Nonlinear Dynamics and Chaos with Applications in Power Systems

Researcher: Bhairavi Premnath
PhD Mathematics, School of Computing and Engineering, University of West London.

Principal Supervisor: Professor Anastasia Sofroniou, Dr
Professor of Mathematics, School of Computing and Engineering, University of West London.

Second Supervisor: Dr Apostolos Georgakis
Associate Professor of Electrical and Electronic Engineering, School of Computing and Engineering, University of West London.

May 2025

Dedicated to my late aunt, Smt. Sivasakthi Sivanesan.

Abstract

This thesis investigates the rich and complex behaviour of nonlinear dynamical systems through the lens of the Swing Equation, a fundamental model in power system dynamics. The Swing Equation, characterised by its nonlinear properties, exhibits diverse dynamical phenomena including period-doubling bifurcations, quasiperiodicity, chaos, and intermittency. The primary aim of this study is to apply the principles of nonlinear dynamics and perturbation theory to uncover the intricate patterns of stability and instability that arise under varying system parameters and external excitations.

A comprehensive exploration of both analytical and numerical techniques is undertaken to examine the system's response to primary and subharmonic resonances, including the transitions leading to chaos. Through methods such as the Floquet theory, method of strained parameters, and tangent instability analysis, the study evaluates the swing equation's sensitivity to perturbations and external forcing.

The investigation further explores the effects of quasiperiodicity specifically, how quasiperiodic forcing influences the system's route to chaos and alters its basins of attraction and Lyapunov exponents. These theoretical insights are supported by detailed graphical simulations, including bifurcation diagrams and Poincaré maps, which visualise the transitions and loss of synchronism.

Moreover, the study incorporates experimental modelling using Matlab Simulink, simulating the swing equation under various resonance conditions and comparing the results with the analytical predictions. Integrity diagrams are constructed to identify regions of stability and quantify chaotic transitions.

An additional focus is placed on the phenomenon of intermittency, exploring how the swing equation responds to small fluctuations in system parameters such as inertia and voltage, and how these contribute to erratic switching between ordered and chaotic states.

Finally, the thesis examines load shedding as a stabilisation strategy. Analytical derivations are presented for both conventional and modified schemes, and their impact on system behaviour is validated through numerical simulation.

This multifaceted approach provides a deeper understanding of nonlinear behaviour in power systems and highlights the importance of robust analytical tools in predicting and mitigating chaotic responses. The findings have direct applications in improving resilience and control in modern electrical grids, particularly under conditions of high variability and complexity.

Acknowledgements

I would like to extend my deepest and most sincere gratitude to my principal supervisor, Professor Anastasia Sofroniou, for her unwavering support, steadfast encouragement, and invaluable guidance throughout the course of this research. Her intellectual generosity, insightful feedback, and patient mentorship have been instrumental not only to the development of this thesis, but also to my growth as a person and a critical thinker. I am profoundly grateful for the countless hours she dedicated to reviewing my work, providing constructive critiques, and nurturing my academic curiosity. Her depth of knowledge, coupled with her humility and genuine interest in the success of her students, has left an indelible mark on my academic journey. Working under her supervision has been a privilege, an experience that has enriched my research and shaped my academic aspirations for the future. I am deeply indebted to her for all that she has done throughout the course of my academic journey.

I am also thankful to my second supervisor, Dr Apostolos Georgakis, for his continuous support, thoughtful suggestions, and kind guidance throughout my doctoral studies. His contributions, especially during key stages of the research, were greatly beneficial, whilst his perspective brought balance and clarity to certain aspects of my work.

I would like to express my heartfelt thanks to the School of Computing and Engineering at the University of West London for providing an environment that promoted intellectual exploration and academic excellence. I am particularly grateful to the university for awarding me the Vice Chancellor's Scholarship, which generously supported me throughout the three years of my PhD programme. This financial assistance played a critical role in enabling me to participate in international conferences, where I had the opportunity to present my work and engage with scholars from around the world, an experience that significantly broadened my academic horizon.

A very special thank you goes to my uncle and aunt, Mr and Mrs Sivanesan, for their enduring love, guidance, and unfaltering belief in me. Their support has been a cornerstone of my personal and academic life. From the very beginning, they have been there to cheer me on, to offer wisdom in times of uncertainty, and to remind me of the importance of perseverance and integrity. Without their help and encouragement, I would not have been able to pursue my education in the United Kingdom. Their sacrifices and commitment to my dreams have inspired me beyond words, and I will forever remain grateful. Their faith in my abilities, even when I doubted myself, has been a powerful source of motivation. Their emotional and moral support formed the bedrock on which I was able to build my endeavours.

Finally, I would also like to express my profound appreciation to my family, whose unconditional love, patience, and encouragement have sustained me through the many challenges and triumphs of this journey.

To all of you, thank you from the bottom of my heart.

Table of Contents

List of Figures

Figure **Page**

List of Tables

Chapter 1

Introduction

1.1 Background and Motivation

The increasing complexity of modern electrical grids, driven by a rising share of renewable energy integration, distributed generation, and responsive loads, poses a substantial challenge to ensuring grid stability and resilience. The operation of a power system is inherently dynamic; even minute disturbances can trigger large-scale oscillations or instabilities due to the nonlinear interactions between components [1, 2]. These phenomena are no longer rare edge cases, they are becoming increasingly prevalent as systems operate closer to their limits to meet modern demand profiles.

A key component of this dynamic behaviour lies in the interaction between mechanical and electrical subsystems in synchronous machines. The swing equation, a second-order nonlinear differential equation, models the rotor angle dynamics of synchronous generators and serves as a fundamental framework in power system stability analysis [3]. While originally developed in the context of small-signal stability, the swing equation has since become a central model in the study of nonlinear dynamics within power systems [4].

Traditionally, power system analysis relied heavily on linearisation techniques, which provide valuable insights under small disturbance assumptions. However, as systems increasingly operate under stressed conditions, these linear methods often fall short of capturing critical dynamical behaviours, such as period doubling, quasiperiodicity, intermittency, and deterministic chaos [5]. These nonlinear phenomena considered, while mathematically rich, pose real engineering risks including loss of synchronism, voltage

collapse, and oscillatory instability.

This research is motivated by the need to apply nonlinear dynamics and perturbation theory to enhance our understanding of these complex behaviours. By constructing an extended formulation of the swing equation that incorporates parametric and external excitations, this work provides a pathway to study how modern power systems respond to disturbances beyond the linear regime. The aim is not only to contribute to theoretical understanding but also to offer practical insights into modelling, prediction, and control of instability in electrical grids.

1.2 Historical Development and Theoretical Context

The swing equation has a long-standing history in electrical engineering, tracing back to the early 20th century. It was initially derived from Newton's second law applied to the rotational motion of synchronous machines, describing the angular acceleration of a rotor in response to the imbalance between mechanical torque and electromagnetic torque. As early as the 1930s, power system engineers recognised its utility in describing transient stability, a system's ability to maintain synchronism following a disturbance.

Over the decades, the swing equation evolved from a basic stability tool into a canvas for nonlinear dynamic exploration. Particularly from the 1970s onward, with the emergence of chaos theory and advances in computational mathematics, researchers began to discover rich dynamical structures embedded within seemingly simple systems. The swing equation, when subjected to periodic or quasiperiodic forcing, exhibits a wide range of behaviours, including strange attractors, bifurcations, and fractal basins of attraction [3].

These findings not only deepened the mathematical appeal of the swing equation but also revealed practical implications for real-world systems. For instance, a generator operating near a bifurcation point may suddenly lose synchronism even under nominal load conditions [2]. Hence, understanding these transitions and their precursors is critical for designing robust control and protection strategies.

1.3 Challenges in Nonlinear Power System Dynamics

The nonlinear nature of power system dynamics introduces several unique challenges. These include:

- Non-uniqueness of solutions: Unlike linear systems, nonlinear systems can exhibit multiple equilibria, some of which may be unstable.
- Sensitivity to initial conditions: Small differences in initial states can lead to vastly different long-term behaviours, especially in chaotic regimes.
- Complex bifurcation structures: Power systems can undergo abrupt qualitative changes in behaviour as parameters are varied, including Hopf, saddle-node, and torus bifurcations.
- Computational burden: Nonlinear simulations require fine temporal resolution and often large-scale computation, especially when including multiple generators and control loops.

Moreover, the presence of non-conservative forces, time delays, and discontinuities in control logic further complicates modelling efforts. To address these challenges, this thesis adopts a hybrid methodology balancing analytical approximations via perturbation theory with numerical simulations and experimental validations using Matlab Simulink.

1.4 Problem Statement and Research Gap

While numerous studies have addressed aspects of nonlinear behaviour in power systems, there remains a critical gap in integrating analytical, numerical, and simulated perspectives under a cohesive framework. Prior research often isolates one method either relying solely on numerical simulations or employing abstract analytical tools without experimental corroboration.

This thesis addresses this gap by:

- Developing a generalised version of the swing equation that incorporates parametric excitation, external forcing, and nonlinear damping.
- Applying multiple-scale perturbation methods to derive approximate solutions under primary and subharmonic resonance conditions.
- Using bifurcation analysis and Lyapunov exponents to characterise stability boundaries.
- Implementing the extended model in Matlab Simulink to simulate and validate behaviours such as chaotic attractors and intermittency.
- Exploring load shedding as a practical control strategy to mitigate instability and chaotic transitions.

This holistic approach allows for the cross-validation of theory and simulation, offering greater confidence in the findings and their applicability to real-world systems.

1.5 Research Objectives

The overarching goal of this research is to investigate the nonlinear dynamics inherent in power systems through a rigorous and multifaceted analysis of the swing equation. This study seeks to go beyond traditional linear approximations and delve into the deeper mathematical structures that govern stability, resonance, and chaotic transitions in dynamic power systems. By constructing an extended form of the swing equation that incorporates parametric and external excitations, nonlinear damping, and time-varying parameters, this work aims to uncover how small perturbations can propagate and evolve into significant instability phenomena.

A key objective is to develop robust analytical methodologies for exploring the dynamic response of the swing equation, particularly under primary and subharmonic resonance conditions. Through the application of perturbation techniques such as the method of strained parameters and multiple time scale analysis, this research aims to derive approximate solutions and interpret their implications for system stability. These analytical tools will be essential for identifying critical parameter thresholds where bifurcations occur, enabling the classification of stability regimes and chaotic behaviour.

Another significant focus is the use of numerical simulations to complement and validate the analytical findings. By generating bifurcation diagrams, Poincaré sections, and Lyapunov exponent plots, the research will provide a detailed map of the system's qualitative dynamics across a wide range of excitation frequencies and amplitudes. These simulations are particularly valuable in regions where analytical solutions become intractable, allowing for visualisation and deeper interpretation of complex dynamical transitions.

Moreover, the research aims to explore the effects of quasiperiodicity, a phenomenon where multiple incommensurate frequencies interact within the system. This component is critical for understanding real-world scenarios in which power systems are subjected to variable frequency disturbances, such as those caused by renewable energy sources. The objective is to examine how quasiperiodic forcing alters the structure of the system's attractors and stability boundaries, and how it influences the routes to chaos, especially in comparison to classical resonance induced transitions.

In addition to theoretical and numerical investigation, this work emphasises practical modelling through the use of Matlab Simulink. The goal is to create an experimental simulation environment that mimics the physical behaviour of the swing equation under various conditions. This includes verifying chaotic behaviour, validating theoretical predictions, and testing the robustness of different stability control strategies. Simulink serves as a bridge between abstract mathematical models and real-world system behaviour, making the findings of this study more applicable to engineering practice.

Finally, the research aims to assess the effectiveness of load shedding as a method of stabilising power systems operating in the nonlinear regime. This includes developing both conventional and modified load shedding schemes, formulating stability equations for each, and analysing their impact on delaying or mitigating the transition to chaos. By integrating these approaches into the overall study, the research aspires to contribute actionable strategies for improving power system resilience in the face of nonlinear disturbances.

1.6 Research Questions

To guide the investigation, the following research questions are posed:

1. How do nonlinear interactions within the swing equation influence the onset of chaotic dynamics?
2. What are the critical parameter regimes where the system transitions from stable periodic motion to chaotic behaviour?
3. How do primary and subharmonic resonances compare in their impact on the stability and response of the system?
4. What role does quasiperiodic forcing play in shaping system behaviour, particularly in terms of bifurcations and attractor structures?
5. Can the swing equation be validated through circuit simulation models on Matlab Simulink, and how well do these align with theoretical predictions?
6. How effective are load shedding strategies in modifying bifurcation structures and delaying the transition to chaos?

1.7 Methodological Overview

The methodology adopted in this research is deliberately multidisciplinary and structured to investigate the swing equation from multiple analytical, numerical, and simulated perspectives. At the core of this approach is the mathematical formulation of an extended swing equation, incorporating both parametric and external excitation terms, damping, and voltage effects. This foundational step enables a more realistic and flexible representation of power system dynamics under varying operational conditions. Once the model is defined, analytical methods are employed to study its behaviour under conditions of resonance. Techniques such as the method of strained parameters, multiple scales, and Floquet theory are used to identify solutions that exhibit primary and subharmonic resonances. These techniques allow the researcher to derive approximate but insightful expressions that characterise the onset of complex behaviour, such as oscillatory instabilities or bifurcations.

Complementing the analytical investigations are detailed numerical simulations, which serve both to validate theoretical findings and to explore the full nonlinear character of the system in parameter regions where analytical techniques lose applicability. Simulations are

used to construct bifurcation diagrams, plot Lyapunov exponents, and generate Poincaré maps, all of which provide critical visual and quantitative insights into the system's stability and its transition into chaos. The influence of forcing amplitude, frequency, damping, and system bias is systematically studied, enabling the construction of integrity diagrams that highlight regions of ordered and disordered dynamics.

Furthermore, Matlab Simulink is employed as a platform for experimental modelling and dynamic simulation. This software environment allows for the construction of virtual circuit models that mimic the behaviour of synchronous machines under dynamic stress. The simulations closely mirror the theoretical formulations of the swing equation and allow for real-time manipulation of system parameters. This step is crucial for validating theoretical predictions and for understanding how chaotic or periodic behaviour manifests in real-world power systems. Simulink simulations also form the basis for implementing and testing stabilisation schemes, including various forms of load shedding. Overall, this hybrid methodology encompassing mathematical derivation, numerical computation, and experimental modelling ensures that the research remains theoretically sound while also grounded in engineering reality.

1.8 Contribution and Originality

This research makes several significant contributions to the field of nonlinear dynamics in power systems, both in terms of theoretical advancement and practical application. One of the key contributions lies in the development and analysis of an extended swing equation model that goes beyond traditional formulations by considering quasiperiodic forcing, intermittency and non-ideal damping. These additions allow the system to capture a broader range of realistic dynamic behaviours, including chaotic attractors and complex bifurcation scenarios that are not readily observed in classical models. This refined mathematical framework provides a more accurate and comprehensive representation of the dynamic response of synchronous machines, particularly under extreme or unstable operating conditions.

Another central contribution is the combined use of analytical, numerical, and simulation-based techniques within a unified study. While many prior studies isolate these approaches, this research demonstrates how their integration can produce richer and

more reliable insights. The application of Floquet theory, method of strained parameters, and tangent instability analysis to power system models remains relatively underexplored in existing literature, and this work highlights their effectiveness in detecting critical thresholds, stability regions, and dynamical transitions. In addition, this research presents a systematic comparison between different types of resonances primary, subharmonic, quasiperiodic and shows how each affects the swing equation's stability in distinct ways. This comparative analysis deepens our understanding of how resonance mechanisms lead to chaotic dynamics and synchronisation loss.

Furthermore, the thesis provides a novel treatment of intermittency in the context of power systems, examining how small changes in parameters such as inertia and voltage can lead to unpredictable switching between periodic and chaotic regimes. The study of intermittency and its characterisation using Lyapunov exponents and bifurcation diagrams brings a fresh perspective to modelling power system instability. A particularly practical contribution is the detailed evaluation of load shedding strategies as a means of suppressing chaos and restoring synchrony. By deriving analytical expressions for both conventional and modified load shedding schemes and validating their performance through simulation, this research offers tangible strategies for improving system resilience. The originality of this work also lies in the experimental modelling using Matlab Simulink, where the theoretical models are brought to life and tested under virtual real-time conditions. Taken together, these contributions position this thesis as a novel, interdisciplinary investigation that enhances both theoretical knowledge and engineering practice in the realm of nonlinear power system dynamics.

1.9 Significance of the Study

The findings of this research hold both theoretical and practical importance. From a theoretical perspective, the thesis advances the mathematical understanding of nonlinear dynamical systems within the context of power system models. It introduces refined analytical tools such as multiple scale perturbation and Floquet analysis to characterise bifurcations, stability boundaries, and transitions to chaos in driven systems.

Practically, the study contributes significantly to enhancing power system resilience. As modern electrical grids become increasingly complex and are influenced by the

variability of renewable energy sources, understanding the conditions that lead to instability becomes critically important. The use of Matlab Simulink to experimentally validate chaotic transitions provides a practical bridge between mathematical models and real-world implementations, offering engineers new strategies for anticipating and mitigating instability.

One of the most crucial contributions of this work is the investigation of load shedding as a stabilisation technique within nonlinear power systems. Load shedding—defined as the deliberate disconnection of certain loads from the grid in response to frequency or voltage deviations, is a well-established control strategy. However, this thesis explores its role from a nonlinear dynamical systems perspective, showing how it can influence the structure of attractors, delay bifurcations, and suppress transitions to chaos.

Furthermore, this research demonstrates that load shedding is not merely a last-resort emergency measure, but can be strategically employed as a preventive control mechanism. It highlights the sensitivity of nonlinear systems to parameter changes and shows how even minimal interventions, when optimally timed and placed, can significantly enhance system robustness.

The insights gained from this work are expected to support the development of smarter, more adaptive grid control strategies. These can integrate nonlinear predictive models to identify early warning signs of instability and apply targeted load shedding to avert cascading failures. As the grid evolves towards higher complexity and interconnectivity, the role of load shedding, as reinterpreted through the lens of nonlinear dynamics will become increasingly central in ensuring system security and operational continuity.

1.10 Structure of the thesis

This thesis is organised in a structured and progressive manner, designed to guide the reader from foundational concepts to advanced analysis and practical applications. Chapter 2 evolves with a comprehensive literature review that explores the key theoretical concepts underpinning nonlinear dynamics, bifurcation theory, chaos, and power system stability. This chapter provides the context and motivation for the study, highlighting existing research gaps and establishing the relevance of the swing equation as a model system.

In Chapter 3, the formulation of the extended swing equation is presented. This chapter derives the mathematical model from physical principles, elaborates on its governing assumptions, and introduces the techniques used for its analysis, focussing on primary resonance. A preliminary exploration into the behaviour of the system is also provided here, laying the groundwork for deeper investigation. Chapters 4 focus on the analytical and numerical examination of the subharmonic resonance, respectively. This chapters detail the conditions under which the system transitions from periodic motion to chaos, with extensive use of graphical tools such as phase portraits, Poincaré sections, and bifurcation diagrams.

Chapter 5 advances the analysis further by introducing sophisticated mathematical techniques, such as Floquet theory, tnagent instability and the method of strained parameters to dissect the system's stability structure. This is followed by Chapter 6, which introduces quasiperiodic forcing into the swing equation, examining how this complicates the system's dynamics and alters its routes to chaos. The discussion includes analysis of Lyapunov exponents, basins of attraction, and golden ratio forcing.

The practical implications of the model are then tested in Chapter 7, where the swing equation is implemented in Matlab Simulink. Here, the theoretical and numerical findings are validated, and new visual tools such as integrity diagrams are introduced. Chapter 8 explores the phenomenon of intermittency, analysing how small fluctuations in parameters can lead to unpredictable dynamic shifts, while Chapter 9 investigates the potential of load shedding as a stabilisation mechanism. Various strategies are developed, analysed, and tested for their effectiveness in delaying or suppressing chaotic behaviour.

The thesis concludes with Chapter 10 that summarises the research findings, implications for both academic and industrial settings, and suggestions for future research. Finally, Chapter 11 outlines the research timeline, project management, and ethical considerations. Throughout the thesis, each chapter builds upon the last, forming a coherent and comprehensive investigation into the nonlinear dynamics of the swing equation and its implications for power system stability.

Chapter 2

Literature Review

2.1 Introduction to Nonlinear Dynamics in Power Systems

The modern power system has evolved into a complex network of highly interconnected and dynamically responsive components. Traditional approaches to power system stability were largely rooted in linear models and small-signal analysis, offering valuable but limited insights into the system's behaviour near equilibrium points [6, 7]. However, as the operational boundaries of the grid are increasingly challenged due to high penetration of renewables, fluctuating loads, and power-electronics-based components, the assumptions underpinning linear models often fail. The resulting dynamics are governed by nonlinear relationships, time-varying parameters, and feedback-driven instabilities, all of which require a fundamentally different analytical approach. This has necessitated a shift in focus toward the field of nonlinear dynamics, which provides the mathematical tools and conceptual framework to understand, predict, and control complex behaviour in engineering systems, particularly those involving oscillatory phenomena and sudden transitions [8, 9].

In this context, nonlinear differential equations, such as the swing equation, emerge as essential tools for investigating transient and long-term stability in power systems. These models can capture behaviours such as limit cycles, bifurcations, chaos, and intermittency, which are often impossible to predict using linear approximations [10, 11]. The nonlinear approach considers a system's global behaviour, how it responds not

just near its equilibrium, but across a broad range of initial conditions and parameter variations. This is especially relevant for critical components like synchronous machines, which play a pivotal role in maintaining synchronism across the grid [12].

Understanding nonlinear dynamics in power systems is not only of academic interest but has direct implications for operational reliability and control strategy design. For example, an operating point close to a bifurcation boundary may appear stable under linear analysis, but can, in reality, be on the verge of transitioning into an unstable or chaotic regime due to a slight parameter change or disturbance [13, 14]. In real systems, such transitions can lead to phenomena like voltage collapse, frequency swings, and cascading failures [15]. By studying these phenomena from a nonlinear standpoint, system operators and engineers can better anticipate instabilities, design more effective controllers, and implement stabilisation mechanisms such as load shedding or adaptive damping [16, 17].

The adoption of nonlinear dynamics into power system analysis has accelerated in recent years due to the increasing availability of computational tools, advanced mathematical methods, and simulation platforms like Matlab Simulink [18, 19]. These tools make it feasible to explore complex systems that were previously too analytically intractable. In this research, the swing equation will be used as a case study to explore a wide range of nonlinear behaviours, including resonances, bifurcations, quasiperiodicity, and chaotic attractors [20]. The goal is not only to understand these behaviours theoretically, but to also test their practical implications through simulations and propose strategies for stabilisation. This literature review aims to contextualise this research within the existing body of knowledge, identify gaps, and highlight where this work offers original contributions.

2.2 Classical Approaches vs Nonlinear Modelling

Traditionally, the analysis of power system stability has relied heavily on classical techniques rooted in linear system theory. These methods include linearisation around equilibrium points, eigenvalue analysis, and frequency response techniques [1–3]. While these approaches have been instrumental in shaping the early development of stability assessment tools, they are inherently limited to small-signal behaviours and are applicable

only under assumptions of near-equilibrium operation. Linearised models can capture local behaviour accurately, but they fail to account for the rich spectrum of dynamics exhibited by nonlinear systems, especially under large disturbances or in the presence of system nonlinearities such as saturation, time-varying inputs, or nonlinear damping.

One of the major limitations of classical modelling lies in its inability to detect and analyse phenomena like bifurcations, chaos, quasiperiodicity, and multistability dynamics that emerge only when the full nonlinear nature of the system is considered. In real-world power systems, particularly those operating near their critical loading points or experiencing fluctuations in generation and demand, such behaviours are not only possible but increasingly likely [6, 7]. This motivates the need for nonlinear dynamic analysis, which is capable of describing both the local and global behaviours of power systems across a wide range of parameter variations and initial conditions.

The swing equation provides a critical link between classical and nonlinear modelling approaches. In its basic form, it resembles a damped second-order differential equation and can be simplified under steady-state conditions. However, as soon as external excitations such as fluctuating loads or varying generator inputs are introduced, the system reveals complex behaviours that cannot be captured through linearisation. It is in this context that nonlinear analysis becomes essential for analysis. For instance, as the damping ratio or input amplitude changes, the swing equation may exhibit transitions from periodic motion to quasiperiodic and even chaotic regimes, signalling the breakdown of synchronism. These transitions are difficult, if not impossible, to observe using classical tools alone [6, 8].

Moreover, classical models often assume time-invariant system parameters, which no longer holds true in modern, renewable-integrated power systems. Today's grids experience rapid variations in generation from wind and solar sources, sudden changes in load patterns, and non-negligible time delays in control systems. These factors introduce a layer of complexity that classical models were never designed to handle. Nonlinear methods, in contrast, are more flexible and can accommodate time-dependent coefficients, forcing functions, and even discontinuities in system response.

Several of the recent studies have begun to adopt nonlinear analysis techniques such as bifurcation theory, perturbation methods, and Lyapunov-based stability analysis to gain deeper insights into power system behaviour [6, 7, 10]. These studies have demonstrated

that nonlinear models provide a more accurate and predictive framework, especially in identifying dangerous transitions that may precede instability or collapse. For example, the presence of a Hopf or saddle-node bifurcation in a power system model may signal an impending loss of synchronism or voltage collapse events that linear tools often miss [17, 18].

The swing equation, when extended and analysed through nonlinear methods, becomes a powerful model for capturing such transitions. It enables the study of resonance phenomena (both primary and subharmonic), quasiperiodic attractors, and chaos through tools such as Poincaré maps, Lyapunov exponents, and integrity diagrams. These nonlinear constructs are essential for visualising and quantifying the onset of instability in power systems under non-ideal, real-world conditions [6, 10].

In essence, while classical approaches have laid the groundwork for power system analysis, they are insufficient for capturing the increasingly complex behaviours found in modern power networks. Nonlinear modelling provides a richer, more accurate depiction of system dynamics and is better equipped to address the challenges posed by instability, high variability, and nonlinearity. This research builds on the nonlinear modelling paradigm, using both analytical and numerical tools to examine the swing equation in regimes where classical analysis fails to provide meaningful insights.

2.3 History and Evolution

The swing equation is one of the most fundamental and widely studied equations in power system dynamics. It models the electromechanical interaction between a synchronous generator's rotor and the rest of the power grid. Its origin can be traced back to the early 20th century, when power system engineers sought to understand how machines behave when subjected to disturbances such as sudden changes in load, generator disconnection, or short circuits. The basic form of the swing equation is derived from Newton's second law for rotational motion, applied to the rotating mass of a synchronous generator [13]. In its classical form, the swing equation relates the acceleration of the rotor angle to the imbalance between mechanical input power and electrical output power.

Mathematically the classical swing equation formulation reveals the dynamical balance between mechanical and electrical forces and serves as the starting point for both transient

and small-signal stability analysis [13, 14].

Historically, the swing equation was primarily used to analyse transient stability, i.e., whether a generator can remain synchronised after a sudden disturbance such as a fault or switching event. For many years, this analysis relied on equal area criteria and other graphical tools, and the model was often solved numerically due to its nonlinear nature. However, with the development of computer simulations in the 1960s and 1970s, the swing equation became central to the design of protection schemes and stability studies in large interconnected grids [14, 15].

In its simplified linear form, the swing equation assumes small deviations from the operating point and constant system parameters. This allows for the use of eigenvalue analysis and linear control theory, which are still commonly employed in traditional power system planning and operation [1, 3]. However, such linear approximations are only valid under idealised conditions. As systems became more complex, particularly with the integration of renewables, fast-switching power electronics, and variable loads, it became increasingly clear that the swing equation's nonlinear nature must be preserved to accurately model and predict system behaviour [6, 7].

In recent decades, researchers have revisited the swing equation from the perspective of nonlinear dynamics and chaos theory, especially in the context of forced oscillations and resonance. By introducing external periodic or quasiperiodic forcing into the swing equation, the model reveals a variety of complex dynamical behaviours, including bifurcations, quasiperiodicity, and deterministic chaos [6, 10, 19]. These behaviours are of particular interest because they closely mirror real-world phenomena observed in power grids such as persistent oscillations, loss of synchronism, and multistable responses that cannot be predicted using classical methods alone.

Furthermore, the swing equation has been extended and adapted to model multi-machine systems, networks of generators, and systems incorporating power-electronic interfaces. In these scenarios, additional terms are added to account for network topology, time delays, and control loop dynamics. These extensions significantly increase the model's dimensionality and complexity, but also its realism and applicability to contemporary grid challenges [6, 10, 19].

In this research, an extended version of the swing equation is studied, incorporating parametric excitation, subharmonic forcing, quasiperiodic terms, and intermittent behaviour.

This formulation allows the investigation of how the system transitions through various dynamical regimes from steady-state synchronism to periodic motion, and ultimately to chaotic oscillations under different configurations. The modified swing equation serves as a gateway to explore nonlinear resonance, intermittency, and stability boundaries, all of which are essential to understanding the performance and vulnerabilities of power systems in the modern era.

Thus, the swing equation has evolved from a classical engineering model to a powerful mathematical framework for nonlinear analysis. It continues to play a central role in theoretical studies, numerical simulations, and experimental validations in the field of power system dynamics.

2.4 Basic Concepts and Theories of Nonlinear Dynamics

2.4.1 Equilibrium Points

Equilibrium points are of utmost importance in comprehending the behaviour of nonlinear dynamical systems. An equilibrium point refers to a condition in which the state variables of a system stay unchanged and stable across time and can exhibit either stability or instability. A stable equilibrium point is characterised by the convergence of neighbouring trajectories towards the point, suggesting the system's inclination to revert to that condition after experiencing minor disturbances. In contrast, an unstable equilibrium point exhibits paths that diverge, demonstrating the system's susceptibility to disturbances and its ability to deviate from this condition. Stability study of equilibrium sites in nonlinear systems entails investigating the eigenvalues of the system's Jacobian matrix, which offers valuable insights into the local dynamics surrounding these points. This is crucial for forecasting the long-term behaviour of complex systems and is extensively utilised in disciplines such as physics, biology, and engineering.

When it comes to determining whether or not power systems are stable within the context of the swing equation, equilibrium points are an extremely important factor to consider. Within the concept of a power grid, the swing equation is a mathematical model that provides a description of the behaviour of synchronous generators. The analysis of

how the system responds to interruptions is a common use of this phenomenon. The stable operating circumstances that correspond to the equilibrium points in the swing equation are those in which the generators are in complete balance with the load. For the purpose of ensuring that the power system is resilient to interruptions, it is vital to conduct stability studies around these equilibrium points. When a system is equated to zero, the solution that becomes available is known as the equilibrium point. The equation can be linearised, which might be helpful in determining whether or not the equilibrium points are stable. In order to analyse a system that is neutrally stable, it is necessary to conduct nonlinear analysis [1, 33, 49].

2.4.2 Bifurcation

Bifurcation takes place when a relatively minor alteration to a parameter value of a system results in a change in the behaviour of the system, regardless of whether the alteration is topological or qualitative in nature. Discrete and continuous systems both have the potential to experience bifurcations. The phenomenon of bifurcation has an effect on power systems and the associated topics, including oscillation and voltage collapse [17, 18]. There is a connection between this subject and the concept of eigenvalues, which can be generalised to be analysed in greater detail [19]. In this work, the primary objective is to provide an explanation for the changes that occur in the bifurcations of power systems and how these changes impact the electric circuits. Despite the fact that bifurcation can be addressed with the assistance of a mathematical model, it can also be described through computer experiments with the assistance of oscillators [20]. These researchers are also aware of the potential drawbacks that may be encountered while employing a physical oscillator. In order to circumvent this difficulty, they propose the utilisation of a computer programme in order to acquire precise and effective results for the purpose of doing additional research on bifurcations. Miles. W. (1984) has provided an explanation of a computer software that works to analyse dynamical systems that contain bifurcations [21]. As an additional point of interest, he mentions that Matlab possesses a few numerical packages, such as MATCONT and CLMATCONT, that are suitable for conducting this particular study on bifurcation [21]. In another research article, the author discusses the peculiar characteristics of a parametrically compressed system and

elucidates the mechanism behind the symmetry-breaking, pitchfork bifurcation that occurs through the utilisation of a pinched cylinder device [22]. Both the stability and the behaviour of the swing equation are influenced by a great number of factors. Additionally, it was discovered that as the time delay is extended, the limit cycle branches expand along the bigger delays, resulting in the combination of bifurcations [23].

In addition, bifurcation analysis has been performed on living beings, which is an interesting development in the field of science. For the purpose of analysing the transmission of malaria, the research conducted by N. Chitnis and colleagues in 2006 [18] has focused on bifurcations. In this case, they take into consideration a mathematical model that contains differential equations in order to determine the duration of the infection and, consequently, the death rate by utilising equilibrium and bifurcations. Bifurcation analysis has been utilised by authors such as Qi et al. (2020) for the purpose of analysing the longitudinal motion of aircraft. By utilising bifurcation theory, they study how the stability is affected in flight dynamics, specifically with regard to the F-8 Crusader [24]. With the assistance of criteria that are derived by Kishida et al. (2014), it is possible to manage systems that are characterised by dynamic uncertainty [25]. This is done in order to ensure that the models remain stable. By altering the values of the variables in the Mathieu equation, the authors demonstrate the transition of bifurcations on the pendulum in a manner that is both analytical and numerical [26].

According to Chin-woo Tan et al. (1993), the change in the load of a power system is also examined after applying some algebraic constraints to the power systems [27]. The researchers come to the conclusion that voltage collapses take place prior to the discovery of saddle-node bifurcation. As the power demand in the systems is increased, it is possible to notice a certain degree of sensitivity in the vicinity of the saddle-node bifurcation. This is because the Jacobian matrix is nearly unique [28]. In situations where the n-dynamics is larger than 3, it is quite challenging to demonstrate the results. It is in the work written by Guckenheimer (1983) that this intricate examination of bifurcations is analysed and presented [29].

In recent studies, bifurcation analysis is utilised to estimate the boundary of the chaotic precursors of a parametrically excited pendulum system [26]. This estimation takes into account the impact of a bias term inclusion in the model, which disrupts the system's symmetry. The objective of this analysis is to acquire more profound

understanding of the bifurcations involved, with the ultimate goal of achieving a higher level of realisation for any specific problem. Additionally, the authors indicate that the simple uneven equation of movement that was proposed on the study results in a variety of nonlinear events. These phenomena include cascades of period doubling bifurcations, which were evaluated and compared with various models.

2.4.3 Limit Cycles

Limit cycles are a captivating and prevalent occurrence in non-linear dynamical systems, wherein the system's trajectory converges to a closed curve in phase space instead of attaining a stable equilibrium. Limit cycles, in contrast to equilibrium points, signify the presence of periodic behaviour within the system [21, 22]. It can exhibit stability, characterised by the convergence of neighbouring trajectories towards it, or instability, denoting divergence. Limit cycles commonly arise due to non-linearities that introduce periodic forces or feedback processes. An essential task in multiple disciplines, including physics, biology, and engineering, is to comprehend and define limit cycles. These cycles play a vital role in elucidating the occurrence of oscillatory patterns in intricate systems. The Van der Pol oscillator and the FitzHugh-Nagumo model are two examples of systems that display limit cycles. These examples highlight the widespread occurrence and significance of limit cycle dynamics in nonlinear systems [30, 31].

The existence of limit cycles in the swing equation of power systems can have substantial consequences for the stability of the system. They can occur as a result of non-linearities in the mechanical and electrical properties of generators, or owing to interactions between generators in a connected grid. These limit cycles have the potential to induce persistent oscillations in the power system, which can result in instability and disruptions. An examination of limit cycles in the framework of the swing equation entails scrutinising the system's reaction to disruptions and comprehending the circumstances under which limit cycles arise.

Limit cycles have been extensively investigated by researchers on the topic of identifying local stability in nonlinear dynamical systems [31]. They are helpful in determining the local stability of these systems and to establish the limits or boundaries of a dynamical system [32]. When a limit cycle undergoes a qualitative shift, a phenomenon

known as orbital bifurcation occurs, which is referred to as bifurcation for a limit cycle [33]. An indirect numerical approach is also described by the researchers, and this is used to derive the eigen values and stability for linearised equations [34]. For the purpose of demonstrating periodic limit cycles and the behaviour of the bifurcation, authors also have used the Bifurcation Theory System Identification (BiTSID) framework [35].

2.4.4 Quasiperiodic Attractors

Quasiperiodic attractors in nonlinear dynamical systems exhibit a more intricate type of dynamics in contrast to the straightforward periodic behaviour observed in limit cycles. This type of attractors display movement when the trajectory of the system does not exactly repeat itself, but instead follows numerous frequencies that are not in a simple ratio to each other, which leads to a more complex and detailed pattern. These attractors frequently emerge in systems with several degrees of freedom and are distinguished by the lack of a direct mathematical depiction, rendering them difficult to analyse. The KAM theorem, also known as the Kolmogorov–Arnold–Moser theorem, is a crucial outcome in the field of quasiperiodic dynamics. It establishes the criteria that determine when a system with almost integrable Hamiltonian dynamics would display quasiperiodic motion [36].

In power systems, quasiperiodic attractors can emerge when the interactions and electrical properties of the generators bring additional difficulties to the dynamics of the system. This is something that can be noticed in the context of the swing equation. Because of the complexity of the power system, there is a possibility that quasi-periodic oscillations would occur, which will make stability analysis more challenging. For the purpose of forecasting the long-term dynamics of power grids that have been disrupted, it is vital to have a solid understanding of the origin and behaviours of quasiperiodic attractors in the swing equation.

Quasiperiodic attractors are characterised by the presence of two or more frequencies that are incommensurate over a time variation [33]. According to researchers, this phenomenon can be investigated in power systems, more specifically in a DC-DC regulator [34]. In a dynamical system, quasiperiodicity is a path that leads to chaos. Additionally, A. R. Bishop and colleagues (1986) investigate the energy transfers that occur between

the states in a nonlinear spectrum (nonlinear spectrum) [37].

2.4.5 Chaotic Attractor

Chaotic attractors in nonlinear dynamical systems exhibit a unique and complex pattern of behaviour characterised by irregular and unpredictable paths. In contrast to periodic attractors like limit cycles, they do not exhibit steady and repeating patterns. On the contrary, they demonstrate a sensitivity to the starting conditions, where their paths diverge rapidly over time, making it difficult to make accurate long-term forecasts. The Lorenz attractor is a renowned illustration of chaotic dynamics, first seen by Edward Lorenz during his investigation of atmospheric convection [32]. Chaotic attractors frequently arise in systems characterised by non-linearities, many interacting components, or feedback loops. They are essential for comprehending the intrinsic complexity of dynamic systems. The examination of chaotic attractors has wide-ranging implications in several scientific fields, including physics, biology, engineering, and economics, enhancing our understanding of intricate events in nature and society.

In power networks, chaotic attractors can form when generators and the system's innate non-linearities interact in a complicated fashion, as seen in the swing equation. This interaction can be viewed in the power network. It is possible for chaotic attractors to arise under certain operating conditions or after interruptions, and the swing equation is a representation of the dynamics of synchronous generators in a connected power grid. It is possible for the reaction of the power system to display a high degree of unpredictability and sensitivity to initial conditions, as shown by the presence of chaotic attractors in the swing equation. In order to evaluate the stability and reliability of power grids, it is vital to have a thorough understanding of the complexities of chaotic attractors in the swing equation. This is especially true when dealing with complex interactions between generators.

According to authors, a chaotic attractor is a type of attractor that does not have an equilibrium point, a limit cycle, or a torus [33]. One sort of attractor is characterised by a fractional dimension, which is further investigated in the works cited in [38, 39]. In addition to this, they state that the attractor is equipped with a broadband power system and that it does not exist in any order that is lower than three.

2.4.6 Chaos

The occurrence of chaos in nonlinear dynamical systems is a result of their sensitivity to initial conditions and the existence of non-linearities, which can give rise to intricate and unpredictable behaviours [26]. In such systems, even slight alterations in the initial conditions might lead to substantially divergent paths over time, posing difficulties in generating accurate long-term forecasts. An exemplary demonstration of chaos may be found in the Lorenz system, which is characterised by the interplay of three interconnected ordinary differential equations governing the behaviour of a dynamic system [3, 16]. Although the equations may appear simple, the system demonstrates chaotic behaviour, which is defined by its sensitivity to initial circumstances, non-repetitive paths, and the existence of a peculiar attractor. The applications of chaos theory span across diverse domains, including weather forecasting, population dynamics, and financial markets. These applications highlight the crucial significance of chaos in comprehending intricate occurrences in both the natural world and civilization.

A nonlinear differential equation that is frequently used to represent the dynamics of power systems is known as the swing equation [1]. It provides a detailed description of the operating characteristics of generators that are part of a linked power system. When the system is working close to its stability restrictions and receives abrupt shocks or load fluctuations, the swing equation may exhibit chaotic behaviour. This can happen when the system is running close to its limits. A description of the rotational movement of generators and the interactions between them is provided by the swing equation. It is possible for it to exhibit chaotic dynamics under certain conditions. The existence of chaos in this equation can lead to adverse results, such as widespread power outages or the onset of cascading malfunctions in the power system. In order to maintain the dependability and stability of electrical networks, it is essential to comprehend and reduce disorder in power systems. This highlights the significance of chaos theory in the process of studying the behaviour of complex engineering systems.

Torus bifurcation, cascade of period doubling bifurcations, and intermittency are the three paths that lead to chaos, according to Berge et al. (1984) [5]. Several studies have been conducted to investigate the phenomenon of chaos in extremely complex power systems. Additionally, an inquiry has been carried out to examine chaos in an autonomous

nonlinear model in a fractional-order format [40, 41].

2.4.7 Lyapunov Exponents

When undertaking an analysis of nonlinear power systems, Lyapunov exponents are an essential component. They offer vital insights into the stability and behaviour of these intricate systems. The rate of exponential divergence or convergence of neighbouring paths in the state space can be quantified using Lyapunov exponents, which are used in the context of nonlinear power systems. The stability of the system may be evaluated with the assistance of these exponents, which indicate whether or not minor changes in the starting conditions will become more pronounced or less pronounced over the course of time [1, 33]. In the process of analysing power systems, Lyapunov exponents can be utilised to locate key points, such as bifurcations or regime transitions. This enables a more comprehensive understanding of the behaviour of the system under a variety of different operating conditions. Lyapunov exponent analysis is frequently utilised by researchers in order to evaluate the stability and robustness of power systems, particularly when nonlinearities and uncertainties are present.

When applied to the swing equation, Lyapunov exponents provide a strong instrument that can be utilised for the purpose of describing the dynamic behaviour of synchronous generators in power systems. The swing equation is used to explain the dynamics of the rotor angle of these generators, and Lyapunov exponents are used to get insights into the stability of the synchronous motion. Researchers are able to locate critical points, bifurcations, and stability boundaries in the parameter space of the system by doing an analysis of the Lyapunov exponents that are related with the swing equation [1, 21]. It is necessary to have this information in order to build control techniques that will ensure the steady operation of power systems and reduce the impact of disturbances. There is a thorough method for understanding the nonlinear dynamics of synchronous generators in power systems that may be obtained through the combination of the swing equation and the Lyapunov exponent analysis.

Both Wolf et al. (1984) and Parker and Chua (1989) created techniques to find Lyapunov exponents. These algorithms were produced through the use of experiments and simulations [42, 43]. It was stated by Newhouse, Ruelle, and Takens (1978) that chaos

occurs after a predetermined number of secondary hopf bifurcations [44]. In a system, the exponents are responsible for monitoring the increase or decrease of disturbances that are considered to be minute [45]. Due to the fact that Lyapunov exponents are only specified for an unlimited length of time, the use of technology to solve them can result in a significant number of inaccuracies. Consequently, the estimation of Lyapunov exponents is performed by using the data of time series that has already been provided [46]. Because they are formed from equations that are quite similar to one another, Lyapunov exponents and floquet multipliers have a close link.

2.4.8 Period Doubling and Poincaré Mapping

The occurrence of period doubling in nonlinear dynamical systems is an important phenomenon that suggests the existence of a path leading to chaos. The phenomenon known as bifurcation takes place when a system goes through a sequence of changes that leads to the doubling of the period of its oscillations. The occurrence of this phenomenon is commonly associated with the presence of nonlinearities and occurs in a wide variety of systems, ranging from straightforward mathematical models to observable physical events. When a parameter is systematically changed, the behaviour of the system shifts from stable periodicity to progressively complicated and chaotic dynamics. This phenomenon is known as the period doubling road to chaos, and it is observed in systems that are governed by logistic maps whenever a parameter is changed. A full explanation of this bifurcation process is provided by the Feigenbaum constants, which were discovered by Mitchell Feigenbaum. These constants also highlight the astonishing self-resemblance that can be found in the period doubling cascade. The examination of period doubling has significant repercussions for understanding the transition from order to chaos in dynamic systems, and it is an essential component of chaos theory [32, 33].

The doubling of the period contained within the swing equation is an essential component of stability analysis in power systems. The swing equation is a representation of the dynamics of synchronous generators in a connected power grid [33]. In this context, period doubling may occur as a result of fluctuations in the parameters of the system. There is the potential for period doubling bifurcations to give rise to a series of occurrences that become progressively more complex, which can ultimately result in the creation of

chaotic dynamics. For the purpose of anticipating the stability thresholds of power systems and analysing the possibility of chaotic responses under given operating circumstances, it is vital to have a solid understanding of the phenomenon of period doubling in the swing equation.

According to Perez et al. (1982), basic models have the ability to demonstrate the existence of period doubling bifurcation and chaos [47]. In this scenario, period doubling proceeds in a cascade that ultimately leads to chaos [48]. In addition to this, they talk about the control of the degree of stability that affects chaos.

In the investigation of nonlinear dynamical systems, Poincaré maps, which were developed by the well-known French mathematician Henri Poincaré, are a powerful instrument that allows for the exploration of these systems. The maps that are displayed here are able to efficiently express the essential dynamics of a continuous system by depicting its intersections with a subspace of lower dimensions, which is generally referred to as a Poincaré maps. When it comes to the dynamics of trajectories in phase space, Poincaré's maps provide valuable insights that may be utilised for the investigation of complex systems and the identification of essential traits such as stable spots, periodic routes, and chaotic attractors. As a result of their ability to provide a means to visually and intellectually grasp the qualitative dynamics of nonlinear systems without the necessity of solving complex differential equations, Poincaré maps have become an essential instrument in the study of dynamical systems. Applications of Poincaré' maps can be found in a variety of domains, including engineering, biology, fluid dynamics, and celestial mechanics, among others. Adaptability is demonstrated by their ability to disclose the intricacy of non-inear occurrences, which is one of their most well-known accomplishments.

Poincaré maps are essential in comprehending the dynamics of power systems and analysing the swing equation. Through the creation of a Poincaré map for the swing equation, scientists can examine the system's dynamics in a space with fewer dimensions, resulting in a more distinct understanding of stability, bifurcations, and attractor structures. Poincaré maps are highly valuable for discerning the influence of parameter fluctuations and disruptions on the power system's enduring dynamics.

Poincaré equation is when there is an intersection in the same direction between the flow of the lines in a system [49]. One of the most significant benefits of using Poincaré is that it reduces the amount of data and separates the time [50]. In addition to being

of great assistance in distinguishing between the attractors, it also reveals the precise number of equilibrium points that are present when plotted on a graph.

2.4.9 Basins of attractions

Basins of attraction are essential principles in the analysis of nonlinear dynamical systems, offering vital understanding into the enduring dynamics and stability of system trajectories. A basin of attraction in a nonlinear dynamical system refers to a specific region in the state space [51]. This zone is characterised by the property that when initial conditions are set within it, the paths of the system will eventually converge towards a certain attractor. An attractor refers to a stable behaviour of a system, which might take the form of a fixed point, periodic orbit, or a more intricate structure. The limits of basins of attraction define the areas where trajectories converge towards different attractors, thereby separating discrete sections of the state space that are linked with diverse long-term behaviours. Comprehending the basins of attraction is essential for forecasting how a system will react to different starting conditions and disturbances, making it a fundamental tool in the examination of intricate dynamical systems.

Basins of attraction are of utmost importance in the analysis of the swing equation in power systems as they significantly influence the stability and dynamics of synchronous generators. The swing equation represents the rotational movement of the rotors in power generators, while basins of attraction provide a visual representation of the areas in the system's state space where the trajectories of the system converge towards stable synchronous operation. Examining the basins of attraction for the swing equation yields valuable insights into how various initial conditions affect the stability of the power system [33]. Researchers utilise this data to develop control algorithms that guarantee the convergence of trajectories towards desirable operating points, hence improving the overall stability and dependability of power systems.

2.5 Quasiperiodicity and Intermittency in Power Systems

Quasiperiodicity and intermittency are critical phenomena in nonlinear dynamics, particularly in systems transitioning toward chaos. In the context of power systems, these behaviours are increasingly observed due to interactions between generators, control systems, and fluctuating sources such as solar and wind. Quasiperiodicity arises when a system is driven by two or more incommensurate frequencies, leading to a motion that never exactly repeats but remains bounded and structured. As discussed above, this behaviour often emerges in systems subjected to dual or multi-frequency excitations, such as parametric forcing and external periodic input acting simultaneously [6, 28, 36].

The importance of quasiperiodicity in power system modelling stems from its role as a precursor to chaos. According to the Ruelle–Takens–Newhouse scenario, a system may transition from periodic to quasiperiodic, and ultimately to chaotic behaviour through successive bifurcations of invariant tori [39]. This pathway is especially relevant in swing equation dynamics where input signals such as load fluctuations or distributed energy control commands introduce additional frequency components. Several studies have demonstrated that under quasiperiodic excitation, the swing equation exhibits complex attractor structures, including toroidal and strange non-chaotic attractors [19, 28].

Another related and equally important concept is intermittency, which refers to irregular switching between different dynamic states. In power systems, intermittency can be triggered by minor variations in system parameters such as inertia, damping, or excitation amplitude. This often leads to abrupt shifts between regular and chaotic regimes, even when the system appears stable for long durations [6, 19]. Intermittency is particularly dangerous because it reflects an underlying system operating near critical thresholds, where small disturbances can trigger large-scale instability.

Three primary types of intermittency are commonly observed: Type I (saddle-node), Type II (Hopf-related), and Type III (crisis-induced). Each corresponds to a different route to chaos and can be detected using time series analysis and phase portraits. In power system contexts, these transitions may result in generator desynchronisation or frequency oscillations, which are difficult to anticipate using classical stability models. This thesis explores the role of intermittency in nonlinear swing equation dynamics and

investigates its occurrence using both numerical simulations and bifurcation tracking techniques.

2.6 Load Shedding Strategies and Nonlinear Stabilisation

Stabilisation of nonlinear power systems is a major engineering concern, especially in systems operating near their bifurcation points or undergoing chaotic oscillations. Among the various control techniques, load shedding remains one of the most widely applied strategies for emergency control in power systems. Load shedding involves the deliberate disconnection of electrical loads to restore power balance and prevent system collapse during periods of stress or instability [47, 48].

While load shedding is typically considered a last-resort protection mechanism, its design and timing are critical, especially in systems exhibiting nonlinear dynamics. Traditional load shedding schemes are usually designed based on frequency thresholds and do not account for the nonlinear trajectories of system states. However, recent research has explored adaptive and model-based load shedding strategies that incorporate bifurcation analysis, Lyapunov exponents, and integrity measures to predict and avoid instability.

In nonlinear systems such as the swing equation under resonance or quasiperiodic forcing, load shedding can be used not just for recovery but also for preventive control. For instance, by reducing the total load at specific frequencies or phases of oscillation, it is possible to shift the system away from a chaotic attractor or delay the onset of a bifurcation. Several studies have proposed load shedding schemes based on phase angle trajectories, damping indices, and chaos indicators, providing more accurate and responsive control mechanisms [49].

This thesis investigates both conventional and modified load shedding models, deriving analytical expressions to evaluate their effect on system stability. Simulations are used to test how load shedding alters the bifurcation structure and basin geometry, and whether it can expand the region of synchrony in phase space. The findings contribute to the growing field of nonlinear control for power systems, where techniques like coordinated

shedding, dynamic relay thresholds, and distributed response mechanisms are being actively researched.

2.7 Experimental Modelling and Matlab Simulink

While theoretical and numerical analyses offer deep insight into nonlinear system behaviour, simulation-based modelling plays a crucial role in validating predictions and testing control strategies under realistic scenarios. Matlab Simulink has emerged as a leading platform for this purpose, especially for power system applications involving complex interdependencies between mechanical, electrical, and control subsystems [50, 51].

In this research, Simulink is used to construct an extended swing equation model, including all nonlinear effects such as parametric excitation, bias, and quasiperiodic forcing. The simulation environment allows for precise control of parameters and input signals, enabling detailed exploration of resonance phenomena, bifurcations, and chaotic transitions. Simulink's graphical environment also facilitates the implementation of feedback loops, load shedding mechanisms, and time-varying excitation sources, offering a dynamic testbed for evaluating nonlinear system behaviour.

Recent studies have utilised Simulink to model synchronisation behaviour under high renewable penetration, power-electronic control dynamics, and forced oscillation analysis [49, 50]. These applications underscore the flexibility of the platform in handling nonlinear, hybrid, and time-delayed systems. Moreover, experimental modelling provides the opportunity to generate integrity diagrams, phase space portraits, and Poincaré sections, which are essential for visualising the system's long-term behaviour under various configurations.

Here within, the Simulink-based model is used to validate the analytical and numerical findings derived from perturbation theory, bifurcation analysis, and Lyapunov exponent computation. The results confirm the presence of stable and unstable regimes, periodic and chaotic attractors, and the influence of nonlinear damping and load modulation on system response. This integrative modelling approach ensures that the theoretical results are not only mathematically sound but also practically relevant.

2.8 Gaps in the Literature and Relevance of the Present Study

Despite the significant progress in nonlinear modelling of power systems, several gaps remain in the literature. First, while many studies address bifurcations and chaos in simplified systems, few offer a comprehensive integration of analytical, numerical, and simulation-based approaches using extended versions of the swing equation. Second, most existing load shedding strategies do not consider the dynamical landscape of the system, such as basin geometry or attractor type, which limits their effectiveness in nonlinear operating regimes.

Additionally, there is a lack of studies exploring quasiperiodicity and intermittency in power systems in sufficient depth. These phenomena are often overlooked in favour of more easily detectable chaos or bifurcation points, yet they offer critical early warning signs of instability. Moreover, few works combine these analyses with practical modelling tools like Simulink to validate theory with near-realistic scenarios.

This thesis addresses these gaps by offering a multi-method investigation of the swing equation's nonlinear behaviour. It contributes to the field by developing a generalised equation that incorporates multiple excitation sources and damping models, applying advanced perturbation techniques and chaos detection tools, and validating all results in a simulation framework. Furthermore, it proposes and tests new load shedding strategies rooted in the geometry of basins of attraction and bifurcation structures bridging the gap between nonlinear theory and control engineering practice.

Through this integrative approach, the research provides not only novel theoretical insights but also practical tools and strategies for predicting, visualising, and mitigating instability in modern power systems.

2.9 Research Paradigm

Within the scope of this investigation, a positivist paradigm is adopted to provide the research questions with a robust framework that is both analytical and empirically grounded. In the context of the social and applied sciences, positivism has long served as a foundational research philosophy. It asserts that reality is objective, external, and

governed by immutable natural laws that can be discovered through observation and reason. Positivist research is built on the belief that the world can be measured and understood through quantitative analysis, and that facts exist independently of the observer [52, 53].

According to authors, research in the scientific domain typically aligns with the explanatory focus of the positivist paradigm [54]. The goal is to explain phenomena through cause-effect relationships and generalisable laws. Importantly, researchers working within this paradigm are expected to maintain a level of detachment from the study subjects in order to minimise bias and uphold objectivity. As researchers note, the philosophical stance of the researcher is embodied in their paradigm, which in turn influences every methodological and analytical decision made throughout the research process [54, 55].

In this study, the positivist approach is manifested through the adoption of a quantitative methodology. Data will be collected through simulations, numerically analysed, and interpreted through structured methods such as numerical simulations, mathematical modelling, and computational analysis. By following a deductive logic, hypotheses can be tested, predictions can be validated, and findings can be replicated, thus ensuring scientific rigour.

Moreover, sufficient theoretical rationale will be presented to support the chosen methods and to frame the interpretation of the results. The use of testable components such as the swing equation and its nonlinear extensions serves as a solid foundation for drawing comparisons, identifying patterns, and evaluating the consistency of outcomes across different scenarios. This structured, methodical approach allows the researcher to not only uncover significant dynamic behaviours (such as bifurcations and chaos), but also to compare these behaviours with theoretical expectations, thereby reinforcing the validity of the research.

Overall, the selected paradigm underpins a structured, measurable, and replicable study that aims to contribute meaningfully to the understanding of nonlinear dynamics in power systems. It provides a philosophical and practical guide for the entire research process, from hypothesis formulation and model development to analysis and interpretation.

Chapter 3

Investigation into the Primary Resonance

3.1 Formulation of the Swing Equation

The swing equation studied here depicts the motion of rotor of machine as shown below in Figure 3.1.

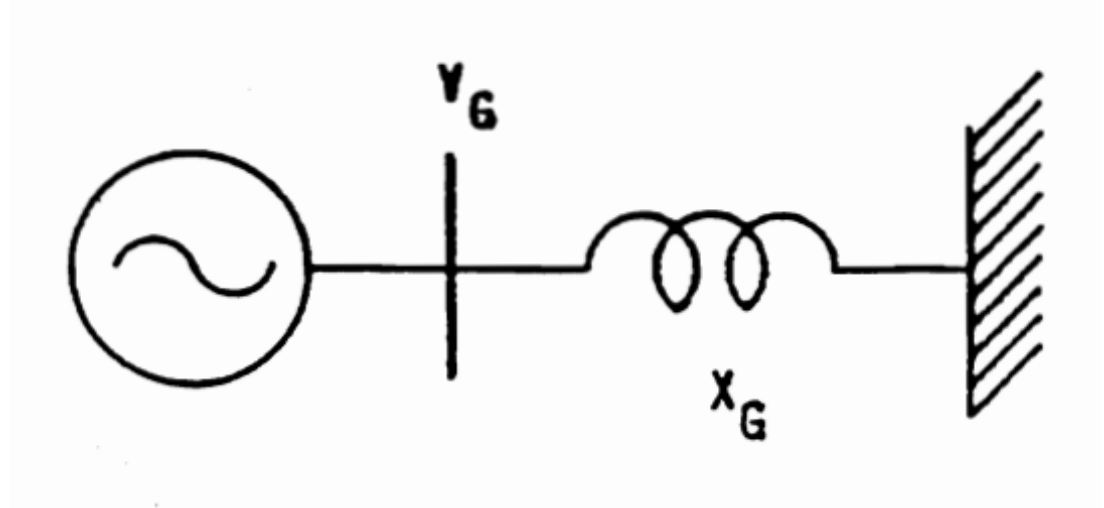

Figure 3.1: Swing equation describing the motion of the rotor of the machine. Figure reproduced from [33].

Initially the classical swing equation is derived in order to understand how the mechanical realisation of the model leads to its formulation.

Considering the Law of rotation,

$$J\frac{d^2\delta_m}{dt^2} = T_a = T_m - T_e \tag{3.1}$$

where J is the moment of combined inertia.

$$\delta_m = \omega_{sm}t + \theta \tag{3.2}$$

The first derivative is given as:

$$\frac{d\delta_m}{dt} = \omega_{sm} + \frac{d\theta}{dt} \tag{3.3}$$

The second derivative is:

$$\frac{d^2\delta_m}{dt^2} = \frac{d^2\theta}{dt^2} \tag{3.4}$$

Substituting into the law of rotation:

$$J\frac{d^2\theta}{dt^2} = T_a = T_m - T_e \tag{3.5}$$

Multiplying throughout by ω_R gives:

$$J\omega_R\frac{d^2\theta}{dt^2} = T_a\omega_R = T_m\omega_R - T_e\omega_R = P_m - P_e \tag{3.6}$$

where

- δ_m: Mechanical rotor angle
- θ: Deviation from synchronous angle (i.e., $\delta_m = \omega_{sm}t + \theta$)
- T_a: Accelerating torque
- T_m: Mechanical torque supplied by the prime mover
- T_e: Electromagnetic torque developed by the generator
- J: Combined moment of inertia of the rotor system
- ω_{sm}: Synchronous angular velocity
- $M = J\omega_R$: Angular momentum

- $P_e = T_e\omega_R$: Electrical power output

$$P_e = \frac{V_G V_B}{X_G} \sin(\theta - \theta_B) \tag{3.7}$$

$$J\omega_R = M = \frac{2H}{\omega_R} \tag{3.8}$$

Finally, converting the swing equation into per unit system leads to:

$$\frac{2H}{\omega_R}\frac{d^2\theta}{dt^2} = P_m - \frac{V_G V_B}{X_G} \sin(\theta - \theta_B) \tag{3.9}$$

Allowing for a damping term, the full swing equation becomes:

$$\frac{2H}{\omega_R}\frac{d^2\theta}{dt^2} + D\frac{d\theta}{dt} = P_m - \frac{V_G V_B}{X_G} \sin(\theta - \theta_B) \tag{3.10}$$

where:

$$V_B = V_{B0} + V_{B1}\cos(\Omega t + \phi_v) \tag{3.11}$$

$$\theta_B = \theta_{B0} + \theta_{B1}\cos(\Omega t + \phi_0) \tag{3.12}$$

with:

- ω_R: Constant angular velocity
- H: Inertia
- D: Damping
- P_m: Mechanical Power
- V_G: Generator voltage
- X_G: Transient reactance
- V_B: Bus voltage
- θ_B: Phase of the bus

The magnitudes V_{B1} and θ_{B1} are assumed to be small.

For the purpose of conducting additional research, a mathematical analysis is performed on this equation. Multiplication and other fundamental mathematical operations, such as algebraic techniques for expanding brackets, are carried out at the beginning of the process. Following that, the Taylor expansion and substitution are carried out in order to generate the final equation that will be utilised for the perturbation experiment.

In the following step, the Floquet theory is taken into consideration for its numerical application. In this step, some analytical work was done in order to extract the equations, which were then utilised for graphical communication.

An additional way of strained parameters, as mentioned by Nayfeh (1981) [9], is the subject of this discussion. Therefore, with the assistance of mathematical processes, the equations are obtained in the appropriate manner.

3.2 Introduction

In the context of a power system, the concept of disturbances, which can be defined as sudden or sequential changes to the system's characteristics or operating quantities, is intimately connected to the concept of stability. When it comes to the dynamics of a system, even a relatively minor disruption can have an effect that is both interesting and important. The process of studying the stability of a system can be accomplished by employing several approaches, such as linearising the equations that represent the system [1, 61], undertaking eigenvalue and frequency response methods [2, 3, 62].

For the purpose of this investigation, a system with a single degree of freedom is taken into consideration. This system will make it possible to investigate nonlinear dynamics and will also take into account chaotic attractors. The nonlinear component of solving a system is the primary emphasis of this investigation. Methods such as perturbation techniques and nonlinear methods are utilised in making this determination. The initial phase of this investigation is the representation of an infinite busbar under the assumption that both the voltage and frequency remain constant. A metallic strip or bar that is utilised for the delivery of high-current power is known as a busbar system. Home circuits, switchgear, and panel boards are the typical applications for this component. In most cases, the busbars are not insulated, and they are supported by insulated pillars that

are exposed to the air. This provides sufficient cooling for the conductors during the process [63]. If a classical representation is taken into consideration, which means that there is a constant voltage behind a transient reactance, then the busbar system can be reduced to a second-order differential equation, but the coefficients will remain constant. The analogous swing equation is considered here within, which includes parametric and external excitations, allowing for the techniques of perturbation theory to be employed under this new formulation of the extended busbar system [5, 6]. This is due to the fact that the resulting equation does not offer a great deal of information that is either useful or novel regarding the response of the system.

This newly formulated swing equation will be analysed analytically and numerically to obtain a better understanding of the stability of the model.

A power system is stable at a particular operating condition when it is able to maintain a steady state. When the system experiences a small disturbance, it is able to return to its pre-disturbance operating conditions or achieve a steady state once again. However, in the event of a large disturbance, the equations that describe the system's behaviour can no longer be linearised, and it becomes necessary to use numerical simulation techniques based on geometric methods to analyse the system's behaviour, which is now considered to be a part of nonlinear dynamics [6, 7]. The focus of this paper is the nonlinear aspect of systems which can be addressed through various dynamical and perturbation techniques [8, 9]. Researchers have studied the swing equation which showed the rotor of the machine's motion [6, 7, 10]. Although power systems have been studied for quite some time now, the growth of the topic is tremendous. The power system in electric applications has seen ongoing development in many areas [11, 64]. With this growth, the conservation of energy and renewing the existing energy have been under the radar by many institutions. To help with the environmental concerns the power systems must be studied further, and new techniques should be introduced [12, 65].

The swing equation which is studied initially in this research work will play a vital part in the analysis of the dynamics of a power system [13, 66]. It does exhibit similar characteristics as other power systems, but it is imperative to analyse it first in detail for a better understanding of the concepts. Recent research has found that the generalised form of the swing equation also helps with understanding transient stability in power-electronic power systems [14, 67]. During any slight disturbance, the rotor of the machine will show

some motion with respect to the synchronously rotating air gap. This in turn starts a relative motion allowing for the swing equation to describe and model this relative motion [15, 16, 68, 69]. Although Tamura et al.[10] initiated the quasi-infinite busbar which is formulated in phase and magnitude, Hamdan and Nayfeh [3, 8] improved the idea to have quadratic and cubic nonlinearities. This helps in applying techniques such as perturbation analysis to the single-machine-quasi-infinite busbar system.

As it is well known, bifurcation occurs when a small change to a parameter value of a system causes a change in the behaviour whether this is a topological or qualitative change occurring in both discrete and continuous systems. A bifurcation has significant effects on power systems, including oscillation and voltage collapse [17, 18, 70, 71]. Eigenvalue analysis may be further utilised to consider stability and to determine the nature of the system [19, 72]. Bifurcations can be studied using both mathematical models and computer simulations involving oscillators [20, 73]. Some authors have pointed out the limitations of using physical oscillators for this purpose and have suggested computer algorithms as an alternative for more accurate and efficient analysis of bifurcations. In a study [21, 22, 74, 75], the unique nature of a parametrically pressurised system was characterised using a pinched cylinder, and the mechanism of symmetry-breaking pitchfork bifurcation was examined. It has been shown that the stability and behaviour of the swing equation can be affected by various factors, and that increasing the time delay can cause limit cycle branches to move and combine through bifurcations [23, 33].

In some studies bifurcation analysis is employed to estimate the boundary of the chaotic precursors of a parametrically excited pendulum system, considering the effect of a bias term inclusion in the model that breaks the symmetry of the system, gaining deeper insights into bifurcations entailed with the purpose of growing a higher realisation for any unique problem [26, 30, 77]. The authors also explain that the easy uneven equation of movement proposed in the study ends in diverse nonlinear phenomena, inclusive of cascades of period doubling bifurcations, which had been tested and compared with different models.

3.3 Analytical Work

Consider the transformations:

$$\theta - \theta_B = \delta_0 + \eta \tag{3.13}$$

$$\delta_0 = \theta_0 - \theta_{B0} \tag{3.14}$$

$$\eta = \Delta\theta - \theta_{B1}\cos(\Omega t + \phi_0) \tag{3.15}$$

From equation (3.13), it follows that:

$$\sin(\theta - \theta_B) = \sin(\delta_0 + \eta) \tag{3.16}$$

Differentiating equation (3.13), the first and second derivatives are retrieved:

$$\frac{d\theta}{dt} = \frac{d\theta_B}{dt} + \frac{d\delta_0}{dt} + \frac{d\eta}{dt} \tag{3.17}$$

$$\frac{d^2\theta}{dt^2} = \frac{d^2\theta_B}{dt^2} + \frac{d^2\delta_0}{dt^2} + \frac{d^2\eta}{dt^2} \tag{3.18}$$

Substituting equations (3.13), (3.14), and (3.15) into the original swing equation (3.10) and multiplying through by $\frac{\omega_R}{2H}$, it is obtained that:

$$\frac{d^2\theta}{dt^2} + \frac{\omega_R D}{2H}\frac{d\theta}{dt} = \frac{\omega_R}{2H}P_m - \frac{\omega_R}{2H}\frac{V_G V_B}{X_G}\sin(\delta_0 + \eta) \tag{3.19}$$

Now substituting the derivatives and rearranging terms, the following is:

$$\frac{d^2\eta}{dt^2} + \frac{\omega_R D}{2H}\frac{d\eta}{dt} = \frac{\omega_R D}{2H}P_m - \frac{\omega_R D}{2H}\left(\frac{d\theta_B}{dt} + \frac{d\delta_0}{dt}\right) - \frac{d^2\delta_0}{dt^2} - \frac{d^2\theta_B}{dt^2} - \frac{\omega_R}{2H}\frac{V_G V_B}{X_G}\sin(\delta_0 + \eta) \tag{3.20}$$

Expanding $\sin(\delta_0 + \eta)$ using the trigonometric identity:

$$\sin(\delta_0 + \eta) = \sin\delta_0\cos\eta + \cos\delta_0\sin\eta, \tag{3.21}$$

applying Taylor series expansion for small η:

$$\cos\eta \approx 1 - \frac{\eta^2}{2!}, \quad \sin\eta \approx \eta - \frac{\eta^3}{3!} \tag{3.22}$$

and substituting these into the equation, there is a reduction of:

$$\frac{d^2\eta}{dt^2} + \frac{\omega_R D}{2H}\frac{d\eta}{dt} + \frac{\omega_R}{2H}\frac{V_G V_B}{X_G}\left[\sin\delta_0\left(1-\frac{\eta^2}{2!}\right) + \cos\delta_0\left(\eta - \frac{\eta^3}{3!}\right)\right] = \frac{\omega_R D}{2H}P_m - \frac{\omega_R D}{2H}\left(\frac{d\theta_B}{dt} + \frac{d\delta_0}{dt}\right) - \frac{d^2\delta_0}{dt^2} - \frac{d^2\theta_B}{dt^2} \quad (3.23)$$

Next substituting the expressions for $V_B = V_{B0} + V_{B1}\cos(\Omega t + \phi_v)$ and expanding gives:

$$\begin{aligned}\frac{d^2\eta}{dt^2} + \frac{\omega_R D}{2H}\frac{d\eta}{dt} + \frac{\omega_R}{2H}\frac{V_G V_{B0}}{X_G}\sin\delta_0 - \frac{\omega_R}{2H}\frac{V_G V_{B0}}{X_G}\frac{\eta^2}{2}\sin\delta_0 + \frac{\omega_R}{2H}\frac{V_G V_{B0}}{X_G}\eta\cos\delta_0 \\ - \frac{\omega_R}{2H}\frac{V_G V_{B0}}{X_G}\frac{\eta^3}{6}\cos\delta_0 = \frac{\omega_R D}{2H}P_m - \frac{\omega_R D}{2H}\left(\frac{d\theta_B}{dt} + \frac{d\delta_0}{dt}\right) - \frac{d^2\delta_0}{dt^2} - \frac{d^2\theta_B}{dt^2} \\ - \frac{\omega_R}{2H}\frac{V_G V_{B1}}{X_G}\cos(\Omega t + \phi_v)\sin\delta_0 + \frac{\omega_R}{2H}\frac{V_G V_{B1}}{X_G}\cos(\Omega t + \phi_v)\frac{\eta^2}{2}\sin\delta_0 \\ - \frac{\omega_R}{2H}\frac{V_G V_{B1}}{X_G}\cos(\Omega t + \phi_v)\eta\cos\delta_0 + \frac{\omega_R}{2H}\frac{V_G V_{B1}}{X_G}\cos(\Omega t + \phi_v)\frac{\eta^3}{6}\cos\delta_0 \quad (3.24)\end{aligned}$$

Defining the following constants:

$$\alpha_2 = \frac{1}{2}K\tan\delta_0, \quad \alpha_3 = \frac{1}{6}K \quad (3.25)$$

$$G_1 = \frac{-V_{B1}}{V_{B0}}K, \quad G_2 = \frac{-V_{B1}}{2V_{B0}}K\tan\delta_0, \quad G_3 = \frac{-V_{B1}}{6V_{B0}}K \quad (3.26)$$

$$Q_1 = \Omega^2\theta_{B1}, \quad Q_2 = \frac{\Omega D\omega_R\theta_{B1}}{2H}, \quad Q_3 = \frac{-V_{B1}}{V_{B0}}K\tan\delta_0 \quad (3.27)$$

$$K = \frac{V_G V_{B0}\omega_R\cos\delta_0}{2HX_G} \quad (3.28)$$

and substituting these definitions gives the final form:

$$\begin{aligned}\frac{d^2\eta}{dt^2} + \frac{\omega_R}{2H}D\frac{d\eta}{dt} + K\eta = \alpha_2\eta^2 + \alpha_3\eta^3 + G_1\eta\cos(\Omega t + \phi_v) + G_2\eta^2\cos(\Omega t + \phi_v) \\ + G_3\eta^3\cos(\Omega t + \phi_v) + Q_1\cos(\Omega t + \phi_\theta) + Q_2\sin(\Omega t + \phi_\theta) + Q_3\cos(\Omega t + \phi_v) \quad (3.29)\end{aligned}$$

Here, the terms involving η, η^2, η^3 multiplied by periodic functions represent parametric excitation, while the Q-terms represent the additive part of the excitation (i.e., effective external forcing).

This nonlinear second order differential equation now forms the basis for perturbation analysis.

3.3.1 Perturbation Analysis for Primary Resonance

To solve the nonlinear swing equation obtained earlier, perturbation analysis is used. Assume:

$$\eta = \mathcal{O}(\varepsilon) \tag{3.30}$$

This implies the damping term is:

$$\frac{\omega_R D}{2H} = \mathcal{O}(\varepsilon^2) \tag{3.31}$$

Also, let:

$$V_{B1} = \mathcal{O}(\varepsilon^3), \quad \theta_{B1} = \mathcal{O}(\varepsilon^3) \tag{3.32}$$

Then the coefficients in the swing equation take the form:

$$G_1 = \varepsilon^3 g_1, \quad G_2 = \varepsilon^3 g_2, \quad G_3 = \varepsilon^3 g_3, \quad Q = \varepsilon^3 q \tag{3.33}$$

Introducing a detuning parameter σ using:

$$\omega_0^2 = \Omega^2 + \varepsilon^2 \sigma \tag{3.34}$$

the governing equation now becomes:

$$\begin{aligned} &\ddot{\eta} + 2\varepsilon^2 \mu \dot{\eta} + (\Omega^2 + \varepsilon^2 \sigma)\eta = \alpha_2 \eta^2 + \alpha_3 \eta^3 \\ &+ \varepsilon^3 g_1 \eta \cos(\Omega t + \phi_v) + \varepsilon^3 g_2 \eta^2 \cos(\Omega t + \phi_v) + \varepsilon^3 g_3 \eta^3 \cos(\Omega t + \phi_v) + \varepsilon^3 q \cos(\Omega t + \phi_e) \end{aligned} \tag{3.35}$$

Looking for a solution in the form:

$$\eta(t;\varepsilon) = \varepsilon\eta_1(T_0,T_1,T_2) + \varepsilon^2\eta_2(T_0,T_1,T_2) + \varepsilon^3\eta_3(T_0,T_1,T_2) + \dots \tag{3.36}$$

The time derivative expansions are defined as:

$$\frac{d}{dt} = D_0 + \varepsilon D_1 + \varepsilon^2 D_2 + \dots \tag{3.37}$$

$$\frac{d^2}{dt^2} = D_0^2 + 2\varepsilon D_0 D_1 + \varepsilon^2(2D_0D_2 + D_1^2) + \dots \tag{3.38}$$

where $D_n = \frac{\partial}{\partial T_n}$.

$$\eta = \varepsilon\eta_1 + \varepsilon^2\eta_2 + \varepsilon^3\eta_3 + \cdots \tag{3.39}$$

Taking the first derivative with respect to t, and using equation (3.39):

$$\begin{aligned}\eta(D_0 + \varepsilon D_1 + \varepsilon^2 D_2 + \cdots) = \varepsilon\eta_1(D_0 + \varepsilon D_1 + \varepsilon^2 D_2 + \cdots) + \\ \varepsilon^2\eta_2(D_0 + \varepsilon D_1 + \varepsilon^2 D_2 + \cdots) + \varepsilon^3\eta_3(D_0 + \varepsilon D_1 + \varepsilon^2 D_2 + \cdots)\end{aligned} \tag{3.40}$$

Taking the second derivative with respect to t, and using equation (3.40):

$$\begin{aligned}\eta(D_0^2+2\varepsilon D_0D_1+\varepsilon^2(2D_0D_2+D_1^2)+\cdots) = \varepsilon\eta_1(D_0^2+2\varepsilon D_0D_1+\varepsilon^2(2D_0D_2+D_1^2)+\cdots)+ \\ \varepsilon^2\eta_2(D_0^2+2\varepsilon D_0D_1+\varepsilon^2(2D_0D_2+D_1^2)+\cdots)+\varepsilon^3\eta_3(D_0^2+2\varepsilon D_0D_1+\varepsilon^2(2D_0D_2+D_1^2)+\cdots)\end{aligned} \tag{3.41}$$

Now substituting equations (3.39), (3.40), and (3.41) into equation (3.35), and squaring equation (3.39) to substitute for η^2:

$$\begin{aligned}\varepsilon\eta_1(D_0^2+2\varepsilon D_0D_1+\varepsilon^2(2D_0D_2+D_1^2)+\cdots) = \varepsilon\eta_1(D_0^2+2\varepsilon D_0D_1+\varepsilon^2(2D_0D_2+D_1^2)+\cdots)+ \\ \varepsilon^2\eta_2(D_0^2+2\varepsilon D_0D_1+\varepsilon^2(2D_0D_2+D_1^2)+\cdots)+\varepsilon^3\eta_3(D_0^2+2\varepsilon D_0D_1+\varepsilon^2(2D_0D_2+D_1^2)+\cdots)+ \\ 2\varepsilon^2\mu\left(\varepsilon\eta_1(D_0 + \varepsilon D_1 + \varepsilon^2 D_2 + \cdots) + \varepsilon^2\eta_2(D_0 + \varepsilon D_1 + \varepsilon^2 D_2 + \cdots) + \varepsilon^3\eta_3(D_0 + \varepsilon D_1 + \varepsilon^2 D_2 + \cdots)\right) + \\ (\Omega^2 + \mathcal{E}^2\sigma)(\varepsilon\eta_1 + \varepsilon^2\eta_2 + \varepsilon^3\eta_3 + \cdots) = \alpha_2(\varepsilon^2\eta_1^2 + \varepsilon^4\eta_2^2 + \varepsilon^6\eta_3^2 + \cdots) + \alpha_3\eta^3 + \\ \varepsilon^3 g_1\eta\cos(\Omega t + \phi_v) + \varepsilon^3 g_2\eta^2\cos(\Omega t + \phi_v) + \varepsilon^3 g_3\eta^3\cos(\Omega t + \phi_v) + \varepsilon^3 g\cos(\Omega t + \phi_e)\end{aligned} \tag{3.42}$$

Comparing coefficients of ε:

$$\varepsilon: \quad \eta_1 D_0^2 + \eta_1 \Omega^2 = 0 \tag{3.43}$$

$$\varepsilon^2: \quad \eta_1 D_0^2 + \eta_2 \Omega^2 + 2D_0 D_1 \eta_1 = \alpha_2 \eta_1^2 \tag{3.44}$$

$$\varepsilon^3: \quad D_0^2 \eta_3 + 2D_0 D_1 \eta_2 + (D_1^2 + 2D_0 D_2)\eta_1 + 2\mu D_0 \eta_1 + \Omega^2 \eta_3 + \sigma \eta_1 = 2\alpha_2 \eta_1 \eta_2 + \alpha_3 \eta_1^3 + g\cos(\Omega t + \phi_e) \tag{3.45}$$

Solution to equation (3.43) is of the form:

$$\eta_1 = A(T_1, T_2)e^{i\Omega T_0} + \bar{A}(T_1, T_2)e^{-i\Omega T_0} \tag{3.46}$$

Where A is an undetermined function and $\bar{A}$ is the complex conjugate. Given that $D_n = \frac{\partial}{\partial T_n}$, then $D_0 = \frac{\partial}{\partial T_0}$, hence by integration $T_0 = \frac{1}{D_0}$.

Substituting equation (3.46)into (3.44):

$$\eta_2 D_0^2 + \eta_2 \Omega^2 = -2D_0 D_1 \left(Ae^{i\Omega T_0} + \bar{A}e^{-i\Omega T_0}\right) + \alpha_2 \left(Ae^{i\Omega T_0} + \bar{A}e^{-i\Omega T_0}\right)^2 \tag{3.47}$$

Expanding the brackets:

$$\eta_2 D_0^2 + \eta_2 \Omega^2 = -2D_0 D_1 A e^{i\Omega T_0} - 2D_0 D_1 \bar{A} e^{-i\Omega T_0} + \alpha_2 \left(A^2 e^{2i\Omega T_0} + \bar{A}^2 e^{-2i\Omega T_0} + 2A\bar{A}\right) \tag{3.48}$$

Using $D_0 = \frac{\partial}{\partial T_0}$:

$$\frac{\partial(2D_0 D_1 A e^{i\Omega T_0})}{\partial T_0} = 2i\Omega D_1 A e^{i\Omega T_0}, \quad \frac{\partial(2D_0 D_1 \bar{A} e^{-i\Omega T_0})}{\partial T_0} = -2i\Omega D_1 \bar{A} e^{-i\Omega T_0}$$

Substituting and rearranging:

$$\eta_2 D_0^2 + \eta_2 \Omega^2 = -2i\Omega D_1 A e^{i\Omega T_0} + 2i\Omega D_1 \bar{A} e^{-i\Omega T_0} + \alpha_2 (A^2 e^{2i\Omega T_0} + \bar{A}^2 e^{-2i\Omega T_0}) + \text{cc} \quad (3.49)$$

Where cc denotes the complex conjugate. For a bounded solution, we require $D_1 A = 0$, implying $A = A(T_2)$.

Using equation (3.43) in (3.49) and simplifying:

$$\eta_2 = -\frac{\alpha_2 A^2 e^{2i\Omega T_0}}{3\Omega^2} - \frac{\alpha_2 \bar{A}^2 e^{-2i\Omega T_0}}{3\Omega^2} + \frac{2\alpha_2 A\bar{A}}{\Omega^2} \quad (3.50)$$

Substituting equations (3.48) and (3.50) into equation (3.45):

$$\begin{aligned} D_0^2\eta_3 + 2D_0D_1 \left(-\frac{\alpha_2 A^2 e^{2i\Omega T_0}}{3\Omega^2} - \frac{\alpha_2 \bar{A}^2 e^{-2i\Omega T_0}}{3\Omega^2} + \frac{2\alpha_2 A\bar{A}}{\Omega^2} \right) + \\ (D_1^2 + 2D_0D_2)(Ae^{i\Omega T_0} + \bar{A}e^{-i\Omega T_0}) + 2\mu D_0(Ae^{i\Omega T_0} + \bar{A}e^{-i\Omega T_0}) + \\ \Omega^2\eta_3 + \sigma(Ae^{i\Omega T_0} + \bar{A}e^{-i\Omega T_0}) = 2\alpha_2(Ae^{i\Omega T_0} + \bar{A}e^{-i\Omega T_0}) \cdot \\ \left(-\frac{\alpha_2 A^2 e^{2i\Omega T_0}}{3\Omega^2} - \frac{\alpha_2 \bar{A}^2 e^{-2i\Omega T_0}}{3\Omega^2} + \frac{2\alpha_2 A\bar{A}}{\Omega^2} \right) + \\ \alpha_3(Ae^{i\Omega T_0} + \bar{A}e^{-i\Omega T_0})^3 + \frac{1}{2}ge^{i\phi} \end{aligned} \quad (3.51)$$

Expanding the cubic bracket:

$$\alpha_3(Ae^{i\Omega T_0} + \bar{A}e^{-i\Omega T_0})^3 = \alpha_3 A^3 e^{3i\Omega T_0} + 3\alpha_3 A^2 \bar{A} e^{i\Omega T_0} + 3\alpha_3 A\bar{A}^2 e^{-i\Omega T_0} + \alpha_3 \bar{A}^3 e^{-3i\Omega T_0} \quad (3.52)$$

Eliminating secular terms and using $D_1 A = 0$:

$$2i\mu\Omega(A' + \mu A) + \sigma A - \frac{1}{2}ge^{i\phi} + 8\alpha_e A^2 \bar{A} = 0 \quad (3.53)$$

where:

$$A' \text{ is the derivative of } A \quad (3.54)$$

$$\alpha_e = -\frac{3}{8}\alpha_3 - \frac{5\alpha_2^2}{12\Omega^2} \tag{3.55}$$

Now, express A and $\bar{A}$ in polar form:

$$A = \frac{1}{2}ae^{-i(\beta+\phi_e)}, \quad \bar{A} = \frac{1}{2}ae^{i(\beta+\phi_e)} \tag{3.56}$$

Substituting into (3.53):

$$2i\mu\Omega\left(\frac{1}{2}a'e^{-i(\beta+\phi_e)} + \mu\cdot\frac{1}{2}ae^{-i(\beta+\phi_e)}\right) + \sigma\cdot\frac{1}{2}ae^{-i(\beta+\phi_e)} - \frac{1}{2}ge^{i\phi} + 8\alpha_e\left(\frac{1}{2}ae^{-i(\beta+\phi_e)}\right)^2\left(\frac{1}{2}ae^{i(\beta+\phi_e)}\right) = 0 \tag{3.57}$$

Separating real and imaginary parts:

$$\Omega(a' + \mu a) + \frac{1}{2}g\sin\beta = 0 \tag{3.58}$$

$$-\Omega a\beta' + \alpha_e a^3 - \frac{1}{2}g\cos\beta + \frac{1}{2}\sigma a = 0 \tag{3.59}$$

To second approximation:

$$\eta = \varepsilon a\cos(\Omega t + \beta + \phi_e) + \frac{\varepsilon^2 a^2\alpha_2}{6\Omega^2}(3 - \cos(2\Omega t + 2\beta + 2\phi_e)) + \cdots \tag{3.60}$$

Let $\varepsilon = 1$ and let a be the perturbation parameter. Then rewriting equation (3.17) and equation (3.61) as:

$$\Delta\theta = \theta_{B_1}\cos(\Omega t + \phi_\theta) + a\cos(\Omega t + \beta + \phi_e) + \frac{a^2\alpha_2}{6\Omega^2}(3 - \cos(2\Omega t + 2\beta + 2\phi_e)) \tag{3.61}$$

$$\frac{a^2\alpha_2}{2\Omega^2}: \quad \text{drift term.} \tag{3.62}$$

Equation (3.61) shows that the rotor deviates from the operating point and undergoes oscillatory motion [54]. The drift term indicates that the motion is not centered due to nonlinearity.

To understand the character of the solutions of equations (3.57) and (3.58), it is necessary to determine their singular or fixed points. The fixed points of equations (3.57) and (3.58) correspond to $a' = \beta' = 0$. They are given by:

$$\mu a = -\frac{g \sin \beta}{2\Omega} \tag{3.63}$$

$$\frac{a\sigma}{2\Omega} + \frac{\alpha_e a^3}{\Omega} = \frac{g \cos \beta}{2\Omega} \tag{3.64}$$

Squaring and adding (3.62) and (3.63):

$$\mu^2 + \left(\frac{\sigma}{2\Omega} + \frac{\alpha_e a^2}{\Omega} \right)^2 = \frac{g^2}{4\Omega^2 a^2} \tag{3.65}$$

This gives an implicit expression for amplitude a as a function of the tuning parameter σ.

Figure 3.2 and Figure 3.3 present both the phase portraits and time histories for the case of primary resonance, that is when the excitation frequency of the system is approximately equal to the natural frequency of the system, specifically at the angular frequency $\Omega = 8.61$ rads^{-1} plotted from the equation (3.13). These plots are instrumental in validating the analytical approximations by providing a direct comparison with the results obtained through numerical simulation. The comparison focuses on evaluating the accuracy of two numerical techniques used in the perturbation analysis: the Runge-Kutta method and the Newton-Raphson method.

The excitation frequency $\Omega = 8.61$ rad s^{-1} was selected because it is approximately equal to the system's natural frequency, corresponding to the primary resonance condition. This provides a representative case to validate the perturbation solutions against numerical simulations. Additional frequencies ($\Omega = 8.43$, 8.282, 8.275, and 8.2601 rad s^{-1}) were also investigated to illustrate the progression from periodic response to period-doubling and chaos, as shown in Figures 3.4–3.8.

The fourth-order Runge-Kutta method was employed in this analysis due to its balance between computational efficiency and numerical accuracy. It provides a higher-order approximation compared to simpler methods such as Euler's method, making it particularly suitable for solving nonlinear differential equations like the swing equation. This method

ensures stable and precise results across a wide range of system parameters, which is essential for capturing complex dynamical behaviours.

A comparative analysis of the numerical outputs reveals that the Newton-Raphson algorithm yields a closer approximation to the true numerical solution, as evidenced by its lower error magnitude. Specifically, the calculated numerical error associated with the Runge-Kutta method was found to be 0.0884, whereas the Newton-Raphson method exhibited a reduced error of 0.0747. This quantifiable difference underscores the higher accuracy of the Newton-Raphson approach for the particular class of problems addressed in the study.

The observed discrepancy in error can be attributed to the inherent strengths of the Newton-Raphson method in handling nonlinear algebraic systems with high precision, especially near equilibrium points. In contrast, the Runge-Kutta method, while versatile and widely applicable, may introduce accumulated numerical inaccuracies over longer time integrations in nonlinear regimes.

In summary, the comparative results demonstrate that the Newton-Raphson method provides a more reliable and accurate solution for capturing the dynamics near primary resonance [30, 58]. This insight is valuable for guiding the selection of numerical techniques in future investigations involving perturbation methods and nonlinear oscillatory systems.

In the simulation process, the Runge-Kutta method, a well-known explicit technique for solving ordinary differential equations was employed to simulate the time evolution of the system under nonlinear excitation. In parallel, the Newton-Raphson method was applied to solve the nonlinear algebraic equations that emerged from the perturbation expansion, particularly in the steady-state approximation. Both methods were tested under identical initial conditions and system parameters to ensure consistency in the evaluation.

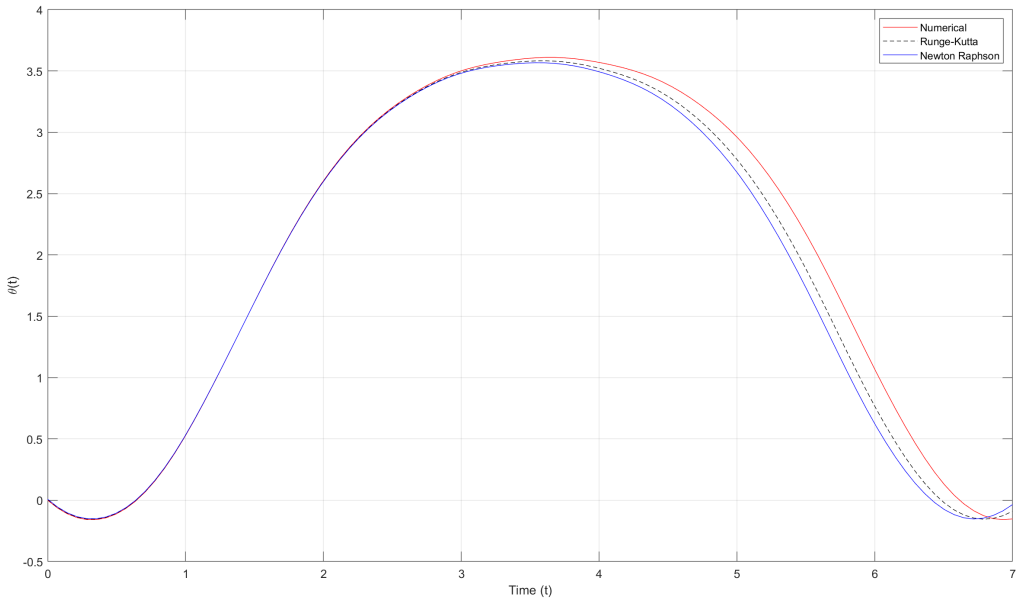

Figure 3.2: Perturbed solution employing Runge-Kutta and Newton Raphson algorithms in comparison to numerical simulations for the case of primary resonance in time history for $\Omega = 8.61$ rads^{-1}.

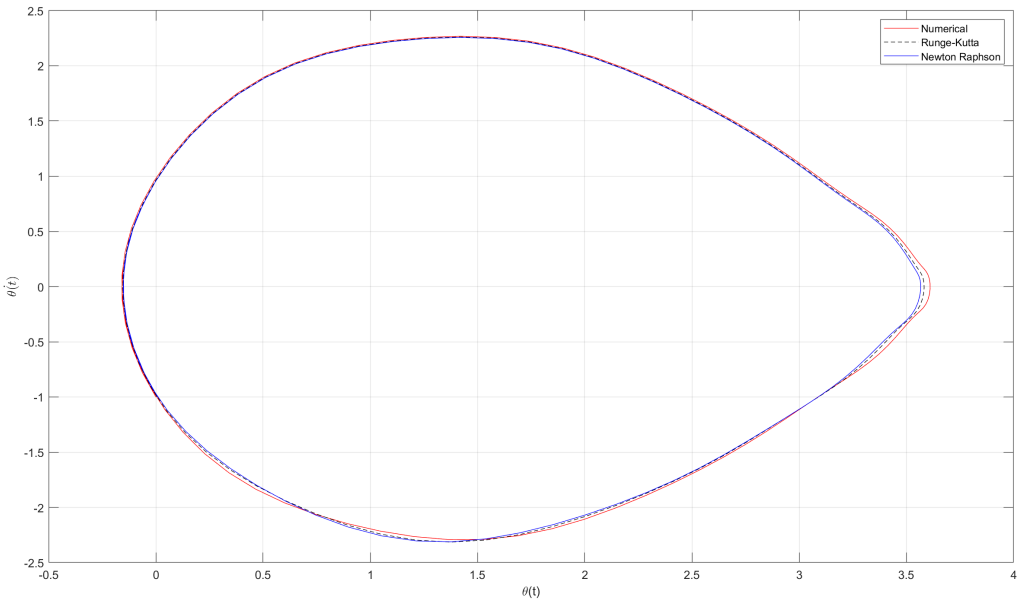

Figure 3.3: Perturbed solution employing Runge-Kutta and Newton Raphson algorithms in comparison to numerical simulations for the case of primary resonance in phase plane for $\Omega = 8.61$ rads^{-1}.

3.4 Numerical Analysis

For the purpose of determining the effect of increasing the excitation frequency Ω, the equations (3.10), (3.11), and (3.12) were set and solved in Matlab using the fourth-order Runge-Kutta method for the parameters given in Appendix [33].

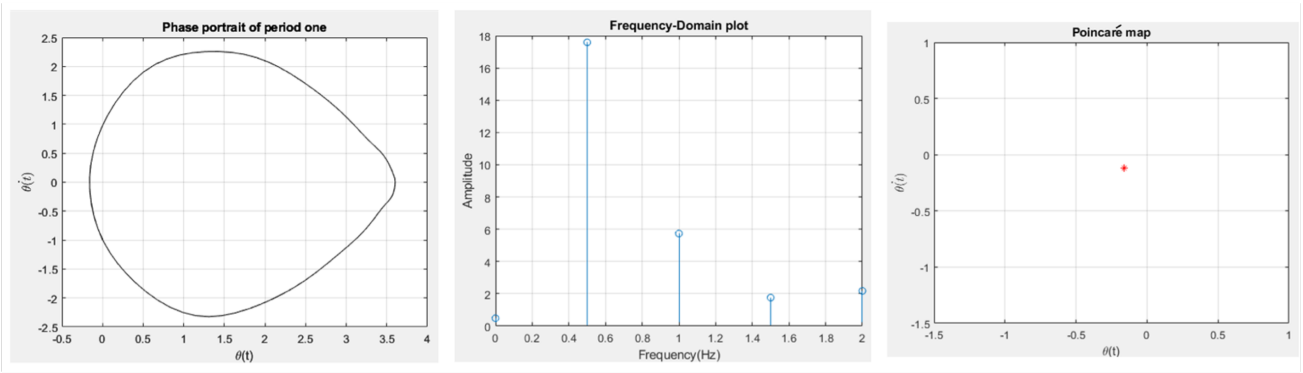

Figure 3.4: Phase portrait, frequency-domain plot and Poincaré map when $\Omega = 8.61$ rads^{-1}.

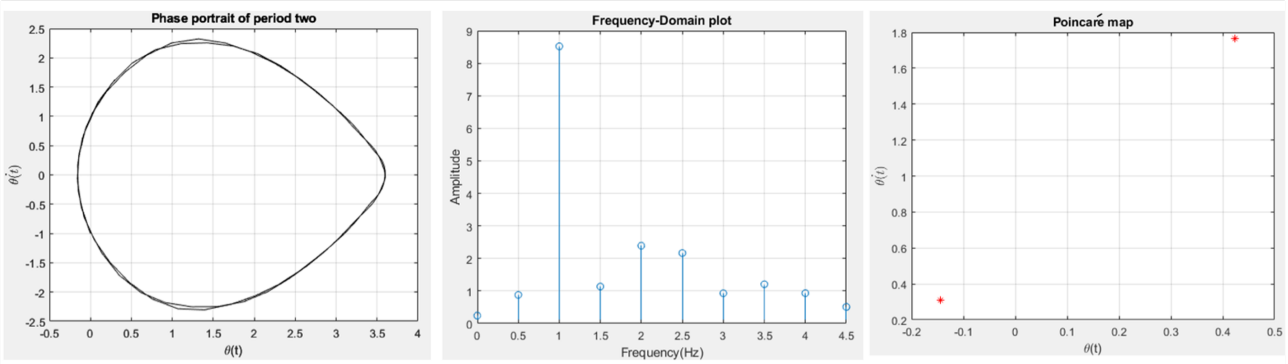

Figure 3.5: Phase portrait, frequency-domain plot and Poincaré map when $\Omega = 8.43$ rads^{-1}.

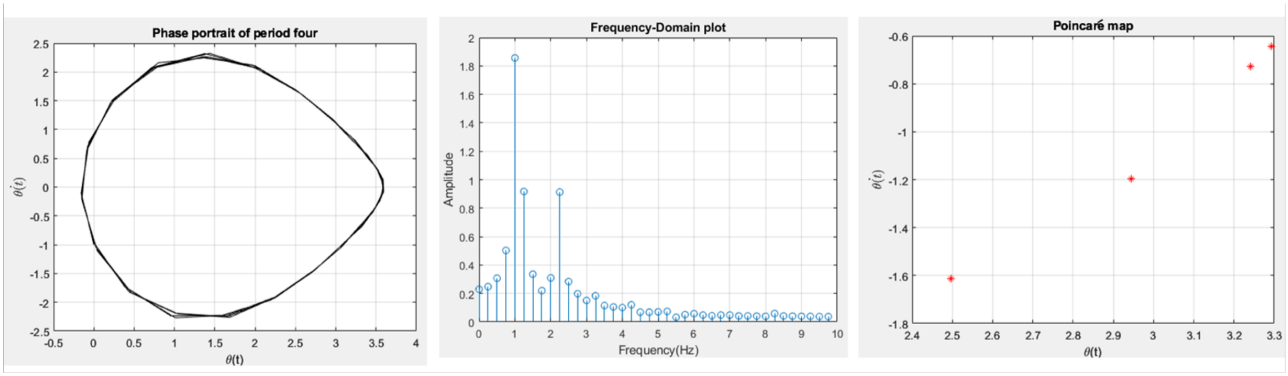

Figure 3.6: Phase portrait, frequency-domain plot and Poincaré map when $\Omega = 8.282$ rads^{-1}.

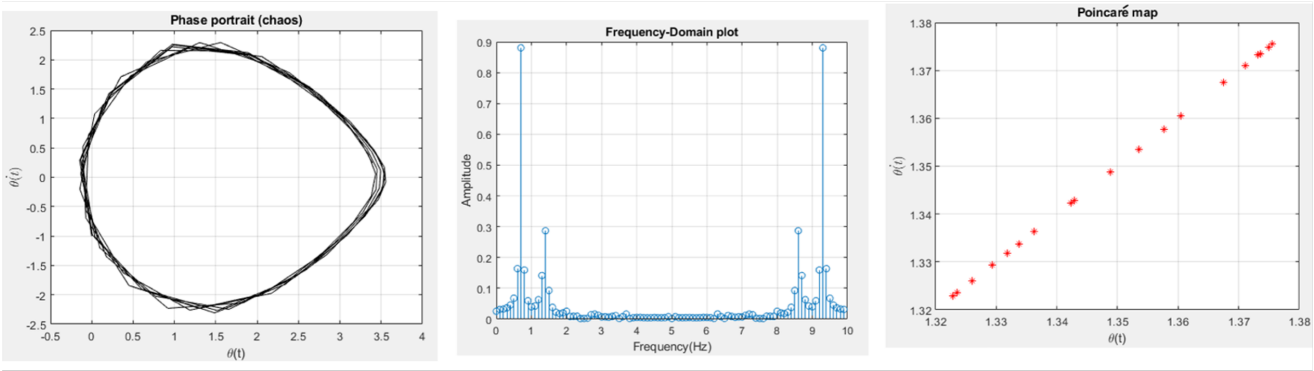

Figure 3.7: Phase portrait, frequency-domain plot and Poincaré map when $\Omega = 8.275$ rads^{-1}.

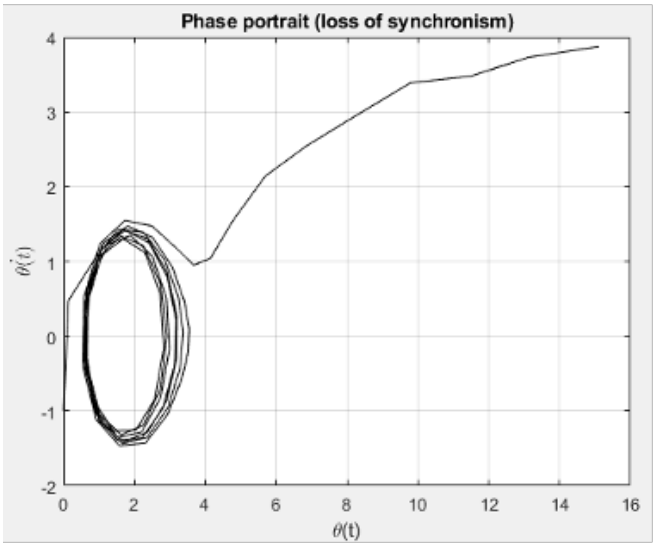

Figure 3.8: Phase portrait (loss of synchronism) when $\Omega = 8.2601$ rads^{-1}.

Plotting the phase portraits, frequency-domain plots, and Poincaré maps generated by varying the excitation frequency in the swing equation (3.10) led to the creation of Figures 3.4, 3.5, 3.6, 3.7, and 3.8. As the excitation frequency Ω decreases, the system progressively loses stability and transitions into chaotic behaviour. Each figure illustrates both the successive period-doubling bifurcations and the manner in which the system loses synchronism.

Figure 3.4 demonstrates that when the excitation frequency is relatively large, specifically $\Omega = 8.61$ rads^{-1}, the system exhibits a single steady-state attractor. The corresponding phase portrait forms a closed loop, indicative of a period-one attractor. This behaviour is further corroborated by the frequency-domain plot and the associated Poincaré map, both of which confirm the periodic nature of the system at this excitation level.

In the process of decreasing the value of Ω, it is possible to see that the graphs experience dynamical transformations, which may include period-doubling solutions. Eventually, as the value of Ω is dropped to a greater extent, around 8.2601 rads^{-1}, a chaotic attractor is displayed, as demonstrated in Figure 3.8.

Using the process of solving the swing equation for a particular value of $\Omega = 8.27$ rads^{-1} and using numerical time integration utilising the traditional fourth order Runge-Kutta technique, the bifurcation diagram that is depicted as Figure 3.9 was built. In the meantime, the value of the forcing r is increased by a small amount, and the time integration process continues to plot the maximum amplitude of the oscillatory solution against r .

$$r = \frac{V_G V_B}{X_G} \sin(\theta - \theta_B) \tag{3.66}$$

Figure 3.9 depicts the first instance of period doubling occurring just before $r = 0.9$, which is also supported by the Poincaré maps shown in Figure 3.10. Additionally, at about $r = 2.36$, the first period doubling in a series of period doubles is displayed, which results in chaotic behaviour. The results of this numerical analysis demonstrate that as the value of r is increased, the swing equation gets closer and closer to losing its synchronisation function.

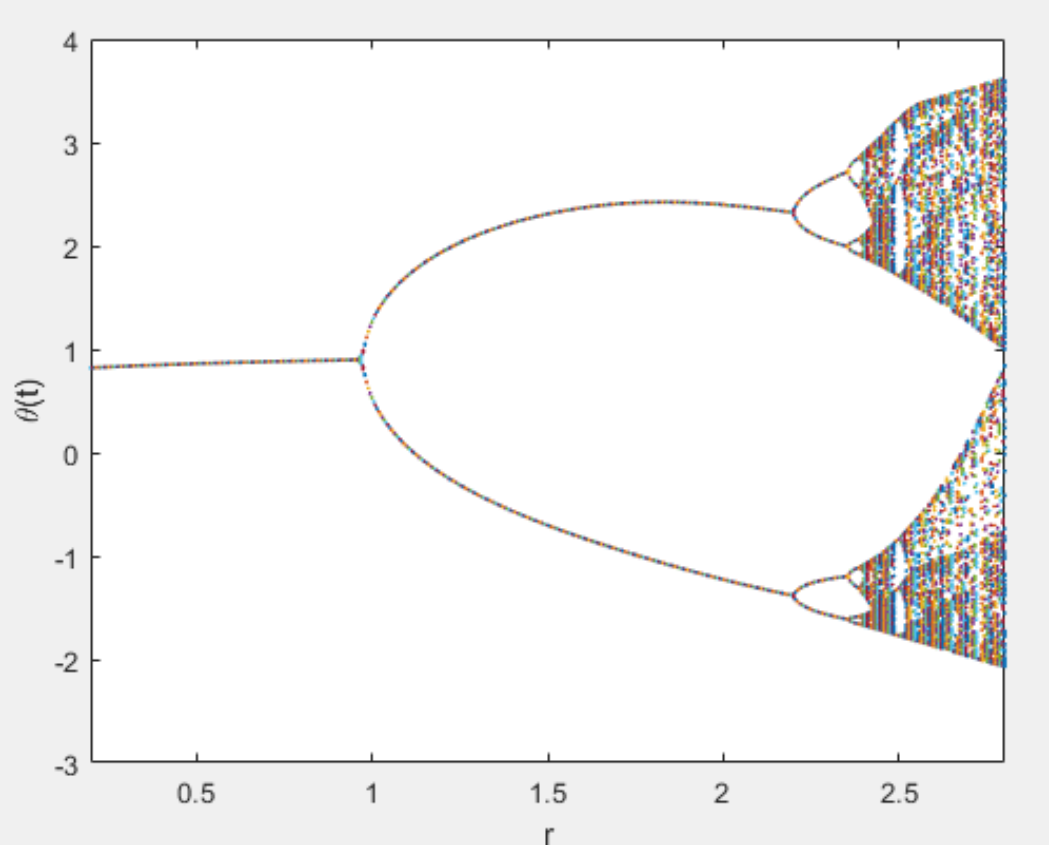

Figure 3.9: Bifurcation diagram when r value is varied and constant $\Omega = 8.27$ rads^{-1}.

The corresponding Poincaré maps are plotted as shown below, Figure 3.10. They clearly depict the points where period doubling occurs and how as r is increased the phenomenon of chaos is verified.

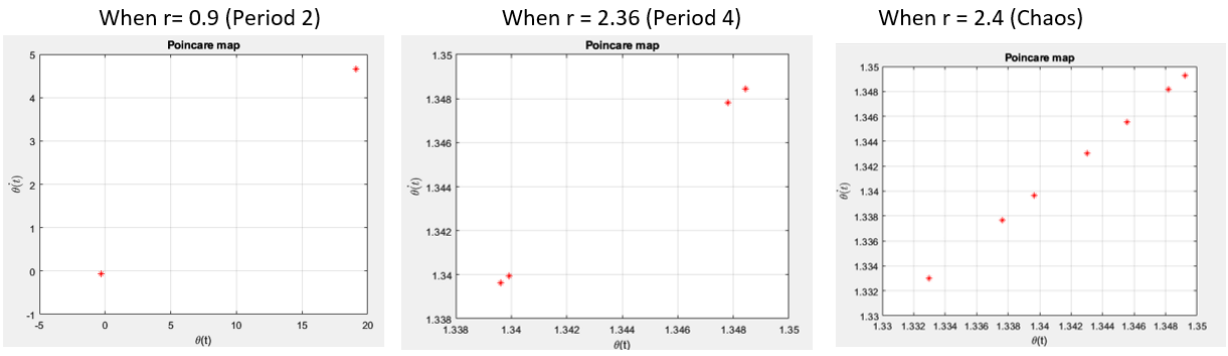

Figure 3.10: Poincaré maps for the different r values.

It is observed that at approximately $r > 2.4$, the chaotic region has commenced where the Lyapunov exponent generally takes positive values. This behaviour is depicted and presented as Figure 3.11, where it is the case when two nearby points, initially separated

by an infinitesimal distance, typically diverge from each other over time and this is quantitatively measured by the Lyapunov exponents. The bifurcation diagram of Figure 3.9, also verifies this behaviour, where at approximately the same value of r , the cascade of period doubling sequence leads to chaos such that is suffices to say that a chaotic attractor can be identified by a positive Lyapunov exponent.

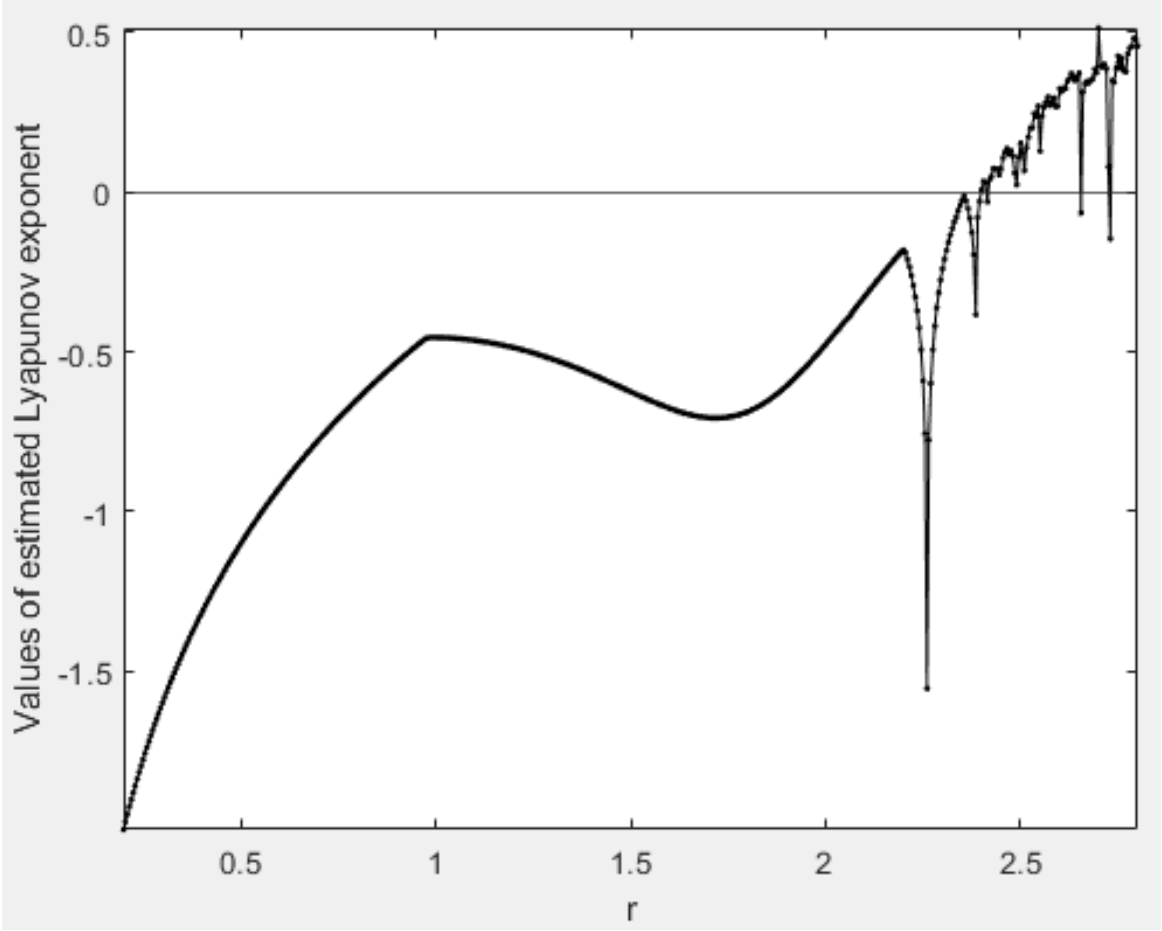

Figure 3.11: Lyapunov exponents as r is varied.

3.5 Discussion

In this section of the chapter, the dynamical behaviour of the swing equation is analysed with respect to variations in key control parameters. These parameters, such as damping, excitation amplitude, and forcing frequency, are systematically altered to examine how the system transitions through different regimes of motion from stable oscillations to complex chaotic dynamics. The investigation integrates both analytical and numerical

approaches, with a particular emphasis on perturbation techniques. The analytical framework, developed using methods such as the method of multiple scales or the Lindstedt–Poincaré technique, provides an approximate solution under the assumption of weak nonlinearity. This solution is then validated against detailed numerical simulations, especially under conditions of primary resonance, where the external forcing frequency is close to the system's natural frequency.

Numerical simulations serve as a critical tool for uncovering the rich and often unpredictable behaviour of nonlinear systems. Among the most notable features observed is the onset of period-doubling bifurcations, which act as a prelude to chaos. The appearance of the first period-doubling event is particularly significant, it marks the beginning of a cascade that can ultimately result in fully developed chaotic motion. This progression is meticulously traced using a combination of diagnostic tools, including numerically constructed bifurcation diagrams, Lyapunov exponents, phase portraits, frequency domain analyses, and Poincaré maps.

Poincaré sections, in particular, provide a useful means of reducing the continuous flow of the dynamical system into a discrete map, thereby revealing underlying patterns and attractor structures that might be obscured in time-domain analysis. These visual tools confirm that the route to chaos is not always linear or singular; although period-doubling is the most commonly recognised scenario, chaos may also arise via other routes, such as intermittency or the breakdown of quasiperiodic motion on a torus.

It is especially important to identify and understand the pre-chaotic motion, those behavioural patterns that occur just before the onset of chaos as they can serve as early warning indicators of instability in practical systems. In power systems, such as those governed by the swing equation, the transition to chaotic behaviour can have serious implications, including synchronisation loss, voltage collapse, and equipment failure. Therefore, recognising the early signs of dynamic degradation is not only of theoretical interest but also of significant practical relevance.

The broader objective of this research is to enrich the existing body of knowledge surrounding the swing equation and its applications in electrical power networks. By combining analytical and numerical tools to explore the onset of chaos, this work offers a deeper understanding of the underlying nonlinear dynamics. In doing so, it provides a foundation for future studies aimed at predicting, controlling, and ultimately mitigating

chaotic phenomena in complex power systems.

3.6 Final Remarks

This section focuses on the analysis of primary resonance in the swing equation and its critical influence on the stability of the underlying dynamical system. Primary resonance occurs when the frequency of external forcing approaches the natural frequency of the system, leading to amplified oscillatory responses that can significantly impact the system's behavior. In the context of power systems, such resonant interactions can give rise to voltage fluctuations, loss of synchronism, or even widespread instability if not properly managed.

The swing equation is studied under conditions that promote primary resonance, and the resulting dynamics are investigated through both analytical and numerical techniques. Analytical methods, such as the method of multiple scales and perturbation analysis, provide approximate solutions that offer insight into the structure of resonance and the associated bifurcation patterns. These are supplemented by numerical simulations, which not only validate the analytical predictions but also allow for the observation of complex phenomena such as limit cycles, quasiperiodic motion, and the transition to chaos, which may not be easily captured by closed-form expressions.

A key focus of this analysis lies in exploring how variations in key system parameters, such as damping, forcing amplitude, and excitation frequency, affect the onset and progression of resonance. It is observed that even slight modifications in these parameters can lead the system into regimes of nonlinear instability and chaotic behavior. The emergence of chaos through primary resonance pathways underscores the sensitive dependence of the system on initial conditions and parameter tuning.

Given the importance of maintaining stability in electrical power grids and interconnected networks, it is imperative to prioritise the study of primary resonance and its dynamic consequences. By identifying the thresholds and critical values that lead to instability, system operators and engineers can develop robust control strategies to mitigate potential failures. Thus, the analysis presented in this section contributes not only to a theoretical understanding of nonlinear dynamics in the swing equation but also to the practical goal of enhancing the resilience and reliability of modern power systems.

Chapter 4

Understanding the Subharmonic Resonance

4.1 Introduction

The swing equation is a basic model that can be explored for the purpose of studying the dynamic behaviour of power systems, specifically the oscillatory motion of synchronous generators. It is vital to have an understanding of the resonance phenomena that can take place in this nonlinear system in order to maintain the dependability and stability of power infrastructures. Within the context of the swing equation, two key types of resonance that are experienced are primary resonance and subharmonic resonance. As a means of providing an explanation for the subharmonic resonance, this section is an expansion of previous chapter, Chapter 3 [77], and builds on the results that were reached in that work.

When it comes to determining the stability of a dynamical system, primary and subharmonic resonances are extremely important factors to consider. There is a close connection between the concept of stability in a power system and the idea of disturbances, which are characterised by sudden changes to the quantities that are being used by the system. Even a relatively slight disturbance can have a rich effect on the dynamics of a system [77]. The dynamical behaviour of this system can be examined by modifying the variables in the equation while maintaining the status quo for the other parameters. During the process of studying the swing equation, the fundamental resonance is regarded

to be a significant resonance. When the criteria of primary resonance are met, a relatively small-amplitude excitation can potentially result in a relatively large-amplitude response if the forcing frequency is reasonably close to the linearised natural frequency, as stated in [78]. Furthermore, it is possible that nonlinear dynamic behaviours, such as saddle-node bifurcations, could be experienced in the steady-state forced response of the nonlinear system, as stated in the reference [58].

When the frequency of the excitation is somewhat near to the frequency that the system naturally produces, a phenomena that is known as primary resonance takes place. The subharmonic resonance takes place when the frequency of the excitation is expressed as a multiple of the frequency of the natural frequency [79]. This is in contrast to the natural frequency, which acts as the frequency of the excitation. Numerous studies have been conducted in order to examine the resonances that take place in nonlinear power systems, to acquire a knowledge of the underlying principles that underpin them, and to design control mechanisms that are effective enough to be implemented. As an illustration, researchers have employed mathematical modelling, simulation studies, and experimental validations in order to investigate the influence that primary and subharmonic resonance have on the stability of power systems. Other methods that have been utilised include experimental validations. Adaptive control, resilient control, and damping controllers are some of the cutting-edge control approaches that have been developed as a result of these research efforts. The purpose of these strategies is to reduce the negative impacts of resonance as much as possible while simultaneously improving the system's stability.

The stability of power systems is an essential component that plays a significant role in ensuring the reliable and efficient operation of electric circuits [80]. A power system is said to be stable when it is able to continue operating within tolerable parameters and maintain its equilibrium in spite of disturbances. It is essential to have a solid understanding of the swing equation in order to comprehend the dynamic behaviour of power systems, in addition to other stability challenges, [33]. The resonance that occurs at the primary and subharmonic levels is yet another significant factor that may have an effect on the stability of the system. There are two primary varieties of power system stability, which are known as transient stability and steady-state stability alike. Transient stability is the capability of the system to recover to a stable operating point after a severe disruption, such as a fault or a sudden loss load, [81]. This capacity ensures that

the system is able to continue functioning normally. One of the topics that is discussed in steady-state stability, which is often referred to as small-signal stability, is the capacity of the system to maintain its stability in the face of little disturbances, such as minute shifts in the amount of power that is required or generated [82].

The swing equation is an important dynamic equation that mimics the behaviour of synchronous generators in a power system. It is used to simulate the behaviour of systems. With regard to synchronous machines, it provides a description of the speed dynamics and rotor angle stability that occur under transient conditions. According to the swing equation, the electrical output of a generator is inversely proportional to the angle between its rotor and the voltage at its terminal, [24]. This is the premise upon which the swing equation is founded.

It is possible for a power system to experience primary resonance when the inherent frequency of the system corresponds with the frequency of an external disturbance that is administered. It is a phenomenon that has the potential to lead to oscillations that are unstable and to bring about instability in the system [83]. The phenomenon of primary resonance is usually associated with low-frequency electromechanical modes of oscillation. These modes of oscillation are frequently demonstrated by the interaction between generators and the control systems that correspond to them [84]. Significant oscillations in generator rotor angles can be caused by it, and if these oscillations are not caught and corrected, they could eventually lead to cascading failures and blackouts [85]. The phenomenon known as subharmonic resonance occurs when the response of a power system exhibits oscillations at frequencies that are lower than the frequency of the external disturbance that is being applied [86]. A power system experiences this phenomenon when the inherent frequency of the system falls below the disturbance frequency. Through their interaction with the power system, power electronic components, such as voltage source converters or thyristor-controlled reactors, have the potential to induce subharmonic resonance [87]. It has the potential to cause oscillations and instability that endure for a long time if it is not minimised. The design and operation of power electronic equipment that is connected to the grid must be carried out in a manner that takes into consideration the phenomenon of subharmonic resonance [88].

When it comes to understanding the various properties of primary and subharmonic resonance, as well as the consequences that these qualities have for the stability of a power

system, it is vital to conduct a comparative examination of the two. For the purpose of conducting a comparison between the two resonance phenomena, the authors utilised both analytical and experimental methods [89] . The research conducted by them shed light on the parallels and differences that exist between primary and subharmonic resonance, hence emphasising the importance of doing a comprehensive analysis on the subject [89]. Improvements in the identification and distinction of primary and subharmonic resonance have been made possible as a result of the development of classification algorithms. It has been established that techniques for machine learning, such as neural networks and support vector machines, are capable of reliably classifying resonance types. Using a neural network-based method, the authors provided a method for the classification of resonance occurrences in real time [90]. This method enables a rapid response to crucial stability events. In their study, the researchers not only investigated the impact of control strategies on subharmonic resonance, but they also underlined the significance of taking into account variations in system parameters when assessing the dynamic behaviour of primary and subharmonic resonances [91].

The stability of the power system is an important factor in determining the reliability and effectiveness of the operation of electrical circuits and grids. The swing equation is an essential tool for analysing the dynamic behaviour of power systems, particularly when analysing the stability of the rotor angle and the dynamics of the speed. Among the many phenomena that can have an effect on the stability of a power system, resonance on the primary and subharmonic scales is a significant one [92]. Therefore, it is of utmost importance when studying the stability of a system, as discussed in [93]. It is essential to have a comprehensive understanding of these phenomena in order to conduct effective stability analysis, regulation, and precautionary actions in power systems. It is vital to conduct additional research and make significant advancements in these areas in order to guarantee the stability and resilience of energy systems in the face of grid situations and challenges that are constantly shifting.

Basins of attraction are geographic areas within the state space that are characterised by the convergence of the paths of the system to specific attractors. Over the course of this chapter, the basins of attraction that are associated with primary and subharmonic resonance in power systems have been investigated. Various methodologies, including bifurcation analysis, numerical simulations, and Lyapunov exponent calculations, have

been utilised in these research to define the limits and properties of the basins of attraction [94]. The impacts of system parameters, initial conditions, and control strategies on systems have been examined by researchers in order to gain a better understanding of the stability boundaries and robustness of power systems.

4.2 Analytical Work

4.2.1 Perturbation Analysis for Subharmonic Resonance

This method uses multiple scales to determine second order approximate expression for period-two solutions for the case $\Omega \simeq 2\omega_0$.

It is possible to use this solution to make a prediction regarding the beginning of the complex dynamics and stability. Due to the fact that the solution is unable to take into account the frequency shift that is caused by the external stimulation, the accuracy of the solution decreases as the magnitude of the excitation grows. The introduction of a minor dimensionless parameter called ε, which is utilised as a mechanism for accurate accounting.

Assume:

$$\eta = \mathcal{O}(\varepsilon) \tag{4.1}$$

Then the damping term is of the order:

$$\frac{\omega_R D}{2H} = \mathcal{O}(\varepsilon) \tag{4.2}$$

And similarly:

$$G_1 = \mathcal{O}(\varepsilon), \quad Q = \mathcal{O}(\varepsilon) \tag{4.3}$$

The excitation magnitudes are also small:

$$V_{B1} = \mathcal{O}(\varepsilon), \quad \theta_{B1} = \mathcal{O}(\varepsilon) \tag{4.4}$$

This leads to the following coefficients in the final perturbed swing equation:

$$G_1 = \varepsilon g_1 \tag{4.5}$$

$$G_2 = \varepsilon g_2 \tag{4.6}$$

$$G_3 = \varepsilon g_3 \tag{4.7}$$

$$Q = \varepsilon q \tag{4.8}$$

After applying these assumptions and simplifying, the governing equation becomes:

$$\begin{aligned}\ddot{\eta} + 2\varepsilon\mu\dot{\eta} + \omega_0^2\eta = \alpha_2\eta^2 + \alpha_3\eta^3 + \varepsilon g_1\eta\cos(\Omega t + \phi_v) \\ + \varepsilon g_2\eta^2\cos(\Omega t + \phi_v) + \varepsilon g_3\eta^3\cos(\Omega t + \phi_v) + \varepsilon q\cos(\Omega t + \phi_e)\end{aligned} \tag{4.9}$$

where

$$\mu = \frac{\omega_R D}{4H} \tag{4.10}$$

Assuming a perturbative solution of the form:

$$\eta(t;\varepsilon) = \varepsilon\eta_1(T_0, T_1, T_2) + \varepsilon^2\eta_2(T_0, T_1, T_2) + \varepsilon^3\eta_3(T_0, T_1, T_2) + \ldots \tag{4.11}$$

The first and second derivatives of the solution are expanded using the chain rule:

$$\frac{d}{dt} = D_0 + \varepsilon D_1 + \varepsilon^2 D_2 + \ldots \tag{4.12}$$

$$\frac{d^2}{dt^2} = D_0^2 + 2\varepsilon D_0 D_1 + \varepsilon^2(2D_0 D_2 + D_1^2) + \ldots \tag{4.13}$$

where:

$$D_n = \frac{\partial}{\partial T_n} \tag{4.14}$$

Also, the natural frequency is detuned using:

$$\omega_0^2 = \frac{1}{4}\Omega^2 + \varepsilon\sigma \tag{4.15}$$

Substituting equations (4.11), (4.12) and (4.13) into equation (3.29) gives,

$$\begin{aligned}\ddot{\eta} + 2\varepsilon\mu\dot{\eta} + \left(\frac{1}{4}\Omega^2 + \varepsilon\sigma\right)\left[\varepsilon\eta_1(T_0,T_1,T_2) + \varepsilon^2\eta_2(T_0,T_1,T_2) + \varepsilon^3\eta_3(T_0,T_1,T_2) + \cdots\right] = \\ \alpha_2\left(\varepsilon^2\eta_1^2 + \varepsilon^4\eta_2^2 + \varepsilon^6\eta_3^2 + \cdots\right) + \alpha_3\left(\varepsilon^3\eta_1^3 + \varepsilon^6\eta_2^3 + \varepsilon^9\eta_3^3 + \cdots\right) \\ + \varepsilon g_1\left(\varepsilon\eta_1 + \varepsilon^2\eta_2 + \varepsilon^3\eta_3\right)\cos\left(\Omega t + \phi_v\right) \\ + \varepsilon g_2\left(\varepsilon^2\eta_1^2 + \varepsilon^4\eta_2^2 + \varepsilon^6\eta_3^2\right)\cos\left(\Omega t + \phi_v\right) \\ + \varepsilon g_3\left(\varepsilon^3\eta_1^3 + \varepsilon^6\eta_2^3 + \varepsilon^9\eta_3^3 + \cdots\right)\cos\left(\Omega t + \phi_v\right) + \varepsilon q\cos\left(\Omega t + \phi_e\right)\end{aligned} \tag{4.16}$$

Substituting these into the main equation and collecting like powers of ε, the following is obtained:

at order ε:

$$D_0^2\eta_1 + \frac{1}{4}\Omega^2\eta_1 = q\cos(\Omega t + \phi_e) \tag{4.17}$$

at order ε^2:

$$D_0^2\eta_2 + \frac{1}{4}\Omega^2\eta_2 + 2D_0D_1\eta_1 + \sigma\eta_1 = \alpha_2\eta_1^2 + g_1\eta_1\cos(\Omega T_0 + \phi_v) \tag{4.18}$$

at order ε^3:

$$\begin{aligned}D_0^2\eta_3 + 2D_0D_1\eta_2 + (D_1^2 + 2D_0D_2)\eta_1 + 2\mu D_0\eta_1 + \frac{1}{4}\Omega^2\eta_3 + \sigma\eta_2 = \\ 2\alpha_2\eta_1\eta_2 + \alpha_3\eta_1^3 + g_1\eta_2\cos(\Omega T_0 + \phi_v) + g_2\eta_1^2\cos(\Omega T_0 + \phi_v)\end{aligned} \tag{4.19}$$

Solving equation (4.17), it admits the following general form:

$$\eta_1 = a(T_0,T_1,T_2)\cos\left(\frac{1}{2}\Omega T_0 + \beta(T_0,T_1,T_2)\right) + 2N\cos(\Omega T_0 + \phi_e) \tag{4.20}$$

or equivalently in exponential form:

$$\eta_1 = A(T_1,T_2)e^{\frac{1}{2}i\Omega T_0} + \bar{A}(T_1,T_2)e^{-\frac{1}{2}i\Omega T_0} + Ne^{i\Omega T_0} + \bar{N}e^{-i\Omega T_0} \tag{4.21}$$

where $\bar{A}$ is the complex conjugate of A and :

$$N = \frac{-2q}{3\Omega^2} e^{i\phi_e} \tag{4.22}$$

Comparing the coefficients in equations (4.20) and (4.21)

$$A = \frac{1}{2} a e^{i\beta} \tag{4.23}$$

Substituting equation (4.21) into equation (4.18) gives,

$$\begin{aligned} D_0^2\eta_2 + \frac{1}{4}\Omega^2\eta_2 = &-2\mu D_0 \left(Ae^{\frac{1}{2}i\Omega T_0} + \bar{A}e^{-\frac{1}{2}i\Omega T_0} + Ne^{i\Omega T_0} + \bar{N}e^{-i\Omega T_0}\right) \\ &- 2D_0D_1 \left(Ae^{\frac{1}{2}i\Omega T_0} + \bar{A}e^{-\frac{1}{2}i\Omega T_0} + Ne^{i\Omega T_0} + \bar{N}e^{-i\Omega T_0}\right) \\ &- \sigma \left(Ae^{\frac{1}{2}i\Omega T_0} + \bar{A}e^{-\frac{1}{2}i\Omega T_0} + Ne^{i\Omega T_0} + \bar{N}e^{-i\Omega T_0}\right) \\ &+ \alpha_2 \left(Ae^{\frac{1}{2}i\Omega T_0} + \bar{A}e^{-\frac{1}{2}i\Omega T_0} + Ne^{i\Omega T_0} + \bar{N}e^{-i\Omega T_0}\right)^2 \\ &+ g_1 \cos(\Omega T_0 + \phi_v) \left(Ae^{\frac{1}{2}i\Omega T_0} + \bar{A}e^{-\frac{1}{2}i\Omega T_0} + Ne^{i\Omega T_0} + \bar{N}e^{-i\Omega T_0}\right) \end{aligned} \tag{4.24}$$

Rearranging the terms,

$$\begin{aligned} D_0^2\eta_2 + \frac{1}{4}\Omega^2\eta_2 = &\, e^{\frac{1}{2}i\Omega T_0} \left[-\sigma A + 2\alpha_2 N\bar{A} - \Omega i(D_1A + \mu A) + \frac{1}{2}g_1\bar{A}e^{i\phi_v}\right] \\ &+ e^{i\Omega T_0}\left[-\sigma N + \alpha_2 A^2 - 2i\mu\Omega N\right] + e^{\frac{3}{2}i\Omega T_0}\left[\frac{1}{2}Af_1e^{i\phi_v}\right] + e^{2i\Omega T_0}\left[\alpha_2 N_2 + 12g_1Ne^{i\phi_v}\right] \\ &+ \left[\alpha_2(A\bar{A} + N\bar{N}) + 12Ng_1e^{i\phi_v}\right] + cc \end{aligned} \tag{4.25}$$

where cc is the complex conjugate.

Eliminating the secular terms,

$$-i\Omega D_1A - i\Omega\mu A - \sigma A + \bar{A}\Gamma e^{i\phi_{ee}} = 0 \tag{4.26}$$

where:

$$\Gamma e^{i\phi_{ee}} = 2\alpha_2 N + \frac{1}{2}g_1e^{i\phi_v} \tag{4.27}$$

The solution of equation (4.25) is of the form,

$$\eta_2 = \frac{-4}{3\Omega^2}\left[\alpha_2 A^2 - (2i\mu\Omega + \sigma)N\right] e^{i\Omega T_0} - \frac{A}{2\Omega^2}\Gamma e^{i\left(\frac{3}{2}\Omega T_0 + \phi_{ee}\right)} + \frac{4}{\Omega^2}\left[\alpha_2(A\bar{A} + N\bar{N}) + 12 g_1 N e^{i\phi_v}\right] - \frac{4}{15\Omega^2}\left[\alpha_2 N^2 + 12 g_1 N e^{i\phi_v}\right] e^{i2\Omega T_0} + \bar{c} \quad (4.28)$$

where $\bar{c}$ is the complex conjugate.

Substituting equations (4.21) and (4.28) into equation (4.19):

$$D_0^2\eta_3 + \frac{1}{4}\Omega^2\eta_3 = -i\Omega D_2 A - D_1^2 A - 2\mu D_1 A - \frac{-8\alpha_2}{3\Omega^2}\left[-(2i\mu\Omega + \sigma)N\bar{A} + \alpha_2 A^2\bar{A}\right] - \frac{\alpha_2 A\bar{\Lambda}}{\Omega^2}\Gamma e^{i\phi_{ee}} + \frac{8\alpha_2}{\Omega^2}\left[2\alpha_2 A^2\bar{A} + 2\alpha_2 A N\bar{N} + \frac{1}{2}g_1 A(\bar{N}e^{i\phi_v} + N e^{-i\phi_v})\right] + 6\alpha_3 A N\bar{N} + 3\alpha_3 A^2\bar{A} - \frac{A_1 g_1\Gamma}{4\Omega^2}e^{i(\phi_{ee}-\phi_v)} + g_2 A(\bar{N}e^{i\phi_v} + N e^{-i\phi_v}) + \mathrm{NST} + \bar{c} \quad (4.29)$$

where NST denotes non significant terms.

Now, we define,

$$D_1 A = -\left(\mu + \frac{i\sigma}{\Omega}\right)\bar{A} + \frac{i}{\Omega}\bar{A}\Gamma e^{i\phi_{ee}} \quad (4.30)$$

$$D_1^2 A = \left(\mu^2 - \frac{2i\mu\sigma}{\Omega} + \frac{\Gamma^2 - \sigma^2}{\Omega^2}\right)A + \frac{2i\mu}{\Omega}\bar{A}\Gamma e^{i\phi_{ee}} \quad (4.31)$$

Eliminating the secular terms in equation (4.29), and substituting equations (4.26) and (4.31),

$$-i\Omega D_2 A + \left[\mu^2 - \frac{\Gamma^2 - \sigma^2}{\Omega^2} - \frac{\alpha_2\bar{N}\Gamma}{\Omega^2}e^{i\phi_{ee}} + \left(6\alpha_3 + \frac{16\alpha_2^2}{\Omega^2}\right)N\bar{N} + (\bar{N}e^{i\phi_v} + N e^{-i\phi_v})\left(\frac{4\alpha_2 f_1}{\Omega^2} + f_2\right) - \frac{\Gamma f_1}{4\Omega^2}e^{i(\phi_{ee}-\phi_v)}\right]A + \left(3\alpha_3 + \frac{40\alpha_2^2}{3\Omega^2}\right)A^2\bar{A} + \frac{8\alpha_2}{3\Omega^2}(2i\mu\Omega + \sigma)N\bar{A} = 0 \quad (4.32)$$

Using method of reconstitution, the derivative of A with respect to t is found and substituting equation (4.26) and (4.32) into (4.12), setting $\varepsilon = 1$, we get,

$$i\Omega(A' + \mu_e A) + \sigma_e A - 4\alpha_e A^2 \bar{A} - \hat{\Gamma} e^{i\hat{\phi}_e} = 0 \tag{4.33}$$

where,

$$\mu_e = \mu - \frac{2\alpha_2 q\Gamma}{3\Omega^5}\sin(\phi_{ee} - \phi_e) + \frac{\Gamma g_1}{4\Omega^3}\sin(\phi_{ee} - \phi_v) \tag{4.34}$$

$$\begin{aligned}\sigma_e = \sigma - \mu^2 + \frac{\Gamma^2 - \sigma^2}{\Omega^2} - \left(\frac{2q}{3\Omega^2}\right)^2 \left(6\alpha_3 + \frac{16\alpha_2^2}{\Omega^2}\right) \\ + \frac{4q}{3\Omega^2}\left(g_2 + \frac{4\alpha_2 g_1}{\Omega^2}\right)\cos(\phi_v - \phi_e) - \frac{2q\Gamma\alpha_2}{3\Omega^4}\cos(\phi_{ee} - \phi_e) + \frac{\Gamma g_1}{4\Omega^2}\cos(\phi_{ee} - \phi_v)\end{aligned} \tag{4.35}$$

$$\alpha_e = \frac{10\alpha_2^2}{3\Omega^2} + \frac{3}{4}\alpha_3 \tag{4.36}$$

$$\hat{\Gamma} e^{i\hat{\phi}_e} = \Gamma e^{i\phi_{ee}} - \frac{16\alpha_2 q}{9\Omega^4}(2i\mu\Omega + \sigma)e^{i\phi_e} \tag{4.37}$$

Separating into real and imaginary parts gives,

$$\Omega(a' + \mu_e a) - a\hat{\Gamma}\sin\gamma = 0 \tag{4.38}$$

$$-\Omega a\beta' + \sigma_e a - \alpha_e a^3 - a\hat{\Gamma}\cos\gamma = 0 \tag{4.39}$$

$$\gamma = \hat{\phi}_e - 2\beta \tag{4.40}$$

Therefore,

$$\eta = a\cos\left(\frac{1}{2}\Omega t + \hat{\phi}_e - \beta\right) - \frac{4q}{3\Omega^2}\cos(\Omega t + \phi_e) + \frac{32\mu q^2}{9\Omega^3}\sin(\Omega t + \phi_e) - \frac{16\sigma q}{9\Omega^4}\cos(\Omega t + \phi_e) - \frac{2a^2\alpha_2}{3\Omega^2}\cos(\Omega t + \hat{\phi}_e - \gamma) - \frac{32\alpha_2 q}{135\Omega^6}\cos[2(\Omega t + \phi_e)] - \frac{ag_1}{4\Omega^2}\cos\left(\frac{3}{2}\Omega t + \phi_v + \frac{1}{2}(\phi_e - \gamma)\right) + \frac{2\alpha_2}{\Omega^2}\left(a^2 + \frac{16q^2}{9\Omega^4}\right) - \frac{8g_1 q}{3\Omega^4}\cos(\phi_v - \phi_e) + \frac{2\alpha_2 aq}{3\Omega^4}\cos\left(\frac{3}{2}\Omega t + \phi_e + \frac{1}{2}(\hat{\phi}_e - \gamma)\right) + \frac{8g_1 q}{45\Omega^4}\cos(2\Omega t + \phi_e + \phi_v) + \ldots \quad (4.41)$$

Similarly, the swing angle is,

$$\Delta\theta = \theta_{B1}\cos(\Omega t + \phi_\theta) + a\cos\left(\frac{1}{2}\Omega t + \hat{\phi}_e - \beta\right) - \frac{4q}{3\Omega^2}\cos(\Omega t + \phi_e) + \frac{32\mu q}{9\Omega^3}\sin(\Omega t + \phi_e) - \frac{16\sigma q}{9\Omega^4}\cos(\Omega t + \phi_e) - \frac{2a^2\alpha_2}{3\Omega^2}\cos(\Omega t + \hat{\phi}_e - \gamma) + \frac{2\alpha_2 aq}{3\Omega^4}\cos\left(\frac{3}{2}\Omega t + \hat{\phi}_e + \frac{1}{2}(\phi_e - \gamma)\right) - \frac{ag_1}{4\Omega^2}\cos\left(\frac{3}{2}\Omega t + \phi_v + \frac{1}{2}(\phi_e - \gamma)\right) + \frac{2\alpha_2}{\Omega^2}\left(a^2 + \frac{16q^2}{9\Omega^4}\right) + \frac{8g_1 q}{3\Omega^4}\cos(\phi_v - \phi_e) + \frac{32\alpha_2 q^2}{135\Omega^6}\cos[2(\Omega t + \phi_e)] + \frac{8g_1 q}{45\Omega^4}\cos(2\Omega t + \phi_e + \phi_v) + \ldots \quad (4.42)$$

Letting $a' = \beta' = 0$ in equation (4.38), (4.39), (4.40) gives,

$$\Omega\mu_e a - \hat{\Gamma} a\sin\gamma = 0 \quad (4.43)$$

$$\sigma_e a - \alpha_e a^3 + \hat{\Gamma} a\cos\gamma = 0 \quad (4.44)$$

when $a = 0$, then:

$$\Delta\theta = \theta_{B1}\cos(\Omega t + \phi_\theta) - \frac{4q}{3\Omega^2}\cos(\Omega t + \phi_e) + \frac{32\mu q}{9\Omega^3}\sin(\Omega t + \phi_e) - \frac{16\sigma q}{9\Omega^4}\cos(\Omega t + \phi_e) + \frac{32\alpha_2 q^2}{9\Omega^6} - \frac{8g_1 q}{3\Omega^4}\cos(\phi_v - \phi_e) + \frac{32\alpha_2 q^2}{135\Omega^6}\cos[2(\Omega t + \phi_e)] + \frac{8g_1 q}{45\Omega^4}\cos(2\Omega t + \phi_e + \phi_v) \quad (4.45)$$

Which is similarly echoed in [33].

When $a \neq 0$, eliminating γ gives the frequency response equation,

$$a^2 = \frac{1}{\alpha_e}\left[\sigma_e \pm \sqrt{\hat{\Gamma}^2 - \Omega^2\mu_e^2}\right] \tag{4.46}$$

Taking into consideration equation (4.46), which presents both the numerical simulation and the perturbation solution, the frequency response plot may be derived.

The accompanying figures, Figure 4.1 and Figure 4.2, display time histories and phase portraits for the case when the excitation frequency is set to $\Omega = 26.01$ rad $\cdot$ s^{-1}. This specific value of Ω was selected because it corresponds to a subharmonic resonance condition. More precisely, it is approximately twice the natural frequency of the system, which leads to a one-half subharmonic resonance. Under such conditions, the system is particularly sensitive to perturbations, and nonlinear interactions become prominent. This makes it an ideal scenario to compare analytical predictions with numerical simulations, as the effects of subharmonic excitation are clearly observable in both the time-domain and phase-space behaviours. The use of this excitation frequency enables a thorough validation of the perturbation methods employed and highlights the resonance-induced instabilities present in the system.

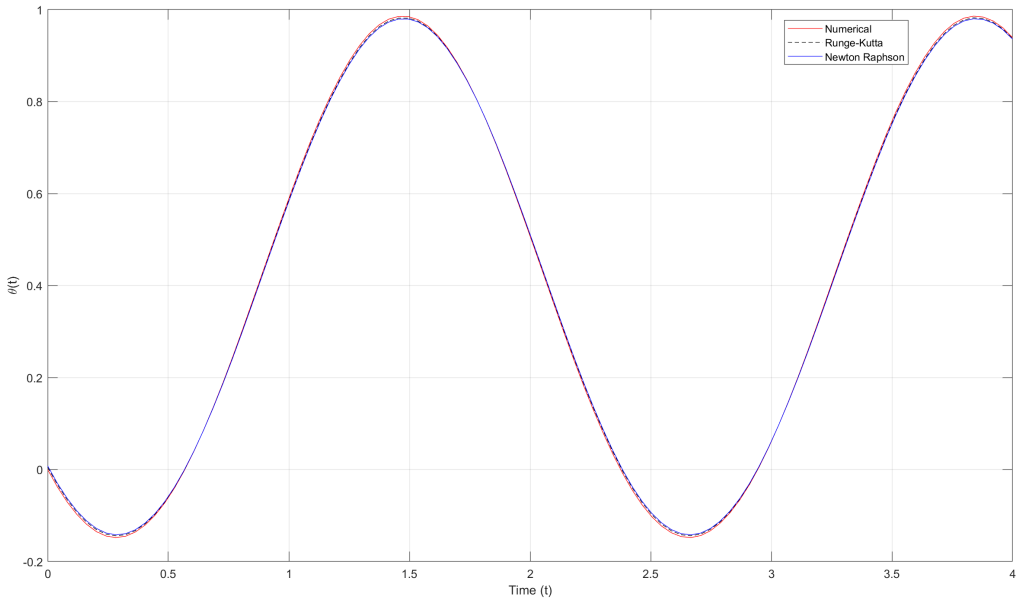

Figure 4.1: Perturbed solution employing Runge-Kutta and Newton Raphson algorithms in comparison to numerical simulations for the case of subahrmonic resonance in time history for $\Omega = 26.01$ rads^{-1}.

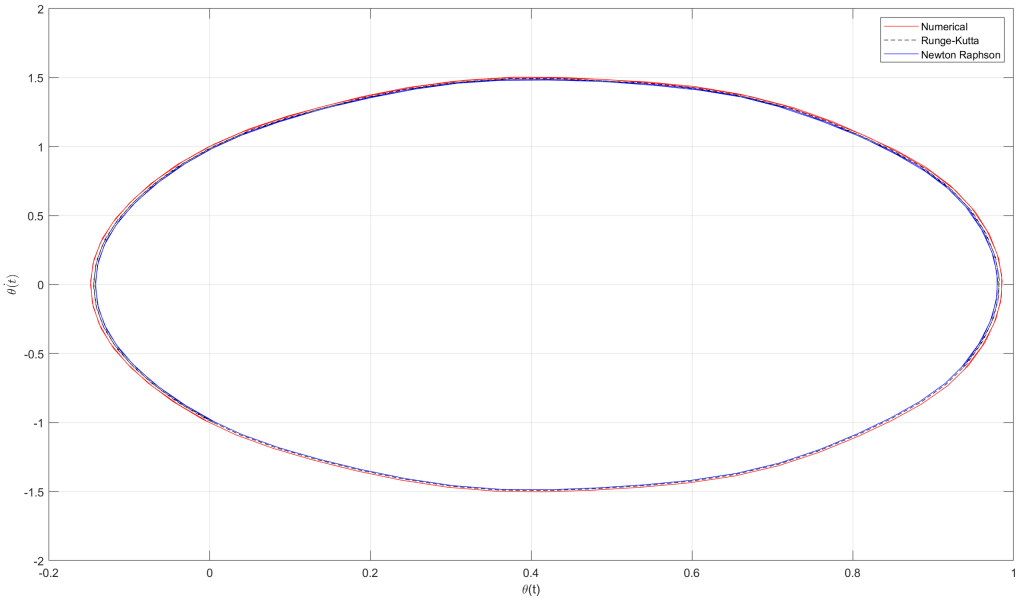

Figure 4.2: Perturbed solution employing Runge-Kutta and Newton Raphson algorithms in comparison to numerical simulations for the case of subhamonic resonance in phase plane for $\Omega = 26.01$ rads^{-1}.

Simulating the perturbation analysis and comparing it to its numerical counterpart was achieved using both the Runge-Kutta and Newton-Raphson numerical methods. Upon evaluation, it was found that the Newton-Raphson method yields a more accurate approximation of the numerical solution. Specifically, for the subharmonic resonance case, the computed numerical errors for the Runge-Kutta and Newton-Raphson methods were 0.0995 and 0.0419, respectively. This indicates that the Newton-Raphson method provides a superior fit to the data due to its lower error value.

This finding is consistent with earlier results obtained for the case of primary resonance, where a similar trend was observed: the Newton-Raphson method produced a closer match to the analytical solution compared to Runge-Kutta. The enhanced accuracy of the Newton-Raphson approach can be attributed to its iterative root-finding nature, which is particularly effective in refining steady-state solutions obtained from nonlinear algebraic equations derived via perturbation techniques. By contrast, the Runge-Kutta method, while reliable for time-domain simulations, is more sensitive to step size and numerical damping, which may affect its accuracy when matching long-term or steady-state behaviours. Hence, the consistent performance of the Newton-Raphson method across both resonance scenarios reinforces its suitability for validating perturbative analytical results in nonlinear dynamic systems.

4.3 Numerical Analysis

4.3.1 Graphical Representation

Using the fourth-order Runge-Kutta method in Matlab, the equations (3.10), (3.11), and (3.12) were set and solved for the parameters given in the Appendix. The primary focus of the analysis was on the effect of altering the excitation frequency Ω for the subharmonic resonance.

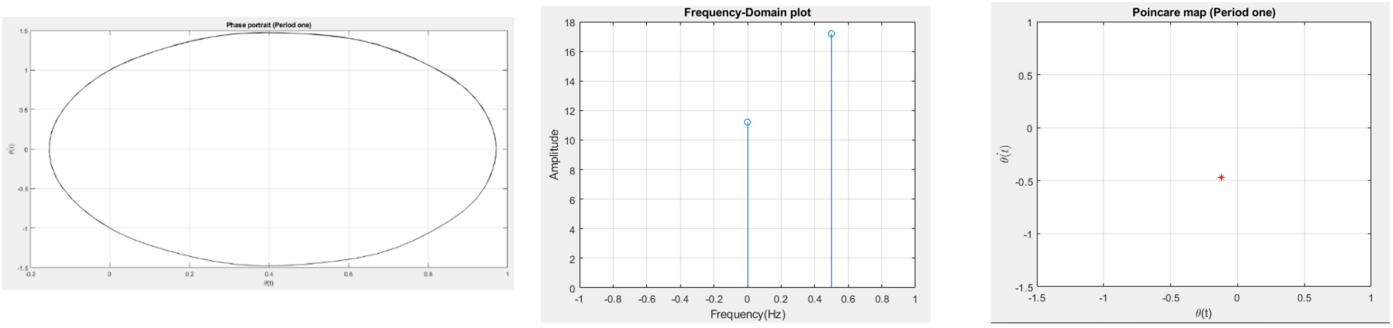

Figure 4.3: Phase portrait, frequency-domain plot and Poincaré map when $\Omega = 26.01$ rads^{-1}.

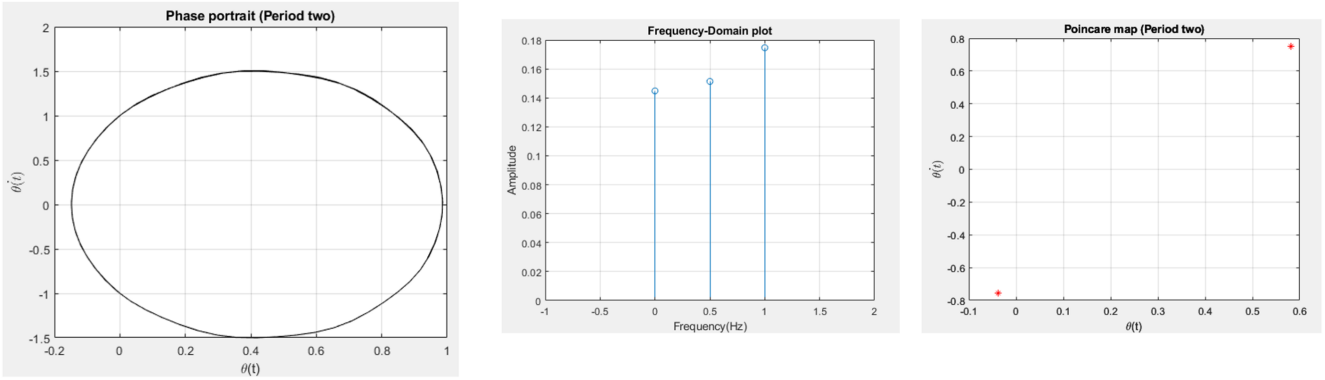

Figure 4.4: Phase portrait, frequency-domain plot and Poincaré map when $\Omega = 21.042$ rads^{-1}.

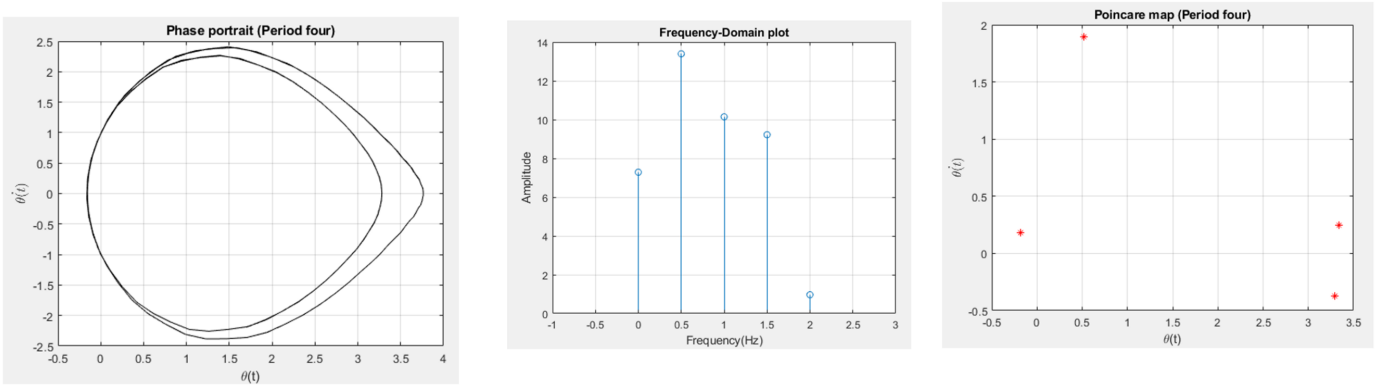

Figure 4.5: Phase portrait, frequency-domain plot and Poincaré map when $\Omega = 19.4162$ rads^{-1}.

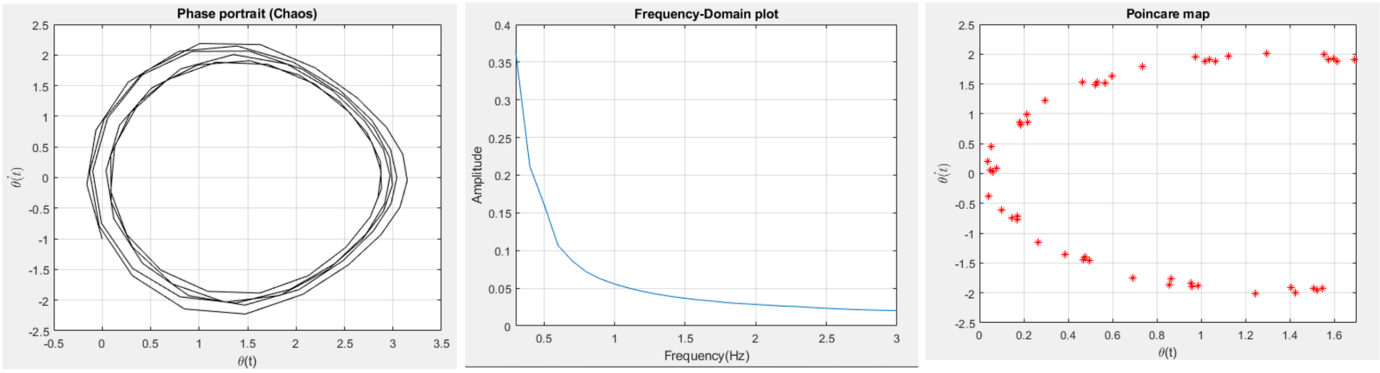

Figure 4.6: Phase portrait, frequency-domain plot and Poincaré map when $\Omega = 19.375$ rads^{-1}.

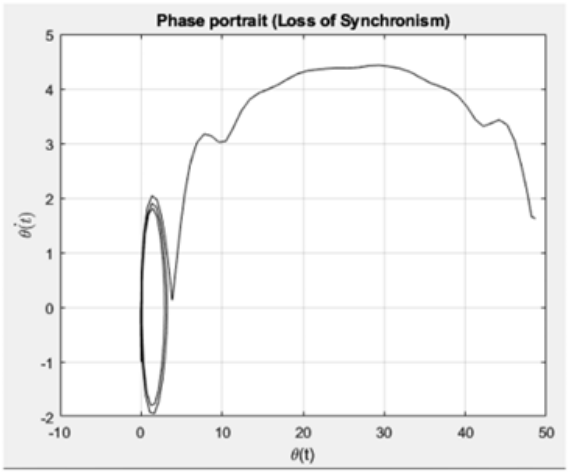

Figure 4.7: Phase portrait (loss of synchronism) when $\Omega = 19.37251$ rads^{-1}.

Figures 4.3, 4.4, 4.5, 4.6, and 4.7 were generated by plotting the phase portraits, frequency-domain plots, and Poincaré maps for various excitation frequencies applied to the swing equation (3.10). These visualisations illustrate how the system's dynamics evolve as the excitation frequency Ω is progressively decreased. As Ω is reduced, the system begins to lose its stability and transitions through a sequence of period doubling bifurcations before ultimately entering a chaotic regime. Each figure captures key dynamical features, including time-doubling phenomena and the gradual loss of synchronism.

The excitation frequencies used in this analysis were carefully selected to explore the onset and progression of subharmonic resonance in the system. These values are situated near resonance conditions, where nonlinear effects become significant and are most easily observable. In particular, Figure 4.3 illustrates the system response at a relatively high

excitation frequency, $\Omega = 26.01$ rad $\cdot$ s^{-1}, where the dynamics are stable and periodic. At this frequency, the phase portrait reveals a closed trajectory corresponding to a period-one attractor. This periodic behaviour is further confirmed by the frequency-domain plot, which shows a dominant single frequency, and by the Poincaré map, which displays a single fixed point.

In addition, as shown in Figure 4.4, the period-one orbit undergoes deformation until the value of Ω reaches 21.042 rads^{-1}. At this point, the period-one attractor loses its stability and is replaced by a period-two attractor. The occurrence of the period doubling bifurcation is demonstrated by the frequency-domain plot as well as the Poincaré map illustration. When the value of Ω is reduced even further to 19.4162 rads^{-1}, the phase picture depicts an attractor that consists of two loops.

In the process of decreasing the value of Ω, it is possible to see that the graphs experience dynamical transformations, which may include period-doubling solutions. Eventually, as the value of Ω is dropped to a greater extent, around 19.375 rads^{-1}, a chaotic attractor is displayed, as demonstrated in Figure 4.6. On the other hand, when the value of Ω is reduced to 19.37251 rads^{-1}, the system loses its synchronism, as depicted in Figure 4.7.

In order to produce the bifurcation diagram depicted in Figure 4.8, the swing equation was numerically solved for a specific excitation frequency of $\Omega = 19.416$ rad s^{-1}. The numerical solution was obtained using the classical fourth-order Runge-Kutta method, a widely accepted technique for time integration in nonlinear dynamical systems. This method was chosen due to its accuracy and stability when handling stiff or oscillatory systems such as the swing equation. The bifurcation diagram was constructed by recording the maximum amplitude of the oscillatory response over time for each value of the forcing parameter r as shown in equation (3.65). To achieve this, the value of r was progressively increased, and for each increment, the system was integrated forward in time to ensure that transient effects were excluded and steady-state dynamics were captured [1].

This process allowed for the identification of critical transitions in the system's behaviour, such as period-doubling bifurcations and the onset of chaos. By plotting the maximum amplitude against the corresponding r values, the bifurcation structure of the system became evident, revealing regions of stability, periodicity, and chaos. This visual representation provides key insights into the sensitivity of the system to parameter

variations and serves as a powerful tool for analysing nonlinear oscillatory dynamics. The detailed structure visible in the bifurcation diagram validates the use of time-domain simulations in exploring the system's response under subharmonic resonance conditions, reinforcing the findings presented in earlier sections.

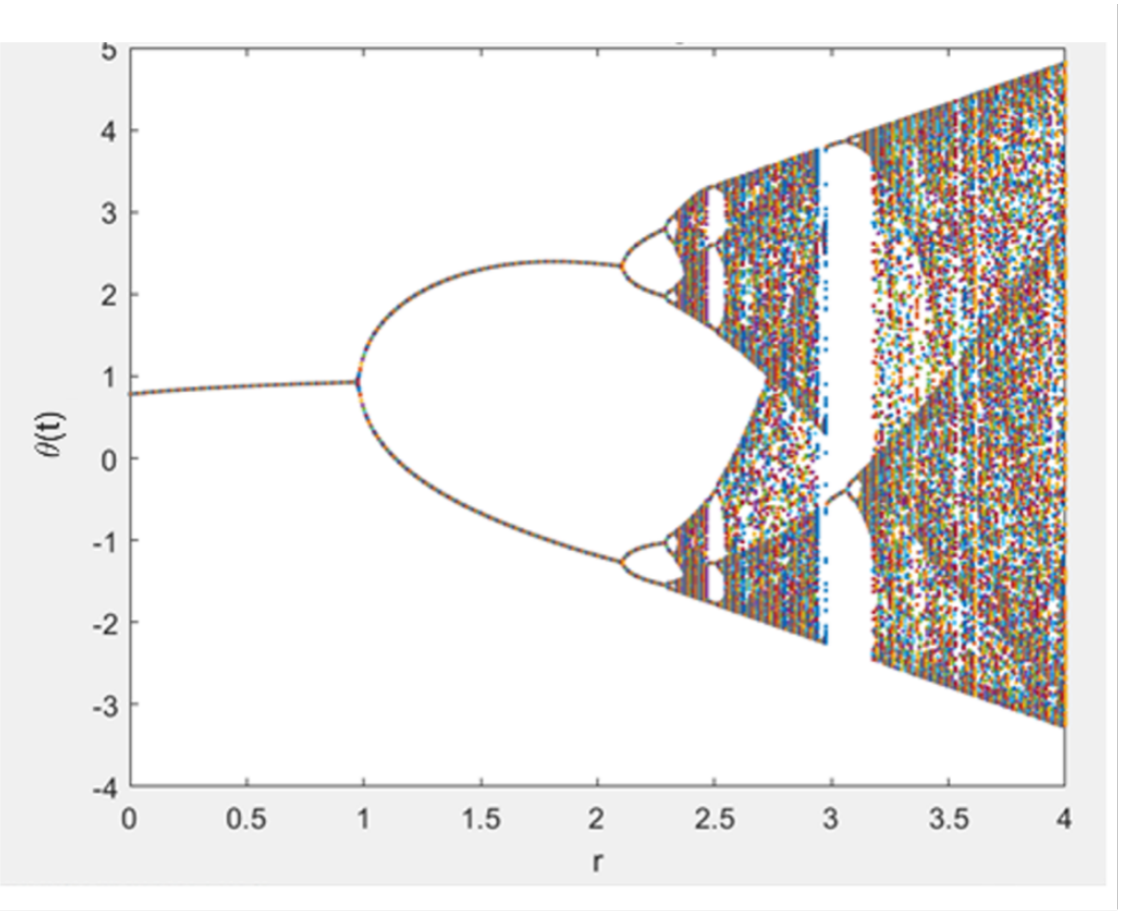

Figure 4.8: Bifurcation diagram when r value is varied and constant $\Omega = 19.4162$ rads^{-1}.

Figure 4.8 depicts the initial period doubling that takes place soon before r = 0.975. This is further supported by the Poincaré's maps shown in Figure 4.9. Additionally, at about r approximately 2.1, the first period doubling in a series of period doubles is displayed, which results in chaotic behaviour.

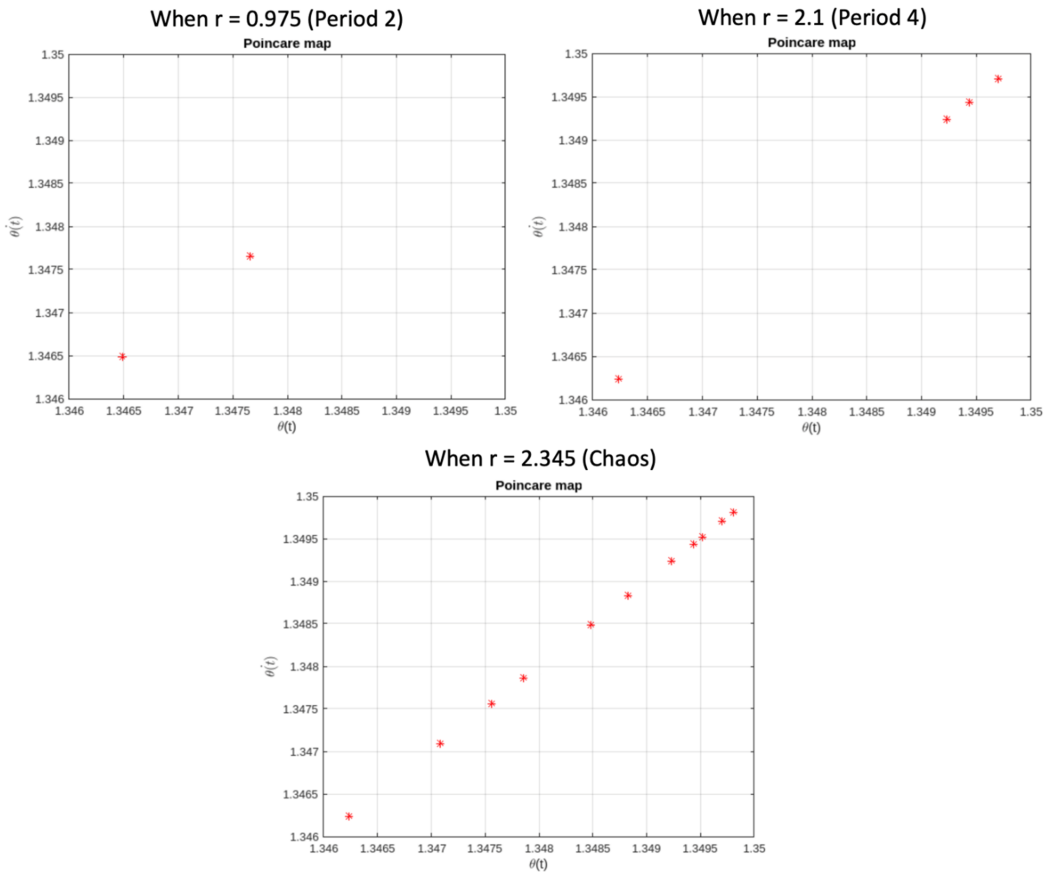

Figure 4.9: Poincaré maps for the different r values.

The results of this numerical analysis demonstrate that as the value of r is increased, the swing equation gets closer and closer to losing its synchronisation function. As can be seen in Figure 4.9, the Poincaré maps that correspond to the coordinates are shown. They provide a clear illustration of the sites at which period doubling takes place, as well as the manner in which the phenomena of chaos is confirmed when r is increased.

When the subharmonic resonance is taken into consideration, it is noted that the chaotic zone has begun at roughly $r > 2.1$. This is the region in which the Lyapunov exponent typically takes on positive values. This behaviour is visualised and displayed in Figure 4.10, which illustrates the situation in which two nearby points, which were initially separated by an infinitesimal distance, normally drift from each other over time. The Lyapunov exponents are used to statistically measure this behaviour. In addition, this behaviour is confirmed by the bifurcation diagram shown in Figure 4.8. This diagram shows that the cascade of period doubling sequence leads to chaos at nearly the same

value of r . This chaos is sufficiently severe that it is sufficient to assert that a chaotic attractor can be characterised by a positive Lyapunov exponent. The Poincaré maps, which are displayed in Figure 4.9, provide additional validation for this assertion.

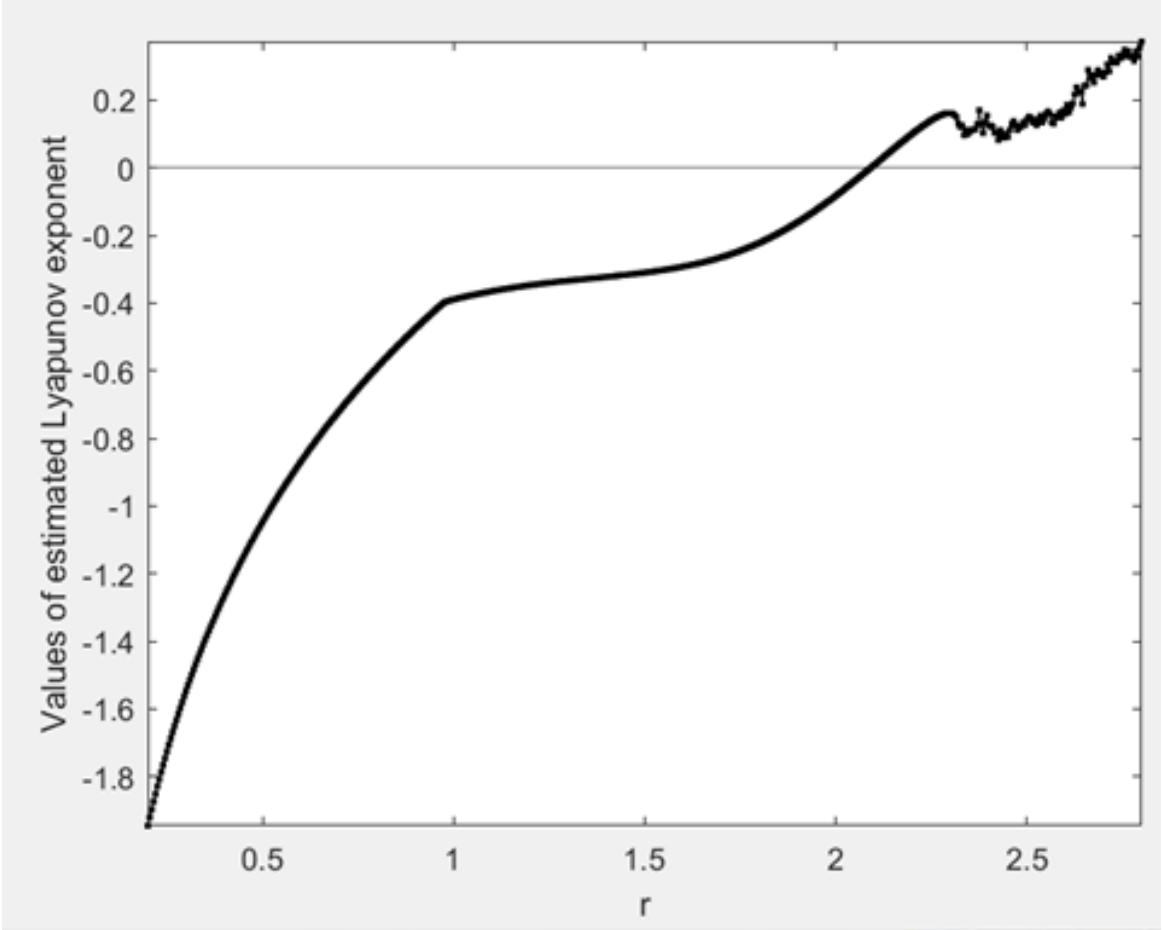

Figure 4.10: Lyapunov exponents as r is varied.

A comparison is made between the analytical solution and the numerical simulation, and the frequency domain plot for equation (4.46) is plotted as shown in Figure 4.11 below. This is done in order to determine whether or not the analytical solution is correct. It is clear from this that the two analyses that were carried out on the swing equation for the subharmonic resonance are in complete agreement with one another. As a result, the analysis that was investigated in this work is validated.

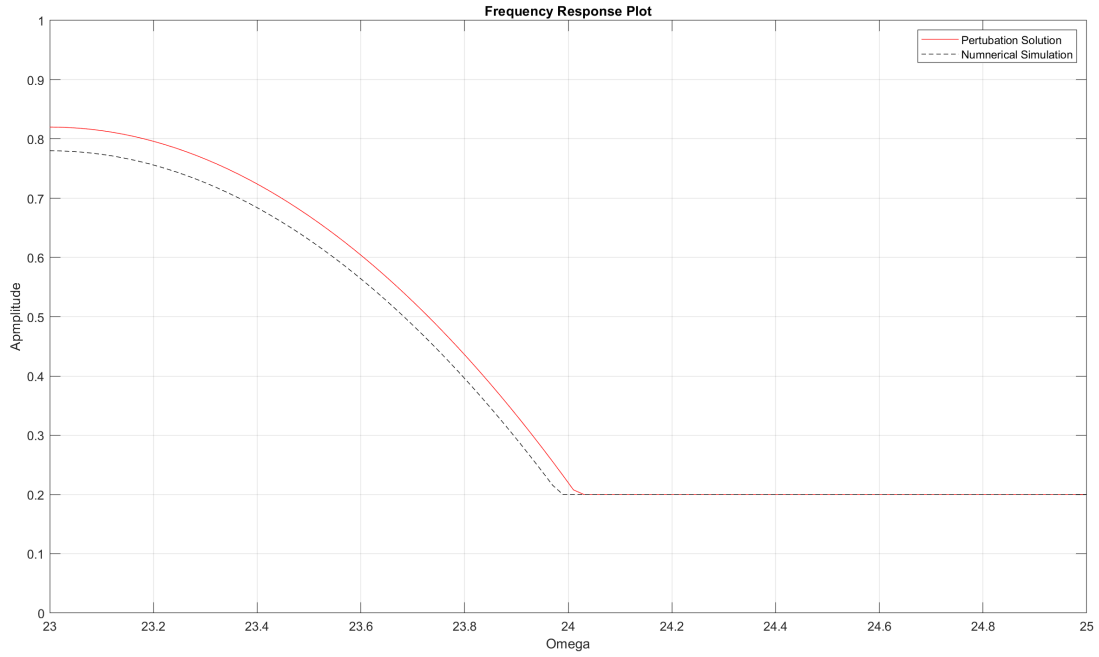

Figure 4.11: Frequency domain plot for subharmonic resonance.

4.4 Comparison of Basins of Attractions for Primary and Subharmonic Resonances

4.4.1 Primary Resonance

This resonance plays a vital role in understanding the stability of a nonlinear system. Hence it is important to study the basins of attraction of the primary resonance to obtain more in-depth information about the system. Basins of attraction shows the stable and unstable regions and helps to analyse the changes made to the system [95]. Plots show the changes in the basins of attraction when variables are altered. It is also necessary to consider boundary conditions when analysing these graphs when arriving at conclusions, [96].

Important insights into the stability behaviour of power systems have been uncovered by studies of the basins of attraction of primary resonance. The effect of parameter variations, including system damping, excitation levels, and control gains, on the shape

and magnitude of the basins of attraction associated with primary resonance has been studied, [97], [98]. In addition, research efforts have concentrated on identifying the critical boundaries separating stable and unstable regions in the state space, [99].

The figures below, Figure 4.12 and Figure 4.13, show the basins of attractions for the primary resonance when the variable V_{B1} is varied whilst Ω= 19.375 rads^{-1}. As the variable is increased the stability of the system changes. The red and green colour show the stable region and the other colours represent the unstable regions of the system. As the variable is increased the system enters a corrupt state with unstable regions, hence a further analysis on the affect of other variables in the system should be considered for sound results in this chapter.

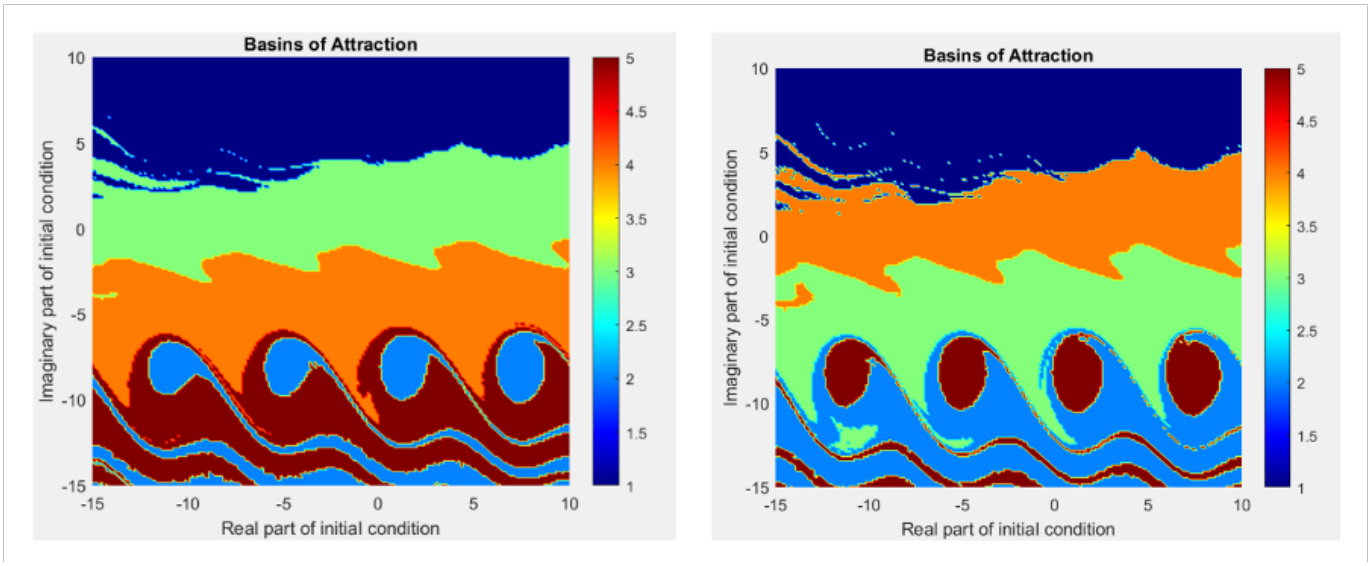

Figure 4.12: Basins of attractions when V_{B1} is 0.051 rad and 0.062 rad respectively for primary resonance.

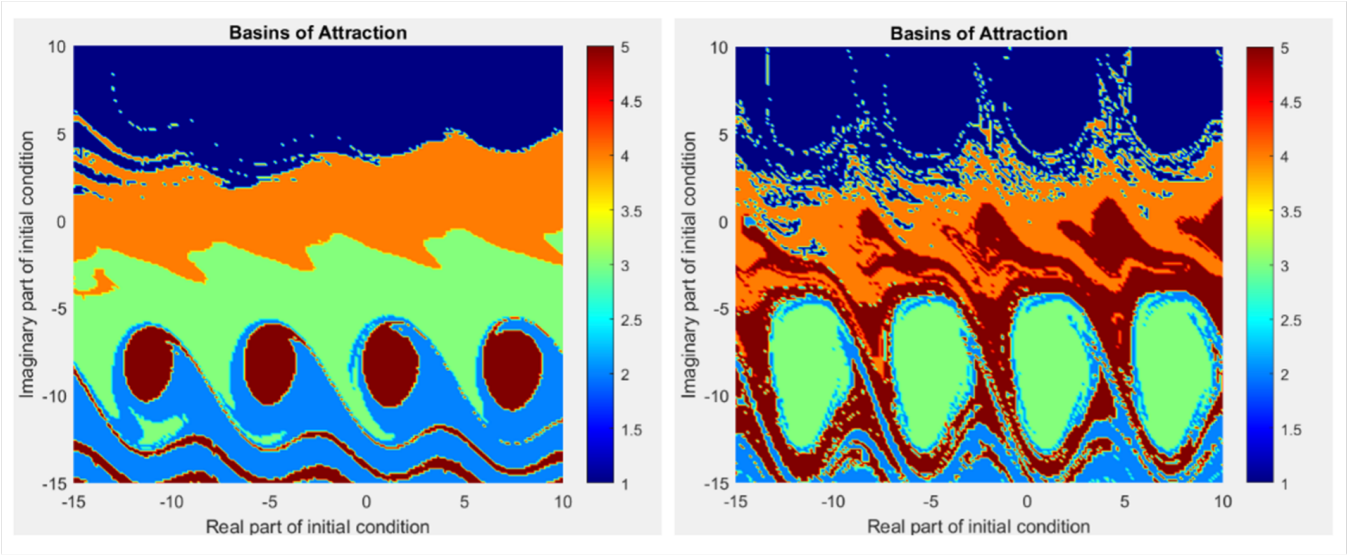

Figure 4.13: Basins of attractions when V_{B1} is 0.071 rad and 0.151 rad respectively for primary resonance.

4.4.2 Subharmonic Resonance

The subharmonic resonance analysed, further provides evidence on the stable regions of the system. The basins of attractions for the subharmonic resonance depicts the stable and unstable regions when the excitation frequency is approximately double the natural frequency of the dynamical system, [100]. This analysis will show the chaos and instability points of the system for further studies, [101].

Subharmonic resonance's sources of attraction have also been studied extensively. In [102], [103], the authors investigated the effects of various parameters, such as the amplitude and frequency of the subharmonic component, on the basins of attraction. Transitions between distinct subharmonic resonant states and the effect of control strategies on the stability boundaries have been studied, [104], [105]. Hence further investigation on the basins of attraction is necessary to analyse the stability when there is a change in parameters, [56].

Figure 4.14 and Figure 4.15 represent the basins of attraction for the subharmonic resonance when V_{B1} and θ_{B1} are varied in the swing equation of the dynamical system. As the variable is changed the system becomes fractal and it becomes corrupt.

Initially only the variable V_{B1} is varied when others are fixed to observe the effect of

this particular variable. Even when $V_{B1} = 0$ the system is still corrupted and this is due to the effect of θ_{B1}.

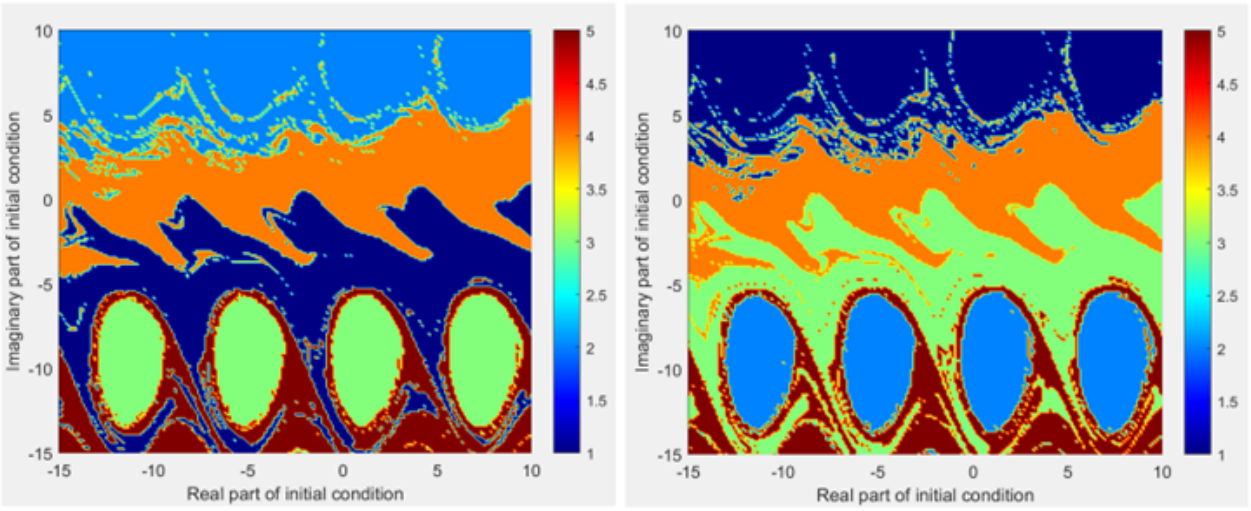

Figure 4.14: Basins of attractions when V_{B1} is 0 rad and 0.051 rad respectively subharmonic resonance.

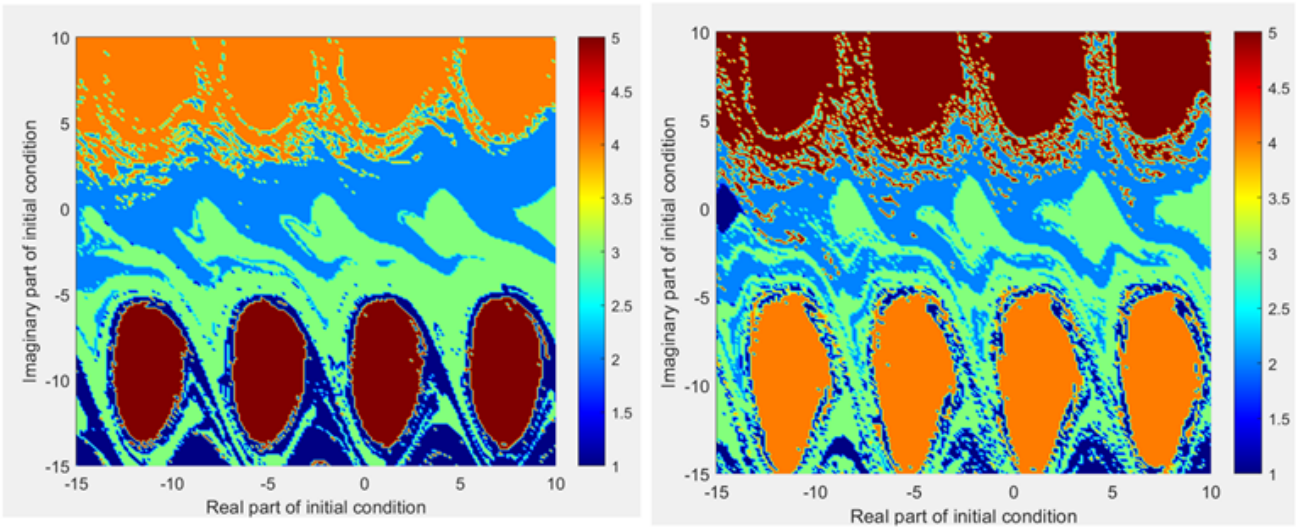

Figure 4.15: Basins of attractions when V_{B1} is 0.151 rad and 0.21 rad respectively for subharmonic resonance.

Furthermore, the variable θ_{B1} is changed to observe the transitions in the basins of attractions for subharmonic resonance.

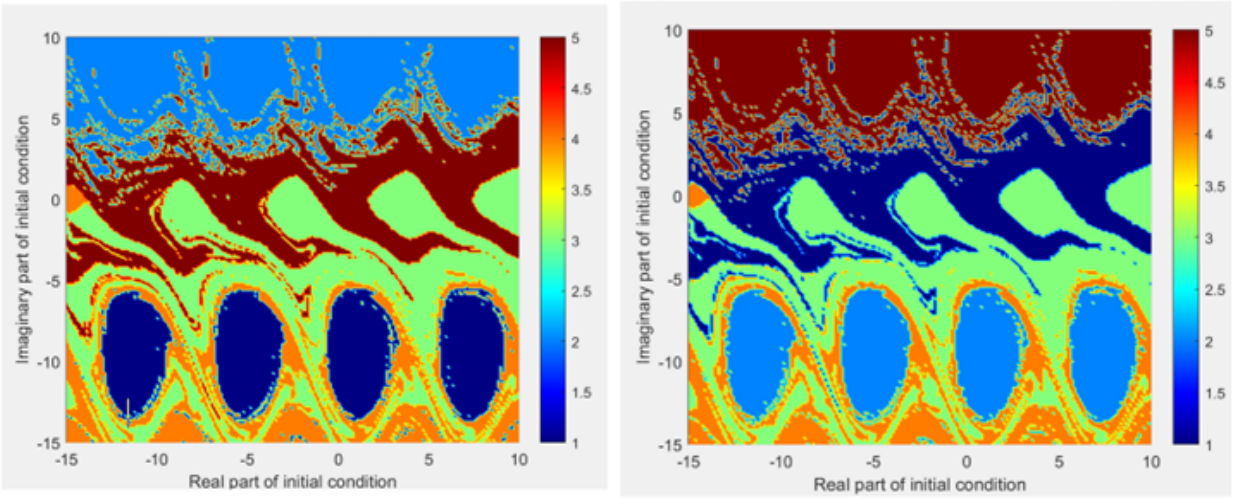

Figure 4.16: Basins of attractions when θ_{B1} is 0.191 rad and 0.181 rad respectively for subharmonic resonance.

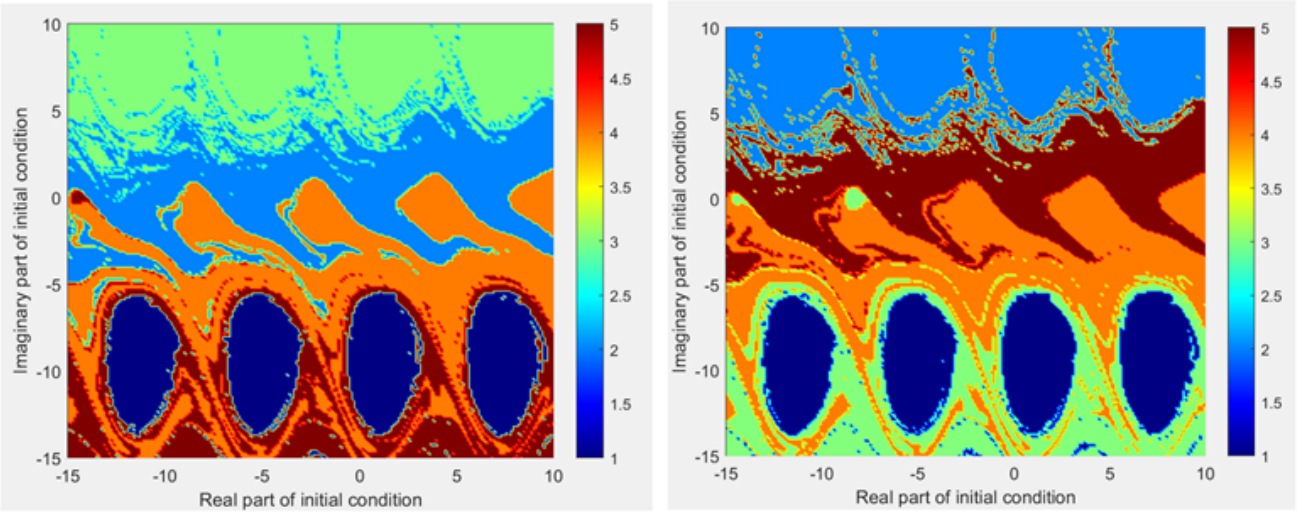

Figure 4.17: Basins of attractions when θ_{B1} is 0.151 rad and 0.141 rad respectively for subharmonic resonance.

Figure 4.16 and Figure 4.17 depict the system when the variable is varied whilst others are kept constant. In this instance as θ_{B1} is decreased the basins of attractions change and the stable and unstable regions can be observed.

4.5 Discussion

An investigation into the dynamic behaviour of the swing equation under a variety of control situations is carried out in this section for the subharmonic resonance. In order to check the correctness of the perturbed solution for subharmonic resonance and the basins of attraction associated with these phenomena, perturbation techniques are compared to numerical simulation. They are used to verify the accuracy of the perturbed solution.

By applying the swing equation to a variety of different circumstances, particularly those involving load displacement, it is easier to make predictions about the behaviour of the system. The administrators of the power system make use of this information in order to ensure the system's consistency and dependability is maintained. It is possible to make use of this methodology in the process of developing and evaluating control systems for power systems, namely in the areas of automatic generation control and load frequency management. The major goal of this initiative is to lower the likelihood of blackouts occurring and, more importantly, to lessen the potentially catastrophic effects that they could have.

The comprehensive numerical analysis that was carried out in this investigation, which made use of a wide range of mathematical tools including bifurcation diagrams, Lyapunov exponents, phase portraits, frequency domain plots, and Poincaré maps, yield significant insights into the way in which the swing equation behaves when subjected to subharmonic resonance. The occurrence of the first period doubling in a sequence has been identified as a significant indicator of oncoming chaos, warning possible risks and operational challenges for power systems. This fact has been highlighted as a key predictor of impending chaos. Furthermore, the research has demonstrated that other phenomena, such as intermittency or the collapse of quasiperiodic torus structures, can also result in systemic chaos. While period doubling is a well-known example of chaotic behaviour, other events, such as these, can also result in chaotic behaviour.

It has effectively depicted both pre-chaotic and post-chaotic alterations by taking into account the effects of various parameter adjustments on the dynamical behaviour of the system. This demonstrates the significance of the work. Having a better understanding of the transitional behaviour of a system before to its entry into a chaotic regime can be achieved through the detection of pre-chaos motion patterns. A further validation

of the system's loss of stability, which leads to chaotic behaviour under conditions of subharmonic resonance, was achieved by the investigation of basins of attraction for primary and subharmonic resonances.

The primary and subharmonic resonances are the focus of this segment, which contributes to a deeper comprehension of the fundamental components of the swing equation and the consequences those aspects have for the maintenance of system stability. Power system engineers and researchers are provided with valuable information as a result of the findings, which enables them to design control systems and protective measures that are more successful in mitigating the risks associated with subharmonic resonance-induced chaos.

The findings of this thesis embedded in this chapter, contribute to a better understanding of the dynamic behaviour of the swing equation and its reaction to subharmonic resonance. Additionally, it sheds light on the essential parameters that govern the stability of the system. The findings also have the potential to contribute to the advancement of the creation of power infrastructures that are more resilient and secure. This is because power systems are always evolving and will continue to face increasingly complex difficulties.

Under conditions of subharmonic resonance, it is possible that future research in this field will investigate novel control methods and technologies with the goal of ensuring the dependability and stability of power systems.

4.6 Final Remarks

Subharmonic resonance plays a critical role in understanding the dynamic stability of nonlinear systems such as the swing equation. In the context of this chapter, a detailed investigation of subharmonic resonance has been undertaken, with the aim of highlighting its influence on the overall system behaviour and its potential to induce instability. Subharmonic resonance occurs when the external forcing frequency is a fraction of the system's natural frequency, and this interaction can give rise to complex oscillatory patterns, including periodic windows, bifurcations, and chaotic attractors.

This chapter has provided a comprehensive explanation of subharmonic resonance and has served to bridge the theoretical insights found in existing literature with the practical analysis of the swing equation. By simulating and analysing the system under various

subharmonic conditions, the chapter has demonstrated how seemingly small parametric variations can lead to significant qualitative changes in the system's dynamics. The inclusion of analytical techniques alongside numerical simulations has further strengthened the validity of the findings and has offered multiple lenses through which the phenomenon can be understood.

Moreover, the study of subharmonic resonance serves as a critical stepping stone toward exploring more complex dynamic behaviours, including the emergence of chaos. Understanding the mechanisms through which energy is transferred across frequencies in nonlinear systems provides key insight into the broader narrative of dynamic instability. As this research has shown, the appearance of subharmonic oscillations often precedes more erratic behaviour and can act as a precursor to bifurcation cascades and the onset of chaos.

Therefore, a thorough comprehension of subharmonic resonance is not merely an academic exercise but a necessary foundation for investigating chaotic behaviour in power system models. It equips researchers and engineers with the theoretical tools and practical awareness needed to predict and mitigate instability in electrical networks. By deepening our understanding of these resonant interactions, this chapter contributes meaningfully to the broader goals of stability analysis and control in nonlinear dynamical systems, particularly in the context of modern power grids.

Chapter 5

Analysing the Dynamical Behaviour using different Mathematical techniques

5.1 Introduction

This section explains different mathematical techniques to analyse the case of bifurcation in the swing equation. Floquet method, Method of strained parameters and Tangent Instability are analysed in depth to understand the intricate behaviour of the system when a disturbance is introduced.

The Floquet approach is a significant tool in the analysis of power system stability, particularly in the context of tiny disruptions, [23], [106]. The mathematical methodology employed in assessing the stability of periodic solutions, such as those seen in the swing equation, involves the examination of the eigenvalues of the linearised equations governing the system. Tangent instability, conversely, refers to a phenomena in which minor disturbances in the operational parameters of a power system can result in prolonged oscillations or instability, [107]. The strained parameters method is a strategy in control theory that is employed to mitigate tangent instability by modifying system characteristics in order to uphold stability, [108]. Collectively, these notions offer a comprehensive theoretical structure for examining and managing the stability of a mathematical problem, thereby guaranteeing their dependable functioning in the presence

of dynamic disturbances.

5.2 Floquet Method

Let $u(t)$ be a small disturbance (arbitrary), then:

$$\hat{\eta}(t) = \eta(t) + u(t) \tag{5.1}$$

The stability of $\eta(t)$ depends on the growth or decay of the perturbation $u(t)$. If $u(t)$ increases over time, the system is unstable around $\eta(t)$; if it decays, the system is stable.

Substituting equation (5.1) into equation (3.10) and eliminating any nonlinear terms with $\zeta(t)$, we obtain the variational equation governing the evolution of $u(t)$:

$$\frac{d^2u}{dt^2} + \frac{\omega_R D}{2H}\frac{du}{dt} + u\left(K - 2\alpha_2\eta - 3\alpha_3\eta^2\right) = 0 \tag{5.2}$$

The behaviour of $u(t)$ can be analysed using Floquet theory, which is suitable for studying the stability of periodic solutions in linear differential equations with periodic coefficients.

If $u_1(t)$, $u_2(t)$ are two independent solutions to equation (5.2), then due to the periodicity of the coefficients, the shifted functions $u_1(t+T)$, $u_2(t+T)$ are also solutions. Therefore, they can be expressed as linear combinations of $u_1(t)$ and $u_2(t)$ as follows:

$$\begin{aligned} u_1(t+T) &= a_{11}u_1(t) + a_{12}u_2(t) \\ u_2(t+T) &= a_{21}u_1(t) + a_{22}u_2(t) \end{aligned}$$

To construct the monodromy matrix, two linearly independent solutions are computed using the following initial conditions:

$$\begin{aligned} u_1(0) &= 1, & \dot{u}_1(0) &= 0 \\ u_2(0) &= 0, & \dot{u}_2(0) &= 1 \end{aligned}$$

After solving the differential equation (5.2) with the above initial conditions over one period T, we evaluate the solutions at $t = T$ to form the monodromy matrix A:

$$A = \begin{bmatrix} u_1(T) & \dot{u}_1(T) \\ u_2(T) & \dot{u}_2(T) \end{bmatrix} \tag{5.3}$$

The eigenvalues of the monodromy matrix A, referred to as Floquet multipliers, govern the stability of the periodic solution $\eta(t)$. If all Floquet multipliers lie strictly within the unit circle in the complex plane, the solution is stable. Conversely, if any multiplier lies on or outside the unit circle, the periodic orbit becomes unstable.

A saddle-node bifurcation of a periodic solution occurs when a pair of fixed points (or periodic orbits) coalesce and eliminate each other as a system parameter varies. In the context of Floquet theory, this bifurcation is analytically predicted when one of the Floquet multipliers approaches and crosses the unit circle at $+1$ on the real axis. This indicates the loss of stability and the disappearance of the periodic orbit.

In the analytical approach used in this thesis, perturbation methods are applied to approximate the solution and derive a linearised variational equation around the periodic orbit. The resulting monodromy matrix captures the fundamental solution over one period. By computing its eigenvalues analytically, it is possible to track when a multiplier reaches the critical value of $+1$, signalling a saddle-node bifurcation. Therefore, the analytical solution accurately predicts the bifurcation point by identifying the parameter value at which the Floquet multiplier crosses the stability threshold, confirming the onset of the bifurcation.

5.3 Method of strained Parameters

Considering equation (3.60) and substituting it into equation (5.2) leads to:

$$\begin{aligned} \ddot{u} + \frac{\omega_R D}{2H}\dot{u} + u\Bigg(K - 2\alpha_2 \left[\varepsilon a \cos(\Omega t + \beta + \varphi_e) + \frac{\varepsilon^2 a^2 \alpha_2}{6\Omega^2} \left(3 - \cos(2\Omega t + 2\beta + 2\varphi_e)\right) \right] \\ -3\alpha_3 \left[\varepsilon a \cos(\Omega t + \beta + \varphi_e) + \frac{\varepsilon^2 a^2 \alpha_2}{6\Omega^2} \left(3 - \cos(2\Omega t + 2\beta + 2\varphi_e)\right) \right]^2 \Bigg) = 0 \end{aligned} \tag{5.4}$$

Expanding the brackets:

$$\ddot{u} + \frac{\omega_R D}{2H}\dot{u} + uK - 2u\alpha_2\varepsilon a\cos(\Omega t + \beta + \varphi_e) + \frac{\varepsilon^2 a^2 u\alpha_2^2}{\Omega^2} - \frac{\varepsilon^2 a^2 u\alpha_2^2}{3\Omega^2}\cos(2\Omega t + 2\beta + 2\varphi_e)$$
$$-3\alpha_3 u\varepsilon^2 a^2\cos^2(\Omega t+\beta+\varphi_e) - \frac{3\alpha_3 u a^3\varepsilon^2\alpha_2}{\Omega^2}\cos(\Omega t+\beta+\varphi_e) + \frac{\alpha_3 u\varepsilon^2 a^3\alpha_2}{\Omega^2}\cos(\Omega t+\beta+\varphi_e)\cos(2\Omega t+2\beta+2\varphi_e)$$
$$- \frac{\alpha_3 u\varepsilon^2 a^4\alpha_2^2}{12\Omega^4}\left(9 + \cos(2\Omega t + 2\beta + 2\varphi_e) - 6\cos(2\Omega t + 2\beta + 2\varphi_e)\right) = 0 \quad (5.5)$$

From equation (3.29), it is known:

$$\frac{\omega_R D}{2H} = 2\varepsilon^2\mu \quad (5.6)$$

and letting:

$$\Phi = \Omega t + \beta + \varphi_e \quad (5.7)$$

In the above expression, Φ represents the total phase of the oscillatory solution. The term Ωt denotes the time-dependent phase component, where Ω is the excitation frequency and t is time. The symbol β is a constant phase shift introduced by the system's nonlinear response, typically arising from the perturbation analysis. Finally, φ_e represents the external or initial phase offset, often associated with the excitation signal or imposed boundary conditions. Together, these components define the instantaneous phase of the system's response.

Then the equation becomes:

$$\ddot{u} + 2\varepsilon^2\mu\dot{u} + uK - 2u\alpha_2\varepsilon a\cos\Phi + \frac{\alpha_2^2 u\varepsilon^2 a^2}{\Omega^2} - \frac{\alpha_2^2 u\varepsilon^2 a^2}{3\Omega^2}\cos 2\Phi - 3\alpha_3 u\varepsilon^2 a^2\cos^2\Phi$$
$$-\frac{3\alpha_3 u a^3\varepsilon^2\alpha_2}{\Omega^2}\cos\Phi + \frac{\alpha_3 u\varepsilon^2 a^3\alpha_2}{\Omega^2}\cos\Phi\cos 2\Phi - \frac{3\alpha_3 u\varepsilon^2 a^4\alpha_2^2}{4\Omega^4} - \frac{\alpha_3 u\varepsilon^2 a^4\alpha_2^2}{12\Omega^4}\cos^2 2\Phi + \frac{\alpha_3 u\varepsilon^2 a^4\alpha_2^2}{2\Omega^4} = 0 \quad (5.8)$$

Now cancelling out ε^2 and simplifying gives:

$$\ddot{u} + 2\mu\dot{u} + uK^* = \chi u\cos\Phi + \Lambda u\cos 2\Phi \quad (5.9)$$

where:

$$K^* = K + \left(\frac{3\alpha_3}{2} - \frac{\alpha_2^2}{3\Omega^2}\right) a^2 - \frac{19\alpha_2^2\alpha_e a^4}{24\Omega^4} \tag{5.10}$$

$$\chi = 2\alpha_2 a + \frac{5\alpha_2\alpha_3 a}{2\Omega^2} \tag{5.11}$$

$$\Lambda = \left(\frac{3\alpha_3}{2} - \frac{\alpha_2^2}{3\Omega^2}\right) a^2 - \frac{\alpha_2^2\alpha_3 a^4}{2\Omega^4} \tag{5.12}$$

$$\Phi = \Omega t + \beta + \varphi_e \tag{5.13}$$

Introducing ε as a bookkeeping parameter, and damping and forcing terms at $O(\varepsilon)$, equation (5.9) is rewritten as:

$$\ddot{u} + 2\mu\varepsilon\dot{u} + uK^* = \varepsilon\chi u\cos\Phi + \varepsilon\Lambda u\cos 2\Phi \tag{5.14}$$

Assuming a uniform expansion of the solution:

$$u(t;\varepsilon) = \varepsilon u_1(t) + \varepsilon^2 u_2(t) + \dots \tag{5.15}$$

And writing:

$$K^* = \frac{1}{4}\Omega^2 + \varepsilon\delta_1 + \varepsilon^2\delta_2 + \dots \tag{5.16}$$

Comparing the powers of ε^0:

$$\ddot{u}_0 + \frac{1}{4}\Omega^2 u_0 = 0 \tag{5.17}$$

Comparing the powers of ε^1:

$$\ddot{u}_1 + \frac{1}{4}\Omega^2 u_1 = -2\mu\dot{u}_0 - \delta_1 u_0 + \chi u_0\cos\Phi + \Lambda u_0\cos 2\Phi \tag{5.18}$$

Comparing the powers of ε^2:

$$\ddot{u}_2 + \frac{1}{4}\Omega^2 u_2 = -2\mu\dot{u}_1 - \delta_1 u_1 - \delta_2 u_0 + \chi u_1\cos\Phi + \Lambda u_1\cos 2\Phi \tag{5.19}$$

Taking the solution:

$$u_0 = a\cos\frac{1}{2}\Phi + b\sin\frac{1}{2}\Phi \tag{5.20}$$

Substituting equation (5.20) into equation (5.18)

$$\ddot{u}_1 + \frac{1}{4}\Omega^2 u_1 = -2\mu\dot{u}_0 - \delta_1(a\cos\tfrac{1}{2}\Phi + b\cos\tfrac{1}{2}\Phi) + \chi\cos\Phi(a\cos\tfrac{1}{2}\Phi + b\sin\tfrac{1}{2}\Phi) + \Lambda\cos 2\Phi(a\cos\tfrac{1}{2}\Phi + b\sin\tfrac{1}{2}\Phi) \quad (5.21)$$

Replacing with,

$$\dot{u}_0 = \frac{-a}{2}\sin\tfrac{1}{2}\Phi + \frac{b}{2}\cos\tfrac{1}{2}\Phi \quad (5.22)$$

gives,

$$\ddot{u}_1 + \frac{1}{4}\Omega^2 u_1 = \mu a\Omega\sin\tfrac{1}{2}\Phi - \mu b\Omega\cos\tfrac{1}{2}\Phi - \delta_1 a\cos\tfrac{1}{2}\Phi - \delta_1 b\sin\tfrac{1}{2}\Phi + a\chi\cos\Phi\cos\tfrac{1}{2}\Phi + b\chi\cos\Phi\sin\tfrac{1}{2}\Phi + a\Lambda\cos 2\Phi\cos\tfrac{1}{2}\Phi + b\Lambda\cos 2\Phi\sin\tfrac{1}{2}\Phi \quad (5.23)$$

Employing trigonometric identities,

$$a\chi\cos\Phi\cos\tfrac{1}{2}\Phi = \frac{a\chi}{2}\left(\cos\tfrac{3}{2}\Phi + \cos\tfrac{1}{2}\Phi\right) \quad (5.24)$$

$$b\chi\cos\Phi\sin\tfrac{1}{2}\Phi = \frac{b\chi}{2}\left(\sin\tfrac{3}{2}\Phi - \sin\tfrac{1}{2}\Phi\right) \quad (5.25)$$

$$a\Lambda\cos 2\Phi\cos\tfrac{1}{2}\Phi = \frac{a\Lambda}{2}\left(\cos\tfrac{5}{2}\Phi + \cos\tfrac{3}{2}\Phi\right) \quad (5.26)$$

$$b\Lambda\cos 2\Phi\sin\tfrac{1}{2}\Phi = \frac{b\Lambda}{2}\left(\sin\tfrac{5}{2}\Phi - \sin\tfrac{3}{2}\Phi\right) \quad (5.27)$$

Substituting the above into the equation and rearranging,

$$\ddot{u}_1 + \frac{1}{4}\Omega^2 u_1 = \cos\tfrac{1}{2}\Phi\left[\left(\frac{1}{2}\chi - \delta_1\right)a - \mu b\Omega\right] + \sin\tfrac{1}{2}\Phi\left[\mu a\Omega - \left(\frac{1}{2}\chi + \delta_1\right)b\right] + \frac{a}{2}(\chi+\Lambda)\cos\tfrac{3}{2}\Phi + \frac{b}{2}(\chi-\Lambda)\sin\tfrac{3}{2}\Phi + \frac{a\Lambda}{2}\cos\tfrac{5}{2}\Phi - \frac{b\Lambda}{2}\sin\tfrac{5}{2}\Phi \quad (5.28)$$

For eliminating secular terms in equation (5.28), consider

$$\left(\frac{1}{2}\chi - \delta_1\right) a - \mu b\Omega = 0 \tag{5.29}$$

$$\mu a\Omega - \left(\frac{1}{2}\chi + \delta_1\right) b = 0 \tag{5.30}$$

It is also given that for non-trivial solution to exist, the following should be satisfied,

$$\delta_1^2 = \frac{1}{4}\chi^2 - \mu^2\Omega^2 \tag{5.31}$$

Using equations (5.29) and (5.30), equation (5.28) becomes

$$u_1 = D\cos\tfrac{1}{2}\Phi + E\sin\tfrac{1}{2}\Phi - \frac{(X+\Lambda)a}{4\Omega^2}\cos\tfrac{3}{2}\Phi - \frac{(X-\Lambda)b}{4\Omega^2}\sin\tfrac{3}{2}\Phi + \ldots \tag{5.32}$$

where D and E are constants.

Substituting equations (5.28) and (5.32) into equation (5.27) the following equations are obtained,

$$\left(\frac{1}{2}\chi - \delta_1\right) D - \mu\Omega E = \left[\delta_2 + \frac{(X+\Lambda)\Lambda}{8\Omega^2}\right] a \tag{5.33}$$

$$\mu\Omega D - \frac{1}{2}(\chi + \delta_1) E = \left[\delta_2 + \frac{(X-\Lambda)\Lambda}{8\Omega^2}\right] b \tag{5.34}$$

Given that equations (5.33) and (5.34) have non-trivial solution, the inhomogeneous equations have solution if and only if consistency (solvability) condition is satisfied,

$$\delta_2 = -\frac{\chi^2 + 4\Lambda\delta_1 + \Lambda^2}{8\Omega^2} \tag{5.35}$$

Hence the equation (5.16) depicts the transition curves determining period doubling as shown below,

$$K^* = \frac{1}{4}\Omega^2 \pm \varepsilon\left(\frac{1}{4}\chi^2 - \mu^2\Omega^2\right)^{1/2} - \varepsilon^2\left(\frac{\chi^2 + 4\Lambda\delta_1 + \Lambda^2}{8\Omega^2}\right) + \ldots \tag{5.36}$$

5.4 Tangent Instabilities

Initially the points corresponding to vertical tangents are in the frequency-response curves given by the equation below, [1],

Beginning with the equation:

$$\mu^2 + \left(\frac{\sigma}{2\Omega} + \frac{\alpha_e a^2}{\Omega}\right)^2 = \frac{g^2}{4\Omega^2 a^2} \tag{5.37}$$

and rearranging the above equation gives:

$$4\mu^2\Omega^2 + \left(\sigma + 2\alpha_e a^2\right)^2 = \left(\frac{g}{a}\right)^2 \tag{5.38}$$

For ease of analysis, the following variable substitutions are defined:

$$s = a^2, \quad x = \Omega^2, \quad \sigma = \omega_0^2 - \Omega^2 \tag{5.39}$$

Then equation (5.38) is written as,

$$4\mu^2 xs + s\left(\omega_0^2 - x - 2\alpha_e s\right)^2 = g^2 \tag{5.40}$$

Next, taking the derivative of the above equation with respect to x:

$$\begin{aligned} 4\mu^2 x\frac{ds}{dx} + \left(\omega_0^2 - x - 2\alpha_e s\right)^2 \frac{ds}{dx} - 4\alpha_e s\left(\omega_0^2 - x - 2\alpha_e s\right)\frac{ds}{dx} \\ +4\mu^2 s - 2s\left(\omega_0^2 - x - 2\alpha_e s\right) = 0 \end{aligned} \tag{5.41}$$

Now, to determine the turning point (i.e., where $\frac{ds}{dx} = 0$), equating the coefficient of $\frac{ds}{dx}$ to zero:

$$4\mu^2 x + \left(\omega_0^2 - x - 2\alpha_e s\right)^2 - 4\alpha_e s\left(\omega_0^2 - x - 2\alpha_e s\right) = 0 \tag{5.42}$$

Now, recall from earlier that:

$$g^2 = 4\alpha_e s\left(\omega_0^2 - x - 2\alpha_e s\right) \tag{5.43}$$

Let us define:

$$z = \omega_0^2 - x - 2\alpha_e s \tag{5.44}$$

Then, rearranging:

$$2(z + x - \omega_0^2) = 4\alpha_e s \tag{5.45}$$

Now substitute equation (5.44) into (5.42) for z back into the earlier turning-point equation:

$$4\mu^2 x + z^2 + 4\alpha_e s z = 0 \tag{5.46}$$

Now use the identity above again to replace $4\alpha_e s$ by $2(z + x - \omega_0^2)$, leading to:

$$4\mu^2 x + z^2 + z \cdot 2(z + x - \omega_0^2) = 0 \tag{5.47}$$

Expanding the brackets and simplifying:

$$3z^2 + 2z(x - \omega_0^2) + 4\mu^2 x = 0 \tag{5.48}$$

In order to calculate the tangent instability using Matlab, the variable z is determined by solving equation (5.48) with specific values assigned to the parameter Ω. Subsequently, by solving equation (5.44) for the variable s and substituting the obtained value into equation (5.43), the variable g can be determined.

5.5 Results

A comprehensive comparison between numerical simulation results and various analytical approaches namely, the Floquet method, the method of strained parameters, and the tangent instability technique is illustrated in Figure 5.1. This figure highlights the accuracy and limitations of each method in predicting the nonlinear dynamic behaviour and bifurcation characteristics of the swing equation.

A detailed investigation of the system's stability and dynamic response has been performed using the Floquet method, implemented numerically via Matlab. This approach facilitates a deep understanding of transient stability phenomena in power systems by examining the periodic nature of small perturbations and their evolution over time. The Floquet method is found to be particularly effective in predicting the onset of saddle-node

bifurcation. However, when its results are compared with those from numerical simulations, a relative error of approximately 9.21% is observed in locating the bifurcation point.

In parallel, analytical solutions derived using the method of strained parameters have been computed by evaluating equation (5.36), which approximates the period-doubling bifurcation curve. This method offers a perturbation-based closed-form expression that provides both qualitative and quantitative insight into the swing equation's nonlinear oscillatory behaviour. Nevertheless, it introduces a prediction error of 10.32% when compared to the numerical benchmark.

The tangent instability criterion has also been applied through the analysis of equation (5.46), offering another perspective on identifying saddle-node bifurcations. While analytically elegant, this method yields a deviation of 12.5% from the numerically determined critical point.

In summary, although all three analytical methods provide valuable predictive capability and theoretical understanding of the system dynamics, each exhibits a certain level of discrepancy relative to the numerically obtained values. Among them, the Floquet method demonstrates the highest accuracy, making it especially useful for applications requiring precise stability assessment. These findings underscore the importance of cross-validating analytical methods with numerical simulations to ensure robust analysis of power system stability.

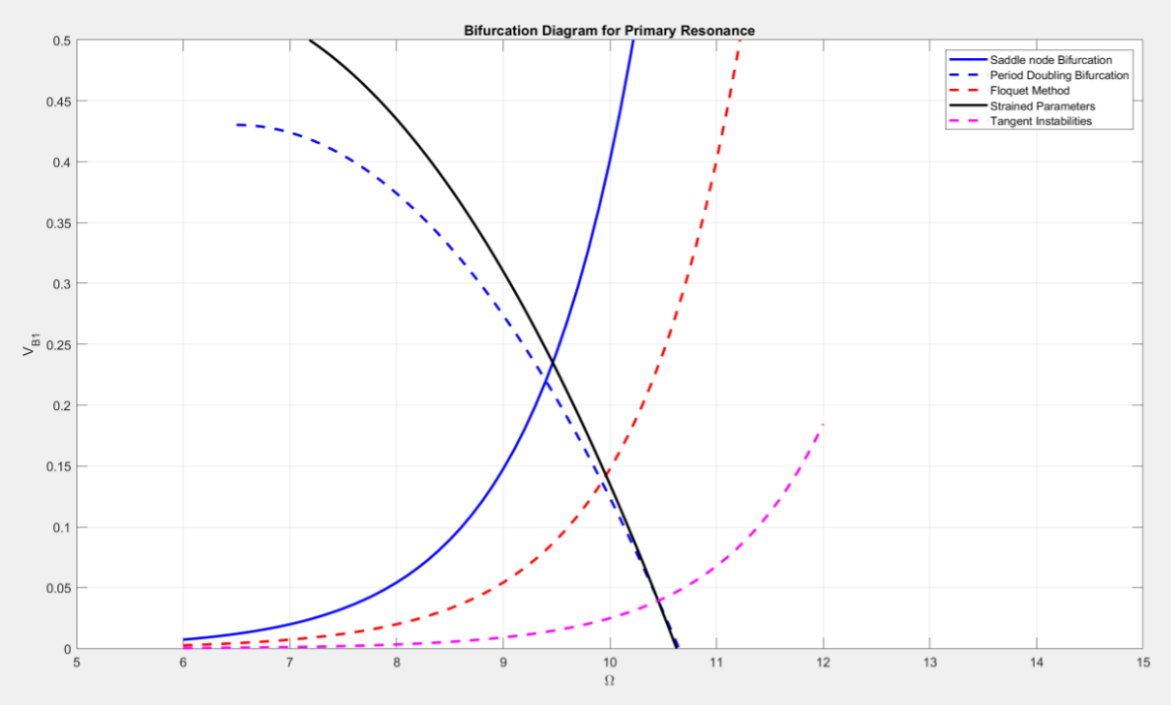

Figure 5.1: Bifurcation diagram showing a comparison of different analytical methods for Primary Resonance.

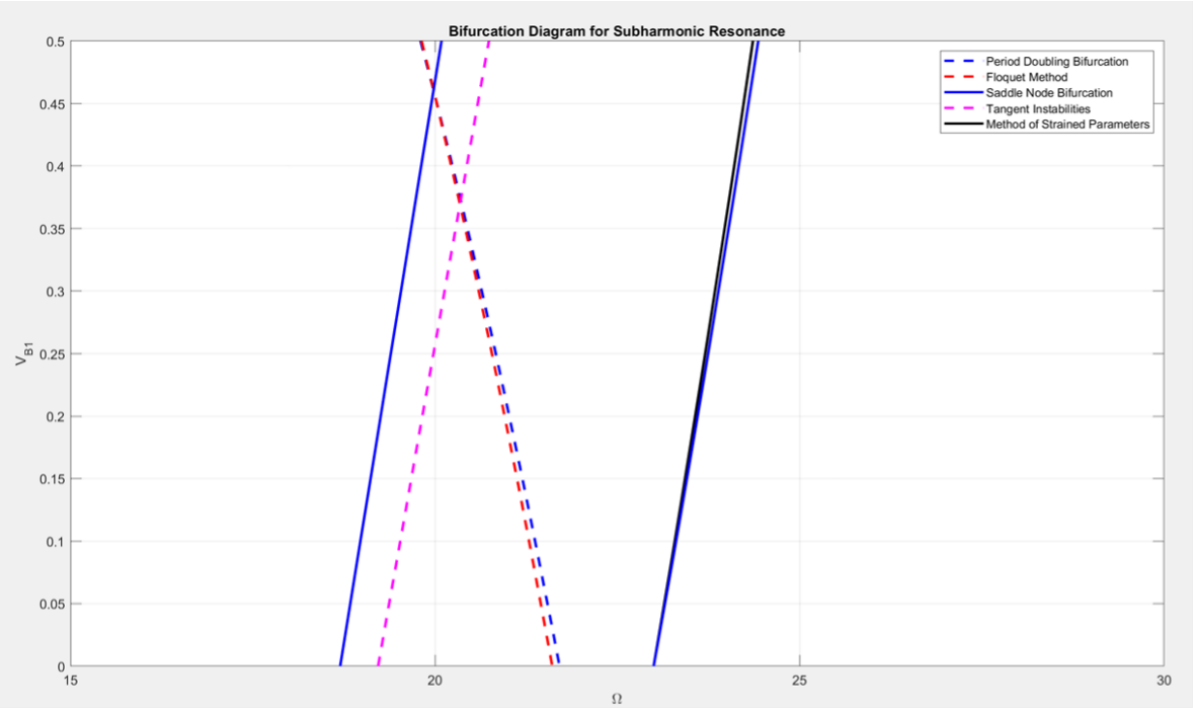

Figure 5.2: Bifurcation diagram showing a comparison of different analytical methods for Subharmonic Resonance.

Similarly, Figure 5.2 presents a comparative analysis between the results obtained from numerical simulations and those derived using various analytical methodologies for the case of subharmonic resonance. In this context, the analysis considers a time scale that is twice that of the primary resonance, allowing for the examination of second-order resonant phenomena such as period doubling and saddle-node bifurcations.

To predict the onset of bifurcations under subharmonic excitation, both the Method of Strained Parameters and the Tangent Instability approach have been employed. These analytical tools are applied to derive expressions that characterise the transition boundaries of the system's dynamic stability. The Method of Strained Parameters demonstrates exceptional agreement with the numerical data, predicting the saddle-node bifurcation with a remarkably low error of only 0.091%. Similarly, the Tangent Instability method forecasts the bifurcation point with a moderate error of 5.43%, reflecting its applicability despite a slightly reduced accuracy in this scenario.

Furthermore, the Floquet method, renowned for its effectiveness in capturing the periodic structure of solutions and their stability, is also applied in this analysis. It successfully predicts the period-doubling bifurcation, yielding an impressively low error of 0.102% when benchmarked against numerical simulation results.

These analytical predictions are not only consistent with the numerical findings but also show strong coherence with specific results presented in the literature, particularly in [86]. The close agreement across methods affirms the robustness of the analytical frameworks and their utility in accurately capturing complex nonlinear behaviours such as subharmonic resonance and bifurcation dynamics in power systems.

5.6 Discussion

The objective of this section of this chapter is to analyse the dynamic characteristics of the swing equation under different variations of control parameters. It compares analytical methods, particularly perturbation techniques, with numerical simulation in order to verify the accuracy of the perturbed solution for subharmonic resonance and the basins of attraction associated with these phenomena.

The examination of the primary and subharmonic resonances of the swing equation

involves the utilisation of many analytical methods, namely the Floquet method, method of strained parameters, and analytical techniques. These approaches give unique perspectives and contribute significant knowledge to the understanding of the stability of the power system in this chapter. The analytical approach generally depends on the utilisation of mathematical modelling and manual computations, resulting in accurate outcomes within the context of simplified assumptions. However, it may encounter difficulties in accurately representing the many interconnections and nonlinear dynamics that manifest in power systems found in real-world scenarios.

On the other hand, the Floquet method and the method of strained parameters utilise numerical and computational techniques to effectively address complex dynamics. These methodologies provide a methodical investigation of the system's reaction to diverse conditions and external disturbances, which can be effectively depicted through graphical illustrations. Researchers can enhance their comprehension of the system's behaviour in the vicinity of the primary resonance by graphing the response of the swing equation across various parameter values or forcing frequencies. Graphical analyses serve as a vital supplement to analytical techniques, providing a more holistic perspective on the stability attributes. This aids power system engineers in making well-informed judgements to guarantee the dependable functioning of the grid.

The anticipated response of the system is determined by employing the swing equation in diverse scenarios, including instances involving load alterations. The data is utilised by power system management in order to guarantee the stability and reliability of the system. The use of this approach extends to the design and analysis of control systems for power systems, namely in the areas of autonomous generation control and load frequency management. For instance in the case to mitigate the occurrence of blackouts and the consequential catastrophic consequences they may entail.

5.7 Final Remarks

This chapter has examined the influence of parameter variations on the dynamic behaviour of the swing equation, with particular emphasis on the transitions observed before and after the onset of chaos. Analytical methods, including the Floquet technique, the method of strained parameters, and tangent instability analysis, were employed to assess the

system's stability characteristics. These techniques offered valuable insights into the mechanisms underpinning the emergence of complex dynamical behaviours.

The identification of pre-chaotic motion proved especially useful in enhancing our understanding of the transient dynamics that precede chaotic regimes. Moreover, the investigation of the basins of attraction associated with both primary and subharmonic resonances confirmed the system's inherent instability under certain excitation conditions particularly those linked to subharmonic resonance, which tends to provoke chaotic responses.

This work makes a significant contribution to the current academic literature on the swing equation, building on recent studies, notably [77] and [115]. By focusing specifically on primary and subharmonic resonances, the findings offer a deeper understanding of the nonlinear dynamics and stability margins in power systems. These insights are of practical relevance to power engineers and researchers seeking to develop advanced control strategies for mitigating chaotic behaviour.

The findings highlight key aspects of system stability and provide a foundation for future research aimed at improving the resilience and reliability of power infrastructures, an increasingly critical objective given the growing complexity and demands placed on modern power networks.

Looking forward, the integration of quasiperiodic forcing into the swing equation framework represents a promising avenue for further investigation. Such an approach could yield important insights into the long-term stability and adaptability of power systems subject to multifrequency disturbances and non-periodic excitations.

Chapter 6

Studying the Effects of Quasiperiodicity on the Swing Equation

6.1 Introduction

The concept of quasiperiodicity describes a type of motion that is characterised by the presence of two or more frequencies that are not rational multiples of one another, which results in the frequencies being incommensurate with one another. In light of this, it may be deduced that the system does not completely return to its initial state, although it does come close to doing so on occasion. The phenomenon of quasiperiodic motion is widely observed in dynamical systems that display perturbations of integrable systems [109]. An illustration of this can be found in the situation of a double pendulum, where the motion displays quasiperiodicity when the amplitudes are at their lowest [110].

The idea of quasiperiodicity is a multidimensional phenomenon that does not have a description that is universally accepted by everyone. Nevertheless, a methodology that is widely utilised entails the construction of a definition for quasiperiodic motion in the manner that is described below: An example of a dynamical system that is considered to be quasiperiodic is one that possesses a solution that can be described as the combination of two or more frequencies that are not in a rational ratio with each other [111].

One other way of thinking about quasiperiodicity is to consider it as a type of motion

that has features that are very similar to those of periodicity. According to the definition provided by authors, a periodic signal is a signal that displays repeating behaviour, meaning that it occurs exactly after a predetermined amount of time has passed [112]. When compared to a perfect periodic signal, a quasiperiodic signal does not exhibit perfect repetition yet, it does exhibit approximate repetition at consistent intervals [113].

Within the area of dynamical systems theory, the idea of quasiperiodicity is thought to be of significant importance. A wide variety of systems, including economic, biological, and physical systems, are all examples of the phenomenon that can be observed. There are a number of events that can serve as examples of quasiperiodicity. These include the motion of the planets within the solar system, as well as the rhythmic patterns that are displayed by the human heartbeat and respiratory cycle [114].

Over the past few years, there has been a substantial amount of focus placed on the investigation of quasiperiodicity in the swing equation. A non-linear differential equation known as the swing equation is a mathematical representation of the dynamics of a machine when it is subjected to the action of a periodic driving force [77, 115]. It is possible that the solution to the swing equation is a combination of two or more frequencies that are not in a clear ratio. This is because the swing equation exhibits quasiperiodic features when specific values are provided to the parameters. Despite the fact that it does get near to returning to its starting state at regular intervals, implying that the system does not completely return to its basic state.

Within the context of the swing equation, the ability of quasiperiodicity to induce chaotic dynamics is the primary reason for its significance. The settings under which chaos begins to take place have a significant impact on the type of movement occurring. It is clear that when two trajectories begin so close to each other, their future divergence follows an exponential growth pattern over a particular length [116]. This is something that can be observed immediately. In order to fully comprehend the fundamental variables, it is necessary to have a comprehensive understanding of chaotic behaviour. This is due to the fact that chaotic behaviour is inherently unpredictable and impossible to manage [23]. Moreover, the capability of this phenomena to produce intricate patterns is another factor that contributes to its relevance. It has been demonstrated through empirical evidence that the utilisation of quasiperiodic solutions to the swing equation can result in the generation of spiral patterns, which are frequently observed in natural systems.

Within the scope of their research work, Chen and Xu [117] investigate the quasiperiodic solutions of discrete dynamical systems that are characterised by mixed-type functional equations. An example of the presence of quasiperiodic solutions is provided by the authors through the application of a fixed-point theorem. In addition to this, they provide instances of systems that are able to fulfil the conditions that are outlined in their proposition. A further inquiry was carried out by the authors, which focused on the examination of quasiperiodic solutions within the context of a fractional differential equation [118]. After that, they make use of a variational approach to show that quasiperiodic solutions do exist, and they also give numerical examples to make their results more clear.

In addition, research is conducted to explore the occurrence of quasiperiodic motion, which is distinguished by two frequencies that are not proportionate, within the context of a non-autonomous differential equation [119]. For the purpose of determining whether or not quasiperiodic solutions are present, the researchers employ a methodology that is founded on the concept of averaging. In addition to that, they provide qualitative and quantitative visualisations to illustrate the findings of their research. In their study, Li and Zhang analyse the existence of quasiperiodic solutions for a fractional differential equation that is not autonomous and has a nonlinear component [120]. In order to verify the presence of quasiperiodic solutions, the researchers employ a methodology that is observed on the concept of fixed points.

An investigation has been carried out that explicitly explores quasiperiodic solutions in a certain category of non-autonomous differential equations that incorporate impulsive effects [121]. For the purpose of demonstrating the existence of quasiperiodic solutions, the authors make use of a methodology that is structured around the concepts of lower and upper solutions theory. Furthermore, in order to make their conclusions more understandable, they include numerical examples.

The method of averaging is utilised to investigate the existence of quasiperiodicity in the swing equation when it is influenced by a sinusoidal driving force [122]. In this chapter, the author demonstrated that the swing equation is capable of displaying quasiperiodic dynamics throughout a broad spectrum of driving force amplitudes and frequencies. In addition, the aforementioned author expanded his research to encompass the influence of damping in a different paper [123]. The author demonstrated that the application of damping can simultaneously generate new sorts of quasiperiodic

behaviour while simultaneously reducing the amount of quasiperiodic behaviour that is observed. A researcher has offered a detailed description of his research on the presence of quasiperiodicity in the swing equation [9]. As an additional point of interest, the author investigated a number of interesting applications of the averaging method in the investigation of nonlinear dynamical systems.

In the context of quasiperiodicity in the swing equation, the term intermittency refers to the rapid and unpredictable shifts that occur between regular and chaotic patterns that are observed in the system [124]. It is distinguished by sporadic episodes of chaos that alternate with periods of regular, quasiperiodic motion, which stands in contrast to the constant irregularities that are observed in traditional chaotic dynamics [125]. Within the framework of the swing equation, these sporadic patterns can be experienced as abrupt transitions between stable quasiperiodic trajectories and chaotic behaviour, emphasising the system's susceptibility to specific changes in parameters or beginning circumstances [126]. Because it can create sudden and unexpected oscillations in the pendulum-like motion, intermittentness in the swing equation has significant repercussions for power systems. These repercussions require careful consideration. According to the researchers, the unforeseen changes that occur during these transitions pose challenges in terms of maintaining system stability and have the potential to have effects that are perceptible on the operations of electrical grids [127]. It is possible to gain a valuable understanding of the underlying processes that regulate the behaviour of the system by doing an examination of the irregular patterns that are present in the periodic motion of the swing equation [33]. This knowledge contributes to the development of control techniques and preventative measures that are more reliable, with the goal of minimising the possibilities of disruptive repercussions resulting from irregularities in power systems.

During the course of the inquiry into quasiperiodicity in the swing equation, it was discovered that the appearance of torus structures is indicative of a distinct and intricate form of dynamic behaviour. A torus is a difficult trajectory that exhibits both periodic and non-periodic properties in the motion of the system [128]. In this context, a torus represents a trajectory that is intricate. It is possible for the swing equation to undergo bifurcations; these bifurcations can lead to the formation of torus shapes when the equation approaches quasiperiodic states. The forms in question are indicative of a fragile equilibrium between regular oscillations and chaotic disturbances being

present. These torus structures provide valuable insights into the complicated interaction of parameters that bring about patterns of motion that are both stable and intricate [129]. An investigation of torus structures is essential for gaining an understanding of the system's potential to withstand and adapt to a variety of conditions. This is because torus structures offer a nuanced perspective on the system's response to shifting conditions. This information is helpful in the development of sophisticated control systems that can make use of the favourable aspects of quasiperiodic dynamics while simultaneously minimising the risks associated with chaotic transitions [130].

When it comes to the field of quasiperiodicity in the swing equation, chaos refers to the occurrence of behaviour that is erratic and appears to be unexpected in a system that, under certain conditions, is expected to exhibit motion that is more organised and periodic [26]. In the swing equation, chaos is characterised by the disturbance of the anticipated quasiperiodic trajectories, which results in movement that is both unpredictable and non-repetitive [89]. As an illustration of the system's susceptibility to disruptions, the creation of this disorderly behaviour can be linked to relatively minor changes in the characteristics of the system or the conditions under which it was initially established. A gripping phenomenon that highlights the inherent complexity of dynamic systems and demonstrates the delicate interaction between deterministic and chaotic dynamics is the phenomenon of transitioning to chaos in quasiperiodic systems, such as the swing equation [131]. This phenomenon is a captivating occurrence that highlights the inherent complexity of dynamic systems. Gaining a full grasp of the chaotic behaviour in the quasiperiodic dynamics of the swing equation is of highest significance, particularly within the field of power systems [132]. It is possible for unpredictable behaviour to lead to unfavourable results, such as increased vulnerability to disruptions and difficulties in maintaining system equilibrium [103]. By examining the conditions under which chaos emerges in the swing equation, one can gain a valuable understanding of the factors that influence the transition from organised to chaotic movement [133]. For the purpose of establishing effective control strategies and preventative actions to manage and decrease the potentially disruptive implications of chaos in power system dynamics, it is essential to have a thorough understanding of this information. The dependable and secure operation of the entire power grid is ensured as a result of this [23, 134].

6.2 Analytical Work

The swing equation is derived from the Law of Rotation, which governs the motion of rotating systems. Specifically, it is formulated by applying Newton's second law to the dynamics of a synchronous generator rotor, as shown in the derivation presented in Chapter 3. This foundational analysis considers the net accelerating torque as the difference between the mechanical input torque and the electrical output torque acting on the rotor.

The analytical framework outlined below builds upon that derivation by further examining the contributions of both mechanical and electrical torques. The resulting swing equation, a second order nonlinear differential equation, describes the evolution of the rotor angle relative to the synchronous reference frame over time. Previous studies addressing this formulation and its applications include the works of [33, 77, 115, 133], which have laid the groundwork for exploring the nonlinear dynamics of the swing equation.

This section extends the initial formulation by considering additional influences such as damping, external excitation, and nonlinear effects, thereby enabling a more comprehensive analysis of system stability and resonance phenomena in power systems.

In order to acquire a deeper comprehension of the intricate nature of quasiperiodicity, it is of the utmost importance to engage in a thorough mathematical investigation of the swing equation. For the purpose of this all-encompassing research, a variety of mathematical approaches, including algebraic algorithms, Taylor series expansion, and substitution, are utilised. Consistently, these methodologies are employed in order to comprehend the intricacies of the swing equation and uncover the subtle effects of quasiperiodicity [77, 115, 134].

The purpose of this section is to make use of the mathematical tools that have been mentioned in order to conduct a thorough investigation of the consequences and ramifications of quasiperiodic behaviour. Through the strategic application of algebraic methods, the purpose is to obtain an understanding of the fundamental patterns and structures that are present in the swing equation. The Taylor expansion is a mathematical technique that is extremely effective and is used to acquire a methodical and precise estimation of an equation. This allows for a more in-depth understanding of the dynamics

of the equation [77, 115].

Furthermore, the strategic application of substitution techniques is introduced into the analytical framework. This has made it possible to investigate alternate representations and transformations, which may disclose elements of quasiperiodic occurrences that were previously hidden. Through the utilisation of mathematical techniques, the objective of this work is to discover the fundamental mechanisms that govern quasiperiodic behaviour in the swing equation [134]. This will be accomplished by revealing the intricate link that exists between variables.

6.3 The Swing Equation Model

One of the most important frameworks for understanding the dynamics of rotor systems in electrical power equipment, specifically synchronous generators, is provided by the swing equation model. In its most basic form, the equation is a representation of the equilibrium that exists between the mechanical inertia and the electrical torque that are present within the rotor. An explanation of how perturbations in the power grid or mechanical forces can cause deviations from the synchronous speed is provided by this equation. These deviations, in turn, can cause oscillations in the rotor angle and speed. Using the language of mathematics, it is possible to characterise it as a differential equation of the second order. Additionally, it is applicable to the acceleration of the rotor angle in relation to the disparity between the mechanical torque and the electrical torque, which is then divided by the inertia of the system [23]. When it comes to evaluating the stability and dynamic response of power systems, the usage of this model is absolutely necessary. This model gives engineers the capacity to build control techniques that are resilient, hence reducing interruptions and ensuring reliable operation.

The rotor of the machine used by the swing equation, explains the intricate behaviour of both electrical and mechanical elements of the system. Hence studying the stability of this machine is vital to comprehend the abrupt alterations to the parameters of the equation. Stability can be observed through changing the load and inputs of the systems over time and hence reducing the cascade of chaos within power systems [133]. Examples of such changes include grid faults and load fluctuations. For the purpose of maintaining

grid stability and preventing cascading failures on account of disturbances, gaining an understanding of these processes is absolutely necessary. The swing equation makes it possible to carry out an accurate analysis of the dynamics of the rotor, which helps to develop complex control systems.

6.4 Hamilton's Principle

Hamilton's principle studies the dynamics of the swing equation system and considering this for the case of quasiperiodicity, this principle uses Lagrangian multiples to formulate the equation [135, 136]. It also provides deeper insight into the behaviour of the variable change within the nonlinear systems [137]. Hence this principle provides a better understanding of the parameters and chaos theory of the swing equation [138].

Over time, within the quasiperiodic domain governed by Hamilton's principle, the swing equation may experience a transition towards chaotic dynamics. Chaos arises when the system's response becomes very sensitive to initial conditions, leading to unpredictable and erratic behaviour. Quasiperiodicity involves a transition to chaos that is marked by the disturbance of stable periodic orbits, the appearance of bifurcations, and the start of complex, non-repetitive paths. The system's vulnerability to disruptions, combined with the incongruous frequencies present in quasiperiodic environments, results in the rapid transition towards chaos. Hamilton's principle, which focuses on minimising action and determining the trajectory of a system, is a valuable tool for understanding how quasiperiodicity can lead to chaotic dynamics in the swing equation over time.

Consider equation (3.10) represents the general form of the swing equation, accounting for damping, mechanical power input, and the electrical power output represented through the sinusoidal term.

Next, we substitute equations (3.11) and (3.12) into the swing equation above and expand the resulting expression. This gives:

$$\begin{aligned}\frac{d^2\theta}{dt^2} = -\frac{\omega_R D}{2H}\frac{d\theta}{dt} + \frac{\omega_R}{2H}P_m \\ - \frac{\omega_R V_G V_{B0}}{2HX_G}\sin\left[\theta - (\theta_{B0} + \theta_{B1}\cos(\Omega t + \phi_\theta))\right] \\ - \frac{\omega_R V_G V_{B1}}{2HX_G}\cos(\Omega t + \phi_v)\sin\left[\theta - (\theta_{B0} + \theta_{B1}\cos(\Omega t + \phi_\theta))\right] \quad (6.1)\end{aligned}$$

Now, simplifying equation (6.1) under the assumption that the quantities θ_{B0}, V_{B0}, ϕ_θ and θ_{B1} are sufficiently small (perturbative terms), we can reduce the expression to a more standard form:

$$\frac{d^2\theta}{dt^2} = -p\frac{d\theta}{dt} + q - r\sin\theta + f\sin(\Omega t) \quad (6.2)$$

where the constants are defined as:

$$p = \frac{\omega_R D}{2H}, \qquad q = \frac{\omega_R}{2H}P_m, \qquad r = \frac{\omega_R V_G}{2HX_G}, \qquad f = \frac{\omega_R V_G V_{B1}}{2HX_G}\cos(\Omega t + \phi_v) \quad (6.3)$$

In order to apply Hamilton's Principle, we first define the Lagrangian $L(\theta, \dot{\theta}, t)$ which consists of kinetic and potential energy terms, as well as non-conservative forces (such as damping) and external periodic excitation:

$$L(\theta, \dot{\theta}, t) = \frac{1}{2}\dot{\theta}^2 + q - p\dot{\theta} - \cos\theta + f\sin(\Omega t)\sin\theta \quad (6.4)$$

We then apply the Euler–Lagrange equation:

$$\frac{d}{dt}\left(\frac{\partial L}{\partial \dot{\theta}}\right) - \frac{\partial L}{\partial \theta} = 0 \quad (6.5)$$

After evaluating the derivatives and simplifying the result, we arrive at the following non-linear differential equation which governs the motion of the system:

$$\ddot{\theta} - \sin\theta + f\sin(\Omega t)\cos\theta = 0 \quad (6.6)$$

After plotting equation (6.6) with angle against time for the case of Hamilton's Principle, comparing this with Method of Strained Parameters and Floquet Theory for further analysis within the context of quasiperiodicity is the next step in the process.

Figure 6.1 is a graph that illustrates the gradual decrease in stability that occurs over the course of time, which ultimately leads to a condition of instability that is characterised

by quasiperiodicity. Throughout the course of time, the movement of the system becomes increasingly erratic and unpredictable, which demonstrates the system's sensitivity to the quasiperiodicity for all of the approaches that are taken into consideration. Based on the behaviour that was seen, it appears that the complex interaction between the system's inherent dynamics and the forces that are located outside of it could potentially result in chaotic motion.

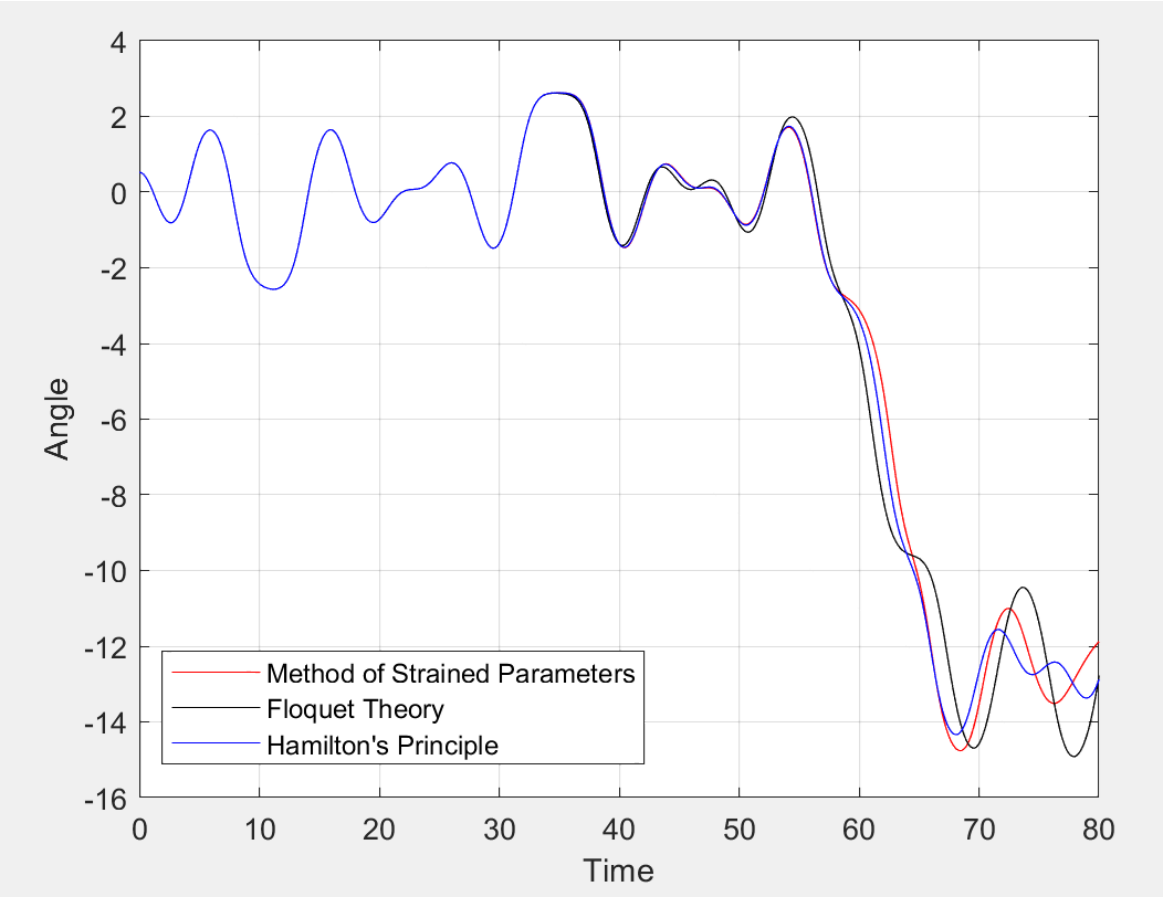

Figure 6.1: Simulation of the Swing Equation with the Hamilton's Principle comparing with Method of Strained Parameters and Floquet Theory when $\Omega = \pi/2$ rads^{-1} [115, 134].

6.5 Basins of Attractions for the case of Quasiperiodicity

The phenomenon of quasiperiodicity is of the utmost relevance when it comes to comprehending the characteristics of stability that are associated with a nonlinear system. Therefore, in order to get a comprehensive understanding of the system, it is absolutely necessary to carry out an in-depth investigation of the basins of attraction that are connected to the core resonance. The utilisation of basins of attraction makes it possible to distinguish between stable and unstable regions within a system, which in turn makes it easier to analyse the modifications that have been made to the system in question [139]. The charts depict the changes that occur in the basins of attraction as a result of the modifications made to the variables. In the process of generating conclusions from these graphs, it is of utmost importance to have the boundary conditions taken into consideration as well [140].

There have been major discoveries made on the stability characteristics of power systems as a result of research conducted on the basins of attraction of quasiperiodicity. An investigation has been conducted to examine the influence of parameter variations, which encompass system damping, excitation levels, and control gains, on the configuration and amplitude of the basins of attraction [98, 140]. Additionally, the majority of the research conducted by academics has concentrated on the discovery of critical borders that serve to differentiate between stable and unstable regions within the state space [99, 141].

6.6 Numerical Analysis

6.6.1 Graphical Representation

Through the use of the fourth-order Runge-Kutta method in Matlab, the equations (3.10), (3.11), and (3.12) were successfully solved. The primary objective was to investigate the impact of altering the excitation frequency Ω on the occurrence of quasiperiodicity with irrational values [77, 115].

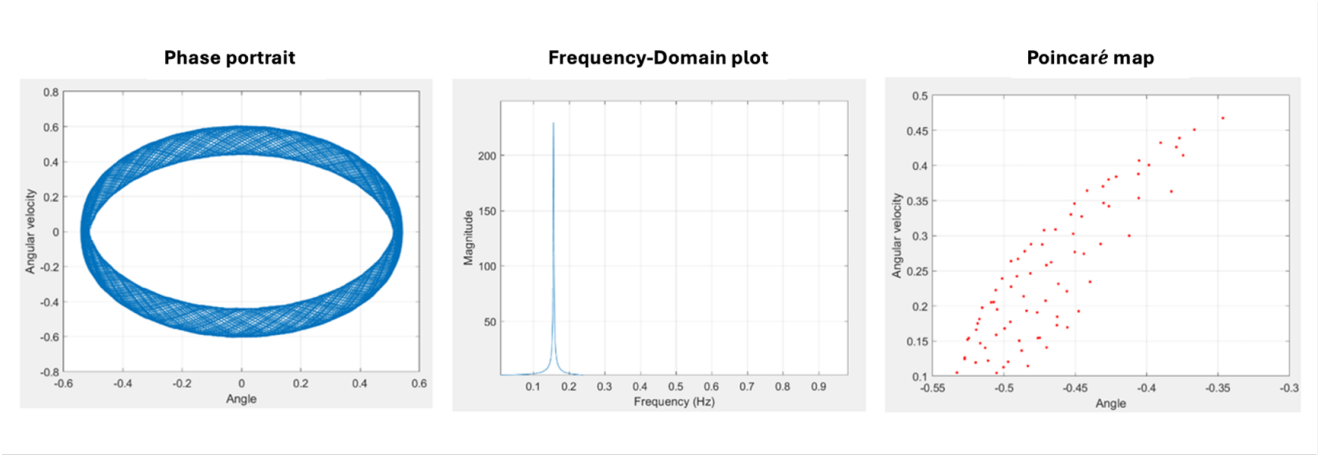

Figure 6.2: Phase portrait, frequency-domain plot and Poincaré map when $\Omega = 2\pi$ rads^{-1}.

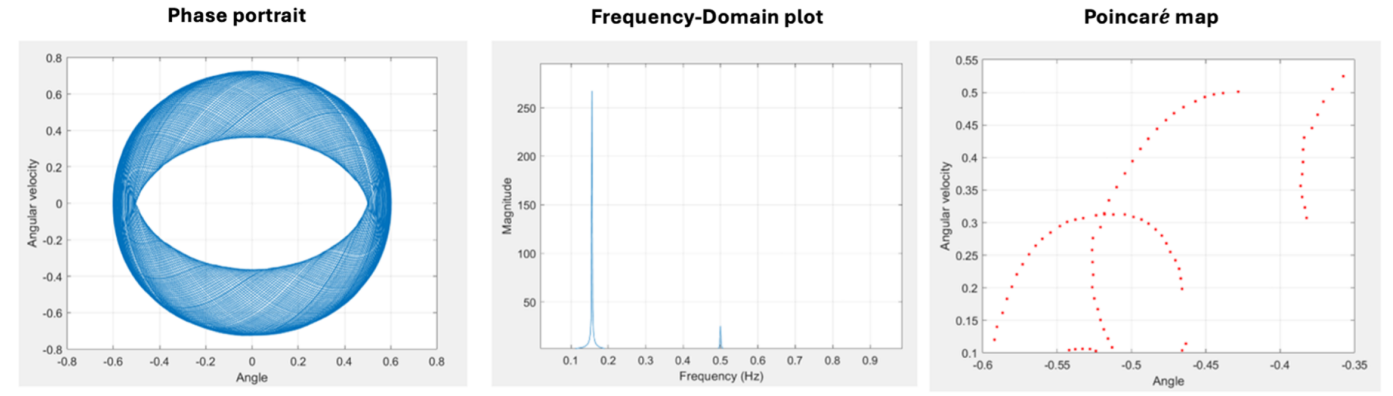

Figure 6.3: Phase portrait, frequency-domain plot and Poincaré map when $\Omega = \pi$ rads^{-1}.

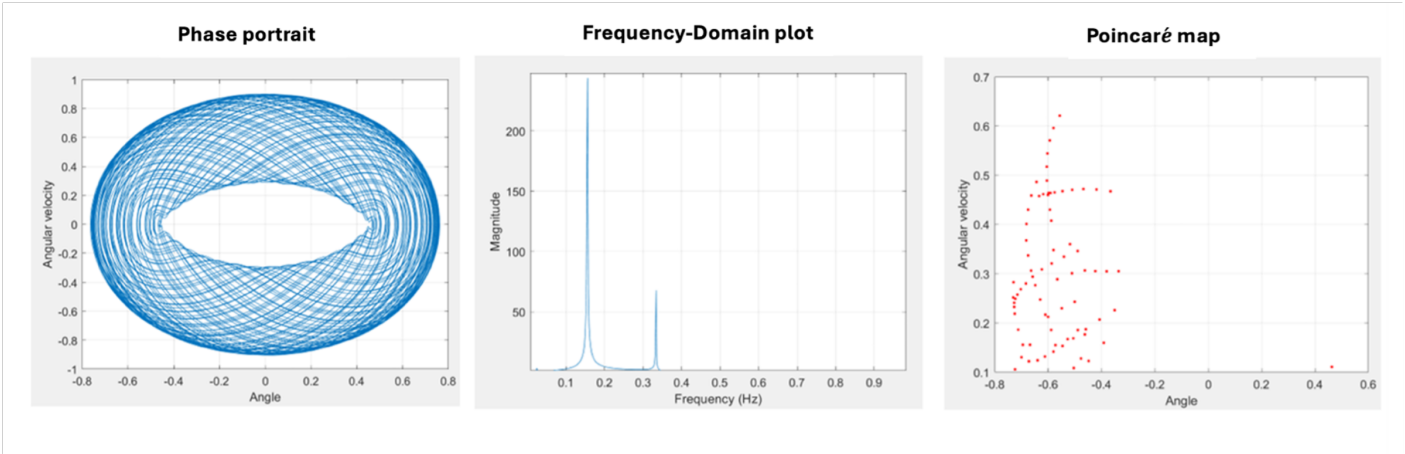

Figure 6.4: Phase portrait, frequency-domain plot and Poincaré map when $\Omega = 2\pi/3$ rads^{-1}.

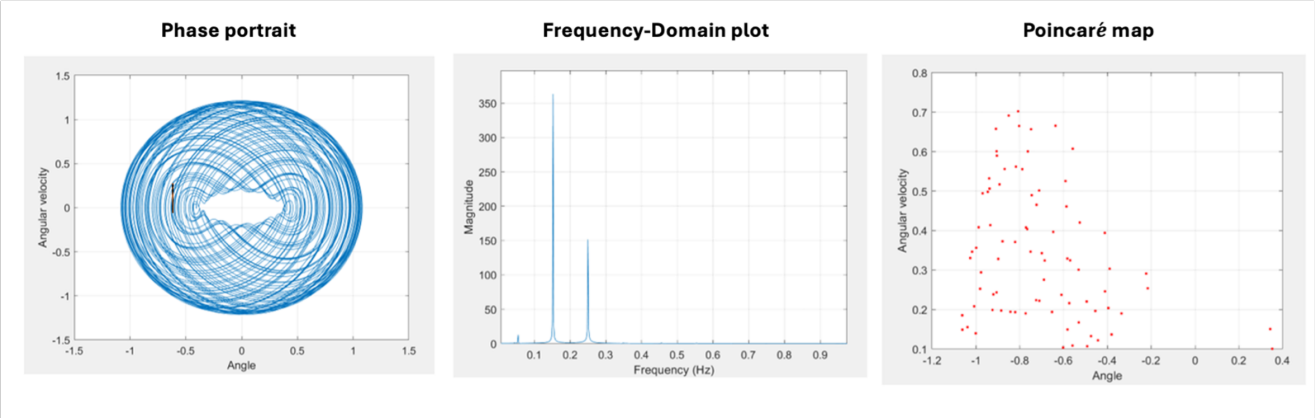

Figure 6.5: Phase portrait, frequency-domain plot and Poincaré map when $\Omega = \pi/2$ rads^{-1}.

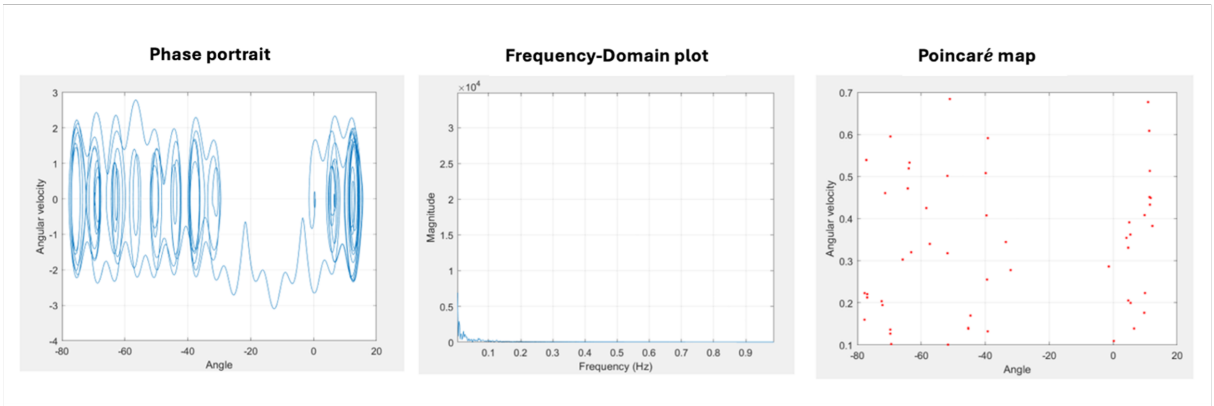

Figure 6.6: Phase portrait, frequency-domain plot and Poincaré map when $\Omega = 2\pi/8$ rads^{-1}.

The swing equation (3.10) was used to examine the system's response to variations in excitation frequency, and Figures 6.2 through 6.6 were constructed to visualise these changes. Each figure includes the corresponding phase portrait, frequency-domain plot, and Poincaré map. The dynamic effects of changing excitation frequency have also been documented in previous studies such as [110].

The selected excitation frequency values for this analysis were chosen to investigate the emergence of quasiperiodic motion and its transition into chaos. In particular, the values of Ω used in Figures 6.2 to 6.5 were carefully set to lie near incommensurate ratios with the system's natural frequency. This encourages the onset of quasiperiodicity, where the system's trajectory evolves on a torus in phase space. As depicted in these figures, the resulting attractors exhibit closed, nested loops indicative of toroidal motion rather

than simple periodic behaviour.

These torus structures suggest that the rotor dynamics of the synchronous generator are governed by two or more incommensurate frequencies, which is a defining characteristic of quasiperiodic motion. The excitation frequencies were gradually lowered in a controlled manner to capture the breakdown of these tori. Figure 6.6 demonstrates this progression, where the attractor degenerates into a strange attractor, confirming the transition to chaos. The chaotic attractor is identified at approximately $2\pi/8$ rad $\cdot$ s^{-1}, marking the endpoint of this route to chaos.

By selecting these specific Ω values, the study aims to illustrate the route to chaos, in which a system transitions from periodic to quasiperiodic dynamics, and eventually to chaos, through torus breakdown. Each frequency step was deliberately chosen to highlight a key phase in this transition, thereby offering insight into the delicate interplay between excitation frequency and nonlinear system behaviour.

6.6.2 Golden Ratio Number

The golden ratio (1.61803398875...), has captivated scientists and mathematicians due to its visually appealing qualities and distinctive mathematical importance [142]. Using the golden ratio as the angular frequency (Ω) in the swing equation makes it possible to conduct an insightful inquiry into the dynamics of quasiperiodicity. A number that is irrational is known as the golden ratio. When it is utilised as the driving frequency, it generates a relationship with other system properties that is not proportional to either dimension. Because of this, there is a possibility that complex quasiperiodic motion will occur. It is envisaged that the reaction of the system will exhibit compelling patterns and frequencies as a result of the introduction of the golden ratio, which will demonstrate the inherent complexity of quasiperiodic behaviour.

A graphical representation of the impact that the golden ratio has on the swing equation may be found in Figure 6.7. A perceptive picture of the system's trajectory as it evolves over time is provided by the phase portrait. This representation highlights the transitions that occur in the system's tilt and angular velocity across time. It is also an illustration of the torus phenomenon for the situation that is being considered. Poincaré

maps offer a concise representation of the behaviour of the system by illustrating the points at which the trajectory interacts with a specific plane through the use of mapping. Furthermore, frequency domain charts make it easier to investigate the spectrum features of the system by illuminating prominent frequencies and potential resonance in the system. The utilisation of the golden ratio in these analyses provides a unique viewpoint that enables one to observe and appreciate the intricate quasiperiodic patterns that emerge in the swing equation. This, in turn, allows a fascinating analysis of the dynamic behaviour of the system.

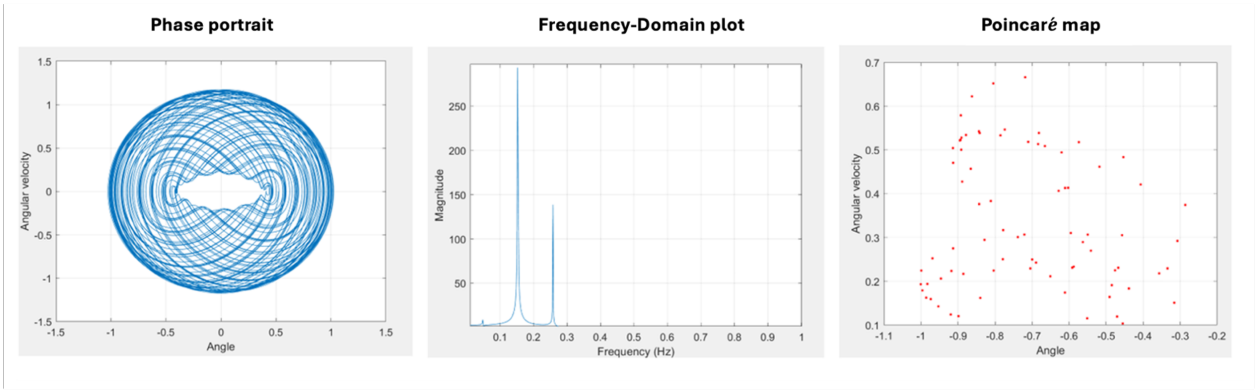

Figure 6.7: Phase portrait, frequency-domain plot and Poincaré map when $\Omega = 1.61803398875...$ rads^{-1}.

6.7 Bifurcation and Lyapunov Exponents

Diagrammatic representation of the bifurcation that is connected with the phenomena of quasiperiodicity is shown in Figure 6.8. After determining the swing equation for a particular angular frequency value of $\Omega = \pi/2$ rads^{-1}, the building procedure involved doing numerical time integration using the widely recognised fourth order Runge-Kutta method. This was done in order to construct the structure. The forcing parameter, which is denoted by the symbol r as shown in equation (3.65), is gradually increased, and the time integration procedure is subsequently extended as a result of this. According to the authors, the data that was acquired is then utilised to build a graph that illustrates the largest amplitude of the oscillatory solution in relation to r as in equation (4.53) [77].

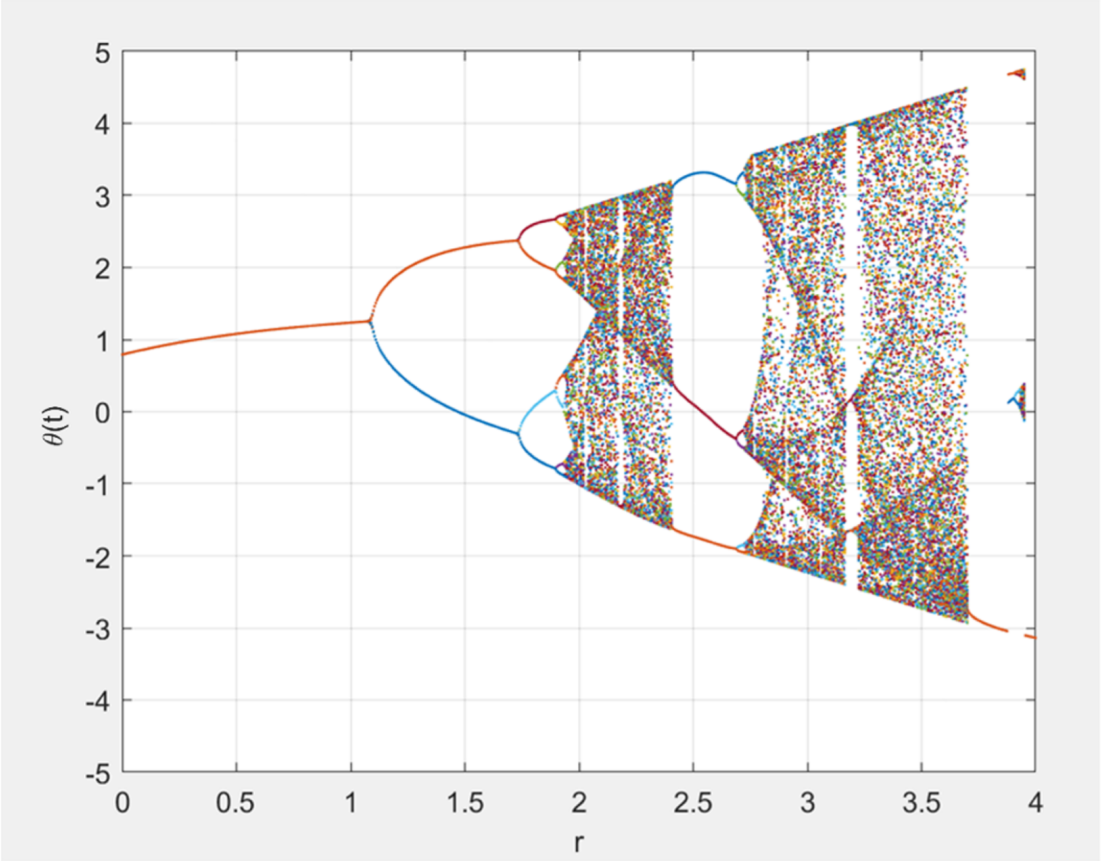

Figure 6.8: Bifurcation diagram for the case of Quasiperiodicity where $\Omega = \pi/2$ rads^{-1}.

Figure 6.8 also illustrates the occurrence of the initial period doubling just before to reaching a value of r that is equal to 1.085 in the case of quasiperiodicity. This is shown in the figure above. Additionally, it is clear that the first instance of period doubling in a series of repeated period doublings is observed at around $r = 1.94$, which ultimately results in the emergence of chaotic behaviour. This is the result of a chain of period doublings that occur in succession. The findings of this numerical component indicate that an increase in the value of parameter r leads to a progressive loss of synchronisation in the swing equation, particularly in regard to quasiperiodicity. This is demonstrated by the fact that the synchronisation gradually deteriorates.

To a large extent, the Lyapunov exponent, as depicted in Figure 6.9, exhibits positive values in the region surrounding the values of $r = 1.9$. Within the context of this scenario, two locations that are initially very close to one another and are separated by an incredibly short distance eventually move further apart from one another over the course

of time. The utilisation of Lyapunov exponents is what allows for the quantification of this divergence to be achieved. Additional corroboration of the phenomenon that was reported earlier is provided by the behaviour that was found in the bifurcation diagram. To provide a more exact explanation, when the value of r hits a specific threshold, a series of period doublings takes place, which ultimately leads to chaotic behaviour. Therefore, it is possible to draw the conclusion that the existence of a chaotic attractor is indicated by the presence of a positive Lyapunov exponent within the system.

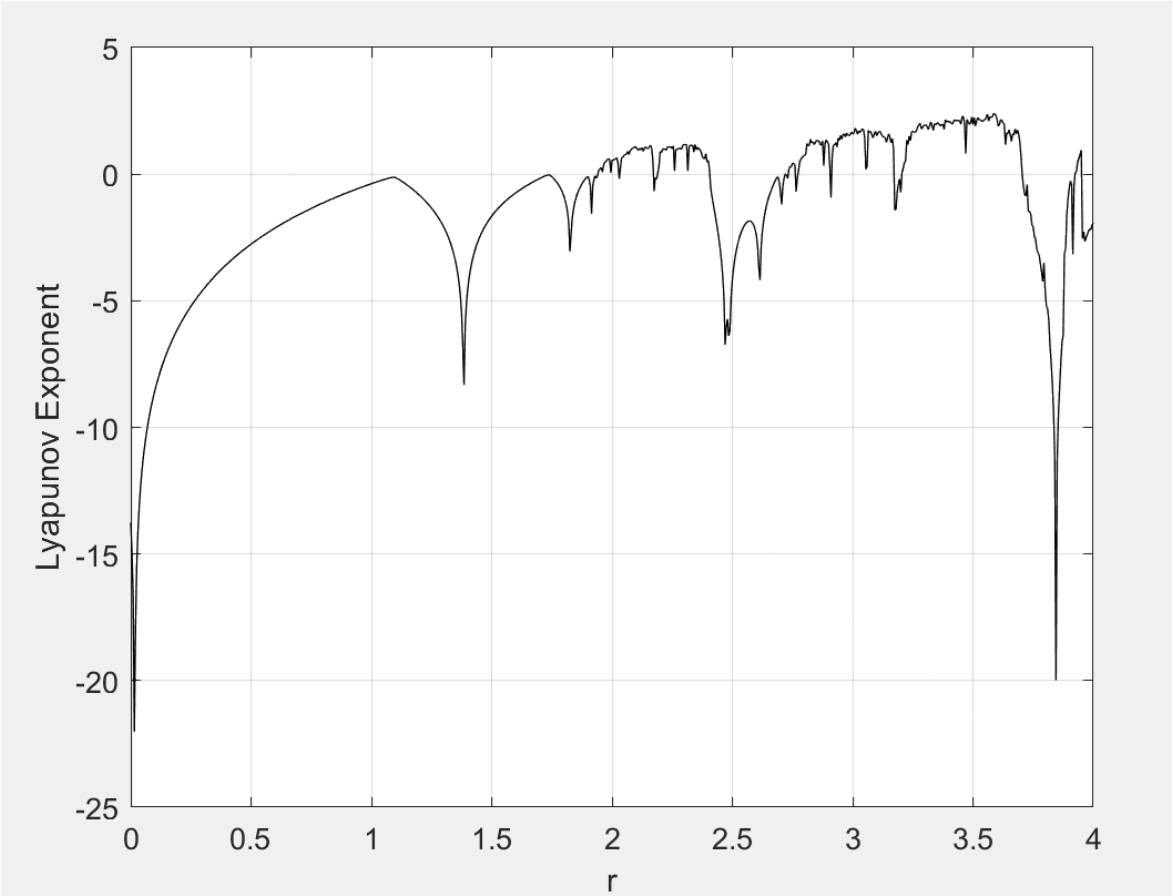

Figure 6.9: Lyapunov exponents as r is varied for quasiperiodicity.

6.8 Comparison of Routes to Chaos for the case of Quasiperiodicity and Primary Resonance

In the process of contrasting the disorder in quasiperiodicity with the primary resonance in the swing equation, it is possible to detect distinct variations in the manner in which the system reacts to the influence of external factors. The term quasiperiodicity describes a circumstance in which the frequency of driving is not a clear rational multiple of the frequency obtained from the natural frequency. In these kinds of situations, the swing equation exhibits patterns that are both complicated and non-repetitive. It is important to note that the complexity of quasiperiodic behaviour is highlighted by the fact that the system is responsive to starting conditions and eventually separates on its courses. On the other hand, when the external frequency coincides with a natural frequency mode, the swing equation can undergo period-doubling bifurcations and ultimately move into chaos. This occurs in primary resonance.

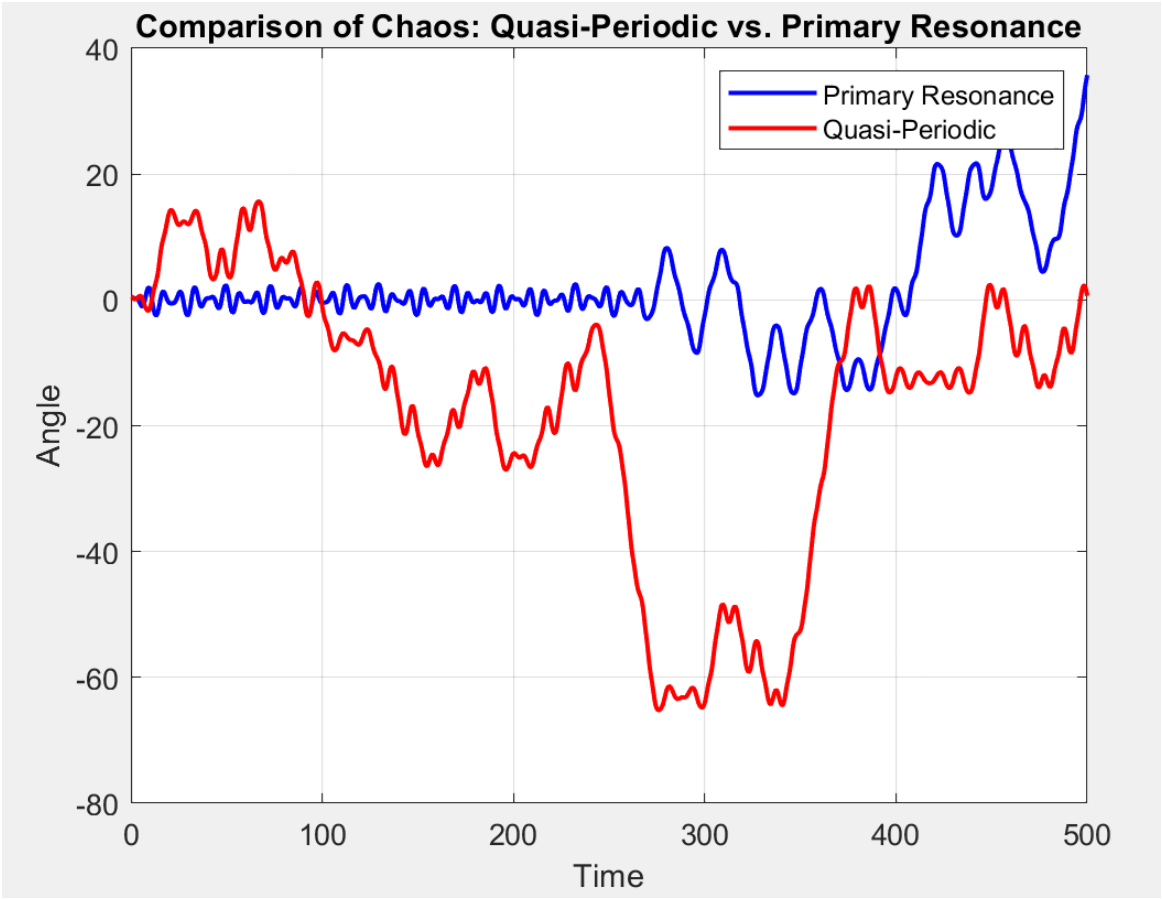

Figure 6.10: Comparison of chaos in the case of Quasiperiodicity($\Omega = 8.27+\pi/2$ rads^{-1}) vs the Primary Resonance ($\Omega = 8.27$ rads^{-1}).

Figure 6.10 is a graph that provides a visual representation of the temporal progression of chaos in quasiperiodicity as contrasted to primary resonance in the swing equation. The primary resonance is believed to be at $\Omega = 8.27$ rads^{-1}, and for the quasiperiodicity, it is therefore considered to be closer to the primary resonance at $\Omega = 8.27 + \pi/2$ rads^{-1}. The graph depicts the irregular trajectories and the early emergence of chaotic behaviour in the quasiperiodic scenario. It also highlights the enhanced susceptibility of the system to slight variations in parameters, which is a characteristic of quasiperiodic dynamics. Compared to the more organised and predictable behaviour associated with primary resonance, this result reveals a tendency for faster transitions into chaotic states, which underscores the necessity of comprehending and tracking the quasiperiodic regime. This is because it demonstrates quicker transitions into chaotic states. When conducting an analysis of the dynamics of the swing equation, it is important to take into consideration both of the possibilities, as the graph illustrates. It provides an in-depth analysis of the

intricate link that exists between the external force and the response of the system.

6.9 Basins of attractions for the case of Quasiperiodicity

The basins of attraction for the case of quasiperiodicity are depicted in Figure 6.11, Figure 6.12, Figure 6.13, and Figure 6.14, respectively. The graphics presented here illustrate the fluctuations that occur in the variables V_{B1} and θ_{B1}, while maintaining the value of Ω at $\pi/2$ rads^{-1}. As the variable is increased, there is a possibility that the stability of the system will be altered. It is clear that the areas of the system that are stable are represented by the presence of the colours red and green, while the other colours are indicative of the regions that are unstable. As the value of the independent variable increases, the system goes through a stage of degradation that is characterised by the presence of unstable zones. For this reason, it is very necessary to conduct an exhaustive investigation into the influence of other components inside the system in order to guarantee the validity and robustness of the conclusions that were reached in this particular research.

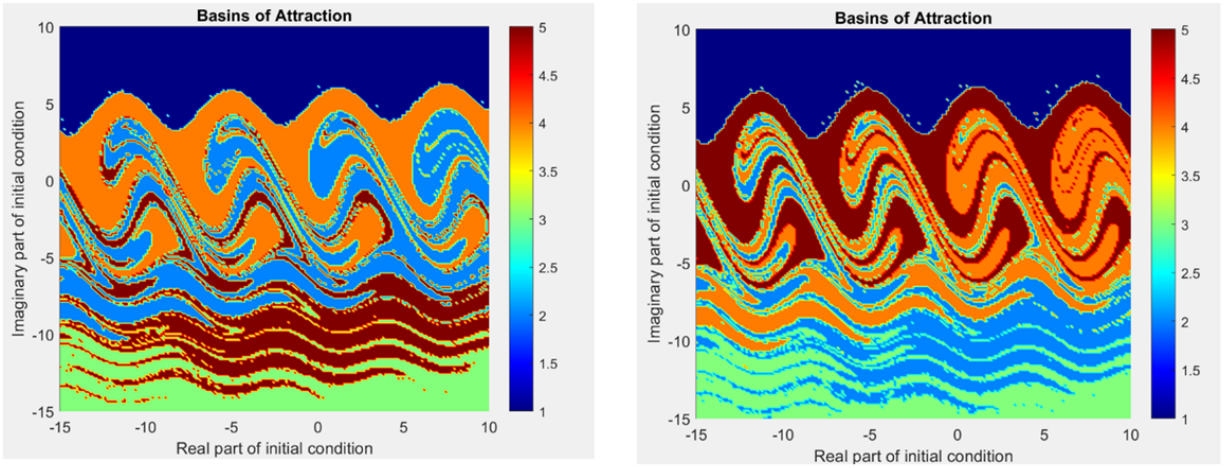

Figure 6.11: Basins of attractions when V_{B1} is 0.051 rad and 0.062 rad respectively for Ω= $\pi/2$ rads^{-1}.

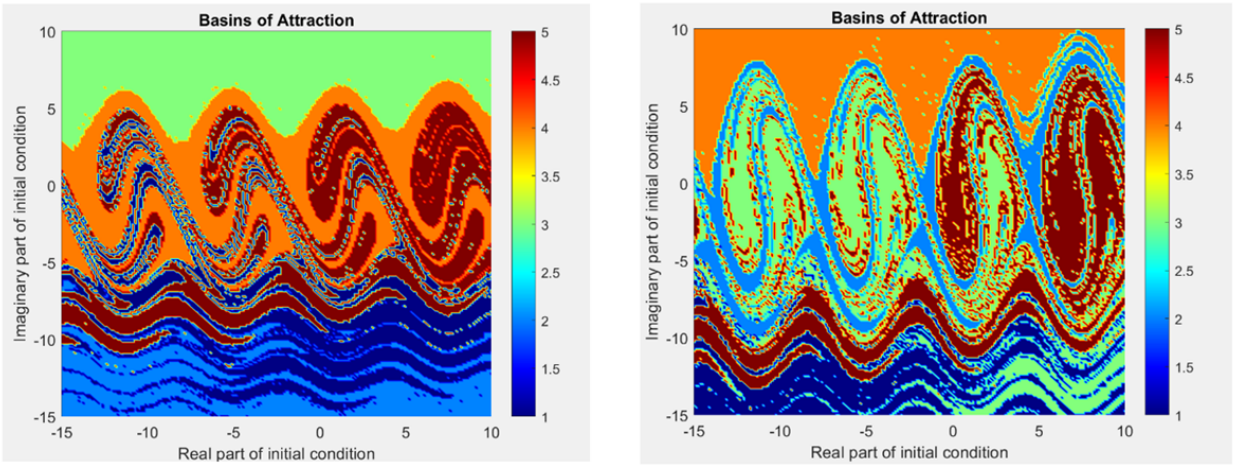

Figure 6.12: Basins of attractions when V_{B1} is 0.071 rad and 0.151 rad respectively for $\Omega = \pi/2$ rads^{-1}.

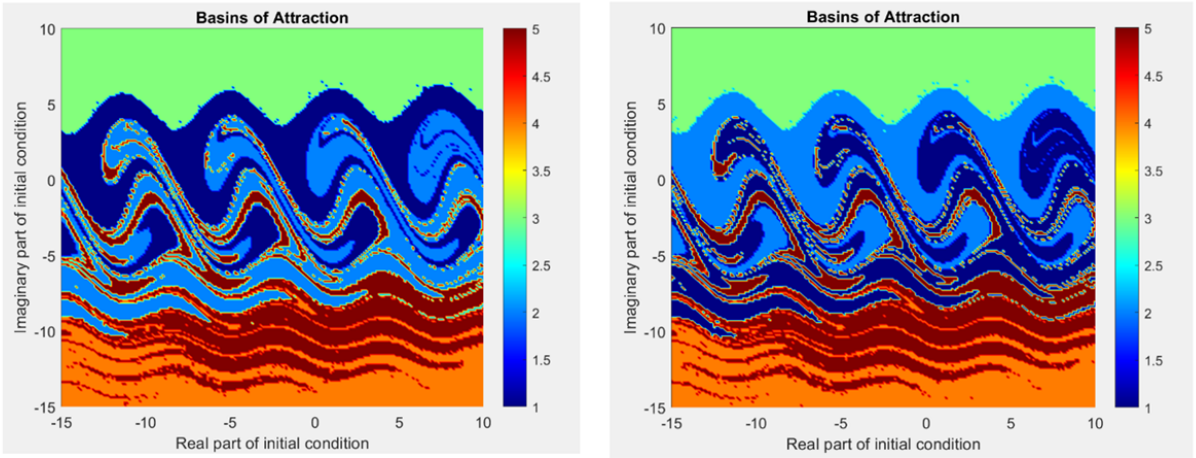

Figure 6.13: Basins of attractions when θ_{B1} is 0.101 rad and 0.05 rad respectively for $\Omega = \pi/2$ rads^{-1}.

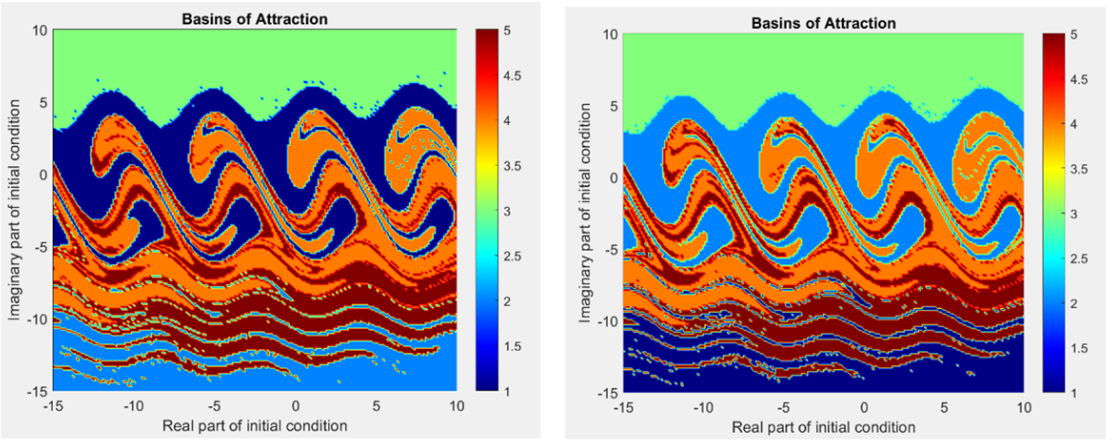

Figure 6.14: Basins of attractions when θ_{B1} is 0.07 rad and 0.181 rad respectively for Ω= $\pi/2$ rads^{-1}.

6.10 Stability Reduction

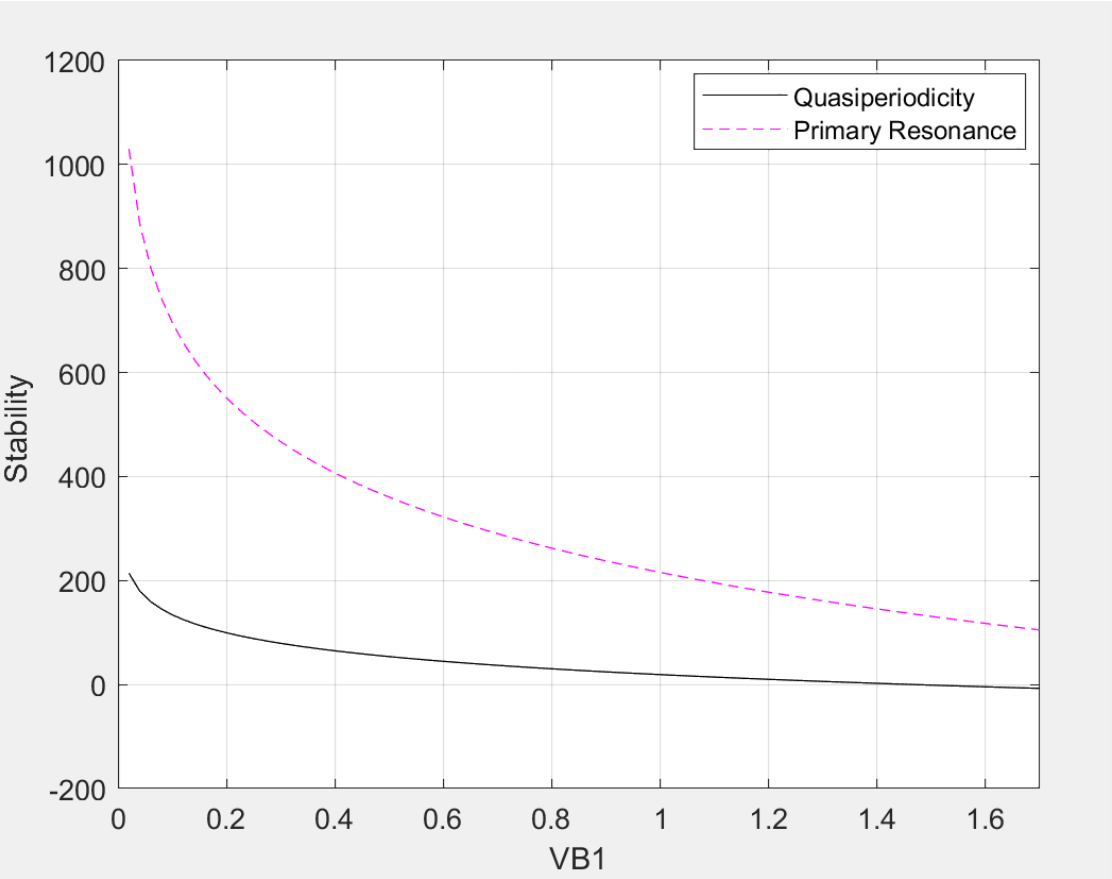

Figure 6.15: Comparing the reduction in stability region for Primary Resonance (Ω=8.27 rads^{-1}) and the case of Quasiperiodicity ($\Omega = 2\pi/8$ rads^{-1}).

The Lyapunov exponents are utilised in the analysis of two different instances of stability degradation in the swing equation, which is depicted in Figure 6.15. When considering the first situation, the estimated value of Ω is to be 8.27 rads^{-1}, which is the frequency that represents the primary resonance. The system is subjected to a driving force that corresponds to its resonant frequency, which results in a gradual reduction in its amplitude. In this case, the value of Ω is investigated by utilising the expression $\frac{2\pi}{8}$ rads^{-1}. This particular expression represents a quasiperiodicity frequency that is distinct from the natural frequency of the system. Within this context, the machine displays a quasiperiodic response as a result of the frequency at which the driving force is given.

According to authors, the Lyapunov exponents offer valuable insights into the stability of a dynamical system, namely the rate at which nearby trajectories either converge

or diverge over the course of time [46]. Within the framework of the swing equation, which is a mathematical expression that represents the movement of a system that is influenced by an external force denoted by V_{B1}, Lyapunov exponents can be utilised to assess the impact of increasing V_{B1} on the stability of the system. Through the process of incrementing V_{B1}, it becomes feasible to compute the Lyapunov exponents at each and every iteration. It is possible to see a loss in stability when there is a transition from negative exponents to less negative or even positive exponents. This is an indication of diminished stability. A steady path is shown by a negative exponent, which indicates that the perturbations in the system are decreasing with time [23, 143]. Consequently, if the Lyapunov exponents fall in size or change sign as the value of V_{B1} increases, this indicates that there is a significant decline in stability. The fact that this is the case suggests that the system is more susceptible to the beginning conditions and that its conduct is less predictable.

As the variable V_{B1} is changed, the Lyapunov exponents provide a precise measurement of the stability of the swing equation. This is important since the swing equation is stable. An observable decline in stability is implied by changes in the exponents, which imply an increased sensitivity of the system to shocks as V_{B1} grows.

6.11 Discussion

The fundamental purpose of this segment is to carry out an in-depth analysis of the dynamic features that are displayed by the swing equation when the control parameters are changed, with a specific emphasis on the complex phenomena of quasiperiodicity as the key area of investigation. An examination of the similarities and differences between analytical methods, particularly perturbation techniques, and numerical simulations is carried out in the course of this investigation. The goal of this comparison is to determine whether or not the perturbed solutions and the basins of attraction that correspond to them are accurate. The purpose is to obtain a full understanding of the quasiperiodic dynamics and the influence that these dynamics have on the stability of the power system. This was accomplished through the use of the analytical technique known as Hamilton's Principle.

It is necessary to make use of analytical techniques and methodologies in order to

conduct an analysis of the resonances that are intrinsically present in the swing equation. Specific insights that are seen on fewer assumptions can be obtained by the utilisation of these techniques, which involve the use of mathematical modelling and computations. It is possible, on the other hand, that their efficiency will decrease when they are confronted with the complexity of actual power networks. By combining numerical and computational tools into Hamilton's Principle, it is possible to solve this limitation, which in turn makes it possible to conduct a more in-depth investigation of how the system reacts to a range of the many scenarios that may arise. Utilising graphical representations, which are obtained from numerical calculations, it is possible to produce a visual depiction of how the swing equation performs under various parameter values and forcing frequencies for the scenario of quasiperiodicity. This may be accomplished by using the process of graphical representations. In order to acquire a more profound understanding of the information that was collected using analytical approaches, these graphical representations are of great use. Using this all-encompassing methodology, power system engineers are able to make well-informed decisions, which is necessary for the purpose of ensuring the grid's reliable functioning in the face of quasiperiodic dynamics.

When it comes to scenarios that occur in real life, it is of the utmost importance to have a solid understanding of the predicted reactions of the system, particularly when quasiperiodicity is present. An illustration that is pertinent is provided by load fluctuations, which are something that regularly occur in power systems. The information that is gathered from these events is extremely important for the management of the power system, as it contributes to the upkeep of the system's dependability and stability. Furthermore, the conclusions that were gained from this research have consequences for the development and evaluation of control systems, namely in the fields of loading frequency management and autonomous generation control. When it comes to efficiently lowering the risk of blackouts and the terrible ramifications that they can have, having a solid understanding of the quasiperiodic dynamics that are involved in the swing equation is absolutely necessary.

6.12 Final Remarks

In order to carry out an in-depth investigation into the complex dynamics of the swing equation within the realm of quasiperiodicity, this extensive analysis utilised a wide range of analytical methods, such as bifurcation diagrams, Lyapunov exponents, phase portraits, frequency domain plots, and Poincaré maps. An oncoming shift towards turbulence is indicated by the introduction of complex behaviours, such as the repetition of periods in sequences of bifurcations. This shift may result in the formation of operational issues and may potentially represent hazards to power systems depending on the circumstances.

The results provided light on the relevance of chaos induction, which is caused by the collapse of quasiperiodic torus structures and the presence of intermittency in the swing equation. The findings of the research shed light on the significance of chaos induction. One example of the system's vulnerability to quasiperiodic transitions is the phenomenon known as period doubling, which is widely recognised. This occurrence is an example of the system's instability. the goal is to investigate such effects in order to better understand how the behaviour of the system is affected by changes in parameters. The outcomes of this inquiry will provide insights into the alterations that are observed both before and after the onset of chaotic behaviour from the perspective of the observers.

It expands upon the recent academic research conducted by the same group of researchers, further developing their previous findings. It aims to enhance existing approaches by offering a more profound understanding of the underlying mathematics, rather than replacing them. This research contributes to the improvement of control strategies and preventive measures for power systems by enhancing the understanding of fundamental principles and system stability, with a specific focus on quasiperiodicity. It aims to mitigate the chaotic effects caused by the phenomena of quasiperiodicity benefiting power system engineers and researchers.

The findings obtained from this work provide a clear grasp of how the swing equation behaves in the presence of quasiperiodic conditions, thereby making significant contributions to the comprehension of system stability. These discoveries could lead to improvements in the creation of power infrastructures that are more durable and safe, especially as power systems face more intricate issues throughout expansion.

In the future, scholars might look at how to include quasiperiodic circumstances in

the framework of swing equations. This may provide important new information about the long-term stability and flexibility of electricity systems. These initiatives have the potential to deepen the knowledge of these intricate nonlinear systems and produce improvements that increase their robustness.

Chapter 7

Analysing the Swing Equation using Matlab Simulink

7.1 Introduction

Matlab is a widely recognised software application employed by numerous researchers for data analysis. In addition, it facilitates the solution of differential equations and the generation of graphical representations, thereby establishing a strong foundation for deeper understanding. Among its various components, the most frequently utilised is Simulink.

Simulink enables the modelling of circuit equations and supports the simulation of reliable data using user-defined inputs. The electrical and electronics industries have undergone significant transformation in recent years, in part due to the capability to simulate a wide range of circuit behaviours.

To accommodate users' specific design requirements, Simulink offers a block diagram interface. This allows users to select and utilise various block diagrams available within its library to construct their desired models for analytical purposes. In the context of this investigation, the swing equation is modelled using Matlab Simulink to conduct both analytical and numerical analyses of the results from a practical standpoint .

Although Matlab Simulink was developed relatively recently, it is currently employed across a wide range of industries and disciplines [144]. It is also used to simulate digital power systems, enabling the examination of data derived from complex post-processing

results [145]. Several authors have developed a simulation toolbox based on power systems that features a user-friendly interface and functionality [146].

Furthermore, a power system model has been proposed by researchers that can be extended for use in various electrical and mechanical systems to explore the interactions between them [147]. In the context of electromechanical systems, multiphase models can also be effectively described and simulated using the Matlab programming environment [148]. Additionally, Matlab has played a significant role in the modelling and design of various fault conditions, facilitating the analysis of their impacts in order to mitigate such adverse effects [149].

The modelling of wireless networks and the investigation of distortion have both been accomplished with the help of Simulink in the setting of nonlinear dynamics [150]. Researchers now have the opportunity to expand their understanding of a variety of systems as a result of this event. A case study is used to highlight the practicability of implementation in the simulation environment in terms of representation and control of nonlinear processes [151]. The authors also employed the adaptive cruise control model as the main focus of the study. The models of any arbitrary nonlinear system are also subjected to an analysis for the purpose of analysing them in Matlab [152]. For the purpose of gaining an understanding of the principles of transfer functions, research is carried out on the computer simulation of nonlinear control systems that are specified in the form of so-called generalised transfer functions [153].

Figure 7.1 presents an example circuit simulation of a synchronous power system, developed by the authors in [154] using Matlab Simulink. This diagram illustrates a model of a transmission system supplying a gearbox line over a distance of 300 kilometres. A shunt inductor is placed at the receiving end to compensate for reactive power. The system parameters, including a voltage level of 735 kV, are based on realistic high-voltage transmission system values typically used in long-distance power delivery networks, such as those in North America or large-scale grid infrastructure projects.

These specific values were adopted from the referenced study to serve as a practical and illustrative benchmark for modelling power systems in Simulink. The 735 kV voltage level is commonly used in extra-high voltage (EHV) transmission networks, as it allows for efficient long-distance power transfer with reduced line losses. Similarly, the 300 km transmission length represents a realistic scenario where line inductance and capacitance

significantly influence system dynamics, making it suitable for studying phenomena such as transient stability and resonance topics central to the swing equation.

This figure was included in the thesis to demonstrate how such a system can be translated into a Simulink model, and to highlight the components relevant to the swing equation analysis presented in this research. The diagram helps to visualise key elements of the power system, including synchronous generators, transmission lines, compensating devices (e.g., shunt inductors), and loads. Understanding the layout and interactions of these components is crucial for correctly configuring the simulation model. This ensures that the swing equation-based model accurately reflects the physical behaviour of real-world power systems, thereby improving the validity and applicability of the numerical results obtained in subsequent chapters.

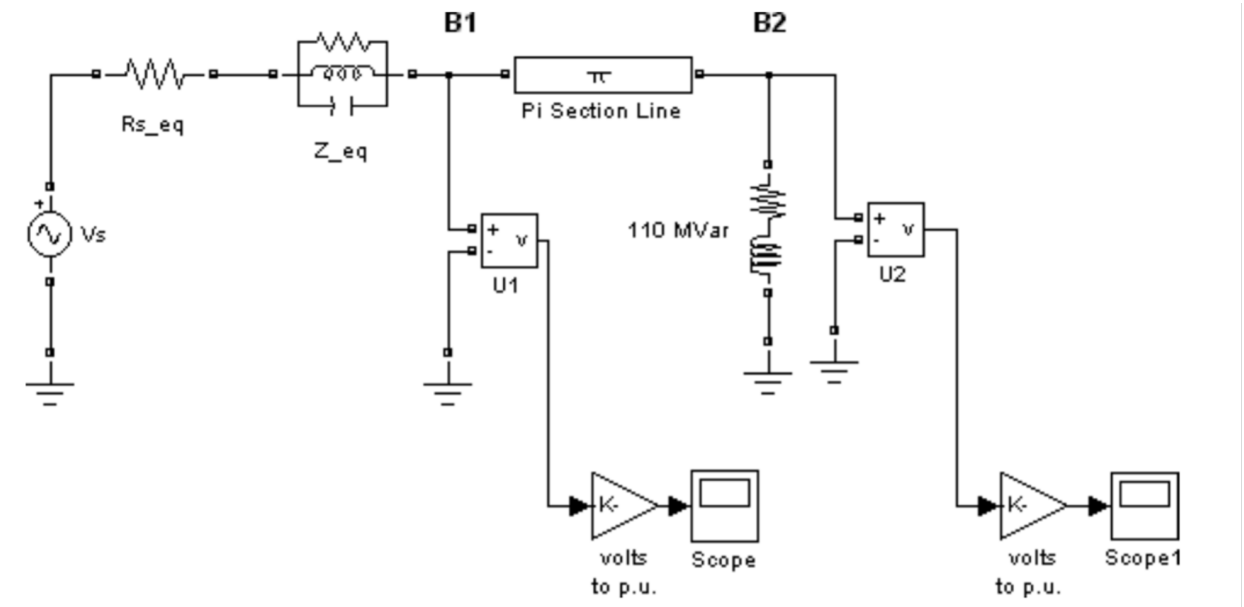

Figure 7.1: Example of a synchronous circuit produced on Matlab Simulink [154].

Simulink offers a flexible platform for modelling intricate dynamical systems, enabling researchers to precisely simulate the behaviour of power circuits and analyse the real-time dynamics of the swing equation. Researchers can utilise the swing equation circuit in Simulink to investigate different situations, modify system parameters, and visually analyse the power system's transient response to shocks.

Furthermore, Simulink provides a user-friendly interface that includes a wide range of pre-built blocks for electrical components. This greatly simplifies the task of developing and simulating the swing equation circuit model. Scientists may incorporate different

components of the power system, including generators, transmission lines, and loads, into their simulations, conducting a thorough examination of system dynamics. Moreover, Simulink offers sophisticated data visualisation tools that allow researchers to properly understand simulation results and obtain significant insights into the power system's behaviour.

Additionally, it simplifies the process of verifying theoretical models and experimental results by conducting simulation-based experiments. Researchers can assess the correctness and dependability of the swing equation model by comparing simulation results with empirical data or analytical answers. This verification process ensures that the model is suitable for forecasting the behaviour of real-world power systems. The validation phase is essential for establishing the legitimacy of the findings and demonstrating the practical applicability of the swing equation technique in addressing stability and reliability issues in power circuits.

The circuit simulation developed in Matlab will be used to support and guide the modelling and analysis conducted in this research. Hence this research should focus on building a circuit model for the synchronous generator considered for the rotor of the machine explaining the swing equation to study the dynamical behaviours.

Matlab Simulink is used to verify the swing equation, which has been examined numerically and analytically in this research. This will strengthen understanding of the equation with analytical results. This will establish a safe foundation for doing an analysis of the differential equation model and keeping track of changes in the parameters in Simulink. In order to discover the results that were anticipated, it is possible to investigate the intricate behaviour of the system by manipulating the simulated model with very tiny disruptions. The findings that are provided by the models will indicate the rate at which the system becomes unstable as well as the precise moment when it takes place.

The swing equation, illustrating the nonlinear behaviour of synchronous generators, has been extensively analysed in many research papers in recent years. These models are essential for assessing the stability of intricate synchronous machines within dynamical systems. Researchers have employed Simulink to develop advanced swing equation models that eliminate simplifying assumptions, yielding a more accurate representation of system dynamics [77, 155]. The enhanced models have been utilised to assess the performance of synchronous generators under diverse conditions, including connections to steady loads

or infinite buses, providing critical insights into stability and frequency regulation, [156], [157]. Moreover, Matlab Simulink offers explicit visualisation when various excitation frequencies are analysed within the systems [158].

The swing equation analyses the dynamic behaviour of the machine's rotor and minor external disturbances [77, 155]. Research has demonstrated that adjusting specific variables in the equation yields distinct behavioural patterns inside the system. Consequently, the system encounters challenges in reverting to its former state, displaying minimal changes that ultimately result in chaos within the structure [116]. Examining the fundamental tenets of chaos theory will provide essential understanding for the management of the nonlinear system [23].

The swing equation is initially modelled in Matlab Simulink, where primary resonance, subharmonic resonance, and quasiperiodicity are studied by varying the system's excitation frequency. The generated results were subsequently examined and validated against the analytical and numerical findings from prior works by the same authors [77, 115, 134, 159]. Various choices of Ω were examined, and Poincaré maps were generated to juxtapose the analytical approaches with the Simulink model, so deriving robust findings for this study.

This chapter seeks to understand the modelling of the swing equation using Simulink and to validate the analytical methods employed to enhance comprehension for academics and researchers. Therefore, the aim is to emphasise progress in the examination of the swing equation through a Matlab model and to concentrate on comprehending this model to provide novel insights into persistent issues related to the stability of dynamical systems.

Matlab Simulink models are essential for analysing the complex behaviour of nonlinear systems. It facilitates the modelling, simulation, and comprehensive analysis of intricate power systems, [160]. This enables engineers and researchers in the electrical domain to visualise the system on a digital computer prior to executing the procedures on actual power grids [161, 162]. Storage facilities utilise Simulink models to analyse processes at varying speeds and loads, hence ensuring system safety [163]. It facilitates the modelling and simulation of systems, hence enabling the creation of innovative chaotic systems exhibiting diverse dynamic behaviours [164].

Numerous studies have explored various uses and approaches within the realm of Simulink modelling. Simulink models have been employed for detecting defects in

control systems and simulating power systems by deconstructing complicated components [165–168]. These models have also been employed in the examination of vehicle gearboxes and memristors within chaotic systems [169–171].

This work additionally analyses the integrity diagrams for primary resonance, subharmonic resonance, and the case of quasiperiodicity when the variable is modified. An analytical method utilising the isolated resonance approximation can be employed to derive integrity diagrams and ascertain their limits before the onset of period doublings [172, 173]. Stochastic bifurcation limits are established by this method, taking into account various amplitudes and beginning circumstances [174, 175]. Attractors lose stability in the absence of chaos when a system enters a bistable state [176, 177].

Primary resonance occurs when the excitation frequency of the system closely matches its natural frequency, whereas subharmonic resonance transpires when disturbances are integer multiples of the natural frequencies. Both resonances may lead to system instability and equipment damage [79, 178]. Techniques like the incremental averaging method and various scales provide accurate analytical solutions that elucidate the resonant behaviour of nonlinear systems, including Duffing oscillators with diverse damping processes [179, 180]. Furthermore, the examination of subharmonic resonance is utilised for diagnostic imaging with ultrasonic contrast agents [181]. Quasiperiodicity occurs when the frequency ratio is an irrational number. All three scenarios are analysed using the Simulink model. Studying all three situations is essential for a comprehensive knowledge of the dynamics of the swing equation system.

Bifurcation diagrams serve as an effective instrument for analysing integrity diagrams in dynamics, as noted in numerous research publications. They furnish essential insights about the dynamical behaviour of the system and its stability [182–184]. Hamiltonian systems employ bifurcation diagrams to analyse the complex and chaotic behaviour within this field [185]. Therefore, it is essential to analyse and acquire bifurcation diagrams for nonlinear systems to comprehend the intricacies of the structure, facilitating a comprehensive examination for future research.

7.2 The Swing Equation Model from the Matlab Simulink

The swing equation, denoted as equation (3.10), elucidates the electrical and mechanical torque of the machine's rotor and examines the behaviour of the rotor's angle and speed in response to a minor perturbation. Analysing the machine's acceleration and torques establishes a robust basis for engineers to address challenges inside the systems [172]. Therefore, modelling this concept to acquire real-time values will be optimal for a detailed examination of the equation.

The rotor of the machine, as described by the swing equation, elucidates the complex interactions between the electrical and mechanical components of the system. Therefore, examining the stability of this machine is essential to understand the sudden changes in the parameters of the equation. Stability can be assessed by varying the load and inputs of the systems over time, hence mitigating the cascade of chaos inside power systems, [180].

The Simulink model depicted in Figure 7.2 was employed to investigate the swing equation for this investigation.

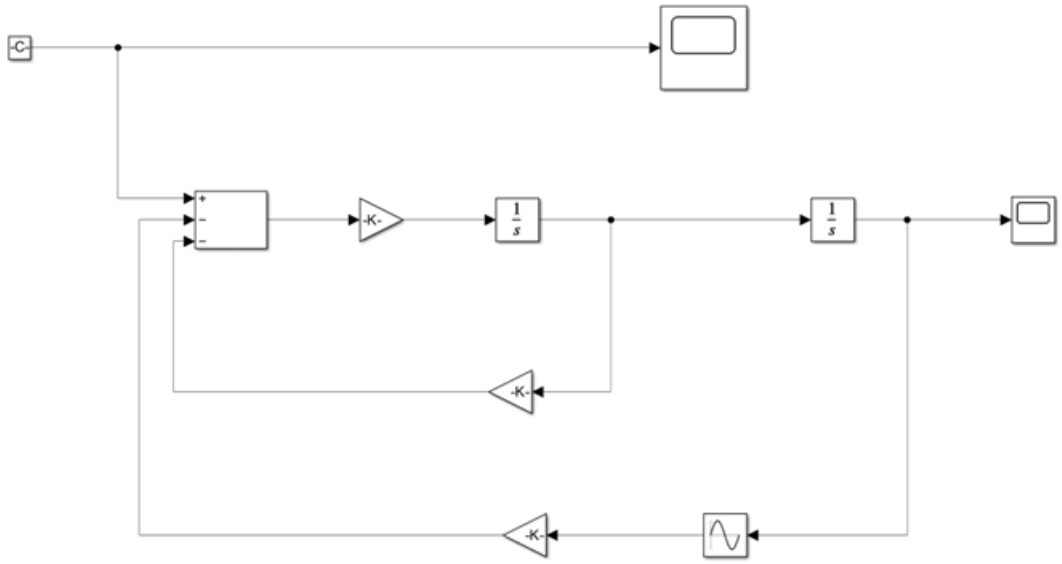

Figure 7.2: MATLAB Simulink model used to represent the Swing Equation.

7.3 Integrity Diagrams

Integrity diagrams are essential in nonlinear dynamics since they facilitate the assessment of the dynamic integrity of systems. These diagrams are essential for assessing the safe basin and erosion profiles, which are critical instruments for studying dynamic integrity, [186]. The concept of dynamical integrity has emerged as a crucial factor in structural design, with extensive study focused on the management of basin erosion processes, [187]. The notion of global safety, an innovative methodology for assessing systems, has significantly impacted the study, regulation, and design of mechanical and structural systems. The integrity diagrams are essential for preserving the stability and performance of the nonlinear system, [188]. This is demonstrated by studying vibrational systems, both with and without discontinuities, [189]. Nonlinear robust control techniques require integrity diagrams to illustrate solutions when several variables are influenced by external disturbances, [190].

These diagrams employ surrogate models to reduce simulation time, maintain accuracy, and facilitate integration into circuit simulators for comprehensive setup analysis throughout the design phase. Adjustable dead bands are examined in networked control systems to reduce network traffic. The main focus is on stability analysis with robust stability theory, [191]. Furthermore, nonlinear robust control techniques that depend on integrity are utilised to tackle unmodeled dynamics and uncertainties in multivariable systems, hence ensuring both robustness and feasibility, [192].

7.4 Results from the Simulink Model

7.4.1 Primary Resonance

The results for primary resonance was obtained for the Simulink model. Figure 7.3, Figure 7.4, Figure 7.5, Figure 7.6 and Figure 7.7 show time series, phase portraits and Poincaré maps that were plotted and compared to the analytical results obtained from the previous research work, [77]. The produced figures from Matlab Simulink show similar behaviour to the analytical work hence providing a strong validation to this study.

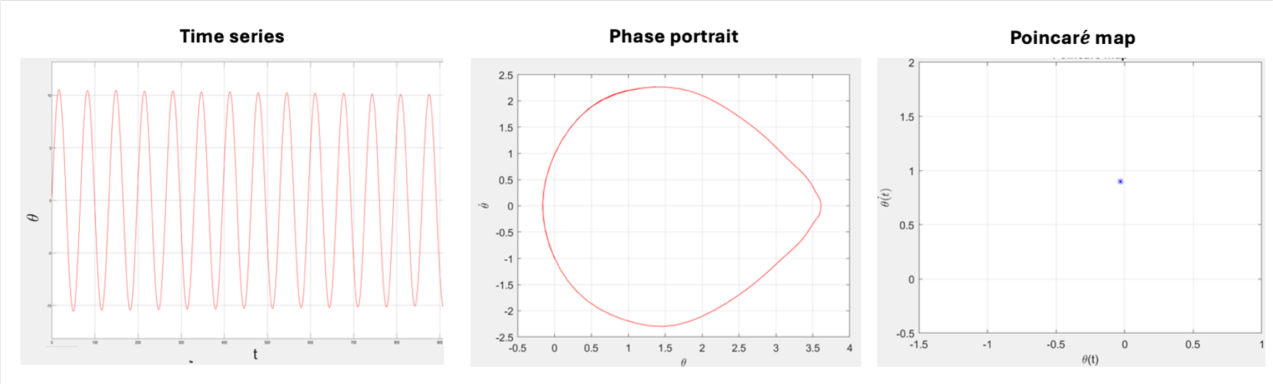

Figure 7.3: Time series, Phase portrait and Poincaré map from Simulink when $\Omega = 8.61$ rads^{-1}.

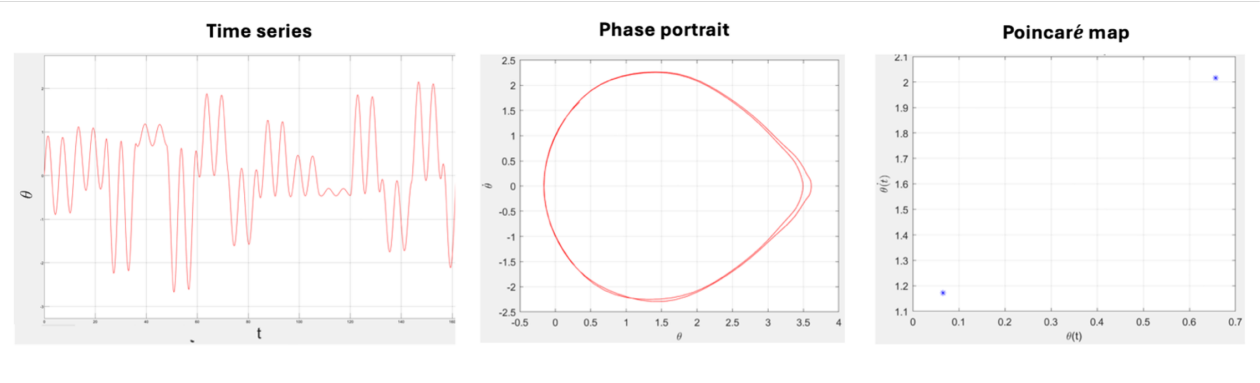

Figure 7.4: Time series, Phase portrait and Poincaré map from Simulink when $\Omega = 8.43$ rads^{-1}.

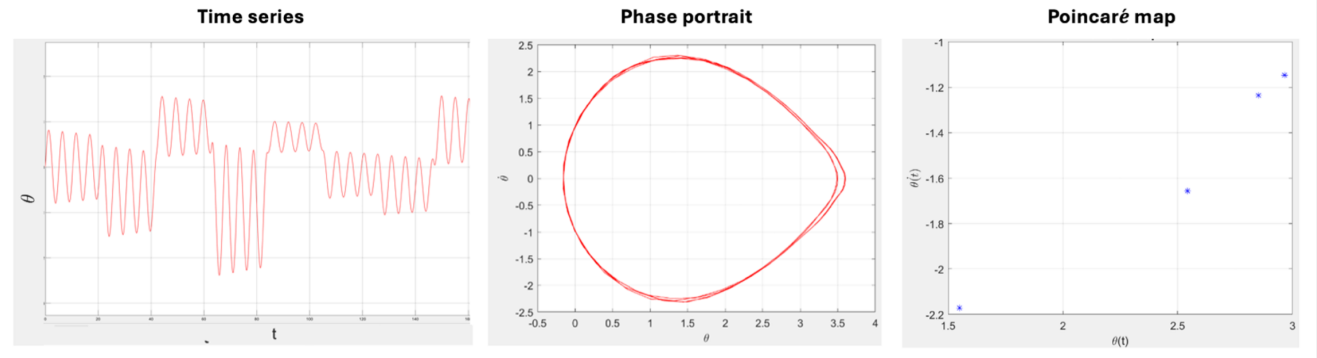

Figure 7.5: Time series, Phase portrait and Poincaré map from Simulink when $\Omega = 8.282$ rads^{-1}.

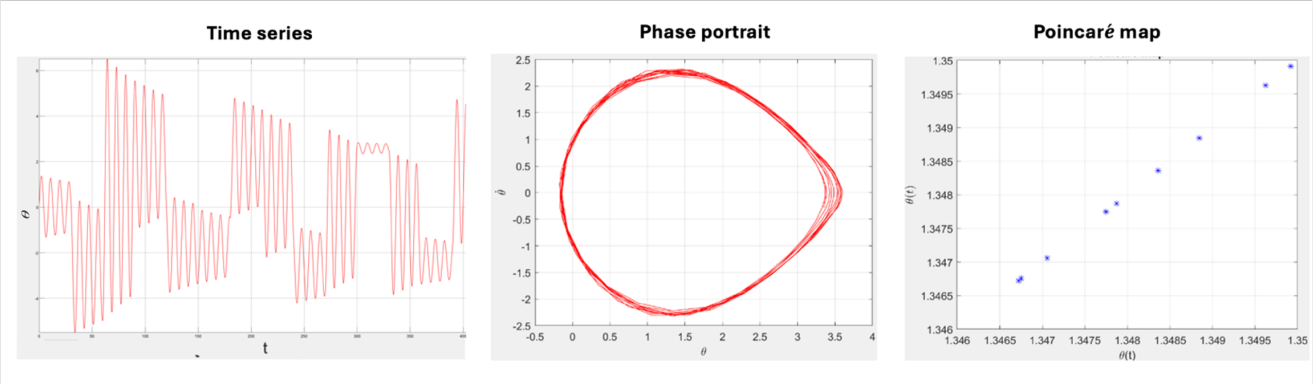

Figure 7.6: Time series, Phase portrait and Poincaré map from Simulink when $\Omega = 8.275$ rads^{-1}.

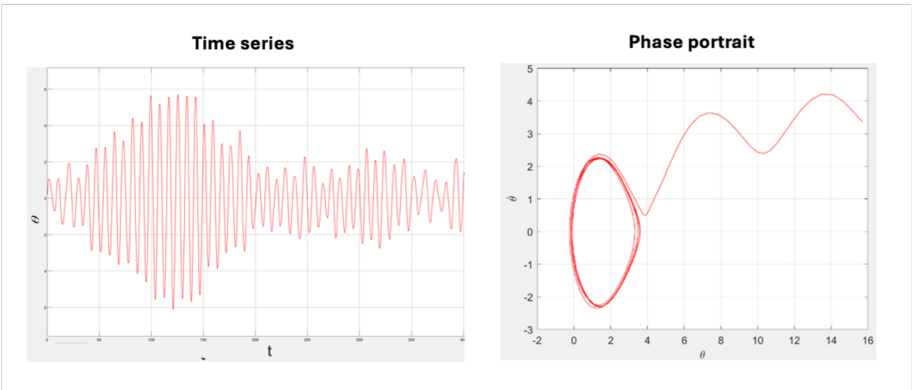

Figure 7.7: Time series and Phase portrait from Simulink when $\Omega = 8.2601$ rads^{-1}.

7.4.2 Subharmonic Resonance

Similarly, Figure 7.8, Figure 7.9, Figure 7.10, Figure 7.11 and Figure 7.12 were obtained for subharmonic resonance from the Simulink model. Results obtained for subharmonic resonance were compared to the analytical findings from previous research [115]. The graphs show similar behaviour to the analytical work, hence providing strong confirmation for this study [115, 134].

Subharmonic resonance is when the excitation frequency is twice the natural frequency of the system. This results in the occurrence of low-frequency oscillations and the possibility of equipment damage [115, 134]. Studies have demonstrated that by employing Melnikov methods, chaos in the pendulum equation may be mitigated during ultra-subharmonic resonance. This allows for the manipulation of chaos patterns, enabling them to be regulated into period-n orbits by making precise adjustments to certain parameters, [193].

The Ω was reduced and it was observed that the system was losing its stability and entering into chaos.

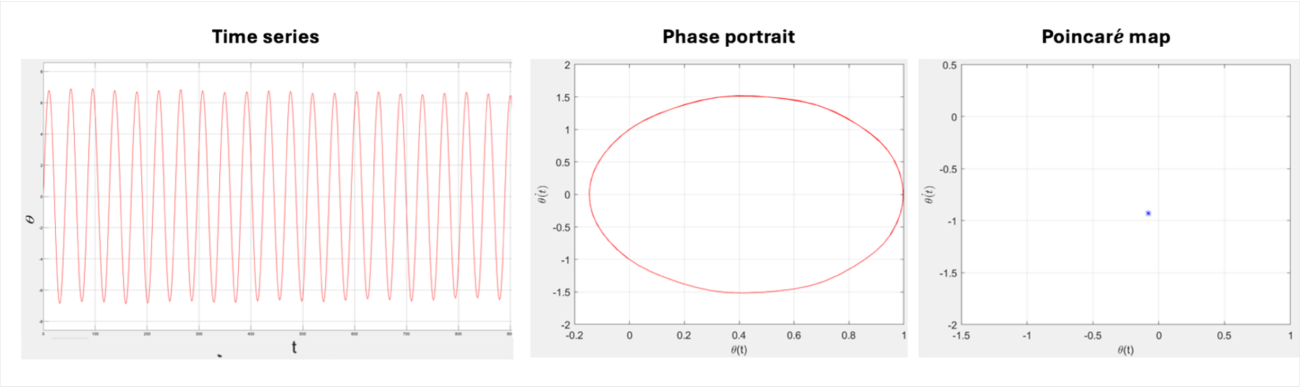

Figure 7.8: Time series, Phase portrait and Poincaré map from Simulink when $\Omega = 26.01$ rads^{-1}.

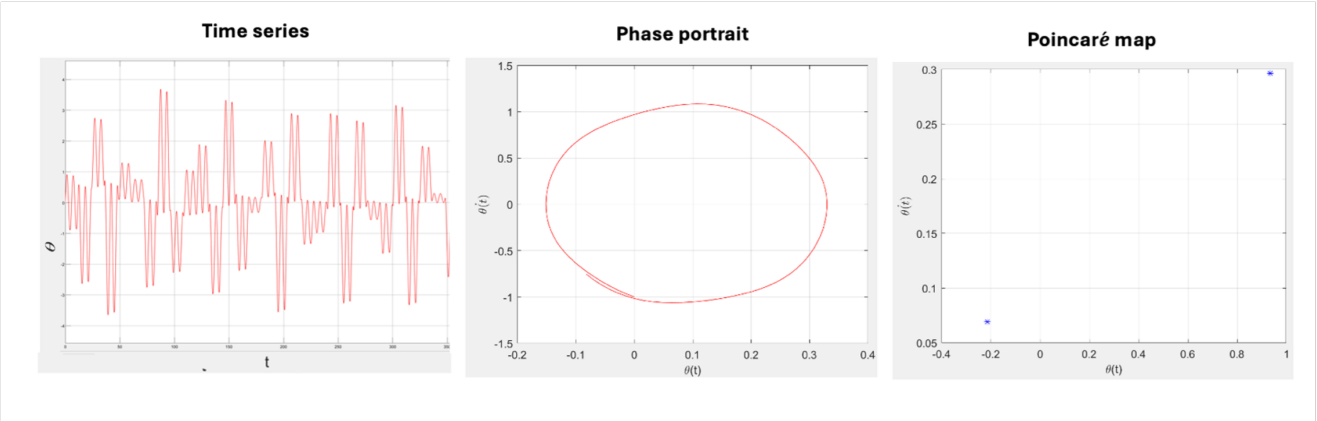

Figure 7.9: Time series, Phase portrait and Poincaré map from Simulink when $\Omega = 21.042$ rads^{-1}.

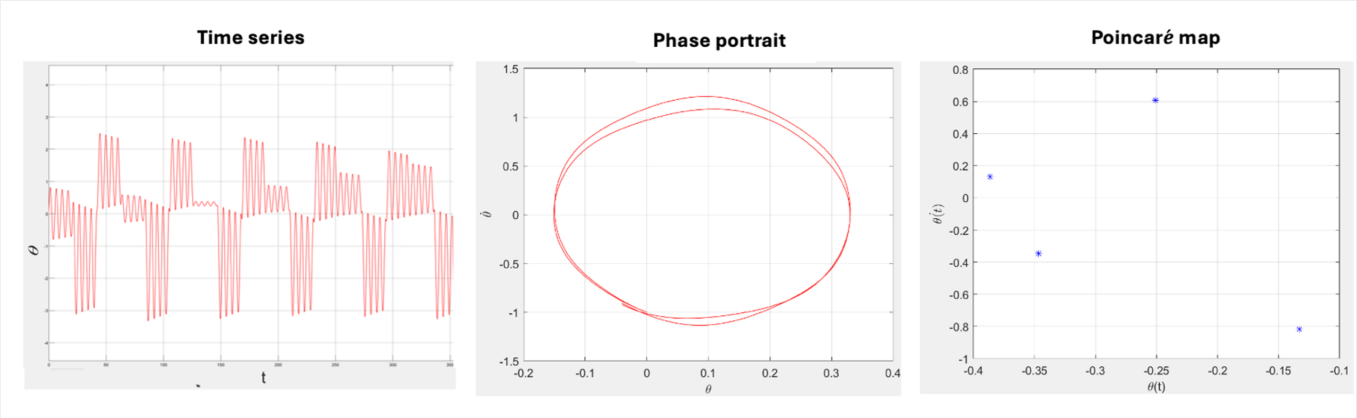

Figure 7.10: Time series, Phase portrait and Poincaré map from Simulink when $\Omega = 19.4162$ rads^{-1}.

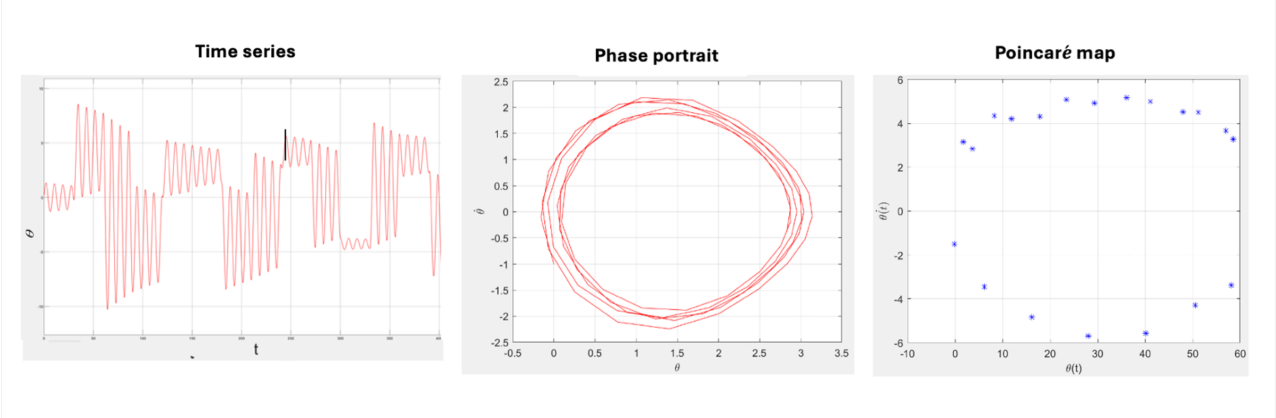

Figure 7.11: Time series, Phase portrait and Poincaré map from Simulink when $\Omega = 19.375$ rads^{-1}.

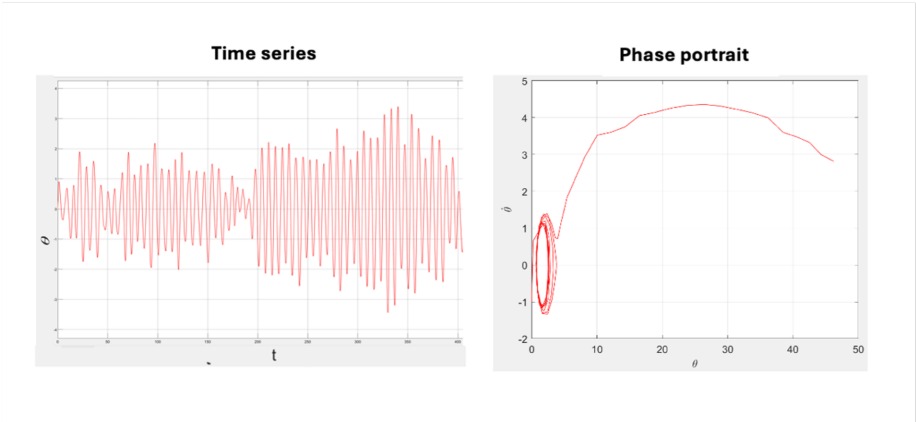

Figure 7.12: Time series and Phase portrait from Simulink when $\Omega = 19.37251$ rads^{-1}.

7.4.3 Quasiperiodicity

Considering quasiperiodicity where the Ω value is considered to be irrational values, figures similar to the analytical work done previously, [159], were produced and compared. Figure 7.13, Figure 7.14, Figure 7.15, Figure 7.16 and Figure 7.17 show the behaviour of the nonlinear system as Ω is reduced exemplifying the significance of the Simulink model.

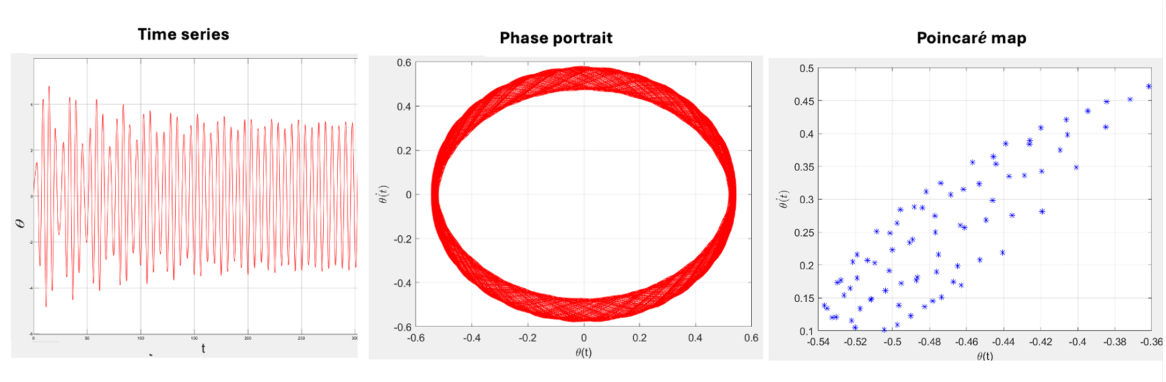

Figure 7.13: Time series, Phase portrait and Poincaré map from Simulink when $\Omega = 2\pi$ rads^{-1}.

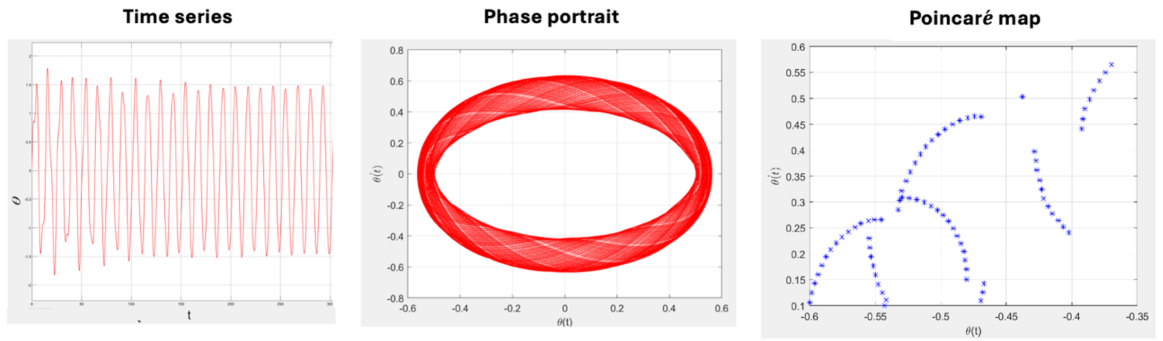

Figure 7.14: Time series, Phase portrait and Poincaré map from Simulink when $\Omega = \pi$ rads^{-1}.

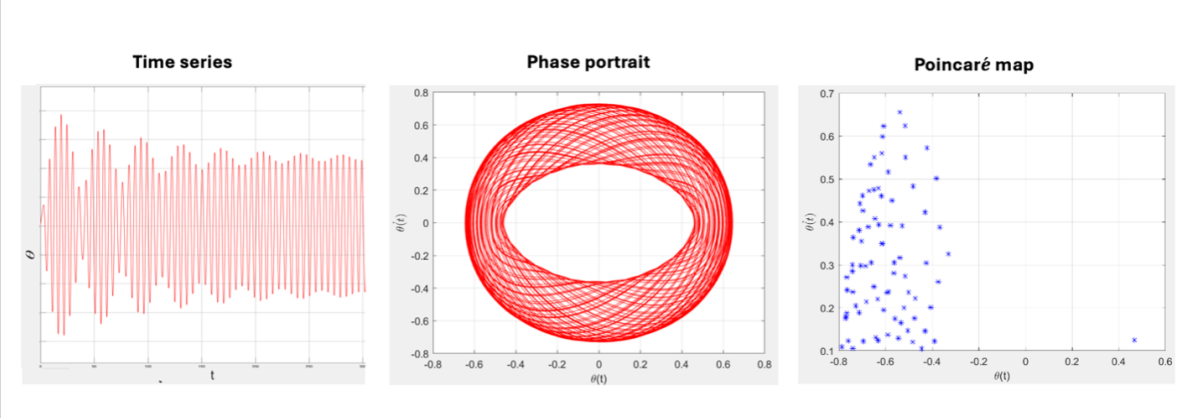

Figure 7.15: Time series, Phase portrait and Poincaré map from Simulink when $\Omega = 2\pi/3$ rads^{-1}.

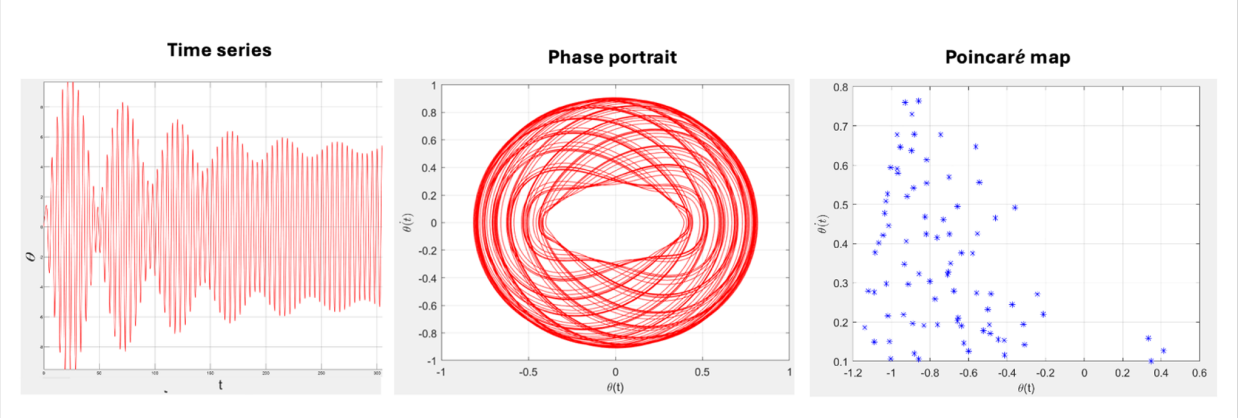

Figure 7.16: Time series, Phase portrait and Poincaré map from Simulink when $\Omega = \pi/2$ rads^{-1}.

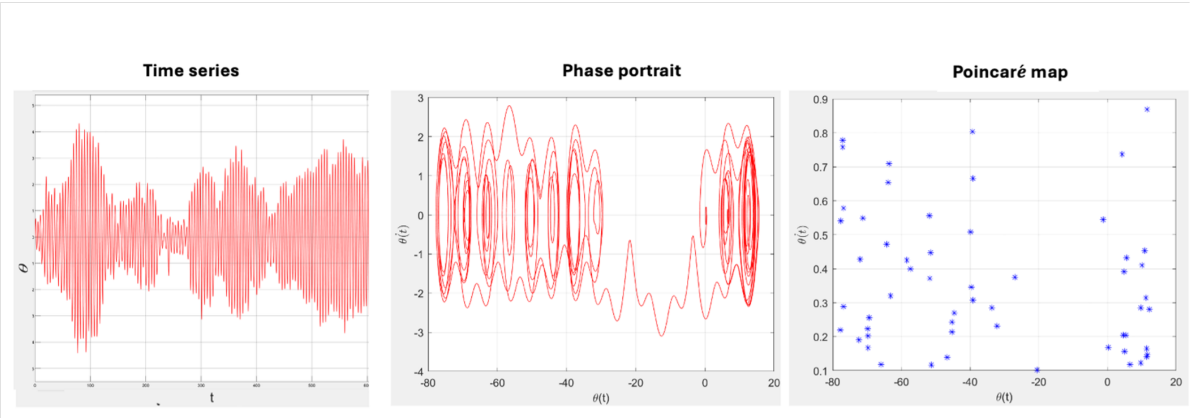

Figure 7.17: Time series, Phase portrait and Poincaré map from Simulink when $\Omega = 2\pi/8$ rads^{-1}.

7.4.4 Comparing Analytical Method with the Simulink model

Figures 7.18, 7.19, and 7.20 were generated to juxtapose the analytical procedure with the Simulink model for further validation of the results.

For the primary resonance depicted in Figure 7.18, a Ω value of 8.2601 rads^{-1}, which is approximately around the system's natural frequency, is utilised, and the Poincaré maps derived from both the analytical analysis and the Simulink model are presented. Both distinctly exhibit analogous patterns in the system's behaviour.

Figure 7.19 illustrates subharmonic resonance at $\Omega = 19.37251$ rads^{-1}. The Poincaré maps derived from both the analytical and simulated models exhibit comparable behaviours, so confirming the Simulink model.

Figure 7.20 was generated under the scenario of quasiperiodicity, with Ω set to $\pi/8.5$ rads^{-1}. This also offers a robust comparison between the analytically derived Poincaré map and the Poincaré map simulated in Simulink.

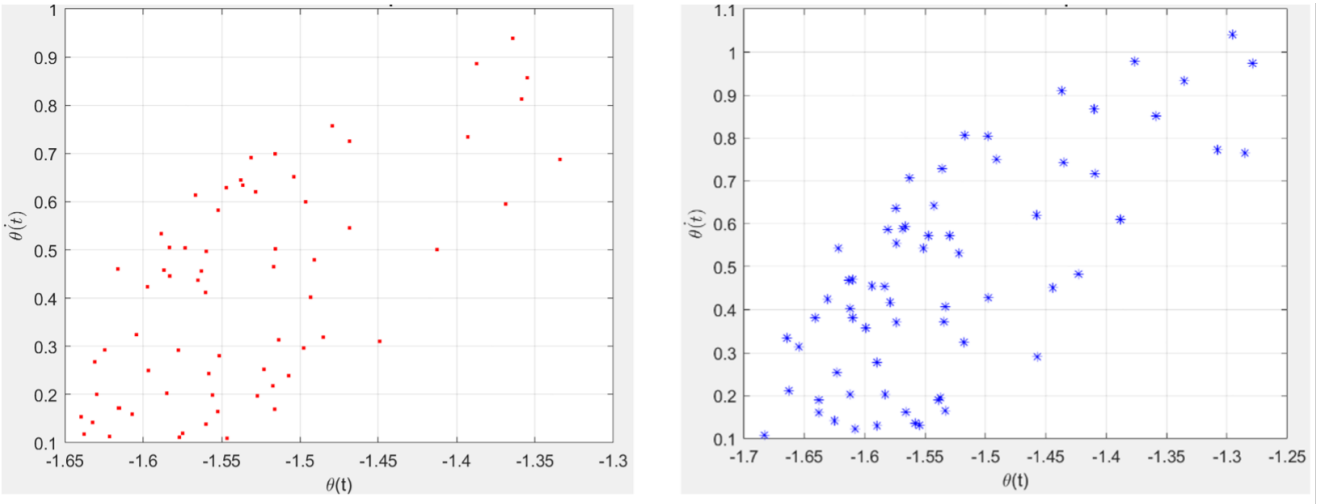

Figure 7.18: Poincaré maps from analytical method and Simulink model respectively for Primary Resonance when Ω = 8.2601 rads^{-1}.

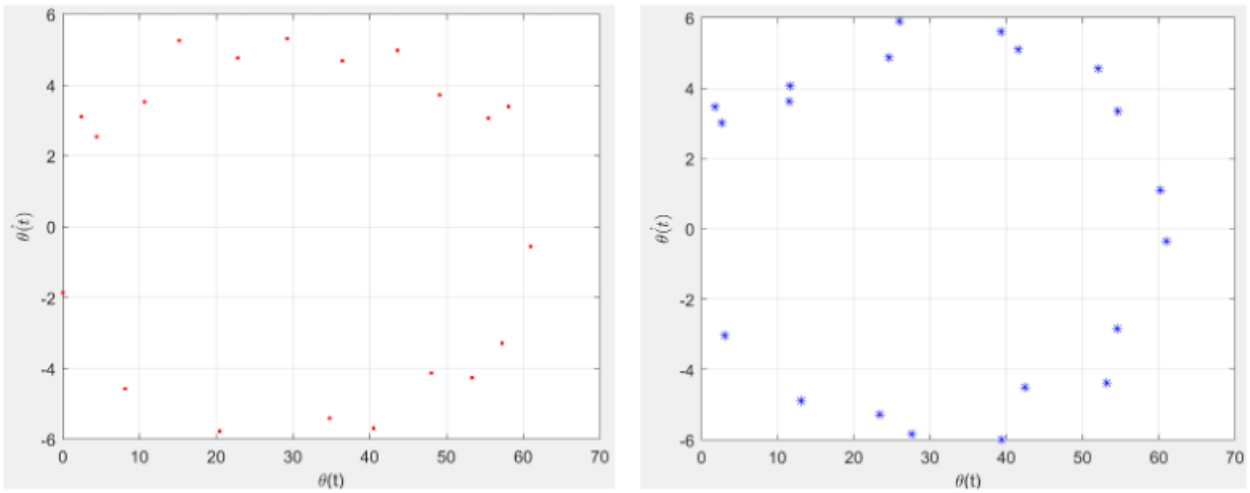

Figure 7.19: Poincaré maps from analytical method and Simulink model respectively for Subharmonic Resonance when $\Omega = 19.37251$ rads^{-1}.

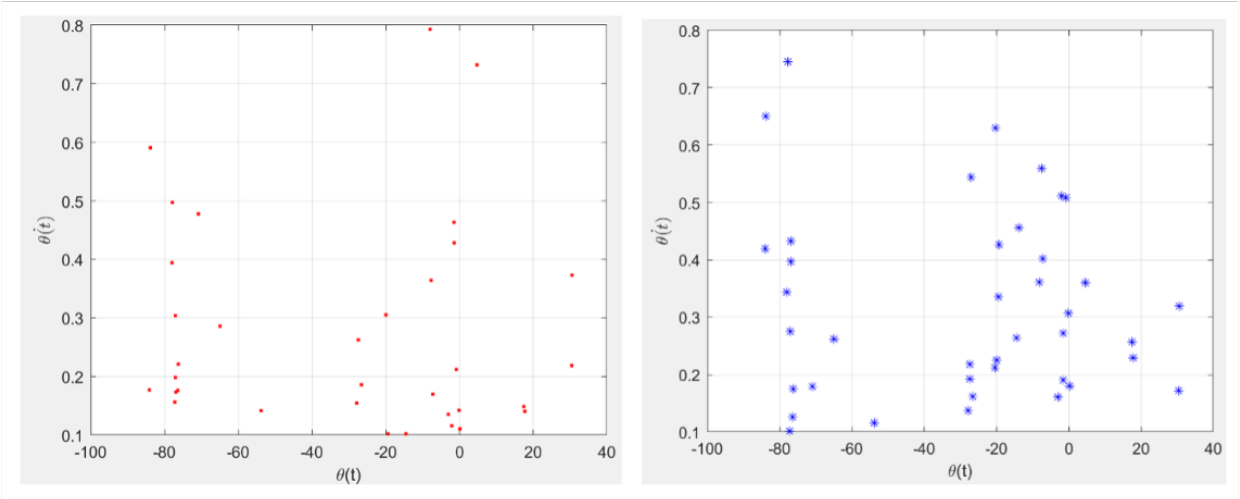

Figure 7.20: Poincaré maps from analytical method and Simulink model respectively for Quaisperiodicity when $\Omega = \pi/8.5$ rads^{-1}.

7.4.5 Results for the Integrity Diagrams

Bifurcation diagrams are crucial instruments for understanding nonlinear dynamical systems, as they visually represent the system's behaviour in response to systematic alterations in the parameter Ω. These diagrams delineate the precise instances at which the system's solutions experience qualitative transformations, transitioning from stable fixed points to either periodic or chaotic behaviour. This can be utilised to pinpoint important moments for deriving relevant parameter values and corresponding state variables. These

inputs are essential for integrity diagrams that depict the dynamic behaviours and resilience of the system within the parameter space. This method also provides a more efficient computational technique for studying system behaviour, [187, 189]. Integrity diagrams delineate the safe zones for the systems, and it is imperative to remain beneath the integrity curve to prevent running at r values that surpass that of the cliff face.

Integrity diagrams are derived by analysing the stability of different behaviours when system parameters vary, utilising bifurcation diagrams. To illustrate the period-doubling precursor to chaos, the first stage entails constructing a bifurcation diagram by varying a control parameter Ω and recording the system's stable or periodic solutions. The identification of pivotal places where period-doubling bifurcations transpire, leading to the onset of chaos, has been achieved. The regions representing stable equilibrium points, periodic paths, and chaotic behaviour are delineated. A study is performed to ascertain how the borders between these behaviours shift in response to perturbations. Before and after disturbances, the integrity zones, which indicate the parameter ranges within which the system sustains a particular stable state, are calculated. The percentage reduction is calculated by comparing the area of these locations prior to and following the disruption.

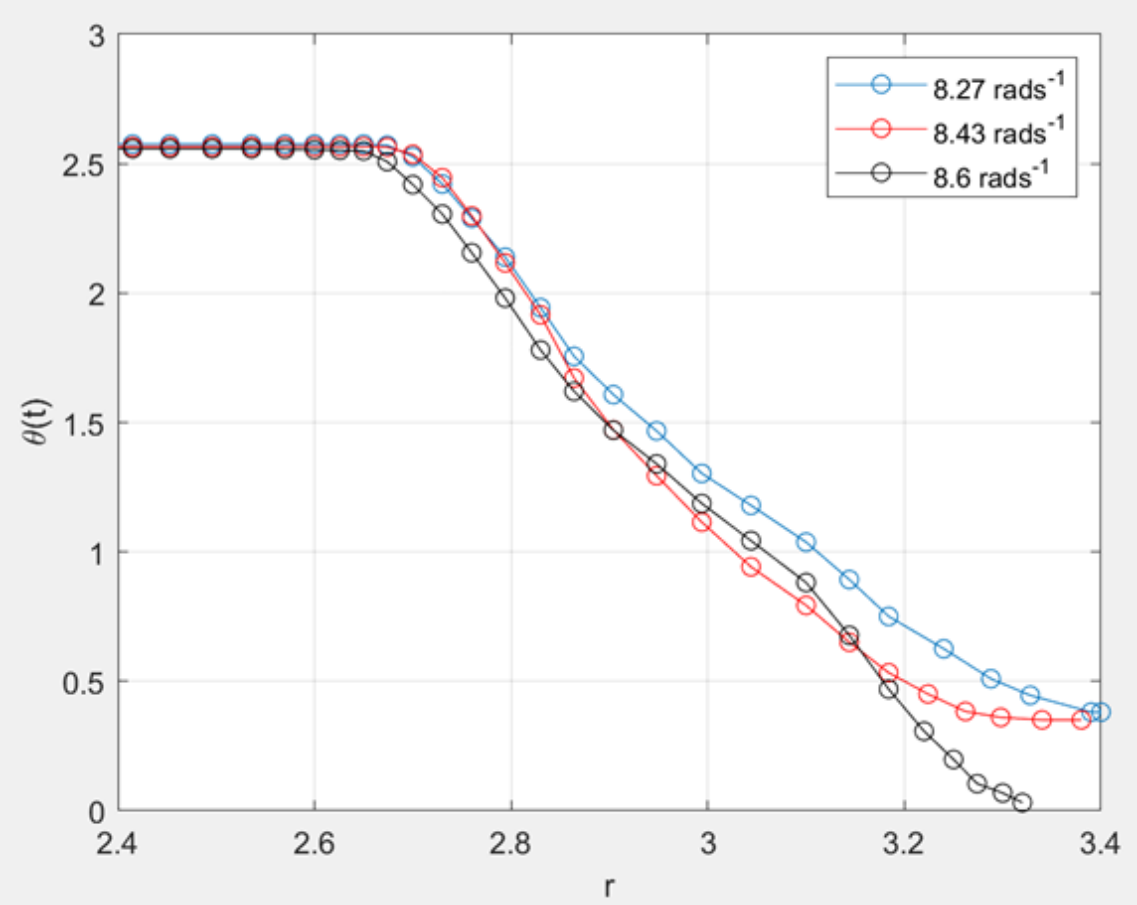

Figure 7.21: Integrity Diagrams for Primary Resonance when Ω = 8.27 rads^{-1}, 8.43 rads^{-1} and 8.61 rads^{-1}.

Figure 7.21 depicts the changes happening within the primary resonance. As the Ω is increased the erosion takes place quicker.

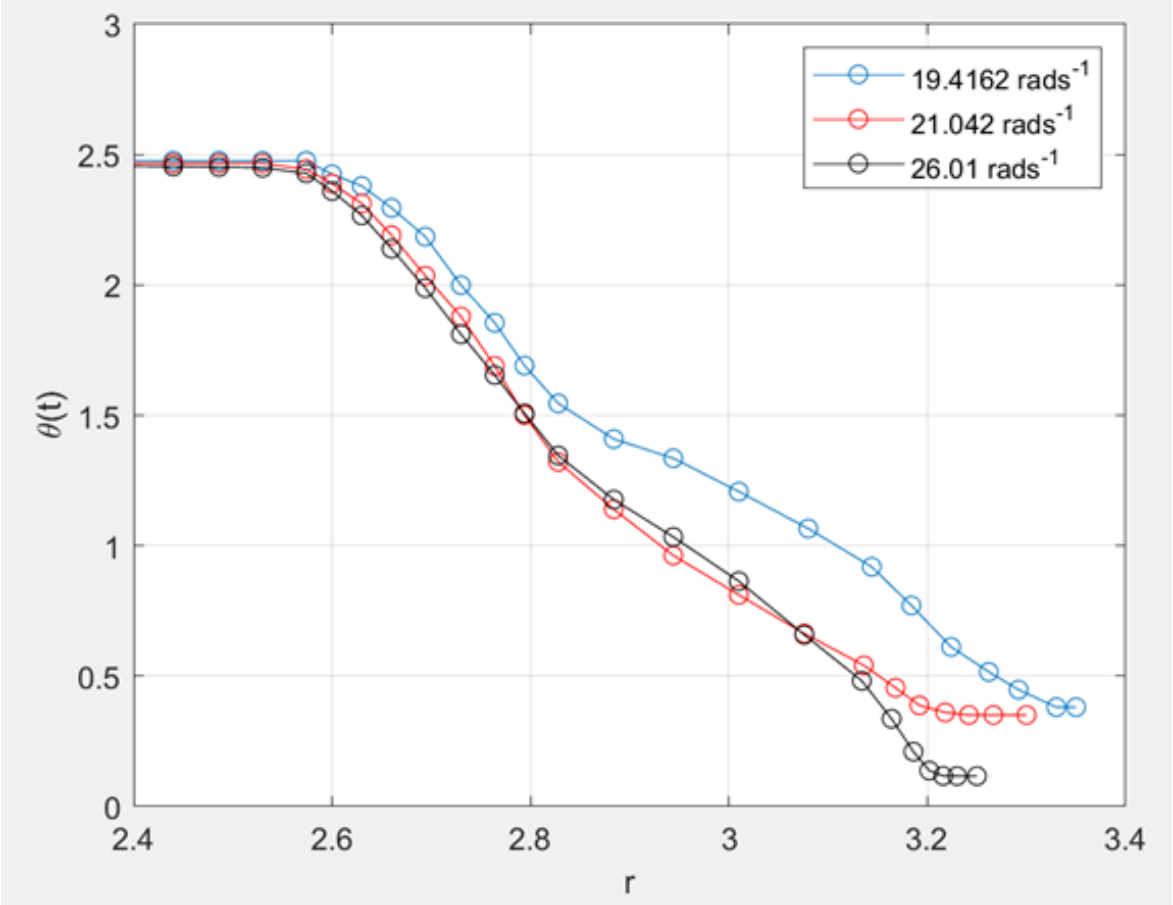

Figure 7.22: Integrity Diagrams for Subharmonic Resonance when $\Omega = 19.4162$ rads^{-1}, 21.042 rads^{-1} and 26.01 rads^{-1}.

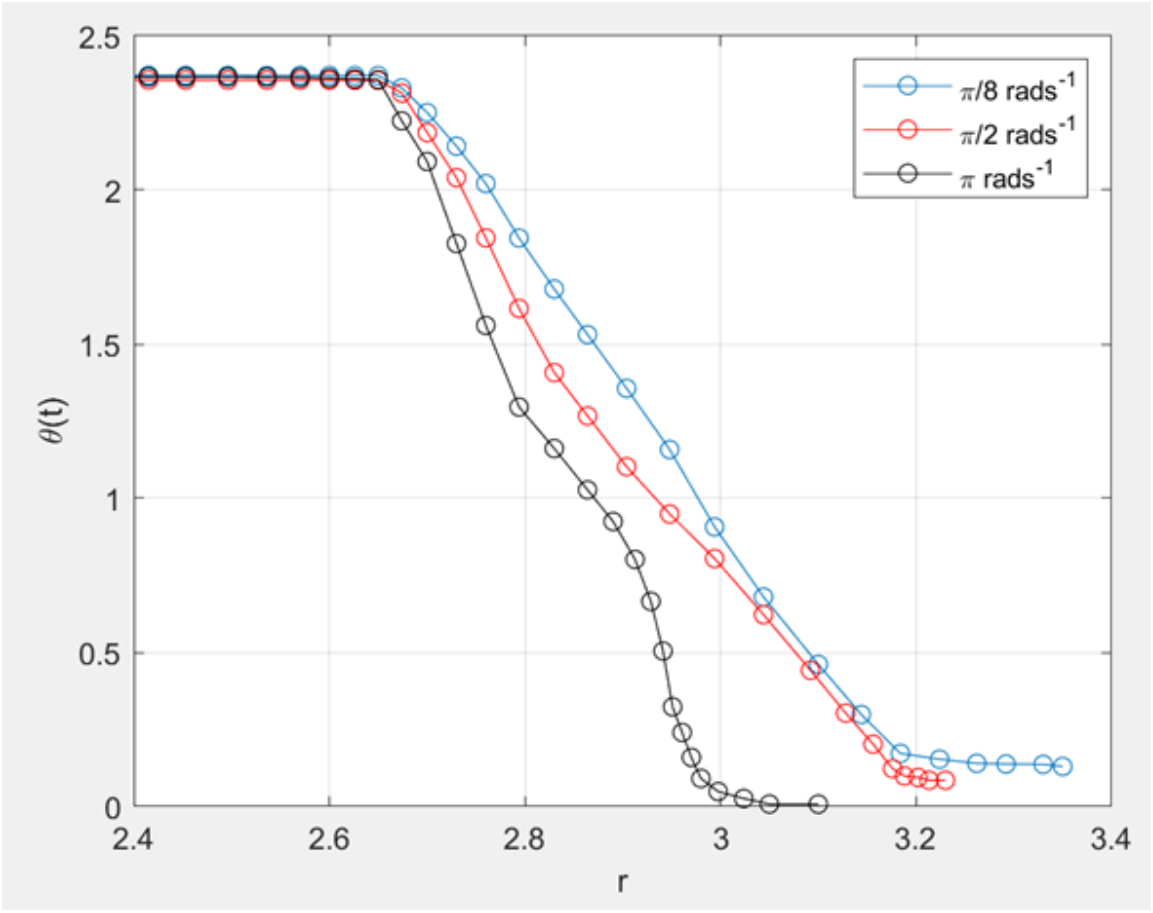

Figure 7.23: Integrity Diagrams for Quasiperiodicity $\Omega = \pi/8$ rads^{-1}, $\pi/2$ rads^{-1} and π rads^{-1}.

Figures 7.22 and 7.23 illustrate the integrity diagrams for subharmonic resonance and quasiperiodicity, respectively. As the r value increases with the augmentation of Ω, the system's behaviour changes.

The percentage reduction is computed for the integrity diagrams pertaining to primary resonance and subsequently evaluated. When Ω equals 8.27 rads^{-1}, the reduction percentage is 24.56%; however, when Ω increases, the reduction percentage rises to 38.17%. 8.6 rads^{-1} illustrates that the stable zone diminishes as the parameter is altered.

Consequently, it has been established that the system's integrity is markedly undermined as the parameter is elevated. Subharmonic resonance occurs when Ω equals 19.4162 rads^{-1}, resulting in an approximate 44.13% reduction in stable behaviour. At $\Omega = 26.01$ rads^{-1}, the increase in bias leads to a decrease of around 51.28%, signifying a substantial decline in the system's consistent performance.

In the context of quasiperiodicity, when Ω transitions from $\pi/8$ rads^{-1} to $\pi/2$ rads^{-1} and subsequently to π rads^{-1}, the stable region contracts. The stable region diminishes to 39.01% when $\Omega = \pi/8$ rads^{-1}, but swiftly escalates to 67.23% when Ω rises to π rads^{-1}.

7.5 Discussion

The primary aim of this section is to meticulously examine the dynamic behaviour of the swing equation while varying factors inside the system. This work compares analytical methodologies and numerical simulations to yield robust results for the investigation. This chapter seeks to thoroughly understand the dynamics of the swing equation and its impact on power system stability through the utilisation of the Simulink tool.

Analytical instruments are crucial for assessing the resonances in the swing equation. By employing mathematical modelling and computations, these methods provide accurate insights grounded in minimal assumptions. The simulated model offers graphical depictions of the swing equation's behaviour under main resonance, subharmonic resonance, and quasiperiodicity as variables are altered. These graphics validate the analytical results achieved. This technology enables engineers to make informed decisions on the reliability of electric grids.

Load fluctuations frequently arise in power systems characterised by nonlinear dynamics. The swing equation executed in Matlab provides clarity on the previously obtained analytical and numerical results. The information obtained from these scenarios is essential for the management of the electrical grid, contributing to the maintenance of system stability and reliability. Enhancing comprehension of the dynamics in the swing equation can facilitate the mitigation of power outages in electrical systems and assist in circumventing unavoidable situations.

This thorough investigation of the swing equation and associated Matlab Simulink model compares and validates the findings from the authors' prior research. The time series, phase portraits, and Poincaré maps derived from the Simulink model illustrate the dynamic behaviour of the power system as Ω is modified. Bifurcation diagrams were meticulously analysed to derive integrity diagrams and enhance the comprehension of the swing equation and its dynamics. The outcomes obtained from the Simulink model for primary resonance, subharmonic resonance, and quasiperiodicity display similar

behavioural patterns to the previous analytical research performed by the same authors.

This chapter also extends the current research conducted by the same researchers, enhancing their previous findings. The idea is to enhance existing approaches by offering a more profound understanding of the underlying mathematics, rather than replacing them. This research improves comprehension of fundamental concepts and system stability in power systems, with a specific emphasis on the Simulink model. It enhances control methodologies and preventive strategies for power systems. The purpose is to mitigate the disruptive effects arising from measures beneficial to power system engineers and researchers.

7.6 Final Remarks

The results also reveal significant insights into the dynamic behaviour of the swing equation. This can enhance power systems that are sophisticated and characterised by detailed details inside the electronics sector.

In the future, researchers may investigate strategies to improve these conditions concerning swing equations in power networks. This may produce substantial new insights into the lasting sustainability and adaptation of electricity networks. They can further our understanding of intricate nonlinear systems and produce advancements that bolster robustness.

Chapter 8

Studying the Phenomena of Intermittency in the Swing Equation

8.1 Introduction

The swing equation, a second-order differential equation, is crucial for comprehending the dynamic behaviour in power systems [33]. It is extensively utilised in engineering applications, particularly within the electrical engineering domain, to simulate the stability of synchronous machines [77, 89]. Despite substantial research on primary and subharmonic resonances and quasiperiodicity, the phenomenon of intermittency remains underexplored in the swing equation. Sudden variations or eruptions within a periodic pattern in a nonlinear system are referred to as intermittency [194]. This study seeks to address this gap by carefully examining the occurrence of intermittency and its role in the transition of the system from stable to chaotic regions [195]. Various classifications of this phenomena, including Type I, Type II, and Type III, have been recognised in experimental contexts, indicating its practical significance [196, 197]. Type I intermittency is frequently linked to saddle-node bifurcation, while Type II is associated with subcritical Hopf bifurcation.

Recent research in nonlinear systems indicates that intermittency may act as a crucial precursor to chaos, consequently influencing the stability of these systems. Intermittency has been found in fluid dynamics, thermoacoustic oscillations, and electrical circuits, where minor parameter changes result in abrupt disruptions [198]. In the realm of power

systems, comprehending intermittency is essential due to the rising incorporation of renewable energy sources, which contribute to diminished inertia and heightened system variability [125]. The observed phenomenon of intermittency may significantly indicate unstable power networks, rendering its research within the swing equation framework essential [199]. Notwithstanding the significance of this phenomenon, many studies on nonlinear power systems neglect intermittency as a distinct pathway to chaos. Previous work has examined period-doubling, quasiperiodicity, and crises; however, few studies have explored intermittency in relation to variable parameters such as inertia and voltage of the machine.

The primary aim of this research is to investigate the influence of intermittency on the swing equation and its implications for the stability of power systems. The study seeks to explore the phenomenon of intermittency when parameters fluctuate, analyse the shift from periodic to chaotic domains, and pinpoint important thresholds for the onset of intermittency. The primary emphasis is on the impact of inertia and voltage of the machine to analyse the stability of the swing equation.

This chapter utilises analytical and numerical methodologies to accomplish its aims and objectives. The fourth-order Runge-Kutta method is employed to solve the swing equation in Matlab. Bifurcation diagrams are utilised to examine stability transitions, whilst heat maps provide insights into the evolution of system dynamics. Lyapunov exponents are computed to confirm the existence of chaos and intermittency. Poincaré maps are utilised to analyse the paths of systems. This segment offers an in-depth analysis of the system's behaviour in response to variations in machine inertia and voltage.

The results have substantial implications for the development of enhanced stability and control solutions, particularly in power circuits experiencing abrupt fluctuations. Addressing intermittent behaviour at an early stage can avert detrimental effects, hence maintaining a dependable nonlinear power system.

The stability of nonlinear power systems is affected by various events, including bifurcations, chaos, and intermittency. Numerous studies have investigated the stability of these systems employing analytical and numerical methods, including bifurcation diagrams, Lyapunov exponents, and phase space analysis [33, 43, 115, 134].

Bifurcation theory is crucial for comprehending the transitions of nonlinear systems between stable and unstable states [200]. Period-doubling bifurcation is a recognised

pathway to chaos, particularly evident in power systems and electrical circuits [33, 89]. Bifurcation diagrams illustrate changes by graphing system states against a control parameter, thereby highlighting zones of stability and intermittency [201].

The Lyapunov exponent is a crucial metric of chaotic behaviour, quantifying the proximity of trajectories inside a system. A positive Lyapunov exponent signifies chaotic motion, whereas a negative exponent denotes stability [115, 134]. This technique has been extensively utilised to examine stability and dynamical behaviour in nonlinear systems. The stability of the swing equation can be analysed by Lyapunov exponents, particularly in relation to intermittent events. Resolving the swing equation necessitates precise numerical integration methods. The fourth-order Runge-Kutta method is extensively employed to solve non-linear differential equations, offering excellent precision in computational systems [33, 89]. Poincaré maps provide a geometric representation of periodic and chaotic attractors, facilitating the visualisation of intermittent regions [134, 202]. An alternative pathway to quasiperiodicity arises when the system possesses irrational frequency values, resulting in irregular transitions [159].

In contrast to the gradual transitions seen in period-doubling, intermittency is marked by abrupt surges of instability inside a periodic system [194]. Intermittency is seen in fluid dynamics, thermoacoustic oscillations [196], and combustion instability [199]. Research indicates that intermittency may commence when essential system characteristics, including inertia, damping, and voltage, exceed stability limits [203, 204].

Three categories of intermittencies exist. Type I intermittency occurs when system trajectories linger at an unstable fixed point prior to abrupt bursts [197]. Type II intermittency is frequently encountered in electrical and mechanical systems [196]. Type III intermittency pertains to quasiperiodicity and arises from non-uniform reinjection in probability densities [198].

Research has demonstrated that the stability of the swing equation may be examined through modelling in Matlab Simulink. It facilitates improved visualisation of the system and offers a thorough comprehension of its dynamic functioning [205].

The swing equation, examined in this research, is a crucial element in the understanding of power system dynamics [13]. It has characteristics akin to those of other power systems; nonetheless, a thorough investigation is necessary to attain a more profound understanding of the concepts. The generalised form of the swing equation has been found to enhance the

understanding of transient stability in power-electronic power systems [206]. In reaction to minimal disturbances, the rotor of the machine will demonstrate motion relative to the air gap, rotating in synchrony. Subsequently, a relative motion is initiated, allowing the swing equation to be employed for characterising and simulating this relative motion [15, 16].

8.2 Analytical Work

Initially the equilibrium points are found. At equilibrium, the time derivatives of θ vanishes.

Begin the analytical realm by considering equilibrium conditions where the system is at rest, that is, no change in rotor angle over time:

$$\frac{d\theta}{dt} = 0, \quad \frac{d^2\theta}{dt^2} = 0 \tag{8.1}$$

Substituting these conditions into the swing equation yields:

$$0 = P_m - \frac{V_G V_B}{X_G} \sin(\theta_0 - \theta_B) \tag{8.2}$$

Rearranging the above, the mechanical power input is found at equilibrium is:

$$P_m = \frac{V_G V_B}{X_G} \sin(\theta_0 - \theta_B) \tag{8.3}$$

where θ_0 is the equilibrium rotor angle.

To linearise the swing equation, a small perturbation is introduced:

$$\delta = \theta - \theta_0 \tag{8.4}$$

This variable δ represents small deviations from the equilibrium. Expanding the sinusoidal term $\sin(\theta - \theta_B)$ using a first-order Taylor series about θ_0 gives:

$$\sin(\theta - \theta_B) \approx \sin(\theta_0 - \theta_B) + (\theta - \theta_0)\cos(\theta_0 - \theta_B) \tag{8.5}$$

Recalling the equation (8.3), substituting this back into the original swing equation, replacing θ with $\theta_0 + \delta$, to obtain:

$$\frac{2H}{\omega_R}\frac{d^2\delta}{dt^2} + D\frac{d\delta}{dt} = -\frac{V_G V_B}{X_G}\cos(\theta_0 - \theta_B)\delta \tag{8.6}$$

Rearranging the terms, the linearised swing equation is thus:

$$\frac{d^2\delta}{dt^2} + \frac{D}{2H}\frac{d\delta}{dt} + \frac{V_G V_B}{2HX_G}\cos(\theta_0 - \theta_B)\delta = 0 \tag{8.7}$$

This is a linear second-order differential equation of the standard form:

$$\ddot{\delta} + \alpha\dot{\delta} + \beta\delta = 0 \tag{8.8}$$

with parameters:

$$\alpha = \frac{D}{2H}, \quad \beta = \frac{V_G V_B}{2HX_G}\cos(\theta_0 - \theta_B) \tag{8.9}$$

To analyse stability, the characteristic equation is derived of the system:

$$\lambda^2 + \alpha\lambda + \beta = 0 \tag{8.10}$$

Solving this quadratic equation for λ using the quadratic formula:

$$\lambda = \frac{-\alpha \pm \sqrt{\alpha^2 - 4\beta}}{2} \tag{8.11}$$

The nature of the eigenvalues λ determines the system's stability:

- **Stable:** When both roots have negative real parts ($\mathrm{Re}(\lambda) < 0$), the system returns to equilibrium after a disturbance. This condition holds when:

$$\alpha^2 - 4\beta > 0, \quad \text{and} \quad \alpha > 0 \tag{8.12}$$

- **Marginally stable:** When at least one root is zero ($\lambda = 0$), the system exhibits quasiperiodic motion, i.e., remains in bounded oscillation.

- **Unstable:** If any root has a positive real part ($\mathrm{Re}(\lambda) > 0$), small perturbations grow exponentially, potentially leading to bifurcation or chaotic dynamics. This happens if:

$$\alpha^2 - 4\beta < 0 \quad \text{or} \quad \alpha < 0 \tag{8.13}$$

8.3 Lyapunov Exponent Analysis

The Lyapunov exponent λ quantifies the system's sensitivity to initial conditions by measuring the average exponential rate of divergence of nearby trajectories in phase space [26, 207, 208]. It is computed as:

$$\lambda = \lim_{t\to\infty} \frac{1}{t} \ln \left| \frac{\delta\theta(t)}{\delta\theta(0)} \right|$$

where $\delta\theta(t)$ represents the perturbation in the rotor angle over time.

The Lyapunov exponent characterises different dynamical behaviors as stated below:

Stable periodic motion: $\lambda < 0$, indicating that small disturbances decay, and the system returns to its steady-state region [33, 195].

Intermittency: λ fluctuates between negative and positive values with sudden bursts, reflecting a system that alternates between stability and chaos [196].

Chaos: $\lambda > 0$, signifying exponential divergence of trajectories, leading to unpredictable behavior and unstable regions [197].

It is found that the system transitions from periodic motion to chaos through intermittent bursts when:

$$\lambda \approx 0, \quad \frac{d\lambda}{dr} > 0 \text{ at } r = r_c.$$

where r_c represents the critical value of the bifurcation parameter r at which the system shifts from stability to chaos. This transition is confirmed through the computed Lyapunov exponents, which align with the bifurcation diagrams and Poincaré maps.

8.4 Bifurcation Diagrams

The bifurcation diagrams are generated by incrementally increasing the forcing parameter r, while continuing the time integration of the system at each step [33, 77, 115]. For each value of r, the maximum amplitude of the oscillatory solution is computed and plotted against r. This process reveals how the system's behavior evolves as the forcing parameter is varied, showing transitions between periodic, chaotic states and even intermittency. The r is considered as mentioned in equation (3.65).

The swing equation (3.10) was solved in Matlab using the fourth-order Runge-Kutta method for numerical accuracy. The inertia and voltage of the machine variables were then altered separately to observe the minute changes that occur within the nonlinear system. Primary and subharmonic resonances are in focus of this research to analyse the intermittent behaviour.

Initially, bifurcation diagrams were obtained for primary and subharmonic resonance of the swing equation. This is then validated with heat maps and Lyapunov exponents. Then this study discusses the changes observed in the system when inertia and voltage of the machine are altered separately. Poincaré maps were then obtained for the time series to compare the results and intermittency was seen when a slight change is made to the nonlinear system. This shows that a small disturbance can lead to a complex behaviour wihtin the system.

Intermittency is considered as a route to chaos. The swing equation also exhibits intermittency when variables are altered. This section will provide a strong foundation for researchers to focus on this topic in nonlinear systems. Previous research by the same authors [77, 115, 134, 203, 204] studied the primary, subharmonic resonances, and quasiperiodicity in the swing equation. This is a continuation to those research and will give a wider knowledge for the case of intermittency.

8.5 Graphical Representation

To investigate the intermittent behaviour, numerical simulations were conducted using fourth-order Runge Kutta method. This method was chosen due to its accuracy in solving second order differential equations. The testing procedure involved selecting parameters such as inertia and voltage of machine and incrementing slightly to observe any sudden bursts within a periodic region. Bifurcation diagrams were plotted and variation of the variable r allowed to identify stability lost.

To ensure validity and reliability different conditions were considered. The findings were cross-validated using bifurcation diagrams, Lyapunov exponents and heat maps. These figures provided insights into the stability regions and confirmed the presence of intermittency. There were limitations in this research method, including computational

complexity during numerical simulations.

8.5.1 Analysing Intermittency around Primary Resonance

Initially, the bifurcation diagram related to $\Omega = 8.3$ rads^{-1}, which is a value closer to the primary resonance $\Omega = 8.27$ rads^{-1} is obtained for analysis as shown in Figure 8.1. At around $r = 0.97$, period doubling bifurcation occurs showing a stable period 2 orbit. Approximately when $r = 2.235$, another period doubling bifurcation occurs depicting a period 4 orbit, which then leads to a period 8 orbit and so on. This happens for 2^n where n takes large values. This then leads to an aperiodic motion eventually cascading to an unstable system [209–211].

At around $r = 2.43$, all periodic orbits would have occurred by then and furthermore that when $r = 3.03$, there are periodic orbits of all periods and all of them are unstable.

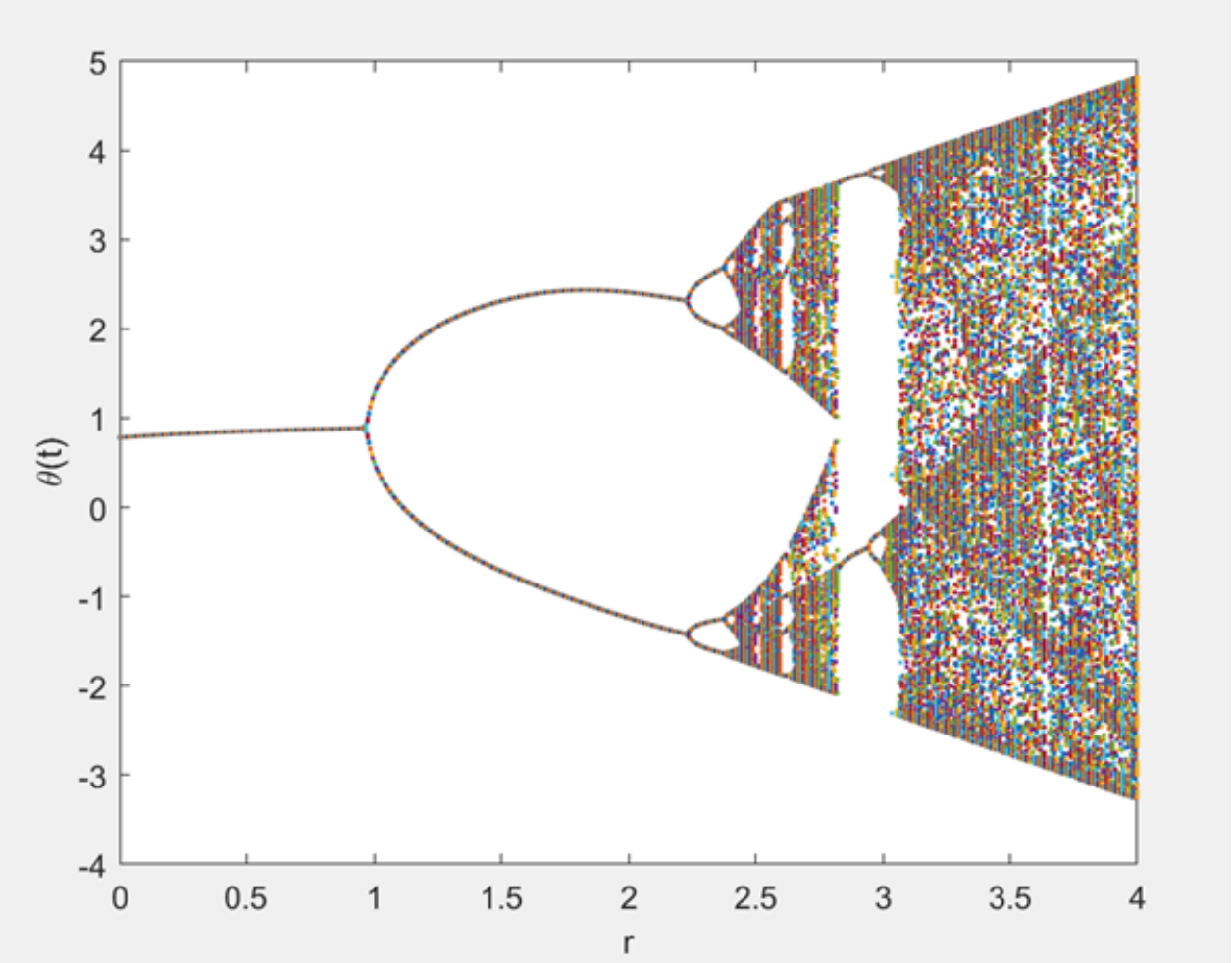

Figure 8.1: Bifurcation diagram for $\Omega = 8.3$ rads^{-1}.

The following heatmap, Figure 8.2, shows the progression of the system into an unstable region. The output heatmap represents the dynamic behaviour of the system over a range of r values and iterations n [212]. Each pixel's color corresponds to the 2π value of x_n, which highlights periodicity and chaos distinctly. Periodic behaviour appears as horizontal bands of uniform color, where the system settles into repeating patterns. Chaotic regions are characterised by irregular, scattered, and mixed color patterns, indicating unpredictable behavior. The marked region at $r = 2.43$ demonstrates intermittency, where the system alternates between chaotic and periodic dynamics. Above $r = 3.03$, the heatmap predominantly shows chaotic behavior, represented by noisy, non-uniform patterns.

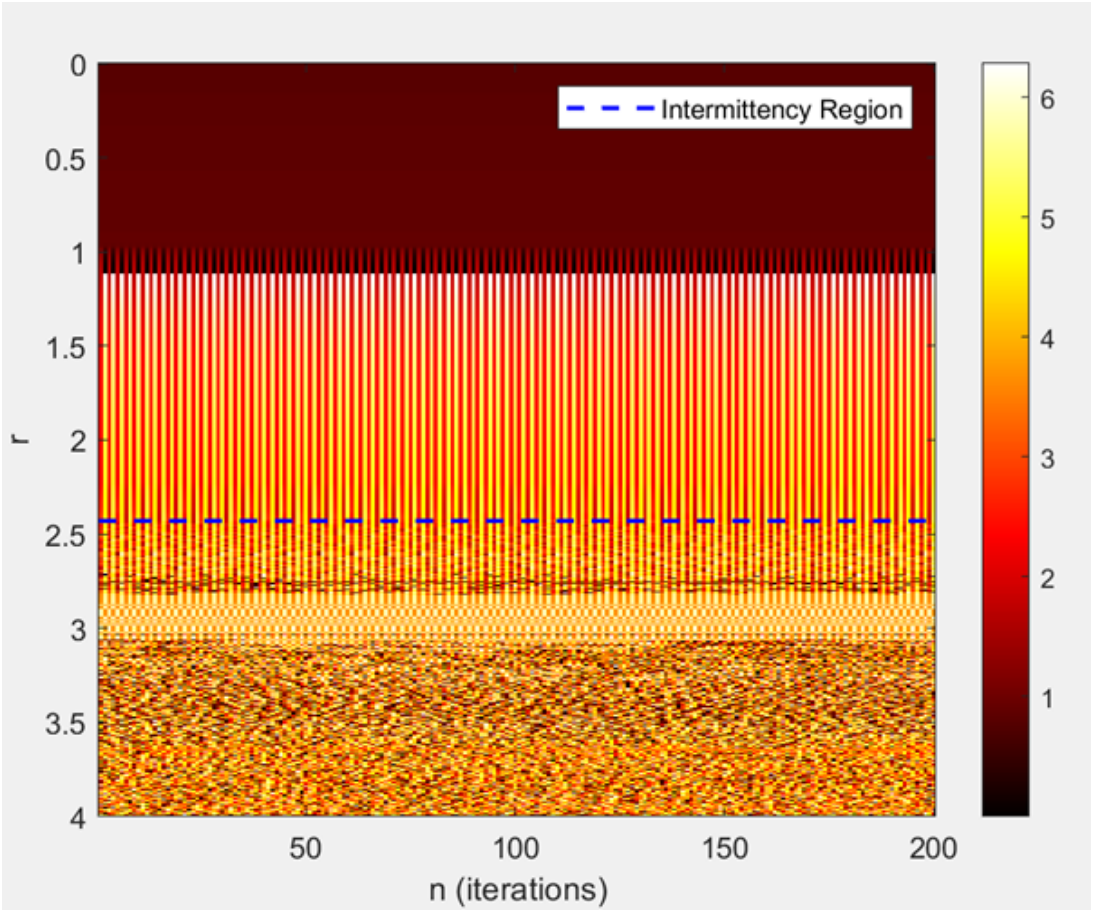

Figure 8.2: Heatmap depicting the dynamical behaviour closer to Primary Resonance.

The following figure, Figure 8.3, shows the corresponding Lyapunov exponents for the corresponding bifurcation diagram. Just below the point of tangency, Lyapunov exponent is positive. This shows that the dynamics just below the tangent bifurcation is actually chaotic. Once this tangency is obtained, there is a bifurcation where the Lyapunov exponent becomes zero. Then it can be seen that the exponent values become negative, and then gradually goes into positive exponents. This validates the results obtained from the bifurcation diagram and the heat map.

Research also found the importance of Lyapunov Exponents in validating the detailed investigation of bifurcation diagrams [207]. Hence, this plays a vital role in studying the intricate dynamic behaviour of nonlinear systems.

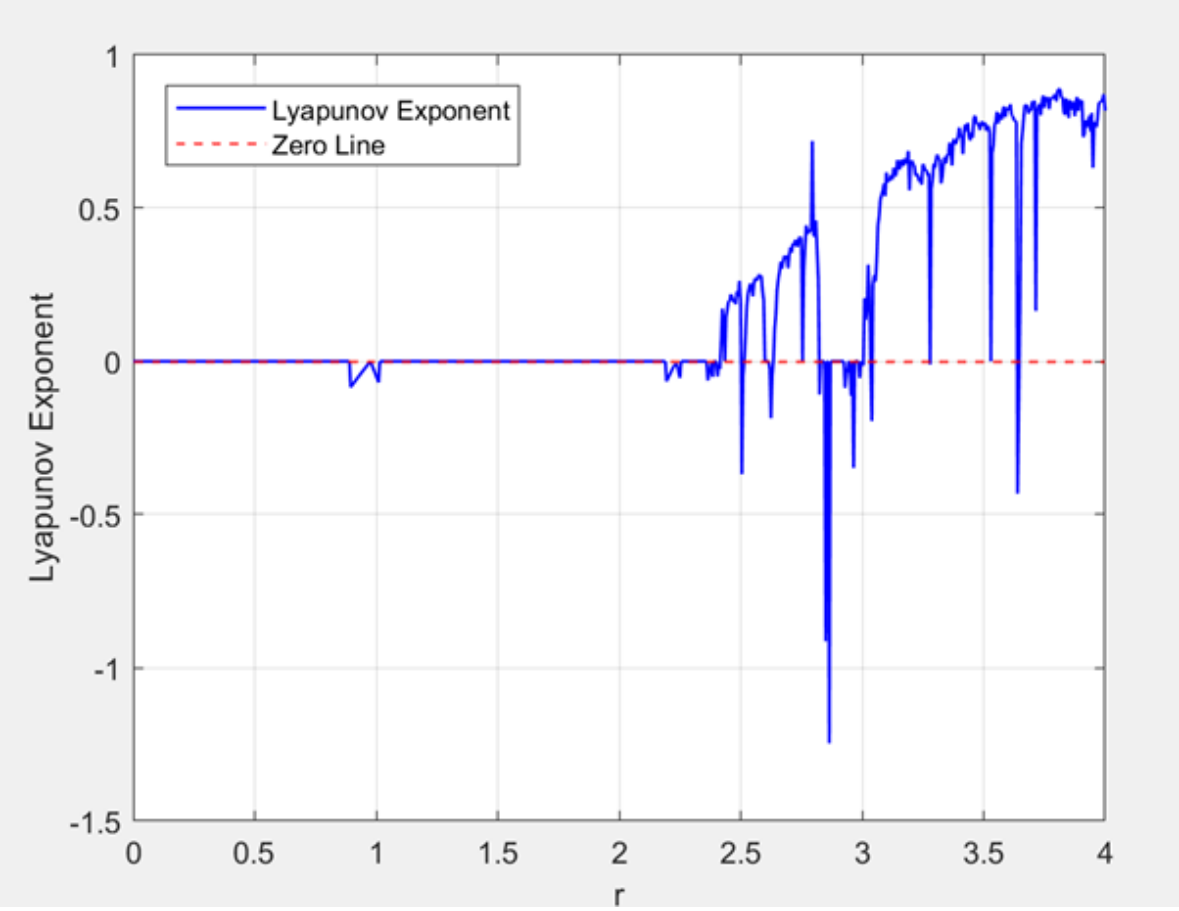

Figure 8.3: Lyapunov Exponents at $\Omega = 8.3$ rads^{-1}.

The results obtained for intermittency around the primary resonance clearly illustrated the presence of intermittent dynamics in the system. The bifurcation diagram revealed a classical route to chaos through period-doubling bifurcations, a hallmark of nonlinear dynamical systems. Notably, at the critical parameter value of $r = 2.43$, the diagram exhibited intermittent windows, regions where the system oscillated irregularly between phases of regular periodic motion and bursts of chaotic behaviour. This intermittent transition indicates a temporary and unpredictable loss of stability, which is a defining characteristic of type-I intermittency commonly observed near the onset of chaos.

This finding was further validated by the corresponding heat map, which visually confirmed the existence of an area at $r = 2.43$ where the system's periodic behaviour unpredictably shifted to chaotic dynamics. The heat map provided a colour-coded depiction of the system's response, with transitions marked by distinct variations in intensity and structure. Additionally, the Lyapunov exponent analysis reinforced this

interpretation: at $r = 2.43$, the exponents fluctuated between positive and negative values, reflecting alternating regimes of divergence and convergence in phase space. This variation is a quantitative indicator of intermittent behaviour, affirming the non-uniform stability of the system. Together, these results demonstrate that the system undergoes a complex transition to chaos characterised by intermittency, and highlight the importance of using multiple analytical tools to detect and interpret such subtle dynamical phenomena.

8.5.2 Analysing Intermittency around the Subharmonic Resonance

The subharmonic resonance for the swing equation in this study occurs at an excitation frequency of $\Omega = 19.41\ \mathrm{rad\,s^{-1}}$. To investigate the system's behaviour near this resonance, a bifurcation diagram was generated at $\Omega = 19.5\ \mathrm{rad\,s^{-1}}$, a value chosen to lie in close proximity to the subharmonic resonance frequency. As illustrated in Figure 8.4, the diagram reveals a rich variety of nonlinear dynamics as the parameter r is varied. At approximately $r = 0.965$, the system undergoes a period-doubling bifurcation, resulting in the emergence of a stable period-2 orbit. This is a classic indicator of a route to chaos through successive period-doublings. As r increases further to around $r = 2.36$, a second period-doubling occurs, giving rise to a period-4 orbit, further demonstrating the system's progression toward chaotic dynamics.

Following these transitions, the system continues to exhibit increasingly complex behaviour. By approximately $r = 2.685$, all lower-order periodic orbits appear to have taken place, and the system enters a fully chaotic regime. This is characterised by irregular, aperiodic oscillations and sensitive dependence on initial conditions. As r is increased beyond this point, specifically around $r = 2.9$, the system becomes unstable, indicating a breakdown of the previously observed attractor structure. The loss of bounded oscillatory behaviour suggests that the swing equation system has exceeded its stability limits, underscoring the significance of parameter tuning and the sensitivity of nonlinear systems near resonance conditions.

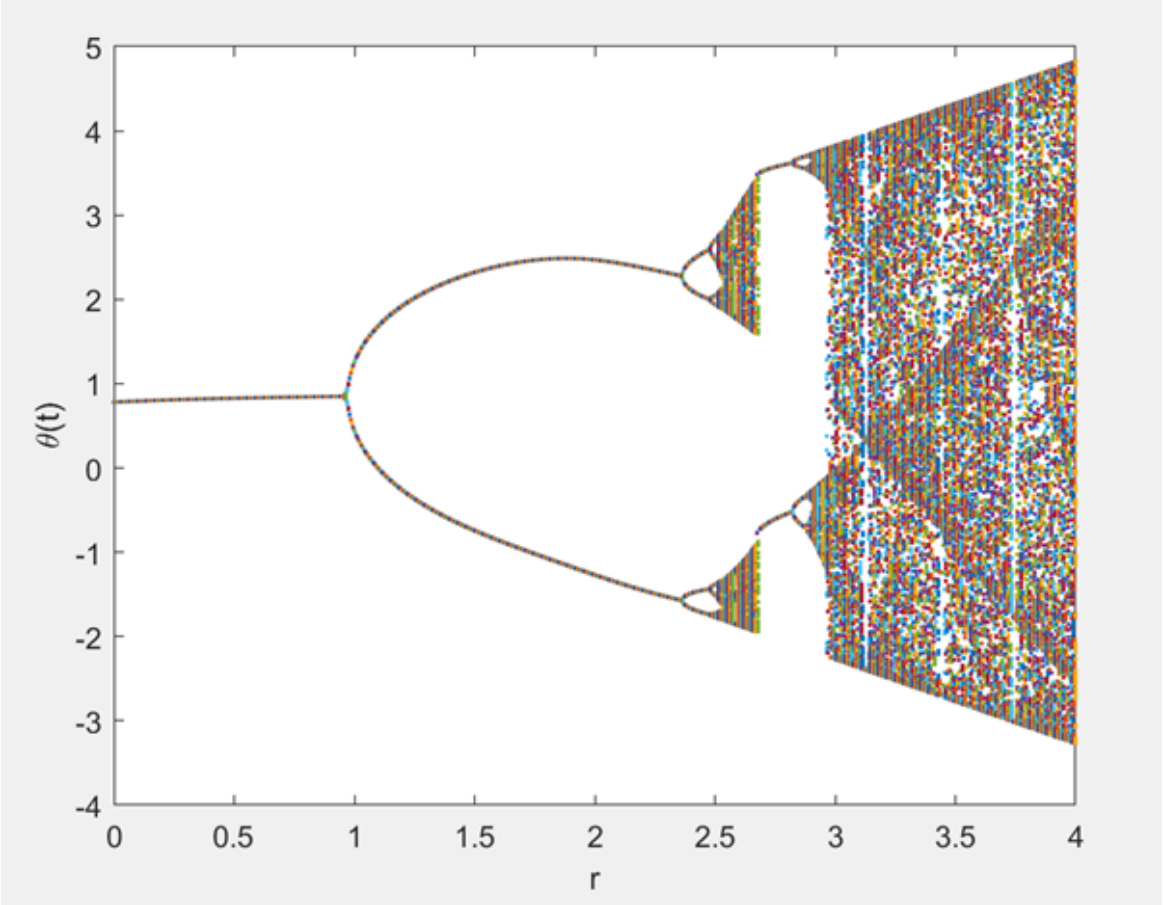

Figure 8.4: Bifurcation diagram at $\Omega = 19.5$ rads^{-1}.

The heatmap presented in Figure 8.5 illustrates the dynamic behaviour of the system under subharmonic resonance conditions. This visual representation provides a clear depiction of how the system transitions through different regimes as the control parameter r is varied. The marked region around $r = 2.68$ highlights the presence of intermittency, a transitional behaviour where the system alternates unpredictably between phases of periodic and chaotic motion. This intermittent window is consistent with the route to chaos identified in the corresponding bifurcation diagram and is characterised by fluctuations in system stability.

Beyond $r = 2.9$, the heatmap reveals a fully chaotic regime, indicated by the irregular and high-intensity patterns typical of sensitive, aperiodic dynamics. The colour gradient in this region intensifies, reflecting the complex and unstable nature of the system's response. These observations reinforce the significance of the intermittency threshold at $r = 2.68$, which serves as a precursor to the complete breakdown of regular motion.

Overall, the heatmap provides strong visual confirmation of the system's transition to chaos and highlights the critical regions in parameter space where control strategies may be most effective.

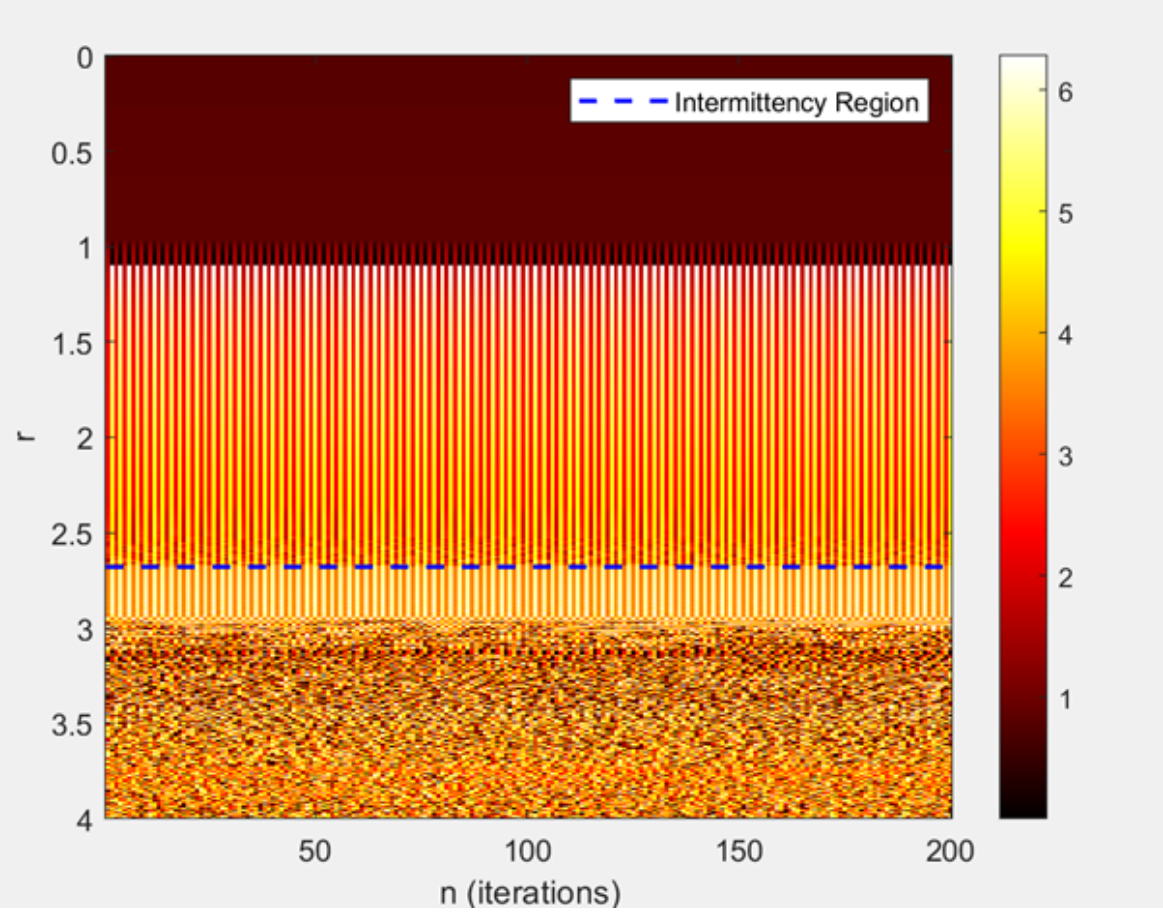

Figure 8.5: Heatmap depicting the dynamical behaviour closer to Subharmonic Resonance.

Figure 8.6 shows the Lyapunov exponents corresponding to the bifurcation diagram for subharmonic resonance. This figure serves to validate the results obtained from both the bifurcation diagram and the heatmap for this case. The Lyapunov exponent becomes positive in regions where chaotic behaviour is observed, particularly beyond $r = 2.68$, confirming the onset of instability. In the intermittent region, the exponent fluctuates near zero, which is characteristic of transitions between periodic and chaotic dynamics. These findings reinforce the diagnostic power of Lyapunov analysis in detecting chaos and verifying the system's nonlinear response near subharmonic resonance.

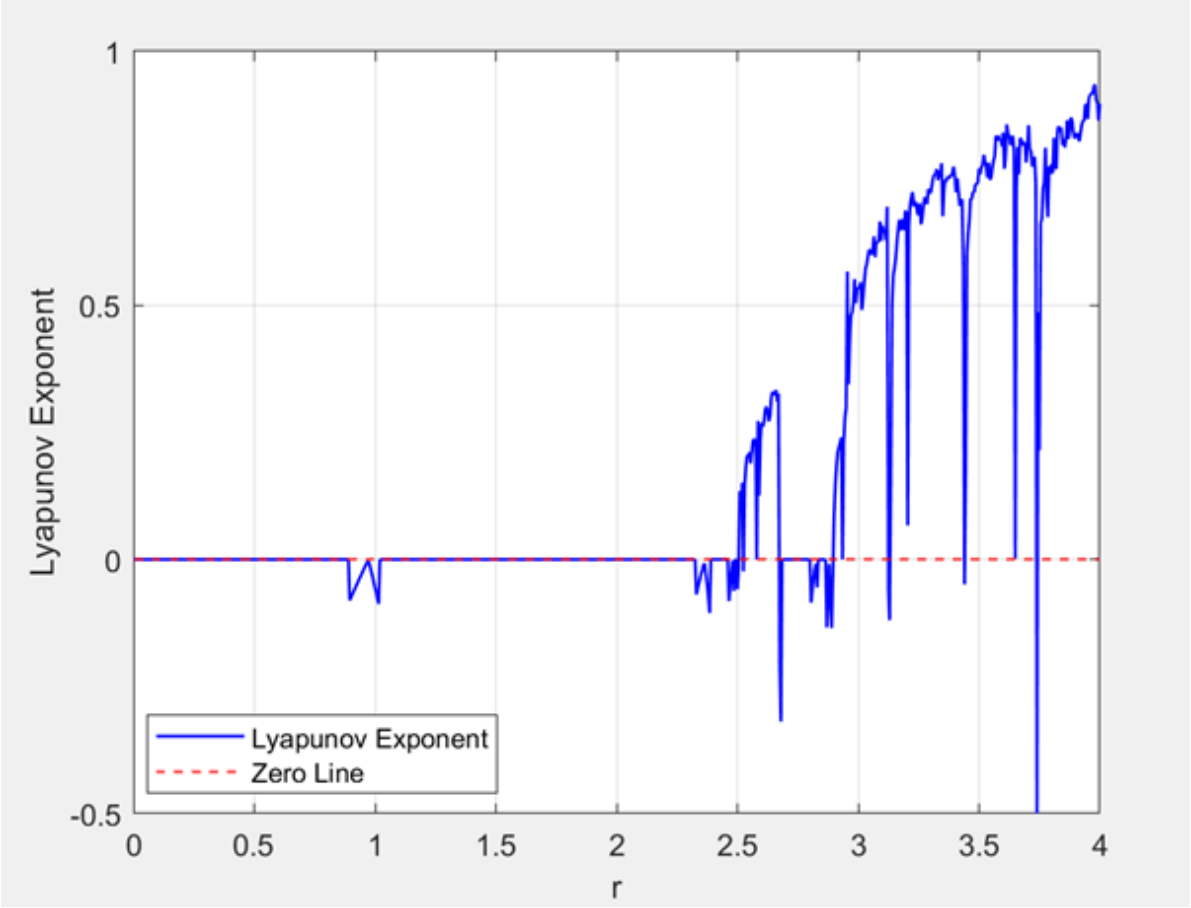

Figure 8.6: Lyapunov Exponents at $\Omega = 19.5$ rads^{-1}.

8.5.3 Analysing Intermittency around the Quasiperiodicity

The bifurcation diagram associated with quasiperiodicity at an excitation frequency of $\Omega = \frac{\pi}{2.5}$ rad s^{-1} was obtained using Matlab for detailed nonlinear analysis, as illustrated in Figure 8.7. This diagram captures the complex dynamic transitions of the system under quasiperiodic excitation and provides valuable insight into the emergence of intermittent and chaotic behaviour. As the system parameter r is varied, several distinct regions of intermittency can be identified, reflecting a gradual and irregular transition between ordered and chaotic states.

At approximately $r = 2.24$, the first clear instance of intermittency becomes evident. Here, the system exhibits alternating phases of regular periodic motion interrupted by unpredictable, short bursts of chaotic activity. This behaviour is indicative of type-I intermittency and marks the system's initial departure from steady-state oscillations. A

second intermittent window is observed around $r = 2.5$, where a similar switching between stable and unstable dynamics is present. Most notably, at $r = 3.701$, the system undergoes a sudden and pronounced burst of intermittent behaviour, suggesting a critical threshold beyond which chaos becomes dominant. These successive occurrences of intermittency highlight the sensitivity of the system under quasiperiodic forcing and underscore the importance of precise parameter control to maintain stable operation.

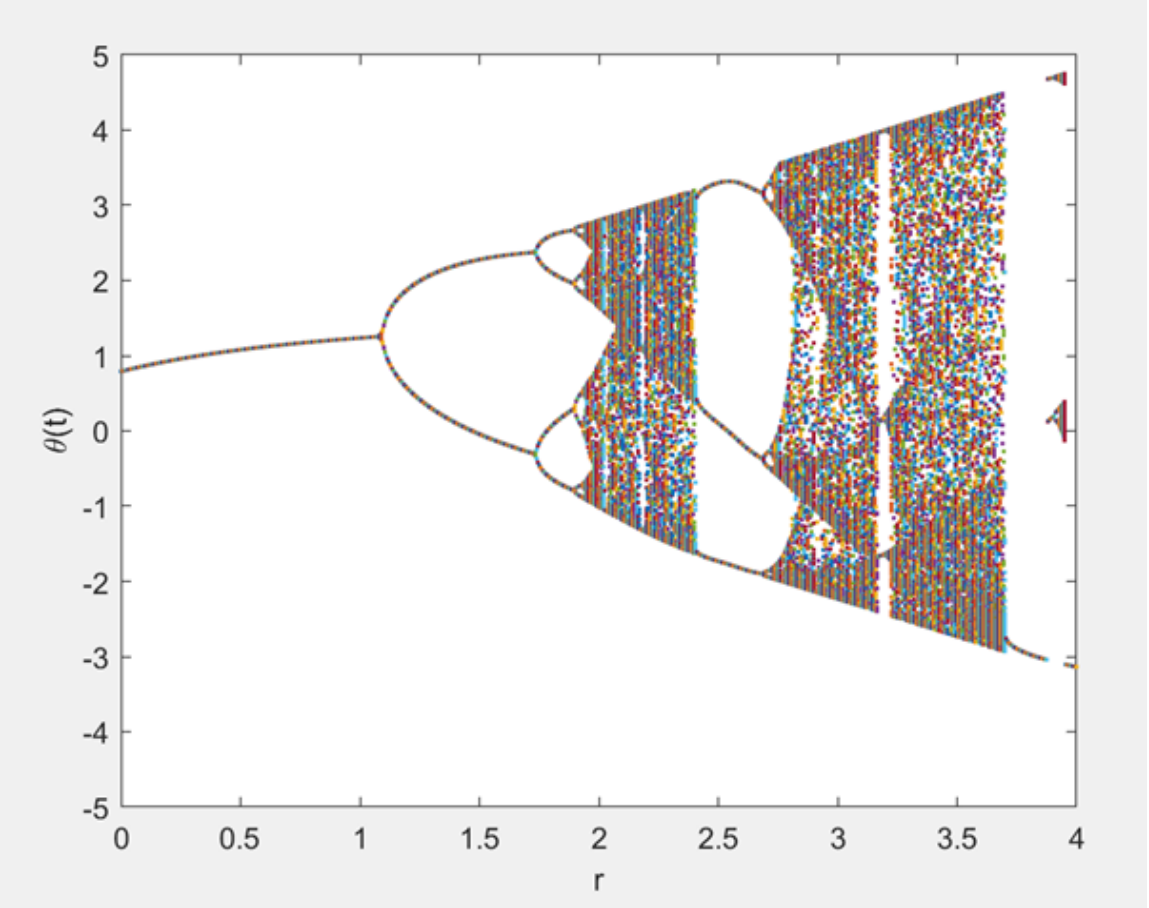

Figure 8.7: Bifurcation diagram for Quasiperiodicity at $\Omega = \pi/2.5$ rads^{-1}.

The following heatmap, Figure 8.8, shows the system for quasiperiodicity. The marked regions at $r = 2.24, 2.5, 3.701$ depict intermittencies, where the system alternates between chaotic and periodic dynamics.

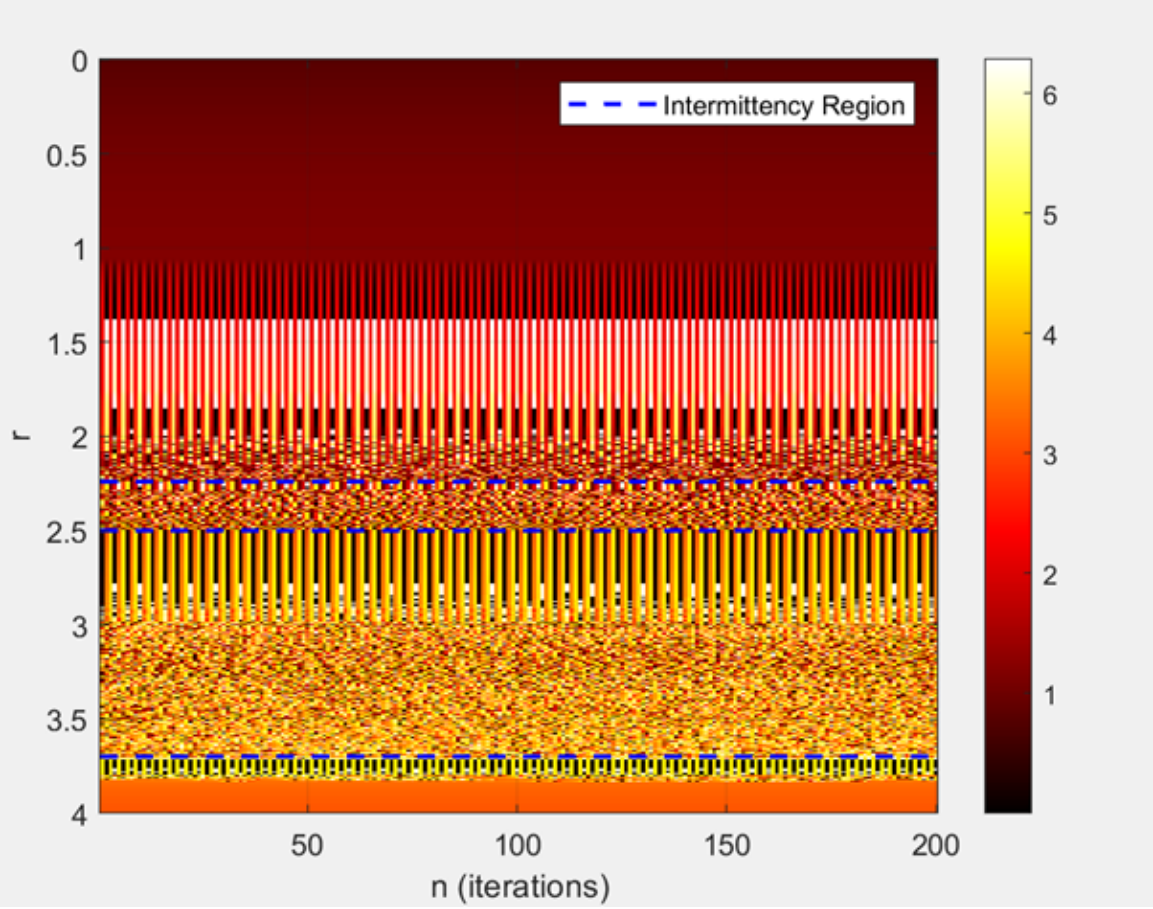

Figure 8.8: Heatmap depicting the dynamical behaviour for Quasiperiodicity.

Figure 8.9 shows the Lyapunov exponents for the corresponding bifurcation diagram in the case of quasiperiodicity. This validates the results obtained from the bifurcation diagram and the heatmap for this case. The regions where the Lyapunov exponent crosses from negative to positive values align with the onset of chaotic behaviour seen in the bifurcation diagram. Near the intermittent windows at $r = 2.24$, $r = 2.5$, and $r = 3.701$, the exponents fluctuate close to zero, confirming transitions between order and chaos. These fluctuations are consistent with quasiperiodic routes to chaos and further support the presence of intermittent dynamics. The use of Lyapunov analysis thus provides a quantitative measure reinforcing the visual observations from other diagnostic tools.

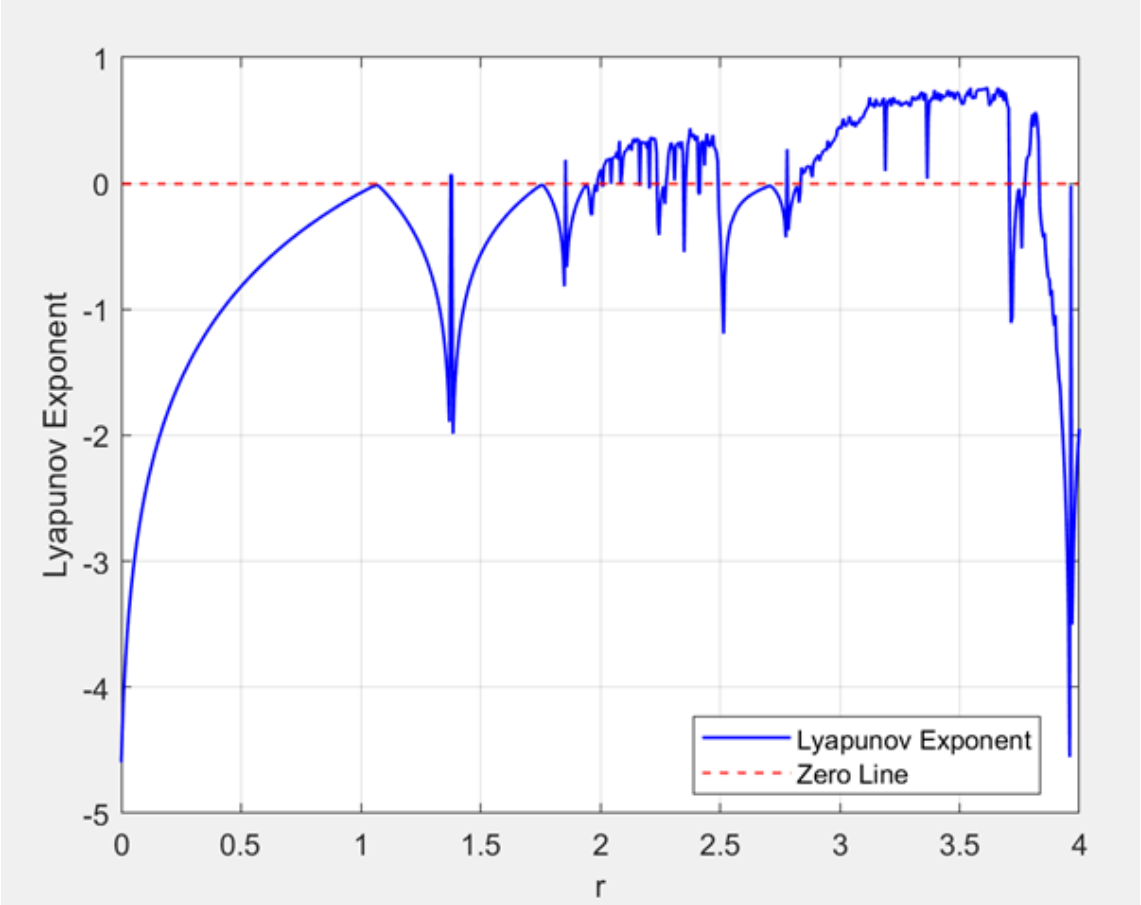

Figure 8.9: Lyapunov Exponents for Quasiperiodicity at $\Omega = \pi/2.5$ rads^{-1}.

8.6 Effects of altering Inertia in the Swing Equation

The following results were obtained when the system inertia was varied and exhibited intermittency in the swing equation. This variation in inertia significantly influenced the dynamic response of the system, leading to observable changes in oscillatory behaviour and stability margins. The presence of intermittent inertia introduces complexity in the modelling process, making it essential to capture transient phenomena accurately. These findings highlight the importance of incorporating realistic, time-varying parameters when analysing power system dynamics using the swing equation.

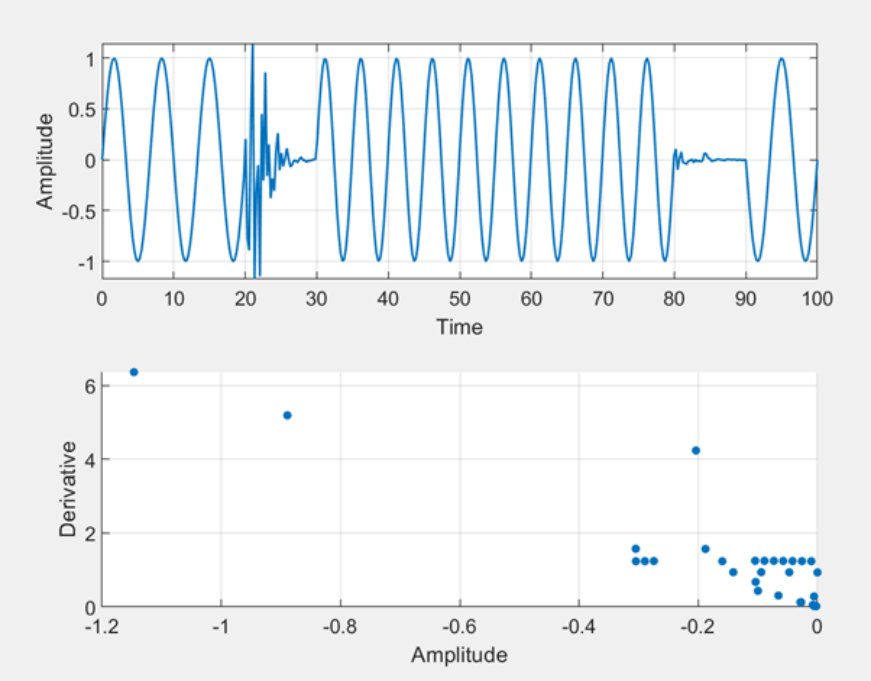

Figure 8.10: Time series and Poincaré map for the case of intermittency when Inertia is 1.81 kgm^2.

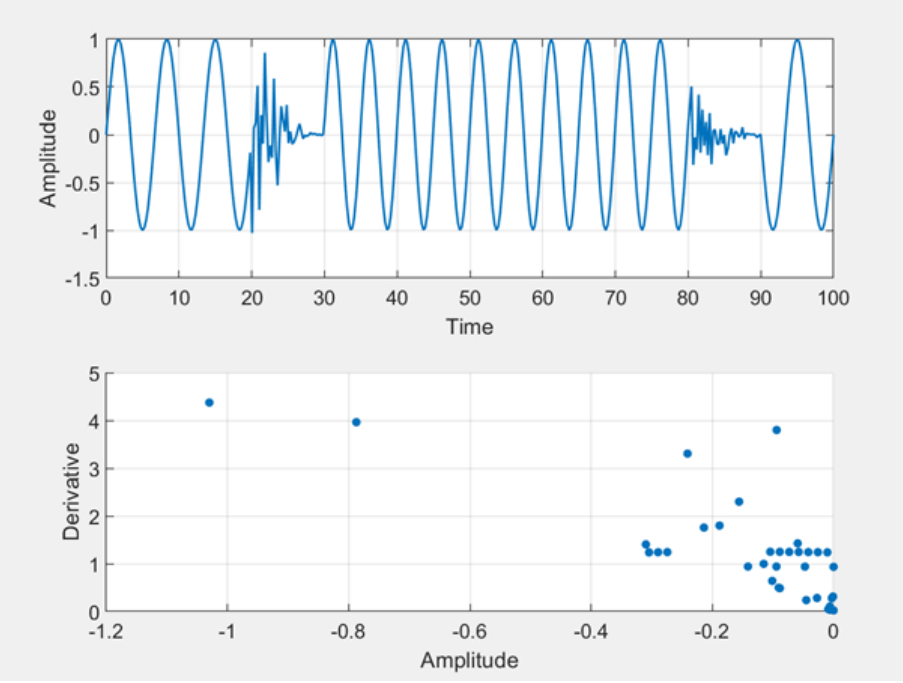

Figure 8.11: Time series and Poincaré map for the case of intermittency when Inertia is 1.75 kgm^2.

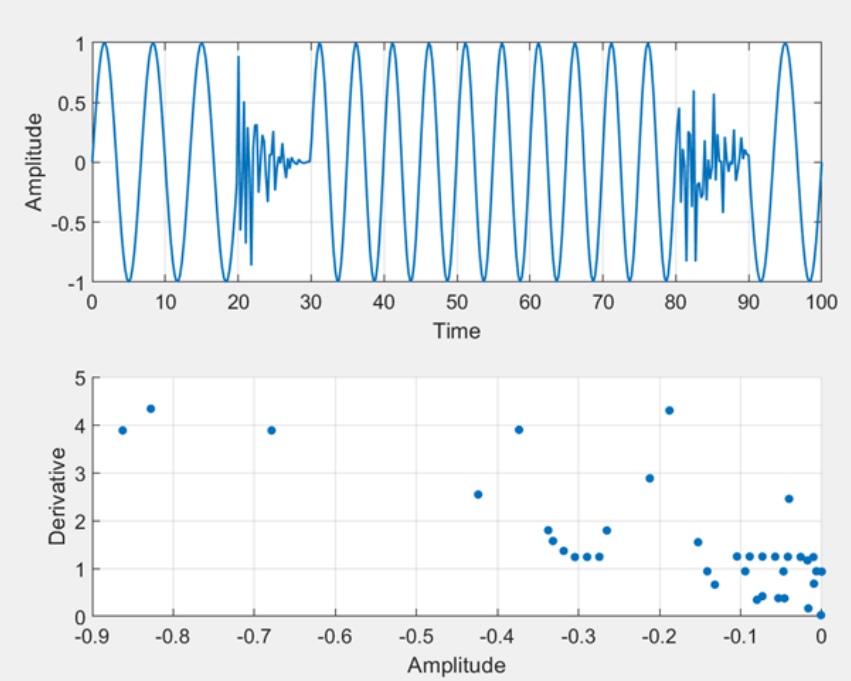

Figure 8.12: Time series and Poincaré map for the case of intermittency when Inertia is 1.7 kgm^2

The figures above Figures 8.10, 8.11, and 8.12 illustrate the time series behaviour of the system as the variable inertia is changed. These figures correspond to different values of the moment of inertia H, and provide insight into the transition from periodic to chaotic dynamics. The associated Poincaré maps offer a complementary view, capturing the qualitative changes in the attractors of the system.

As the value of H is varied, the system exhibits a range of dynamical behaviours. For instance, when $H = 1.81\,\text{kgm}^2$, the system predominantly exhibits periodic orbits. However, intermittent bursts of chaotic motion appear suddenly within these regular intervals. This phenomenon indicates that the system is near a bifurcation point, where small changes in inertia lead to drastic changes in the long-term dynamics.

The corresponding Poincaré map for $H = 1.81\,\text{kgm}^2$ initially displays a periodic attractor represented by discrete, regularly spaced points. As the chaotic bursts begin to appear, the map evolves and begins to show a gradual expansion of the attractor, signifying the emergence of instability in the system. The transition is marked by the spreading of points in the Poincaré map, which is indicative of the system entering a chaotic regime.

Overall, these figures and maps highlight the sensitivity of the system's behaviour to changes in the moment of inertia and demonstrate a classical route to chaos via intermittency and attractor destabilisation.

8.7 Effects of altering Voltage of machine in the Swing Equation

The following intermittency graphs were obtained when the machine voltage (V_G) was varied. Altering the machine voltage has a direct impact on the power output and stability characteristics of the system, influencing the overall dynamic behaviour. The results demonstrate how fluctuations in V_G can lead to intermittent patterns in the system's response, particularly affecting the synchronisation and damping properties. These graphical representations provide valuable insights into the sensitivity of the system to voltage variations, which is critical for the design and stability assessment of power systems under varying operating conditions.

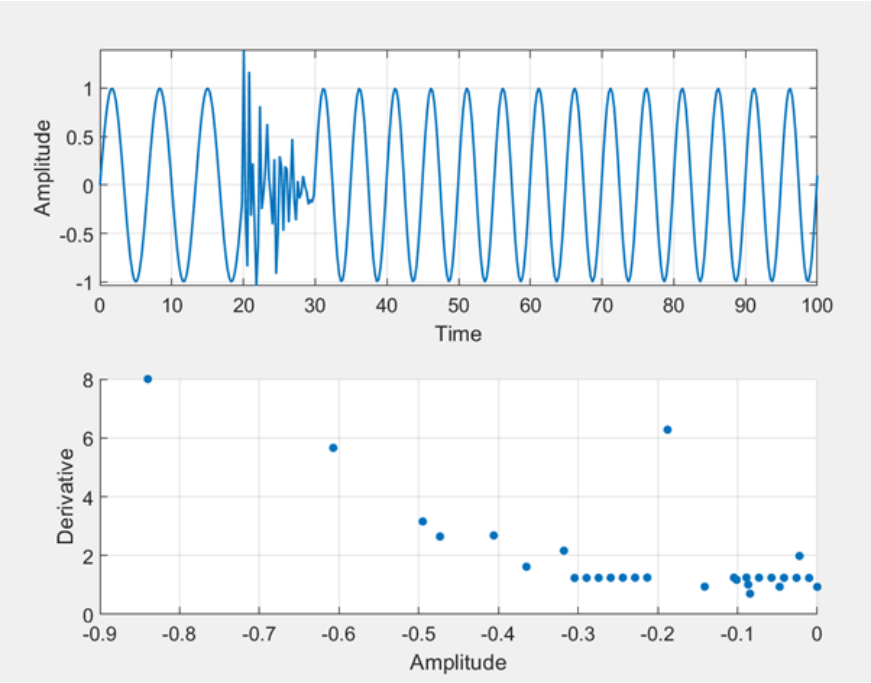

Figure 8.13: Time series and Poincaré map for the case of intermittency when V_G is 0.05.

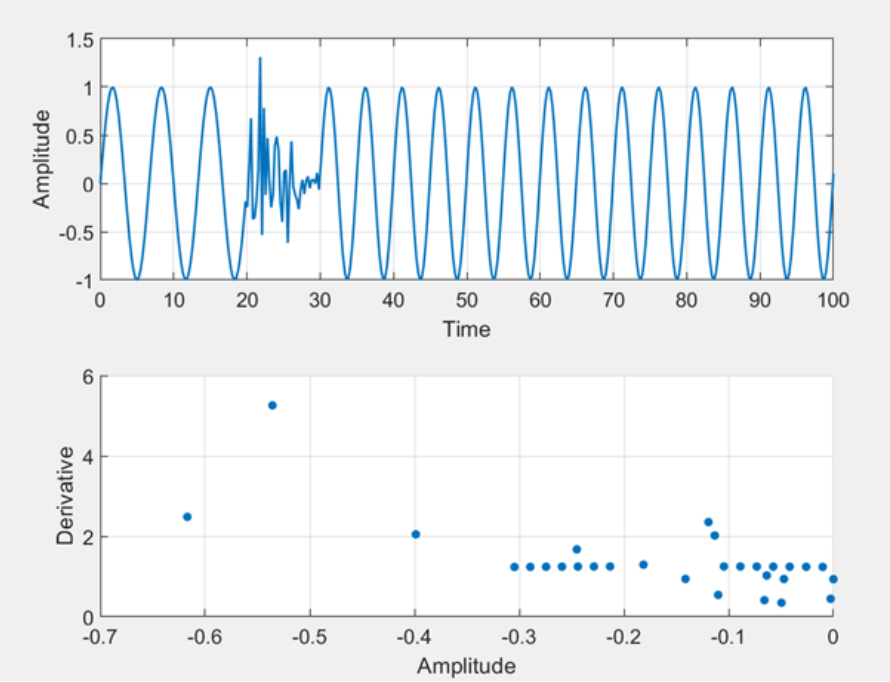

Figure 8.14: Time series and Poincaré map for the case of intermittency when V_G is 0.04.

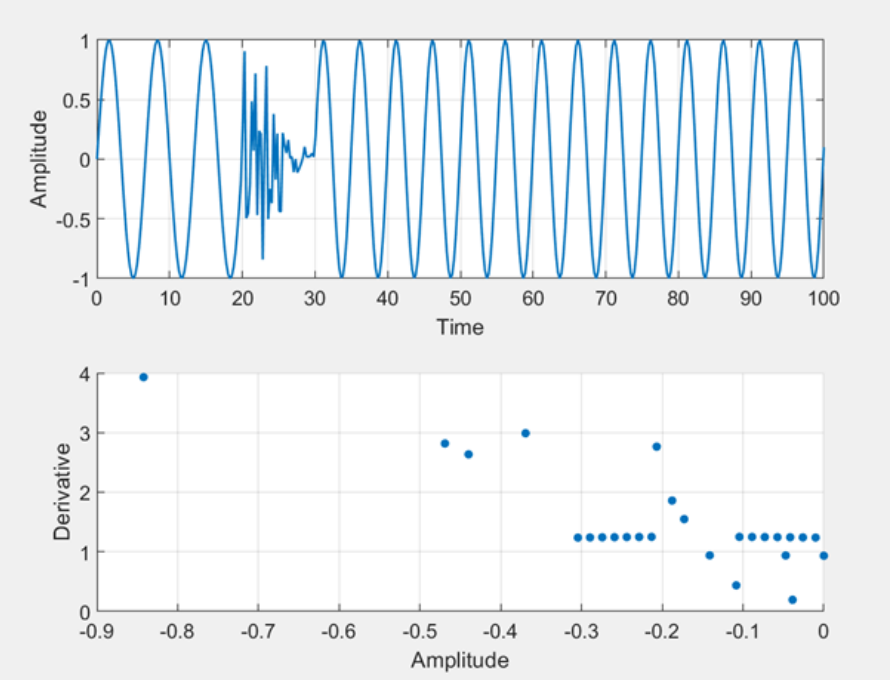

Figure 8.15: Time series and Poincaré map for the case of intermittency when V_G is 0.03.

Figures 8.13, 8.14, and 8.15 present the time series and corresponding Poincaré maps for varying values of the machine voltage. Similar to the earlier analysis involving moment of inertia, these figures reveal that changes in the machine voltage significantly affect

the dynamic behaviour of the system. Specifically, the system transitions from periodic motion to sudden bursts of instability, a phenomenon characteristic of intermittent behaviour. This intermittent instability is clearly visible in the time series, where regular oscillations are interrupted by erratic fluctuations. The corresponding Poincaré maps reflect this transition, initially showing periodic attractors which then begin to scatter, indicating a move toward chaotic dynamics.

To further explore the system's sensitivity, both the inertia and machine voltage were systematically varied. When the moment of inertia was adjusted within the range $1.70\,\mathrm{kgm}^2 \leq H \leq 1.81\,\mathrm{kgm}^2$, the system began to display clear signs of intermittent instability. This suggests that the system is operating near a bifurcation threshold, where small changes in physical parameters can trigger complex dynamical transitions.

Similarly, variations in the machine voltage, specifically in the range from 0.05 to 0.03, led to an observable increase in instability. As the voltage decreased, the system's periodic nature was disrupted more frequently by irregular and chaotic bursts. This behaviour indicates that lower voltages may reduce system damping or alter the excitation dynamics, thereby enhancing the system's susceptibility to intermittency and chaotic transitions.

In both cases whether through changes in inertia or voltage, the system consistently demonstrated a tendency toward intermittent chaos, underscoring the nonlinear and sensitive dependence of the system's dynamics on its governing parameters.

8.8 Discussion

The findings from this section underscore the importance of intermittency as a prelude to chaos in the swing equation. Identifying the pivotal values of intermittent behaviour can assist in recognising instability in power systems. This is especially pertinent in real-world power systems characterised by low inertia.

In comparison with previous research, the validation of Lyapunov exponents adheres to analogous techniques [207] for identifying chaos. This verifies that intermittency phenomena can be evaluated via exponent fluctuations. The findings align with the intermittency observed in fluid dynamics [194], indicating that the analysis of intermittency is relevant across diverse nonlinear systems.

This chapter possesses certain limitations that warrant consideration. The swing

equation is examined in an idealised context, excluding external influences such as power grid disturbances and abrupt load variations. While inertia and voltage of the machine are examined, additional characteristics like as damping and network architecture must also be considered to analyse intermittent behaviour.

This work elucidates the concept of intermittency in power systems by linking it to chaotic transitions in the swing equation, so enabling engineers to mitigate its detrimental impacts.

This chapter examined intermittency in the swing equation, illustrating its function as a precursor to chaos in power systems. Bifurcation diagrams, Lyapunov exponents, heat maps, and Poincaré maps were utilised to detect intermittency. The findings validate that intermittency can be noticed when the machine's inertia and voltage fluctuate, underscoring the significance of analysing minor disruptions within the system.

Power grids that include renewable energy with low inertia demonstrate intermittent behaviour. This chapter emphasises that low-inertia systems exhibit a heightened potential for intermittent instability, underscoring the significance and necessity of stability management techniques. The examination of the machine's voltage indicates that precise voltage regulation measures can mitigate chaotic transitions.

8.9 Final Remarks

The findings of this chapter establish a foundational framework for developing early warning indicators aimed at detecting potential instability within power networks. One of the key insights is the potential deployment of Lyapunov exponent monitoring instruments as diagnostic tools. These instruments can be used to detect the onset of intermittent behaviour, which serves as a precursor to chaotic transitions in system dynamics. By identifying these early signals, system operators could take preventive actions before instability manifests in a disruptive manner, thereby enhancing grid reliability and resilience.

Although this research contributes significantly to the understanding of nonlinear dynamics in power systems, it is not without limitations. The analysis of the swing equation was conducted under idealised conditions, deliberately excluding extraneous influences such as load variations, stochastic fluctuations, and grid faults. These were

necessary for isolating the primary dynamic behaviour; however, they also highlight the scope for future research. Subsequent studies should focus on real-time operational environments to better assess the impact of intermittency and identify other precursors to chaotic transitions. In addition, the methodology can be extended to multi-machine or large-scale interconnected power systems to explore the interplay between resonance, intermittency, and chaos as grid complexity increases.

Furthermore, future investigations may consider the integration of advanced data-driven techniques such as machine learning and predictive analytics with traditional nonlinear dynamical models. This hybrid approach could lead to more robust forecasting tools capable of capturing subtle precursors to instability. As modern power systems evolve with the incorporation of renewable energy sources, electric vehicles, and decentralised control strategies, understanding and managing nonlinear behaviours will become increasingly critical. Hence, this line of inquiry not only advances theoretical insight but also holds considerable promise for enhancing the operational security of future smart grids.

Chapter 9

Analysing Load Shedding Technique to Increase Stability

9.1 Introduction

Examining the stability of nonlinear systems is of paramount importance, particularly in the context of sudden, minor perturbations that may escalate into large-scale failures or blackouts [33, 89]. Power systems, by their nature, are highly sensitive to fluctuations, and even small deviations can produce cascading effects that threaten the integrity of the entire grid. A crucial aspect of maintaining system stability lies in ensuring that the system's frequency remains within specified operational limits. Frequency deviations are typically caused by abrupt mismatches between electricity demand and generation capacity, which, if not addressed promptly, may lead to destabilisation and equipment damage [213].

To mitigate such adverse outcomes, a range of control strategies have been implemented, aimed at preserving frequency stability during short-term disturbances. These strategies are essential for ensuring that transients do not lead to critical instability or chaotic dynamics. Frequency regulation mechanisms, both primary and secondary, serve to restore balance between supply and demand in the immediate aftermath of a disturbance, thereby reducing the risk of cascading failures.

The swing equation, a second-order nonlinear differential equation, is central to the analysis of power system dynamics. It models the motion of the rotor in synchronous

machines and captures the essential behaviour of generators under various operating conditions [33, 77]. While numerical simulations have long been the standard approach for exploring these nonlinear dynamics [214], recent advancements have seen the adoption of more sophisticated analytical tools. These methods have been employed to define and explore stability boundaries under a wide range of parameter settings and disturbances [115, 134], providing deeper insight into the onset of instability and the conditions that facilitate transitions to chaos.

Historical approaches to mitigating frequency instability have focused on load shedding techniques. These have evolved from rigid, rule-based mechanisms to more nuanced, adaptive strategies. Classical methods such as Under Frequency Load Shedding (UFLS) are relatively simple and easy to implement; however, they suffer from several shortcomings. Chief among them is the use of fixed frequency thresholds, which often result in either excessive or insufficient load shedding [216, 217]. Such static approaches are unable to account for the real-time state of the grid and fail to adapt to varying levels of perturbation.

To overcome these limitations, recent research has shifted towards data-driven methodologies capable of dynamically responding to grid conditions. These advanced techniques integrate real-time system monitoring, predictive analytics, and machine learning models to execute more accurate and efficient load shedding operations [215, 218–221]. These strategies not only provide improved resilience against disturbances but also enable more economical and sustainable grid operations. The transition from traditional to intelligent systems marks a pivotal step towards the development of future-proof, smart grid infrastructures that can better withstand nonlinear instabilities and unpredictable perturbations.

Although a variety of contemporary control tools are available, ranging from voltage stability indicators to AI-driven, game-theoretic optimisation models many researchers still perceive load shedding as an external corrective measure, operating independently of the fundamental equations that govern system dynamics. Traditional perspectives often treat load shedding as a post-fault emergency response, rather than a proactive, system-integrated control variable.

This chapter aims to bridge this critical gap by proposing a control-integrated load shedding mechanism that is embedded directly within the dynamic equations of the

system. The approach draws inspiration from the classical equation of motion for a pendulum, adapting it to the context of synchronous machines governed by the nonlinear swing equation. The principal goal is to analytically determine the minimum amount of load curtailment required to restore system stability following minor disturbances, and to explore the extent to which the integration of a load shedding term can mitigate the onset of chaotic behaviour. By modifying the damping characteristics of the swing equation via a shedding factor, this method enables real-time control to be analytically understood within the context of nonlinear dynamics.

The proposed work derives an analytical formulation of the swing equation that explicitly includes a load shedding component. It subsequently evaluates the system's stability using a suite of well-established analytical tools, including eigenvalue analysis, Lyapunov exponents, bifurcation diagrams, and perturbation techniques. The proposed approach is then compared with conventional load shedding strategies, using both analytical derivations and numerical simulations. The methodology's robustness is tested across a range of system parameters, and its effectiveness is validated through simulations conducted in Matlab Simulink.

The stability of nonlinear systems in the presence of small and abrupt perturbations has become an area of increasing importance, especially given the growing complexity and decentralisation of modern power grids. Load shedding remains one of the most widely implemented emergency control mechanisms used to prevent system-wide blackouts and to preserve frequency stability under stress conditions [222]. However, its implementation has traditionally remained detached from the governing dynamic equations of the power system.

The swing equation, which models the rotor dynamics of synchronous generators, is a cornerstone in the analysis of transient stability. Represented as a second-order nonlinear differential equation, it captures the essential response of power systems to disturbances [159, 205]. Due to its inherent nonlinearity, solving the swing equation analytically has historically posed considerable challenges, with early investigations relying almost exclusively on numerical techniques. Nevertheless, recent advances have introduced novel analytical approaches that provide deeper insights into system stability boundaries [214, 223]. For instance, reformulating the swing equation in Cartesian coordinates has enabled approximate analytical solutions that align well with traditional numerical

outcomes [224]. Similarly, enhancements to ZIP load models, incorporating constant impedance, current, and power elements, have increased the applicability of such analyses to real-world scenarios [225].

Despite these analytical advances, many industrial systems continue to employ conventional load shedding techniques such as Under Frequency Load Shedding (UFLS), primarily due to their simplicity and ease of implementation. These methods operate by disconnecting predefined load blocks once frequency thresholds are breached [226]. However, these static and reactive methods are fundamentally limited, they neither adapt to the nature of the disturbance nor incorporate real-time system conditions. As a result, they often lead to either over-shedding or under-shedding, exacerbating instability instead of alleviating it.

To improve upon UFLS, voltage-indicator-based techniques have been proposed. These strategies evaluate the system's voltage margin to forecast the maximum sustainable load curtailment before instability ensues [227]. While more adaptive than traditional UFLS, their scope is generally confined to voltage-related instabilities and may not perform well in scenarios dominated by frequency dynamics.

In recent years, data-driven strategies employing machine learning techniques have garnered significant attention. These methods leverage historical operational data and simulated scenarios to forecast optimal load shedding actions in real time [219, 220]. Although they offer impressive predictive capabilities, these techniques require large volumes of high-quality training data and often struggle with generalisability across different grid topologies. Furthermore, they lack analytical transparency and are often treated as black-box solutions, which can be problematic in critical infrastructure contexts where interpretability and auditability are paramount.

Game-theoretic frameworks represent another emerging class of solutions, modelling power systems as multi-agent environments where entities such as regional operators, generators, and consumers engage in cooperative or competitive decision-making processes [221]. These models are capable of producing equilibrium-based load shedding strategies that balance local objectives with global system stability. However, they introduce complex optimisation problems and often rely on strong assumptions about agent behaviour, which can be difficult to realise in a real-time physical power system.

The methodology introduced in this chapter offers a distinct departure from these

approaches by embedding the load shedding mechanism directly within the swing equation. This integration enables load shedding to be treated as a dynamic system variable rather than an external intervention. The resulting modified swing equation allows for the derivation of closed-form expressions for key system parameters, such as natural frequency and damping ratio, under the influence of load curtailment. Through this formulation, the real-time effects of load shedding on system stability can be analytically traced, offering both interpretability and predictive capability.

By synthesising nonlinear dynamics theory with practical control applications, this approach serves as a promising foundation for future research and implementation. It aligns with the broader goal of developing intelligent, adaptive control strategies that are deeply rooted in the fundamental physics of power systems. Moreover, the method has the potential to enhance system resilience, reduce the frequency and severity of blackouts, and provide a theoretical framework that bridges the gap between simulation-based design and real-world control systems.

Table 9.1 below delineates several load shedding methodologies to elucidate the significance of the technique proposed in this article.

Table 9.1: Comparison of Load Shedding Strategies

Strategy Type	Real-Time Capable	Embedded in System	Control Flexibility	Limitations
UFLS (Conventional)	No	No	Low	Rigid thresholds; lacks adaptability to varying conditions
Voltage Indicator-Based	Partial	No	Medium	Dependent on reactive power data; not predictive under frequency-dominated instability
Machine Learning / Predictive	Yes	No	High	Requires extensive training data; may lack generalisation and interpretability
Game-Theory Approaches	Yes	No	High	Computationally intensive; assumes idealised agent behaviour
Proposed Embedded Method	Yes	Yes	Medium–High	Currently validated for single-machine models; requires extension for large-scale grids

9.2 Analytical Work

Deriving an equation for system frequency $f(t)$, which relates to the time derivative of the rotor angle:

$$f(t) = f_0 + \frac{1}{2\pi}\frac{d\theta}{dt} \tag{9.1}$$

where f_0 is the rated system frequency.

Differentiating both sides with respect to time:

$$\frac{df}{dt} = \frac{1}{2\pi}\frac{d^2\theta}{dt^2} \tag{9.2}$$

Substituting into the swing equation (3.10):

$$\frac{df}{dt} = \frac{\omega_R}{2H}\left(P_m - \frac{V_G V_B}{X_G}\sin\left(\theta - \theta_B\right) - D\frac{d\theta}{dt}\right) \tag{9.3}$$

This equation describes how the frequency $f(t)$ evolves over time based on power input, electrical power transfer, and damping.

9.2.1 Frequency Deviation Analysis

The aim is to make sure that the system frequency remains above the minimum threshold $f_{\min}$ to reduce unstable regions. During a small perturbation the electrical power P_e, might drop because of faults in the grids. This might adversely affect the nonlinear systems.

$$P_e = \frac{V_G V_B}{X_G} \sin(\theta - \theta_B) \tag{9.4}$$

To study the effect of these perturbations, it is required to approximate $\sin(\theta - \theta_B)$ using a first-order Taylor expansion around the steady-state condition $\theta \approx \theta_{B0}$:

$$\sin(\theta - \theta_B) \approx \sin\theta_{B0} + \cos\theta_{B0}(\theta - \theta_{B0}) \tag{9.5}$$

Introducing Load Shedding

Load shedding is introduced to alter P_e, reducing the effective electrical power. Let P_{LS} be the load shed, so that:

$$P_e' = P_e - P_{\text{LS}} \tag{9.6}$$

$$\frac{df}{dt} = \frac{\omega_R}{2H}\left(P_m - (P_e - P_{\text{LS}}) - D\frac{d\theta}{dt}\right) \tag{9.7}$$

Expanding P_e in the swing equation:

$$\begin{aligned}\frac{df}{dt} = \frac{\omega_R}{2H}\Bigg(P_m - \Bigg[&\frac{V_G(V_{B0} + V_{B1}\cos(\Omega t + \phi_v))}{X_G} \\ &\times(\sin\theta_{B0} + \cos\theta_{B0}(\theta - \theta_{B0})) - P_{\text{LS}}\Bigg] - D\frac{d\theta}{dt}\Bigg)\end{aligned} \tag{9.8}$$

The load shedding objective is to determine P_{LS} such that:

$$f(t) \geq f_{\min}, \quad \forall t \tag{9.9}$$

The load shedding term, P_{LS} , was introduced into the swing equation to evaluate its effect on system stability [218]. Load shedding was triggered when the rotor angle deviation exceeded a defined threshold. At each time step, if this threshold was breached, the system shed a fixed percentage of electrical power. The values of tested were 0.05, 0.1 and 1.2 per unit (pu). The values were carefully selected to represent light, moderate, and high levels of load reduction respectively and were chosen to examine how increasing control effort influences system dynamics. The effect of load shedding was studied by comparing the delay in chaotic parts in bifurcation diagrams and were validated from the Lyapunov Exponents.

9.2.2 Derivation of the Stability Equation without Load Shedding

Consider the swing equation (3.10) and approximate it using a Taylor series. Then simplifying gives:

$$\frac{d^2\theta}{dt^2} + \frac{D\omega_R}{2H}\frac{d\theta}{dt} + \frac{\omega_R}{2H}\frac{V_G V_B}{X_G}(\sin\theta_{B0} + \cos\theta_{B0}(\theta - \theta_{B0})) = 0 \tag{9.10}$$

The natural frequency is defined as:

$$\omega_n = \sqrt{\frac{\omega_R}{2H}\frac{V_G V_B}{X_G}\cos\theta_{B0}} \tag{9.11}$$

The damping ratio is:

$$\zeta = \frac{D}{2}\sqrt{\frac{\omega_R}{2H}\frac{V_G V_B}{X_G}\cos\theta_{B0}} \tag{9.12}$$

Thus, the characteristic equation is:

$$s^2 + 2\zeta\omega_n s + \omega_n^2 = 0 \tag{9.13}$$

Solving the above equation to find the eigenvalues:

$$s = -\zeta\omega_n \pm \omega_n\sqrt{\zeta^2 - 1} \tag{9.14}$$

The stability of the system is determined by the damping ratio ζ and the real part of the eigenvalues s.

The system is stable if the damping ratio is positive and the real part of the eigenvalues is negative:

$$\zeta > 0, \quad \mathrm{Re}(s) < 0. \tag{9.15}$$

If the damping ratio is between 0 and 1, the system oscillates but eventually stabilises:

$$0 < \zeta < 1. \tag{9.16}$$

If the damping ratio is exactly 1 it is called critically damped, the system returns to equilibrium in the shortest possible time without oscillations:

$$\zeta = 1. \tag{9.17}$$

If the damping ratio is negative, the real part of the eigenvalues is positive, leading to exponential growth and system instability:

$$\zeta < 0, \quad \mathrm{Re}(s) > 0. \tag{9.18}$$

9.2.3 Derivation of the Stability Equation with Load Shedding

The modified swing equation including load shedding is given by:

$$\frac{df}{dt} = \frac{\omega_R}{2H}\left(P_m - (P_e - P_{\mathrm{LS}}) - D\frac{d\theta}{dt}\right) \tag{9.19}$$

Expanding P_e:

$$\frac{df}{dt} = \frac{\omega_R}{2H}\left(P_m - \left[\frac{V_G(V_{B0} + V_{B1}\cos(\Omega t + \phi_v))}{X_G} \times (\sin\theta_{B0} + \cos\theta_{B0}(\theta - \theta_{B0})) - P_{\mathrm{LS}}\right] - D\frac{d\theta}{dt}\right) \tag{9.20}$$

Considering small deviations around the equilibrium $\theta \approx \theta_{B0}$, leading to the linearised system:

$$\frac{d^2\theta}{dt^2} + \frac{D + P_{\text{LS}}}{2H}\frac{d\theta}{dt} + \frac{\omega_R}{2H}\frac{V_G V_B}{X_G}\cos\theta_{B0}(\theta - \theta_{B0}) = 0 \tag{9.21}$$

This equation follows the form of a standard second-order differential equation:

$$\frac{d^2\theta}{dt^2} + 2\zeta\omega_n\frac{d\theta}{dt} + \omega_n^2(\theta - \theta_{B0}) = 0 \tag{9.22}$$

The natural frequency ω_n is:

$$\omega_n = \sqrt{\frac{\omega_R}{2H}\frac{V_G V_B}{X_G}\cos\theta_{B0}} \tag{9.23}$$

The damping ratio ζ is modified due to the incorporation of load shedding P_{LS}:

$$\zeta = \frac{D + P_{\text{LS}}}{2}\sqrt{\frac{\omega_R}{2H}\frac{V_G V_B}{X_G}\cos\theta_{B0}} \tag{9.24}$$

The characteristic equation was:

$$s^2 + 2\zeta\omega_n s + \omega_n^2 = 0 \tag{9.25}$$

Solving for the eigenvalues:

$$s = -\zeta\omega_n \pm \omega_n\sqrt{\zeta^2 - 1} \tag{9.26}$$

The eigenvalues were plotted in Figure 9.3, for different values of P_{LS}, depicting a leftward shift as load shedding increased. This confirms that higher values enhanced system damping and reduced oscillations, leading to delayed chaos within the system.

9.2.4 Perturbation Analysis

The standard swing equation, which governs the rotor dynamics of a synchronous machine including damping and electrical power terms, is given by [77]:

$$\frac{2H}{\omega_R}\frac{d^2\theta}{dt^2} + D\frac{d\theta}{dt} = P_m - P_e \tag{9.27}$$

where:

- P_m is the mechanical power input.

- P_e is the electrical power output.

To enhance stability, introducing the load shedding term within the equation P_{LS},

$$\frac{2H}{\omega_R}\frac{d^2\theta}{dt^2} + D\frac{d\theta}{dt} = P_m - (P_e - P_{\text{LS}}) \tag{9.28}$$

where

$$P_{\text{LS}} = P_{LS0} + P_{LS1}\cos(\Omega t + \phi_{ls}) \tag{9.29}$$

This equation (9.29) shows a small perturbation effect on the load shedding term where P_{LS0} which depicts the initial state and is assumed to be very small.

Expanding P_e using a first-order Taylor series approximation:

$$P_e = \frac{V_G(V_{B0} + V_{B1}\cos(\Omega t + \phi_v))}{X_G}(\sin\theta_{B0} + \cos\theta_{B0}(\theta - \theta_{B0})) \tag{9.30}$$

By introducing perturbations in rotor angle,

$$\theta - \theta_B = \eta \tag{9.31}$$

Allowing consideration for the transformations,

$$\theta - \theta_B = \delta_0 + \eta \tag{9.32}$$

$$\delta_0 = \theta_0 - \theta_{B0} \tag{9.33}$$

$$\eta = \Delta\theta - \theta_{B1}\cos(\omega t + \phi_0) \tag{9.34}$$

Equation (9.32) becomes,

$$\sin(\theta - \theta_B) = \sin(\delta_0 + \eta) \tag{9.35}$$

Substituting equations (9.32), (9.33) and (9.34) into equations (3.10), (3.11), and (3.12), we derive the modified swing equation with excitation:

$$\frac{d^2\eta}{dt^2} + \frac{\omega_R D}{2H}\frac{d\eta}{dt} + K\eta = \alpha_2\eta^2 + \alpha_3\eta^3 + G_1\eta\cos(\Omega t + \phi_v) + G_2\eta^2\cos(\Omega t + \phi_v) + G_3\eta^3\cos(\Omega t + \phi_v) + Q_1\cos(\Omega t + \phi_\theta) + Q_2\sin(\Omega t + \phi_\theta) + Q_3\cos(\Omega t + \phi_v) + P_1\cos(\Omega t + \phi_{LS}) \quad (9.36)$$

$$\alpha_2 = \frac{1}{2}K\tan\delta_0, \quad \alpha_3 = \frac{1}{6}K$$

$$G_1 = \frac{-V_{B1}}{V_{B0}}K, \quad G_2 = \frac{-V_{B1}}{2V_{B0}}K\tan\delta_0, \quad G_3 = \frac{-V_{B1}}{6V_{B0}}K$$

$$Q_1 = \Omega^2\theta_{B1}, \quad Q_2 = \frac{\Omega D\omega_R\theta_{B1}}{2H}, \quad Q_3 = \frac{-V_{B1}}{V_{B0}}K\tan\delta_0, \quad P_1 = \frac{\omega_R}{2H}P_{LS1}$$

$$K = \frac{V_G V_{B0}\omega_R\cos\delta_0}{2HX_G}$$

where,

$$Q\cos(\Omega t + \phi_e) = Q_1\cos(\Omega t + \phi_\theta) + Q_2\sin(\Omega t + \phi_\theta) + Q_3\cos(\Omega t + \phi_v) \quad (9.37)$$

Thus, equation (9.36) reduces to:

$$\frac{d^2\eta}{dt^2} + \frac{\omega_R D}{2H}\frac{d\eta}{dt} + K\eta = \alpha_2\eta^2 + \alpha_3\eta^3 + G_1\eta\cos(\Omega t + \phi_v) + G_2\eta^2\cos(\Omega t + \phi_v) + G_3\eta^3\cos(\Omega t + \phi_v) + Q\cos(\Omega t + \phi_e) + P_1\cos(\Omega t + \phi_{LS}) \quad (9.38)$$

Initially, the focus of the analysis is on primary resonance. To study this, multiple scales is used to find a uniform solution for equation (9.38). A small, dimensionless parameter ε is introduced to account for the effects of damping, nonlinearities, and the excitation frequency, which occur in a specific order.

Letting

$$\eta = O(\varepsilon), \quad \frac{\omega_R D}{2H} = O(\varepsilon^2) \quad (9.39)$$

and

$$V_{B1} = O(\varepsilon^3), \quad \theta_{B1} = O(\varepsilon^3), \quad P_{LS1} = O(\varepsilon^3) \tag{9.40}$$

then the final equation from the swing equation derivation above has the following coefficients:

$$G_1 = \varepsilon^3 g_1, \quad G_2 = \varepsilon^3 g_2, \quad G_3 = \varepsilon^3 g_3, \tag{9.41}$$

$$Q = \varepsilon^3 q, \quad P_1 = \varepsilon^3 p. \tag{9.42}$$

Also, considering the equation with the detuning parameter σ,

$$\omega_0^2 = \Omega^2 + \mathcal{E}^2\sigma, \tag{9.43}$$

to allow for the derived final swing equation (9.38) to be rewritten as,

$$\begin{aligned}\ddot{\eta} + 2\varepsilon^2\mu\dot{\eta} + (\Omega^2 + \mathcal{E}^2\sigma)\eta = \alpha_2\eta^2 + \alpha_3\eta^3 + \varepsilon^3 g_1\eta\cos(\Omega t + \phi_v) \\ + \varepsilon^3 g_2\eta^2\cos(\Omega t + \phi_v) + \varepsilon^3 g_3\eta^3\cos(\Omega t + \phi_v) + \varepsilon^3 q\cos(\Omega t + \phi_e) + \varepsilon^3 p\cos(\Omega t + \phi_{LS}).\end{aligned} \tag{9.44}$$

The solution to the above equation is of the form:

$$\eta(t;\varepsilon) = \varepsilon\eta_1(T_0, T_1, T_2) + \varepsilon^2\eta_2(T_0, T_1, T_2) + \varepsilon^3\eta_3(T_0, T_1, T_2) + \ldots \tag{9.45}$$

where T_0 is a fast scale describing motions of frequencies, and T_1, T_2 are slow scales describing amplitude variation [33].

The first derivative of this equation is:

$$\frac{d}{dt} = D_0 + \varepsilon D_1 + \varepsilon^2 D_2 + \ldots \tag{9.46}$$

The second derivative is:

$$\frac{d^2}{dt^2} = D_0^2 + 2\varepsilon D_0 D_1 + \varepsilon^2(2D_0 D_2 + D_1^2) + \ldots \tag{9.47}$$

where

$$D_n = \frac{\partial}{\partial T_n}. \tag{9.48}$$

Equation (9.45) can be rewritten as:

$$\eta = \varepsilon\eta_1 + \varepsilon^2\eta_2 + \varepsilon^3\eta_3 + \dots \tag{9.49}$$

Finding the first derivative with respect to t for equation (9.49) and substituting equation (9.46) gives:

$$\begin{aligned}\eta(D_0 + \varepsilon D_1 + \varepsilon^2 D_2 + \dots) = \varepsilon\eta_1(D_0 + \varepsilon D_1 + \varepsilon^2 D_2 + \dots) \\ + \varepsilon^2\eta_2(D_0 + \varepsilon D_1 + \varepsilon^2 D_2 + \dots) + \varepsilon^3\eta_3(D_0 + \varepsilon D_1 + \varepsilon^2 D_2 + \dots).\end{aligned} \tag{9.50}$$

Differentiating for the second derivative with respect to t for equation (9.49) and substituting equation (9.47) gives:

$$\begin{aligned}\eta(D_0^2 + 2\varepsilon D_0 D_1 + \varepsilon^2(2D_0 D_2 + D_1^2) + \dots) = \\ \varepsilon\eta_1(D_0^2 + 2\varepsilon D_0 D_1 + \varepsilon^2(2D_0 D_2 + D_1^2) + \dots) \\ + \varepsilon^2\eta_2(D_0^2 + 2\varepsilon D_0 D_1 + \varepsilon^2(2D_0 D_2 + D_1^2) + \dots) \\ + \varepsilon^3\eta_3(D_0^2 + 2\varepsilon D_0 D_1 + \varepsilon^2(2D_0 D_2 + D_1^2) + \dots).\end{aligned} \tag{9.51}$$

Substituting equations (9.49), (9.50), and (9.51) into equation (9.38) and comparing coefficients of ε gives,

$$\varepsilon^1/: \quad \eta_1 D_0^2 + \eta_1\Omega^2 = 0 \tag{9.52}$$

$$\varepsilon^2/: \quad \eta_1 D_0^2 + \eta_2\Omega^2 + 2D_0 D_1\eta_1 = \alpha_2\eta_1^2 \tag{9.53}$$

$$\begin{aligned}\varepsilon^3/: \quad & D_0^2\eta_3 + 2D_0 D_1\eta_2 + (D_1^2 + 2D_0 D_2)\eta_1 + 2\mu D_0\eta_1 + \Omega^2\eta_3 + \sigma\eta_1 \\ & = 2\alpha_2\eta_1\eta_2 + \alpha_3\eta_1^3 + q\cos(\Omega t + \phi_e) + p\cos(\Omega t + \phi_{LS})\end{aligned} \tag{9.54}$$

From equations (9.52), (9.53) and (9.54), it can be seen that the parametric terms do not have key effects on the system. Hence, only the external forcing term remains [33, 77].

The solution to equation (9.52) is of the form:

$$\eta_1 = A(T_1, T_2)e^{i\Omega T_0} + \bar{A}(T_1, T_2)e^{-i\Omega T_0} \tag{9.55}$$

where A is an undetermined function. Given that

$$D_n = \frac{\partial}{\partial T_n}, \quad D_0 = \frac{\partial}{\partial T_0}$$

by integration,

$$T_0 = \frac{1}{D_0}.$$

Substituting equation (9.55) into (9.53),

$$\begin{aligned} \eta_2 D_0^2 + \eta_2 \Omega^2 = & -2D_0 D_1 \left(A(T_1, T_2)e^{i\Omega T_0} + \bar{A}(T_1, T_2)e^{-i\Omega T_0}\right) \\ & + \alpha_2 \left(A(T_1, T_2)e^{i\Omega T_0} + \bar{A}(T_1, T_2)e^{-i\Omega T_0}\right)^2 \end{aligned} \tag{9.56}$$

Expanding the brackets,

$$\begin{aligned} \eta_2 D_0^2 + \eta_2 \Omega^2 = & -2D_0 D_1 A(T_1, T_2)e^{i\Omega T_0} - 2D_0 D_1 \bar{A}(T_1, T_2)e^{-i\Omega T_0} \\ & + \alpha_2 \left(A^2 e^{2i\Omega T_0} + \bar{A}^2 e^{-2i\Omega T_0} + 2A\bar{A}\right) \end{aligned} \tag{9.57}$$

Due to $D_0 = \frac{\partial}{\partial T_0}$ and

$$\frac{\partial \left(2D_0 D_1 A\, e^{i\Omega T_0}\right)}{\partial T_0} = 2i\Omega D_1 A\, e^{i\Omega T_0} \tag{9.58}$$

$$\frac{\partial \left(2D_0 D_1 \bar{A}\, e^{-i\Omega T_0}\right)}{\partial T_0} = -2i\Omega D_1 \bar{A}\, e^{-i\Omega T_0} \tag{9.59}$$

Substituting into the equation and rearranging leads to,

$$\eta_2 D_0^2 + \eta_2 \Omega^2 = -2i\Omega D_1 A e^{i\Omega T_0} + \alpha_2 (A^2 e^{2i\Omega T_0} + \bar{A}^2 e^{-2i\Omega T_0}) + cc \tag{9.60}$$

where cc is the complex conjugate. In this equation, $D_1 A = 0$, to avoid secular terms η_2 and hence $A = A(T_2)$. Replacing equation (9.52) into (9.55) and simplifying,

$$\eta_2 = -\frac{\alpha_2 A^2 e^{2i\Omega T_0}}{3\Omega^2} - \frac{\alpha_2 \bar{A}^2 e^{-2i\Omega T_0}}{3\Omega^2} + \frac{2\alpha_2 A\bar{A}}{\Omega^2} \tag{9.61}$$

which is also echoed in [33, 77].

Replacing equations (9.55) and (9.61) into equation (9.54),

$$2i\mu\Omega(A' + \mu A) + \sigma A - \frac{1}{2}qe^{i\phi} - \frac{1}{2}pe^{i\phi} + 8\alpha_e A^2\bar{A} = 0 \tag{9.62}$$

where

$$\alpha_e = -\frac{3}{8}\alpha_3 - \frac{5\alpha_2^2}{12\Omega^2}.$$

Expressing A in polar form,

$$A = \frac{1}{2}ae^{-i(\beta+\phi_e)} \tag{9.63}$$

Substituting equation (9.63) into equation (9.62) gives,

$$\Omega(a' + \mu a) + \frac{1}{2}q\sin\beta + \frac{1}{2}p\sin\beta = 0 \tag{9.64}$$

$$-\Omega a\beta' + \alpha_e a^3 - \frac{1}{2}q\cos\beta - \frac{1}{2}p\cos\beta + \frac{1}{2}\sigma a = 0. \tag{9.65}$$

Equation (9.63) can also be written in the form:

$$A = \frac{1}{2}a\cos(\beta + \phi_e). \tag{9.66}$$

Substituting A and its conjugate into equation (9.55) leads to:

$$\eta_1 = a\cos(2\Omega t + \beta + \phi_e). \tag{9.67}$$

Similarly, replacing into equation (9.61) gives:

$$\eta_2 = \frac{\alpha_2 a^2}{2\Omega^2} - \frac{\alpha_2 a^2}{6\Omega^2}\cos(2\Omega t + 2\beta + 2\phi_e). \tag{9.68}$$

Substituting the above derivations for η_1 and η_2 in equation (9.45) to obtain the second approximation,

$$\eta = \varepsilon a \cos(\Omega t + \beta + \phi_e) + \frac{\varepsilon^2 a^2 \alpha_2}{6\Omega^2}\left[3 - \cos(2\Omega t + 2\beta + 2\phi_e)\right] + \dots \tag{9.69}$$

Setting $\varepsilon = 1$ and letting "a" be the perturbation parameter, using equation (9.69), equation (9.34) may be rewritten as,

$$\Delta\theta = \theta_{B1}\cos(\Omega t + \phi_\theta) + a\cos(\Omega t + \beta + \phi_e) + \frac{a^2\alpha_2}{6\Omega^2}(3 - \cos(2\Omega t + 2\beta + 2\phi_e)) + ... \tag{9.70}$$

with $\frac{a^2\alpha_2}{2\Omega^2}$ defined as the drift term, which because of its quadratic nonlinearity the oscillatory motion is not centered as seen also in [33, 77].

To understand the character of equations (9.64) and (9.65), fixed points are found in alignment with $a' = \beta' = 0$ to reduce to:

$$\mu a = -\frac{q\sin\beta}{2\Omega} - \frac{p\sin\beta}{2\Omega} \tag{9.71}$$

$$\frac{a\sigma}{2\Omega} + \frac{\alpha_e a^3}{\Omega} = \frac{q\cos\beta}{2\Omega} + \frac{p\cos\beta}{2\Omega} \tag{9.72}$$

Squaring and adding equations (9.71) and (9.72) will give,

$$\mu^2 + \left(\frac{\sigma}{2\Omega} + \frac{\alpha_e a^2}{\Omega}\right)^2 = \frac{(q+p)^2}{4\Omega^2 a^2} \tag{9.73}$$

The analytical results are compared with the numerical simulations for the primary resonance when $\Omega = 8.61$ rads^{-1} with the load shedding term. The Runge-Kutta fourth order and Newton Raphson methods were used for the simulation perturbation analysis and compared with the numerical results as shown in Figure 9.1. It can be seen that the Newton Raphson Method gives a better approximation to the numerical solution. The calculated numerical error of the Runge-Kutta method versus the Newton Raphson technique compared to the actual numerical solution error was 0.04192 and 0.02314 respectively, ensuring that the Newton Raphson method is a suitable fit because of its small error value.

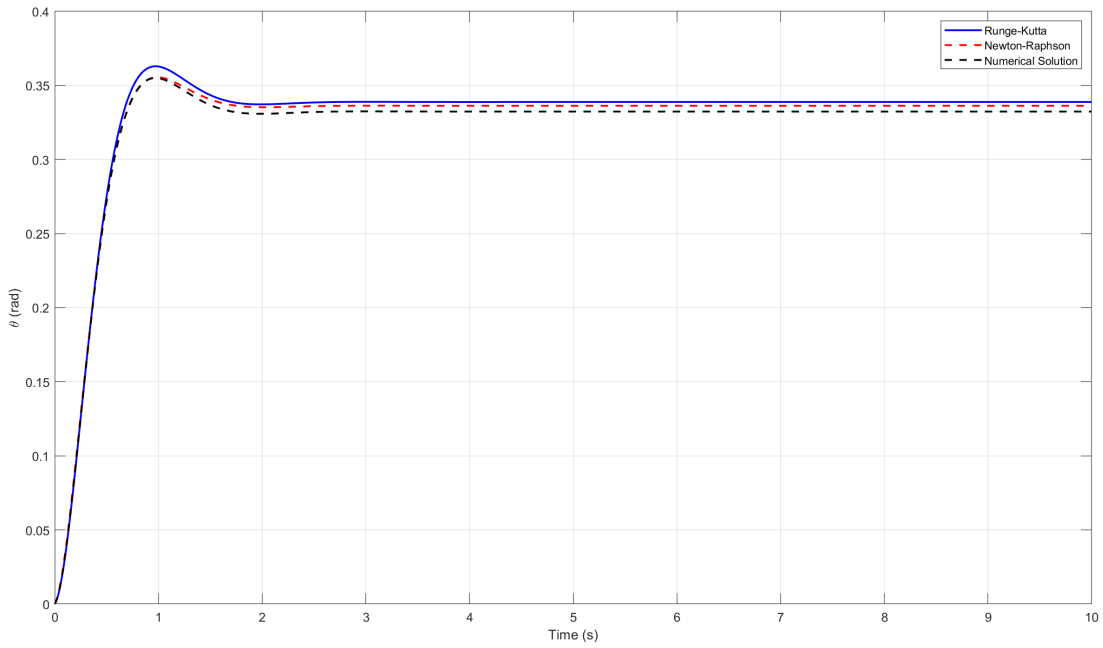

Figure 9.1: Perturbed solution employing Runge-Kutta and Newton Raphson algorithms in comparison to numerical simulations for the case of primary resonance in the phase plane and time history for $\Omega = 8.61$ rads^{-1}.

The bifurcation diagrams are produced by incrementally increasing the forcing parameter r, while simultaneously continuing the time integration of the system at each step [16, 33, 77]. For each value of r, the maximum amplitude of the oscillatory solution is calculated and graphed against r. This procedure elucidates the evolution of the system's behaviour when the forcing parameter is altered, demonstrating transitions among periodic, chaotic states, and intermittency. The r is regarded as mentioned in the equation (3.65)

The modified swing equation was resolved in Matlab with the fourth-order Runge-Kutta method for numerical precision, incorporating the load shedding term. As load shedding intensified, a critical threshold was identified that mitigated chaos inside the system.

Conventional scheme bifurcation diagrams were generated, wherein the system was resolved incrementally. The results indicated that the confusion occurred prior to the introduction of the load shedding term into the system.

The Lyapunov exponents were generated to measure the system's sensitivity to beginning circumstances [42]. A positive Lyapunov exponent indicates chaos, whereas

a negative exponent signifies stability. As load shedding values grew, the Lyapunov exponents transitioned to negative values, indicating diminished chaos. The turmoil commenced later than the period characterised by the absence of load shedding in the system.

A traditional load shedding technique was employed for comparison, wherein the electric power was executed in a sequential manner with designated time intervals [200]. Rather than reducing load solely during instances of instability, predetermined shedding intervals were implemented every 5 seconds. This method resulted in earlier confusion, indicating that the load shedding strategy examined in this research is more effective in postponing anarchy. Therefore, it is essential to evaluate the impact of the parameters on the system [26, 228].

The model presumes a single-machine infinite bus system with fixed parameters, including damping, inertia, and generating voltage. These simplifications are essential for deriving analytical results and understanding stability mechanisms. Although the actual system encompasses more intricate variables and reactive power dynamics, as well as varying topologies, these assumptions are applicable for analysing local generator behaviour during short-term transients. Consequently, subsequent research may broaden this methodology to intricate power grid configurations and examine the stability dynamics when other elements are incorporated [229].

9.3 Results

9.3.1 Representation of the Analytical Work

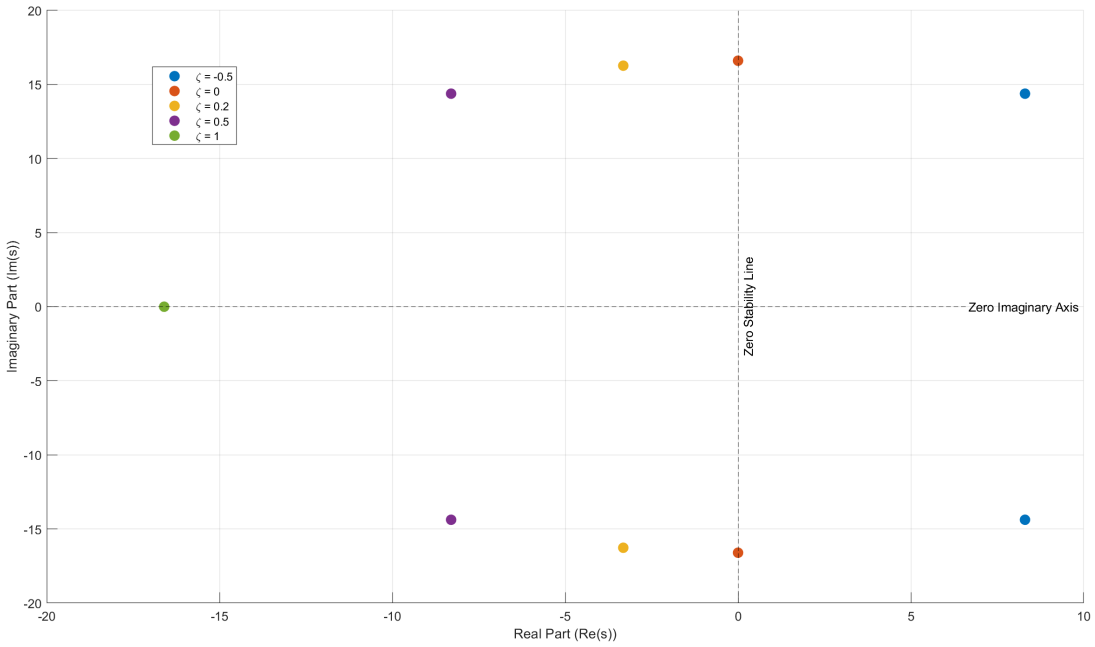

Figure 9.2: Eigenvalues obtained from the swing equation with load shedding term when $\Omega = 8.61$ rads^{-1}.

Figure 9.2 illustrates the eigenvalues computed for the swing equation devoid of any load shedding component. In the case of negative damping ($\zeta = -0.5$), the eigenvalues possess positive real components, indicating that the system undergoes exponentially amplifying oscillations. This signifies an unstable system characterised by the amplification of disturbances.

When the damping ratio is null, the eigenvalues reside only on the imaginary axis. The system demonstrates persistent oscillations without attenuation.

In underdamped scenarios ($0 < \zeta < 1$), such as ζ=0.2 and ζ=0.5, the eigenvalues move to the left while retaining imaginary components. This indicates that the system oscillates but eventually stabilises over time. A damping ratio approaching 1 is preferable, as it facilitates rapid decline.

In the case of critical damping (ζ=1), the eigenvalues are real and negative, indicating

that the system reverts to equilibrium without oscillatory behaviour. This is the optimal damping scenario sought by researchers and engineers in the field.

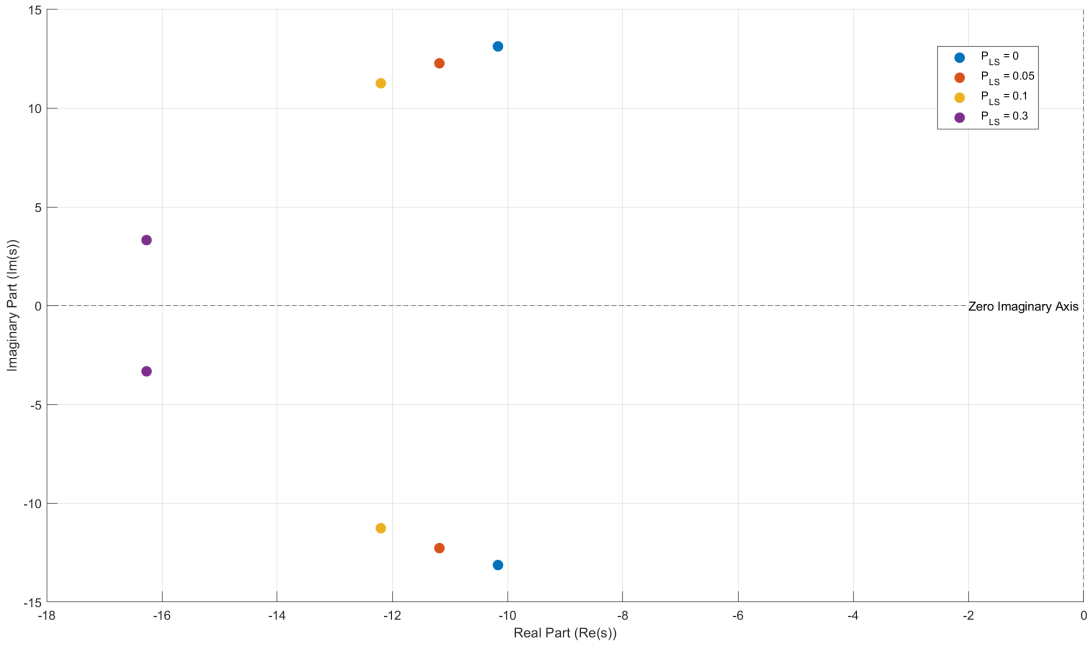

Figure 9.3: Eigenvalues obtained from the swing equation with load shedding term when $\Omega = 8.61$ rads^{-1}.

Figure 9.3 depicts the eigenvalues obtained for the swing equation with the load shedding term. For zero load shedding the eigenvalues remain close to the imaginary axis.

As load shedding is increased, the eigenvalues shift leftward, signifying improved damping and enhanced stability. For higher load shedding values the eigenvalues move further into the left-half plane, reducing the imaginary component.

9.3.2 Representation for the Primary Resonance

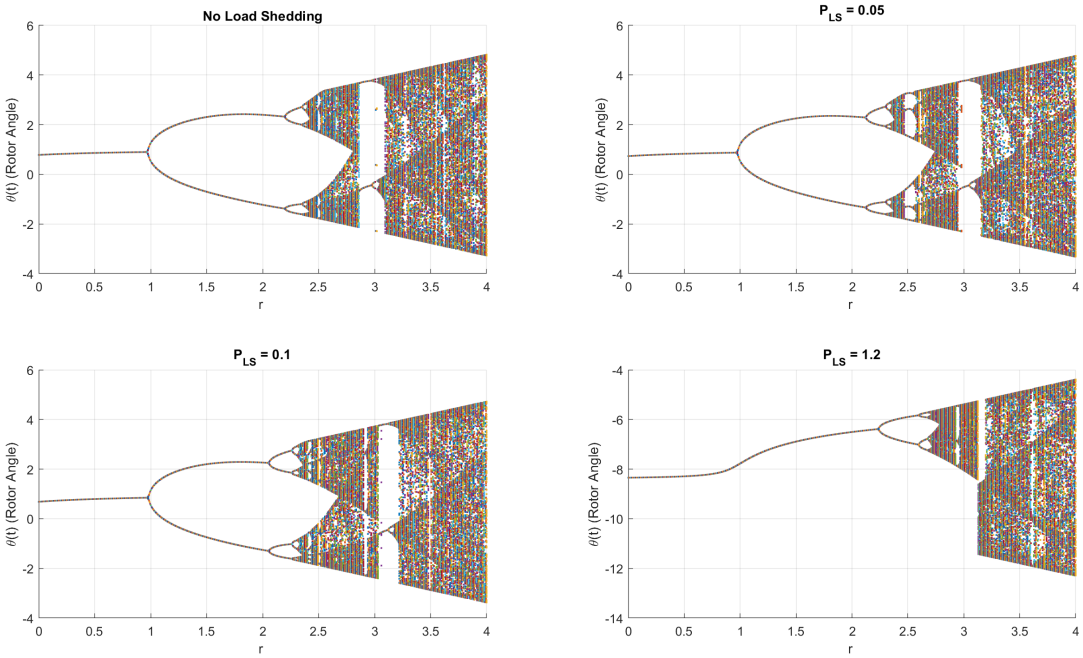

Figure 9.4: Bifurcation diagrams when the load shedding terms are increasing in the scheme analysed in this study for primary resonance at $\Omega = 8.61$ rads^{-1}.

Figure 9.4 presents bifurcation diagrams generated for the swing equation using the load shedding factor. The swing equation devoid of load shedding exhibits initial chaotic behaviour [77]. The incorporation of the load shedding term within the system is reflected in a minor alteration in the diagrams.

At elevated load shedding values ($P_{\text{LS}} = 1.2$), the bifurcation diagram indicates a predominantly stable zone, characterised by diminished chaotic oscillations. The system displays a singular, stable trajectory rather than many bifurcation branches, so validating that load shedding facilitates consistent frequency responses. Excessive load shedding may overly stabilise the system, thereby hindering its ability to adjust to transient changes. When P_{LS} exceeds 1.2, the system demonstrates chaotic behaviour, indicating that at $P_{\text{LS}} = 1.2$, the system experiences a delay in chaos and remains stable for an extended period.

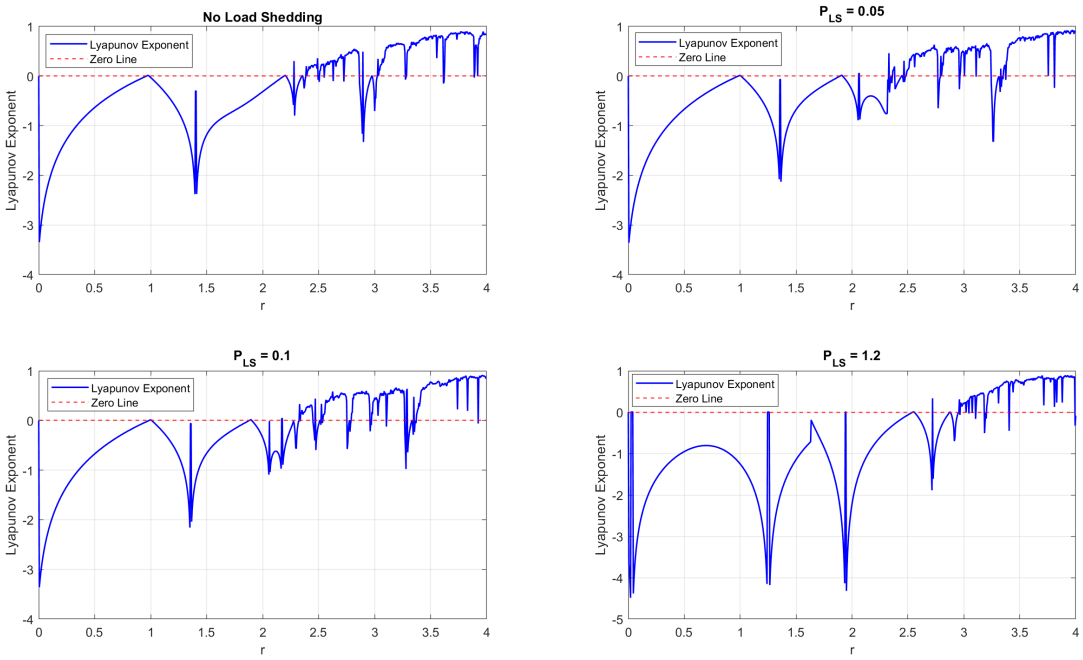

Figure 9.5: Lyapunov Exponents for the primary resonance for the Load shedding scheme when $\Omega = 8.61$ rads^{-1}.

Figure 9.5 illustrates the Lyapunov exponents corresponding to the bifurcation diagrams derived from the aforementioned load shedding strategy. In the absence of load shedding, positive Lyapunov exponents are seen, indicating that the system demonstrates sensitivity to initial conditions. As P_{LS} grows, the Lyapunov exponents transition to negative values, indicating that load shedding successfully alleviates chaotic dynamics and guarantees predictable system behaviour. Chaos ensues in the system when $P_{\text{LS}} = 0$ and $r = 2.2$ [4]. However, when the load shedding parameter is elevated to 0.05, disorder ensues at $r = 2.3$. With the load shedding term elevated to 1.2, it is evident that chaos initiates at $r = 2.72$, indicating that the proposed technique has postponed the system's transition into an unstable region.

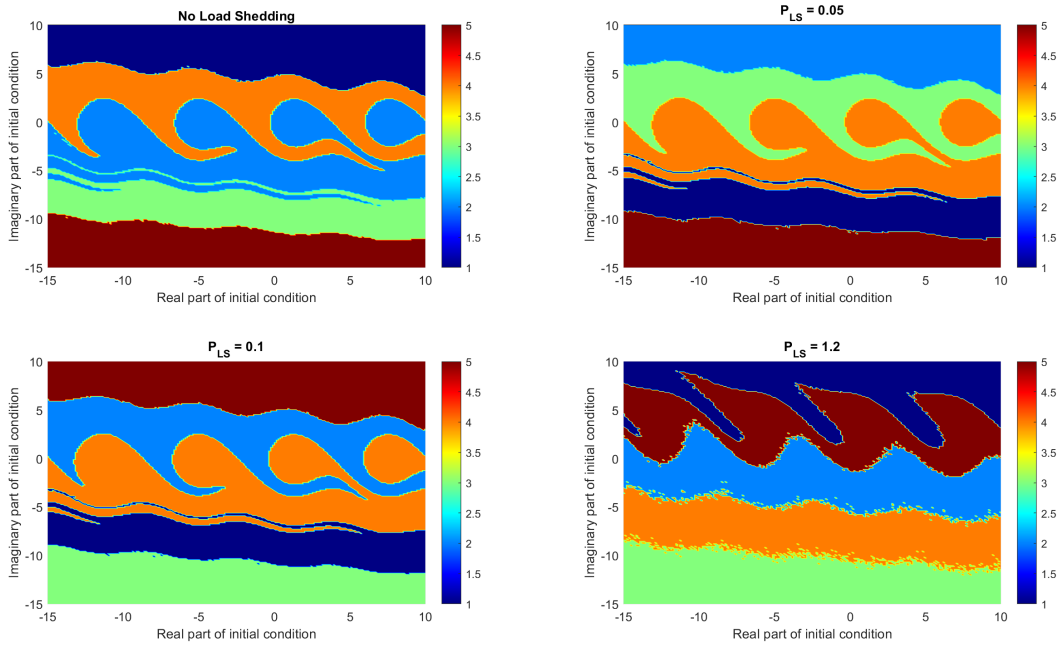

Figure 9.6: Basins of attractions with load shedding term within the swing equation for primary resonance when $\Omega = 8.61$ rads^{-1}.

The basins of attraction depicted in Figure 9.6 illustrate the domains of beginning conditions that result in steady operation. The red and green areas represent the stable sections. In the absence of load shedding, the stable basin is comparatively limited, indicating that even slight disruptions might induce system instability. As P_{LS} grows, the stable basin enlarges, indicating that load shedding improves the system's capacity to revert to equilibrium following perturbations. The stability region expands, indicating a rise in pixel count, which reflects a significant enhancement in the system's dynamic reactivity. These findings underscore the necessity for dynamic optimisation of load shedding to enhance stability while minimising energy loss.

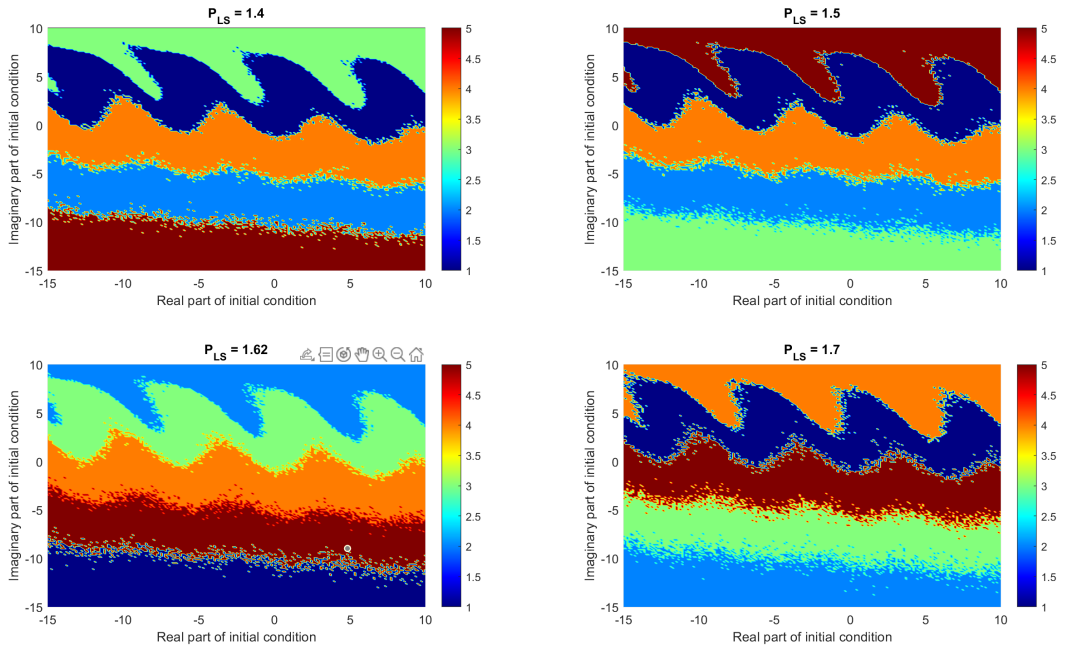

Figure 9.7: Basins of attractions when increasing the load shedding term within the swing equation for primary resonance when $\Omega = 8.61$ rads^{-1}.

Figure 9.7 illustrates the dynamic changes that the system undergoes as the load shedding term is progressively increased in the context of primary resonance. Primary resonance, being a fundamental type of resonance that occurs when the system's natural frequency aligns closely with the excitation frequency, is highly sensitive to external perturbations. As shown above, the introduction and subsequent amplification of the load shedding term have a marked influence on the system's behaviour. Initially, when the load shedding is absent or minimal, the system exhibits greater susceptibility to irregularities and instabilities. The oscillations are more erratic, and signs of chaotic behaviour begin to emerge earlier in the response.

However, as the load shedding term is incrementally increased, the system transitions into a more stable regime. The figure reveals a significant reduction in the amplitude and irregularity of the oscillations, as well as a delay in the onset of chaotic motion. This stabilising effect demonstrates the efficacy of load shedding in modulating the system's energy balance and preventing uncontrolled dynamic responses. The results shown in Figure 9.7 thus underscore the critical role of load shedding as a control strategy during primary resonance, effectively enhancing the overall robustness and resilience.

9.3.3 Representation for the Conventional Scheme

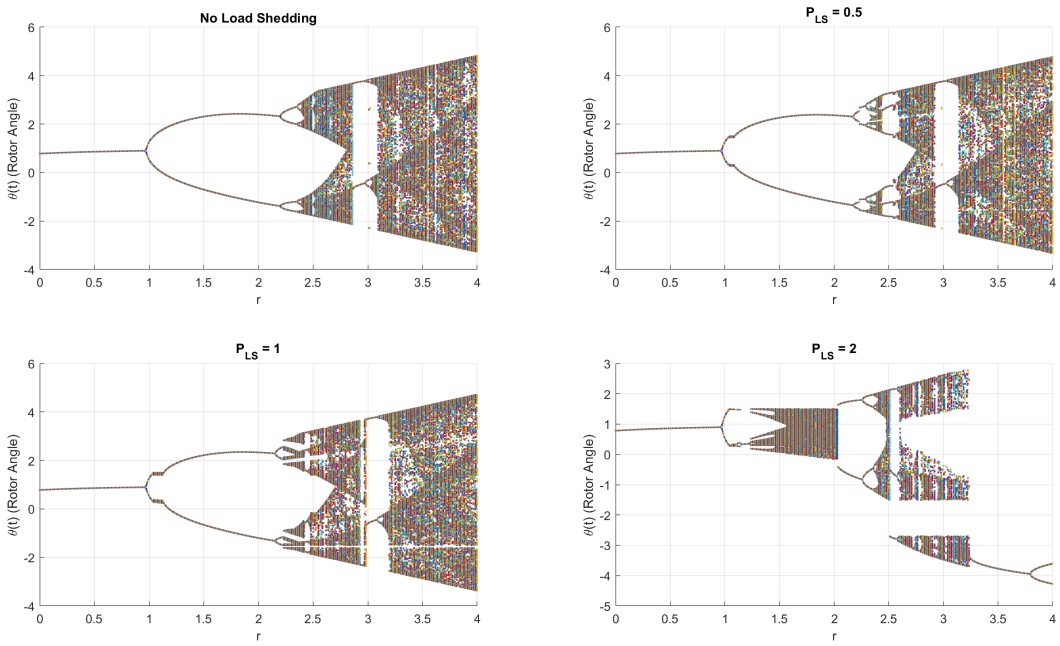

Figure 9.8: Bifurcation diagrams when the load shedding terms are increasing using the conventional scheme when $\Omega = 8.61$ rads^{-1}.

Figure 9.8 illustrates the bifurcation diagrams for the conventional load shedding scheme, emphasising a significant divergence in stability behaviour relative to the adaptive load shedding technique. In the traditional method, where load shedding is activated at predetermined frequency thresholds, the system continues to display chaotic oscillations, albeit with an earlier onset of instability. The bifurcation graphic illustrates chaotic behaviour manifesting at reduced parameter values of r, indicating that the system transitions into an unstable zone more rapidly. This indicates that the conventional progressive load shedding method fails to adequately postpone pandemonium.

In contrast to the load shedding methodology examined in this paper, which progressively relocates bifurcations deeper into the stability domain, the traditional scheme exhibits a lack of control, leading to both excessive and insufficient shedding in electrical power circuits, hence fostering chaotic oscillations. Moreover, rather than a seamless transition to stability, the bifurcation diagram for the typical system displays sudden shifts between periodic and chaotic behaviour, further validating the inadequacy of a fixed threshold

method in mitigating instability.

9.3.4 Representation for the Subharmonic Resonance

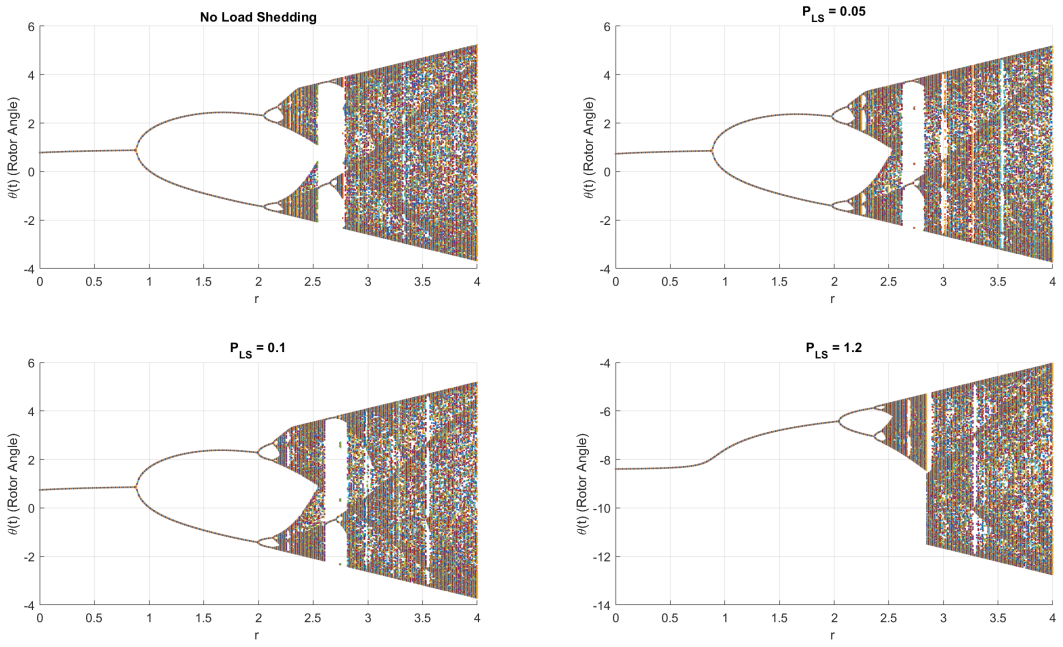

Figure 9.9: Bifurcation diagrams when the load shedding terms are increasing in the scheme analysed in this study for subharmonic resonance when $\Omega = 19.375$ rads^{-1}.

Figure 9.9 illustrates bifurcation diagrams for subharmonic resonance at $\Omega = 19.375$ rads^{-1}. The swing equation incorporates a load shedding factor, and the output is examined to observe chaotic behaviour.

The initial diagram illustrates the dynamic behaviour in the absence of a load shedding factor in the swing equation [6, 7]. Chaotic behaviour is seen at around $r = 2.15$. Chaos can only be observed at $r = 2.2$ with the load shedding parameter, $P_{\text{LS}} = 0.05$. As the load shedding parameter escalates to 1.2, the system descends into anarchy at $r = 2.47$. This indicates that pandemonium is postponed when the load shedding parameter is incrementally increased, corroborating the findings of the controlled load shedding scheme examined in this work.

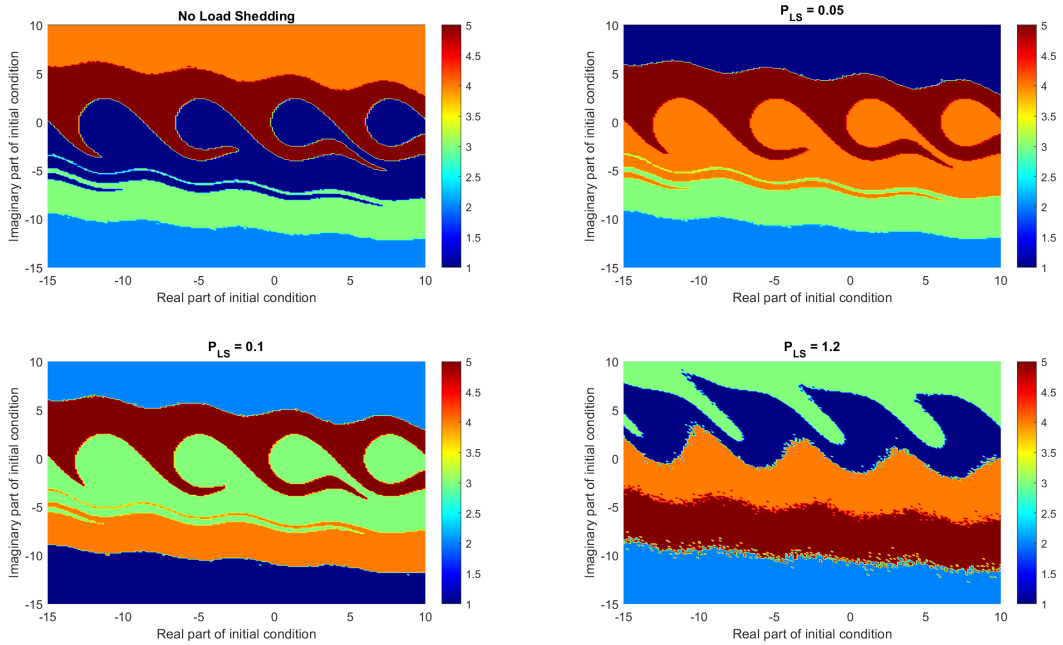

Figure 9.10: Basins of attractions with load shedding term within the swing equation when $\Omega = 19.375$ rads^{-1}.

The basins of attraction depicted in Figure 9.10 illustrate the regions of initial conditions that lead the system to stable equilibrium states under the phenomenon of subharmonic resonance. These basins serve as a visual representation of the system's stability landscape. In the figure, the red and green regions represent areas of stability where the system eventually settles into periodic or quasi-periodic behaviour.

When there is no load shedding mechanism incorporated into the system, the size of the stable basin remains relatively small, indicating limited tolerance to perturbations in initial conditions. This suggests that the system is more prone to instability under such circumstances. However, as the load shedding term is increased, a notable expansion in the stable basin can be observed. This expansion implies that the system becomes more robust and less sensitive to variations in initial states.

Figure 9.11 further reinforces this observation by illustrating additional basins of attraction corresponding to progressively higher values of the load shedding term. The sequence of graphs captures the dynamic evolution of the system's stability landscape as the load shedding parameter is varied. As the parameter increases, the basins of attraction become larger and more inclusive, thereby confirming that load shedding contributes

significantly to the enhancement of system stability and the enlargement of the domain of attraction.

Hence, both figures underscore the positive influence of load shedding on system dynamics, particularly under conditions of subharmonic resonance. The increasing area of the stable regions with higher load shedding indicates that such a control strategy can effectively mitigate instability.

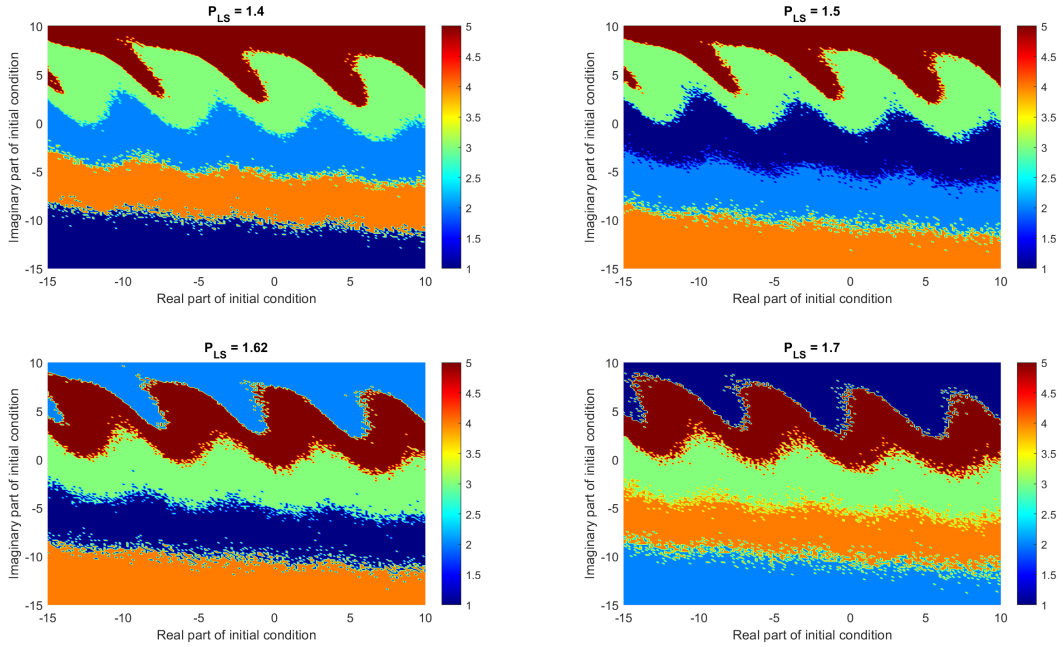

Figure 9.11: Basins of attractions when increasing the load shedding term within the swing equation when $\Omega = 19.375$ rads^{-1}.

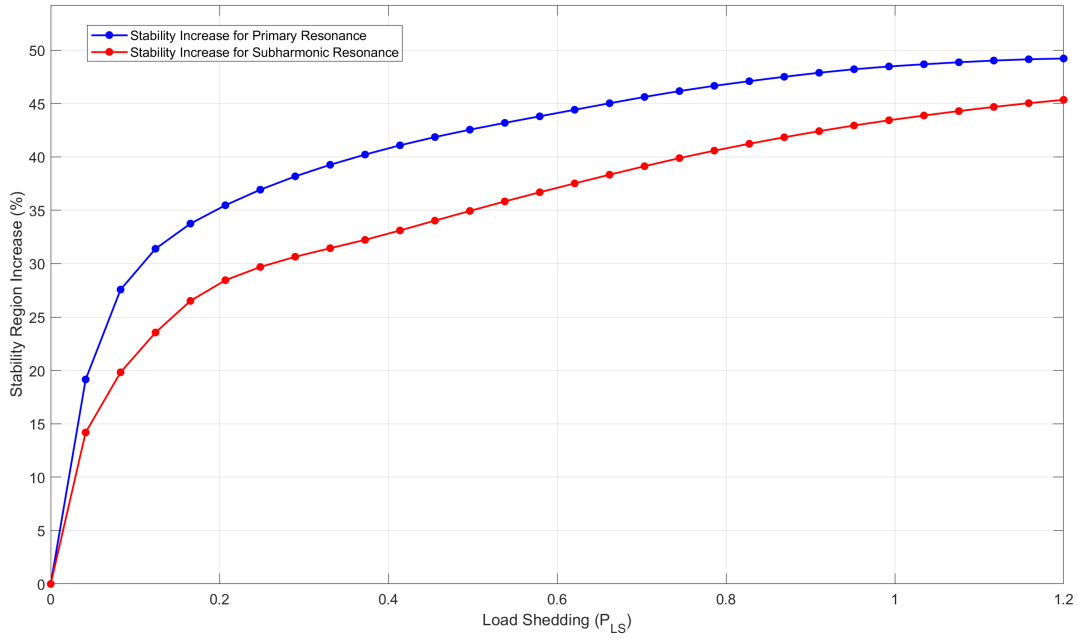

Figure 9.12: Increase in stability as the load shedding term is incremented for Primary Resonance when $\Omega = 8.61$ rads^{-1} and Subharmonic Resonance when $\Omega = 19.375$ rads^{-1}.

Figure 9.12 shows the relationship between load shedding P_{LS} and the increase in the stability region for both primary resonance, when $\Omega = 8.61\ \text{rad}\,\text{s}^{-1}$, and subharmonic resonance, when $\Omega = 19.375\ \text{rad}\,\text{s}^{-1}$. It can be observed that stability increases as the load shedding term is incremented. At $P_{\text{LS}} = 1.2$, the stability region increases to a maximum by 49.21% for primary resonance and 45.34% for subharmonic resonance. These results validate the bifurcation diagrams and Lyapunov exponents, confirming that the load shedding term contributes to delaying the onset of chaotic oscillations.

The clear trend indicates that load shedding not only suppresses chaos but also enhances the system's tolerance to initial perturbations. This improved stability is especially critical in energy systems, where maintaining operational continuity is essential. The differing percentages of improvement between primary and subharmonic resonances suggest that the system's response to load shedding is frequency-dependent, with primary resonance exhibiting a slightly greater sensitivity to control interventions. This distinction may be attributed to differences in nonlinear energy transfer mechanisms active at different excitation frequencies. Overall, the results reinforce the role of load shedding as an effective control strategy for managing dynamic instabilities in nonlinear oscillatory

systems.

9.3.5 Load Shedding in the Matlab Simulink Model

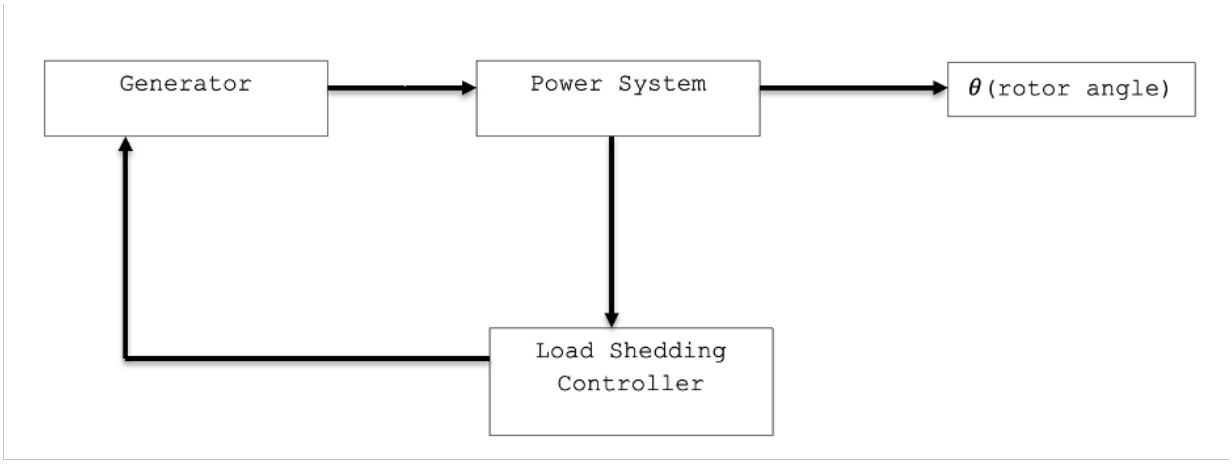

Figure 9.13: Conceptual schematic of the power system integrated with the proposed load shedding control loop.

Figure 9.13 presents a generic block diagram representing a power system with integrated load shedding control. This diagram captures the essential dynamic interactions between generation, system response, and real-time control mechanisms, framed within the context of the modified swing equation.

The Generator block represents the mechanical power input, denoted by P_m, which is typically provided by a turbine or other prime mover. This mechanical input serves as the driving force of the system and is a critical component in the balance of energy within the generator.

The Power System block models the fundamental swing dynamics of the generator, which are governed by the classical swing equation. This block includes parameters such as the system's moment of inertia H, the damping coefficient D, and the electrical power output P_e. Together, these variables define the generator's response to imbalances between mechanical input and electrical output power. The swing equation characterises the evolution of the rotor angle θ, which represents the angular displacement of the generator rotor and serves as a key indicator of system stability.

The output of the Power System block is the rotor angle θ, which is continuously monitored. Both θ and its time derivative $\dot{\theta}$, representing the rotor speed deviation,

are essential for assessing the system's dynamic behaviour and detecting the onset of instability.

The Control block receives θ and $\dot{\theta}$ as inputs and computes the appropriate load shedding response. This response is determined based on deviations from nominal operating conditions, and the control strategy aims to stabilise the system by curtailing a calculated portion of the load. The resulting control signal is then fed back into the Power System block, effectively modifying the damping characteristics of the swing equation through the introduction of a load shedding term.

This closed-loop structure reflects the implementation of a modified swing equation, such as that expressed in Equation (9.19), where the effective damping is dynamically enhanced by the control input. As a result, the integrated system is capable of reacting in real time to disturbances, reducing the likelihood of instability and chaotic behaviour, and maintaining operational security within the power grid.

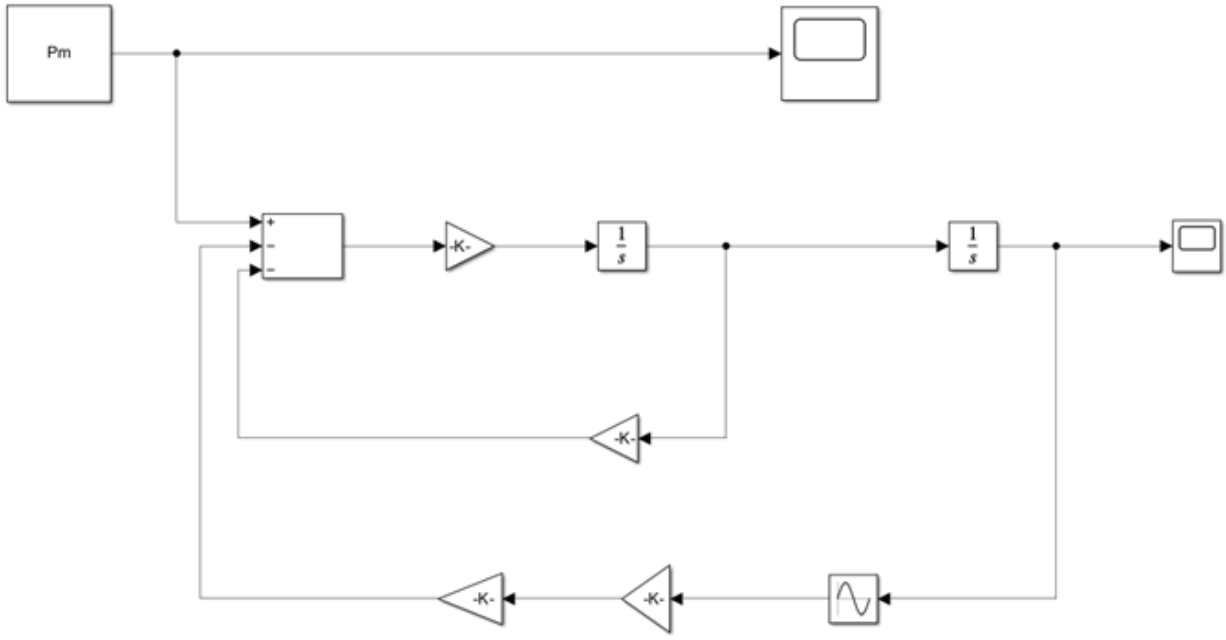

Figure 9.14: Simulink model of the swing equation with the load shedding term when $\Omega = 7.5$ rads^{-1}.

The Simulink model illustrated in Figure 9.14 represents the implementation of the swing equation with an integrated load shedding term. This model facilitates the

simulation and analysis of power system dynamics under various operational conditions and disturbance scenarios. It allows for real-time observation of system responses, including frequency deviations, rotor angle oscillations, and the impact of load curtailment on overall stability. By incorporating the modified swing equation directly into the model, this setup serves as a valuable tool for validating analytical findings and evaluating the performance of control strategies.

To investigate the system's behaviour around resonance conditions, specific excitation frequencies were chosen. For the analysis of primary resonance phenomena, an excitation frequency of $\Omega = 7.5\,\mathrm{rad\,s^{-1}}$ was selected. This value is situated near the system's primary resonance frequency and enables the observation of characteristic nonlinear responses such as increased amplitude oscillations and potential bifurcations. The choice of this frequency provides insight into how the system responds when it is near its natural frequency, where small disturbances can result in significant dynamic amplification.

In addition, a higher excitation frequency of $\Omega = 18.9\,\mathrm{rad\,s^{-1}}$ was chosen to investigate the system's behaviour near subharmonic resonance. At this frequency, the system exhibits complex dynamic behaviours, such as period-doubling and intermittent instability, which are typical precursors to chaos in nonlinear systems. Analysing the model's response at this frequency helps to identify the thresholds at which the system transitions from stable to chaotic regimes. The comparative study of system dynamics at both primary and subharmonic resonance frequencies underscores the importance of frequency-dependent stability analysis and demonstrates the efficacy of the control-based load shedding mechanism in mitigating undesirable nonlinear effects.

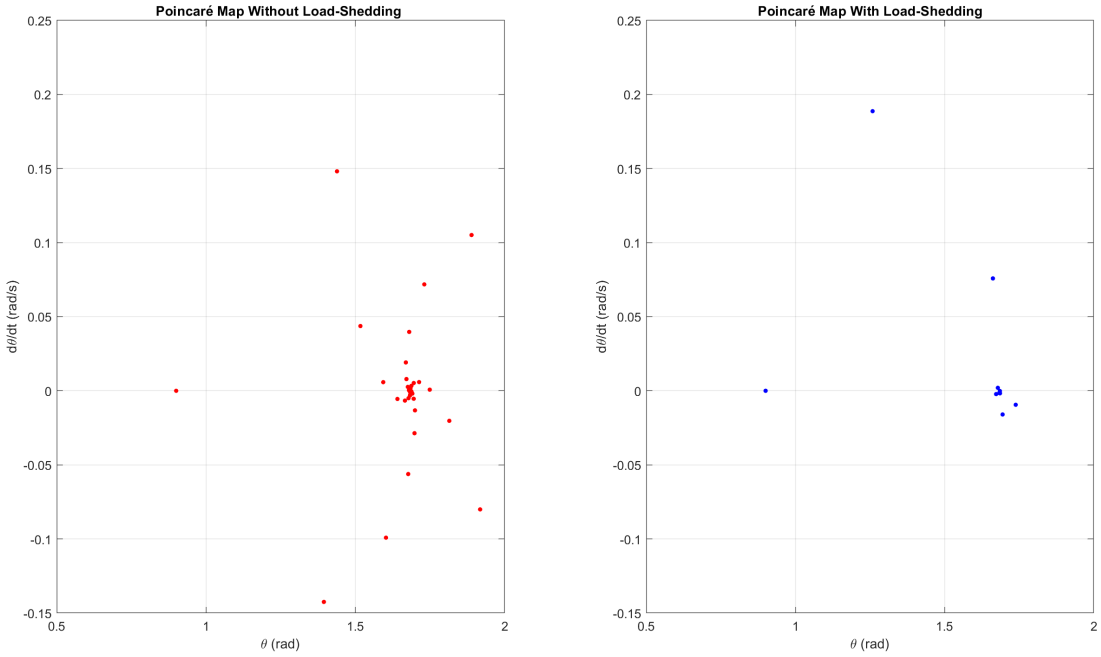

Figure 9.15: Poincaré maps from the Simulink model showing the delay in chaos after the load shedding term is included for $\Omega = 7.5$ rads^{-1}.

The Poincaré maps in Figure 9.15 were derived using the aforementioned Simulink model to illustrate the delay in the onset of chaos as a result of incorporating the load shedding factor. These maps offer valuable insights into the system's phase space dynamics by sampling the system at regular intervals, thus enabling the visual detection of periodicity and chaos. The first map illustrates the system's behaviour in the absence of a load shedding term at an excitation frequency of $\Omega = 7.5$ rad s^{-1}. Under these conditions, chaotic behaviour becomes evident when the angular displacement $\theta \approx 1.6$, as characterised by the presence of widely dispersed points on the map, indicative of a loss of regularity in the system's motion.

Upon introducing a load shedding term of 1.2 pu, the system exhibits a significant delay in the manifestation of chaotic dynamics. The corresponding Poincaré map shows that chaos now arises around $\theta \approx 1.7$, as reflected by the scattered distribution of points, though the onset is clearly postponed. This shift in the threshold of chaotic behaviour highlights the stabilising influence of load shedding, which acts to suppress the system's transition into chaotic regimes. The observed delay suggests that the system remains in

a more ordered state over a broader range of operating conditions, thereby enhancing its dynamic reliability.

The implications of these findings are particularly important for power system stability and control. By effectively delaying the onset of chaos, load shedding allows system operators greater flexibility in maintaining control, especially under fluctuating demand or disturbances. This capacity to defer instability can be critical during peak loads or fault conditions, providing valuable time for corrective action. Furthermore, the analysis reinforces the importance of non-linear diagnostic tools such as Poincaré maps in understanding complex dynamical systems and evaluating control strategies like load shedding. Overall, the results demonstrate that targeted intervention via load shedding can play a pivotal role in improving the resilience and operational robustness of non-linear oscillatory systems.

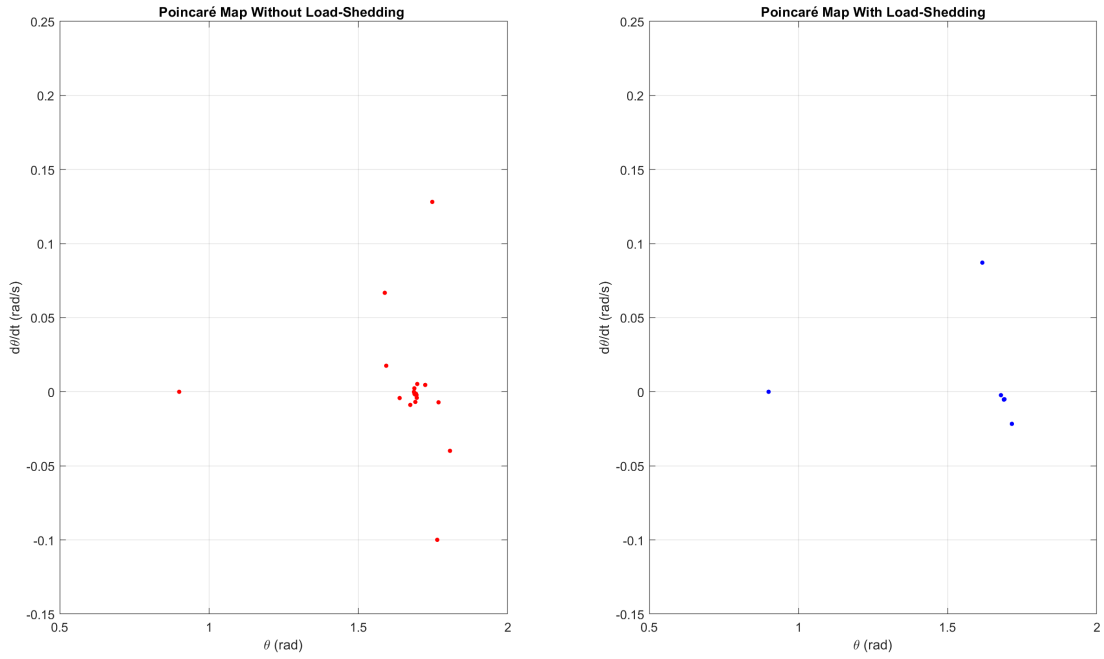

Figure 9.16: Poincaré maps from the Simulink model showing the delay in chaos after the load shedding term is included for $\Omega = 18.9$ rads^{-1}.

Figure 9.16 illustrates the Poincaré maps both with and without the load shedding term at $\Omega = 18.9$ rads^{-1}. Chaos commences at $\theta \approx 1.6103$ in the absence of the load shedding term, however with the inclusion of the load shedding term, chaos manifests at

$\theta \approx 1.652$, accompanied by a limited number of locations on the map. This underscores the significance of the load shedding methodology for the swing equation.

Time series data regarding the rotor speed is acquired to validate the results obtained.

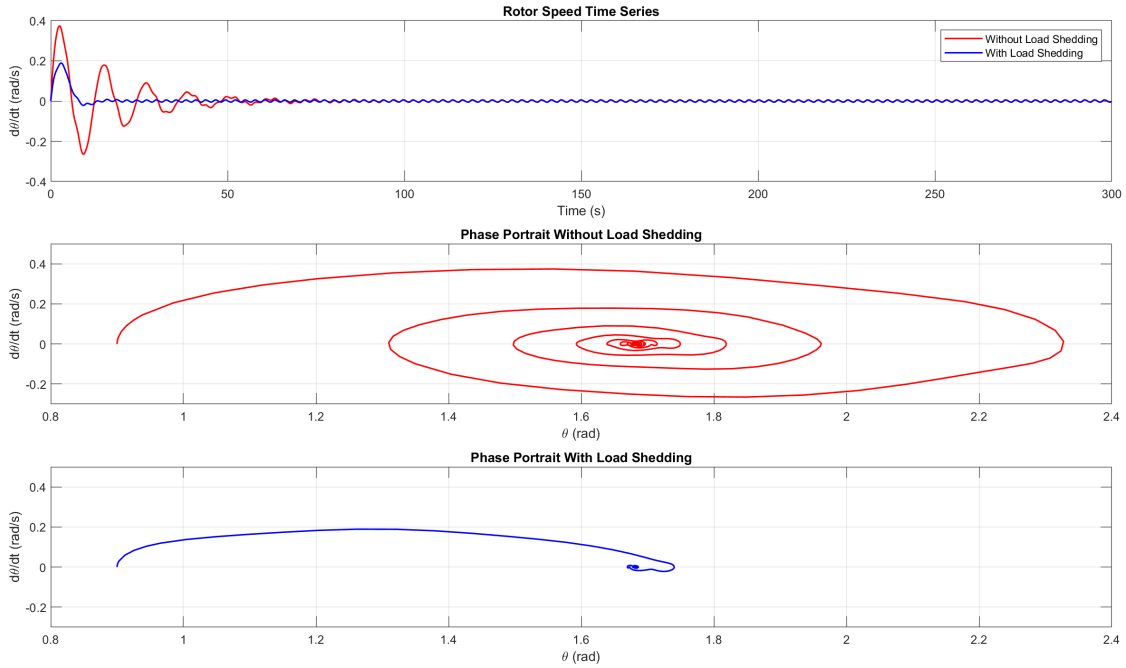

Figure 9.17: Time series and Phase portraits for the rotor speed with load shedding and without load shedding for $\Omega = 7.5$ rads^{-1}.

Figure 9.17 illustrates the time series and phase pictures of rotor speed in the swing equation, contrasting the system's behaviour with and without load shedding at $\Omega = 7.5$ rads^{-1}, which is near the primary resonance value. In the absence of load shedding, erratic oscillations persist for an extended duration before progressively stabilising into a consistent oscillatory pattern. This signifies that disturbances endure for an extended duration within the system. The phase pictures indicate that, with load shedding, the system enters a stable area characterised by fewer spirals compared to the scenario without the load shedding term. Thus, demonstrating that the system attains stability rapidly with the introduction of a load shedding factor in the equation.

The load shedding method enables the rotor speed to attain stable oscillations more rapidly. The supplementary damping effect from load shedding significantly diminishes oscillation amplitude and curtails chaotic activity, resulting in expedited stabilisation.

This underscores the significance of incorporating the load shedding approach to mitigate volatility.

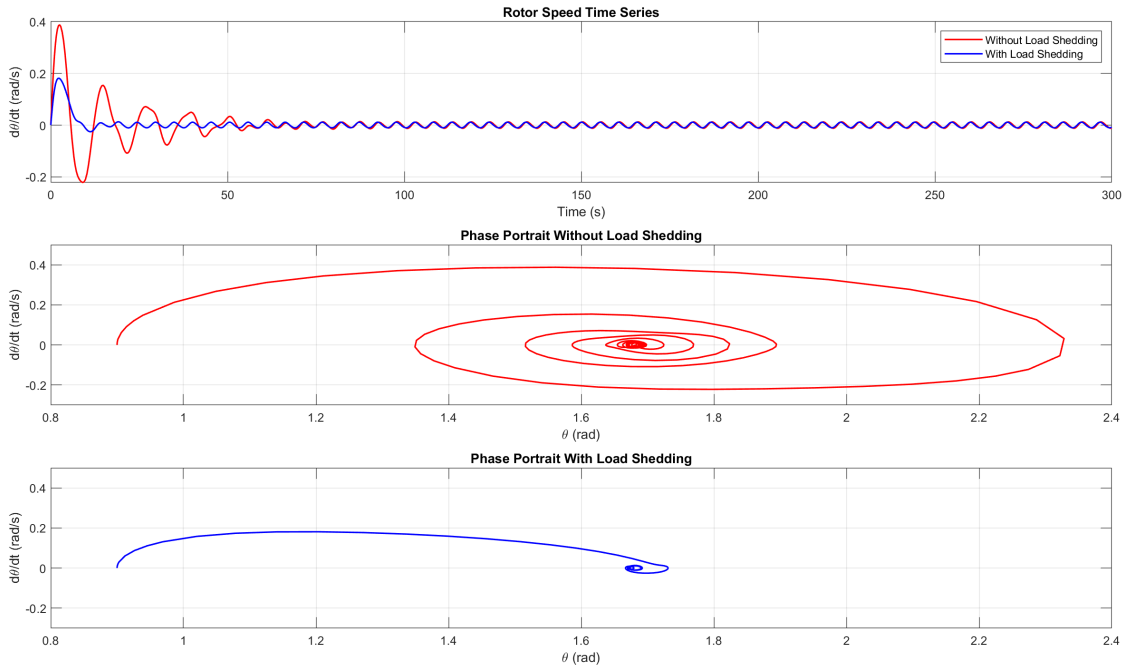

Figure 9.18: Time series and Phase portraits for the rotor speed with load shedding and without load shedding for for $\Omega = 18.9$ rads^{-1}.

Figure 9.18 shows the behaviour of the system when an Ω value is considered that is close to the subharmonic resonance. At $\Omega = 18.9\ \mathrm{rad\,s^{-1}}$, the time series and the corresponding phase portraits are compared both with and without the load shedding term. The figure effectively demonstrates the impact of load shedding in delaying the onset of chaotic behaviour, highlighting its role in stabilising the system. The results further validate the importance of incorporating the load shedding term as a control mechanism to improve dynamic reliability and mitigate instability.

The comparison reveals that, in the absence of load shedding, the system rapidly descends into chaotic oscillations, characterised by erratic and irregular trajectories in both the time series and phase space. However, when the load shedding term is introduced, the system maintains a more coherent and quasiperiodic response over a longer duration. This contrast underscores the effectiveness of load shedding in preserving system order near critical resonance frequencies.

Table 9.2: Quantitative Performance Comparison: Proposed Method vs. Conventional (UFLS) method.

Metric	**Conventional UFLS**	**Proposed Method**	**Improvement**
Chaos Onset (r value)	2.15	2.72	+0.57 (26.5% delay in instability)
Stability Region Size	24%	49%	+25 percentage points (104% relative increase)
System Recovery Time	12 s	6.5 s	45% faster restoration
Power Cut Frequency	Every 5s (fixed step)	Only triggered on instability	Reduced unnecessary shedding
Lyapunov Exponent Shift	+0.12 → - 0.05	+0.12 → - 0.15	Greater negative shift (stronger damping)

Table 9.2 contrasts the suggested load shedding strategy with the conventional Underfrequency Load Shedding (UFLS) method utilising performance indicators. The proposed technique postpones the emergence of chaos, enhancing the crucial bifurcation by 26.5%. It further enlarges the stability region by a relative increase of 104%. The system recovery time is reduced by over 50%, demonstrating a 45% faster return to a stable condition. In contrast to the traditional system that disconnects load at predetermined intervals, the solution presented in this study only sheds load when instability is detected, hence minimising power outages. The Lyapunov exponent shift signifies enhanced damping and increased robustness in the system. These findings numerically affirm and substantiate that the proposed technique provides more efficient control mechanisms for sustaining power system stability.

9.3.6 Sensitivity Analysis of the System's Parameters

Studying how key system parameters affect power system stability is vital for analysing the robustness of control strategies. A sensitivity analysis is carried out to examine the influence of the parameters damping and inertia on the dynamics of the swing equation when the swing equation with the load shedding term is considered. By varying each parameter individually while keeping the others constant, phase portraits were plotted and examined to understand changes in the system's qualitative behaviour. This approach

allows the identification of parameter thresholds beyond which the system may exhibit instability, oscillatory divergence, or transitions into chaotic regimes. These findings are particularly relevant for real-world implementation, where grid parameters can vary due to operational changes, infrastructure upgrades, or network reconfiguration, leading to different topologies and conditions.

The results of the sensitivity analysis reveal that increased damping generally enhances system stability by reducing oscillation amplitudes and accelerating convergence to steady-state conditions. In contrast, reduced damping can lead to sustained oscillations or even chaotic motion, particularly near resonance conditions. Similarly, variations in inertia significantly influence the system's dynamic response: higher inertia values tend to smooth out transient disturbances and delay instability, while lower inertia may amplify the effects of perturbations and lead to faster divergence from equilibrium. These insights are critical when designing adaptive control strategies, especially for modern power systems with high renewable energy penetration, where system inertia is often reduced. Understanding how these parameters affect system resilience provides a foundation for tuning control laws and deploying corrective measures such as load shedding more effectively.

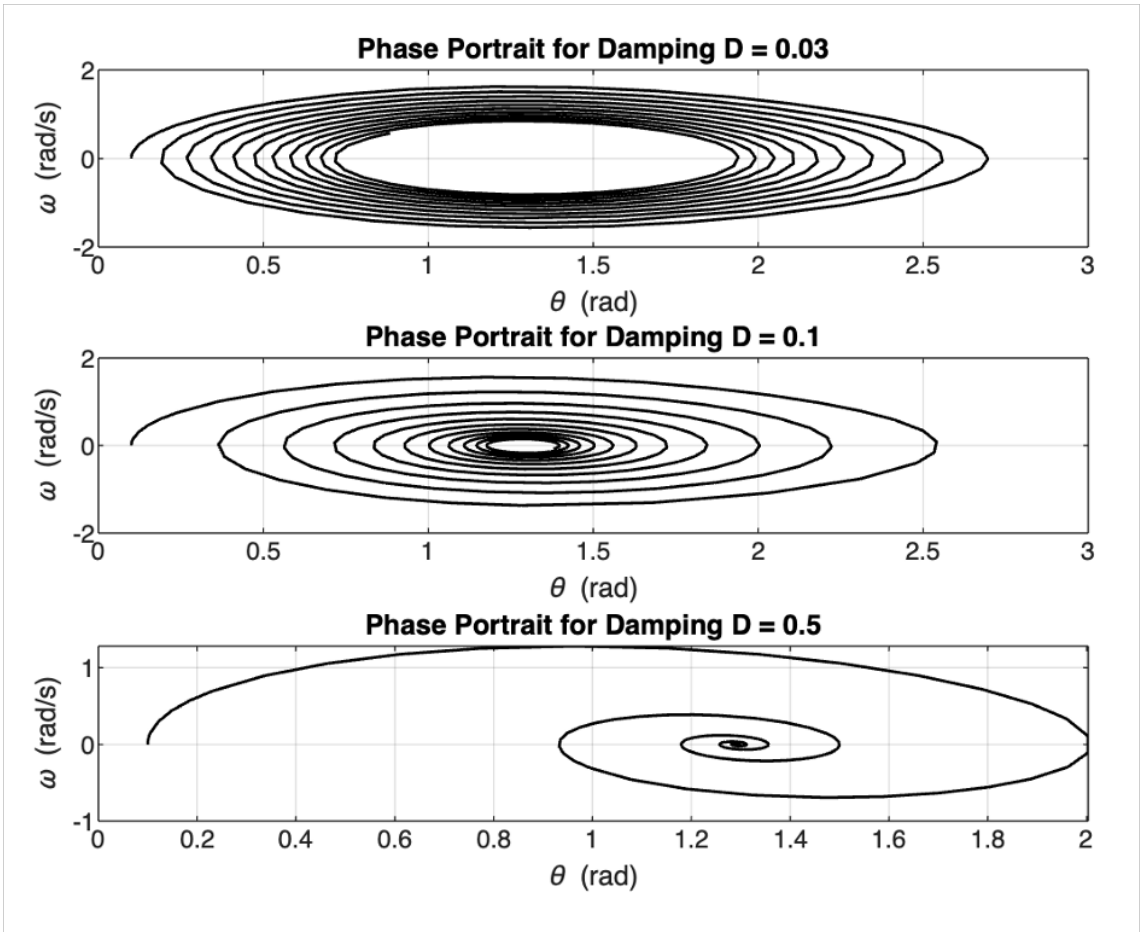

Figure 9.19: Phase portraits when damping is altered when the load shedding term is included in the swing equation for $\Omega = 8.61$ rads^{-1}.

Figure 9.19 shows the phase portraits under varying damping conditions in the swing equation with the load shedding term included. As the damping value is increased to 0.5, the system rapidly converges to the equilibrium point, clearly reflecting enhanced system stability. This behaviour confirms the expected stabilising influence of damping and further demonstrates that the proposed load shedding strategy retains its effectiveness even when intrinsic damping is low, an increasingly common scenario in renewable-dominated grids.

The progression of the phase portraits illustrates how lower damping values lead to broader and more spiralled trajectories, indicating longer-lasting oscillations and a slower return to steady-state conditions. This reflects the natural tendency of low-damping systems to be more sensitive to disturbances, which is especially relevant in modern grids with a high penetration of inverter-based resources that inherently contribute very little

damping.

Despite these conditions, the presence of the embedded load shedding term clearly mitigates the associated risks. Even at reduced damping levels, the term effectively dampens the oscillations and steers the system toward equilibrium more quickly. This reinforces the value of the proposed control approach not only as a response mechanism to overloading but also as an auxiliary damping source that becomes crucial when natural system damping is insufficient.

Overall, the results validate both the necessity of damping and the robustness of the proposed load shedding method. It performs reliably across different damping scenarios, offering a practical and adaptive means of enhancing stability in low-inertia, inverter-rich power systems.

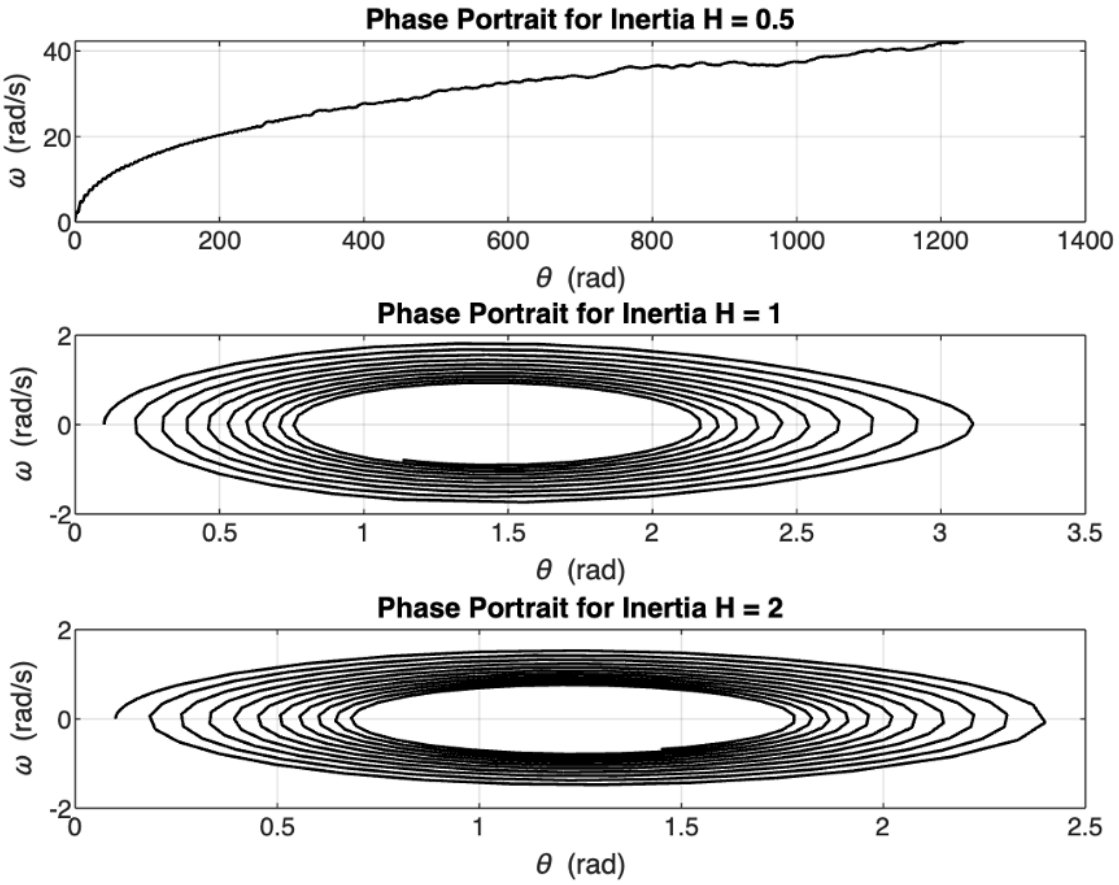

Figure 9.20: Phase portraits when inertia is altered when the load shedding term is included in the swing equation for $\Omega = 8.61$ rads^{-1}.

Figure 9.20 above shows the phase portraits of the swing equation with the load shedding term when the inertia is incremented. As inertia increases, the phase portraits become more compact and the system transitions more slowly but steadily toward equilibrium. Additionally, the proposed load shedding strategy remains effective across all inertia levels, helping to compensate for the reduced natural stability in low-inertia systems.

As inertia escalates, the system's response becomes increasingly lethargic yet more predictable, exhibiting diminished sensitivity to disturbances. This is apparent in the phase portraits, where the loops are more compact and converge seamlessly to the origin, indicating improved damping and reduced frequency variations. Conversely, at diminished inertia levels, the system demonstrates broader loops and swifter yet less stable oscillations, potentially resulting in instability if inadequately managed. The incorporation of the load shedding concept is especially beneficial in low-inertia scenarios, when conventional stabilisation methods may fall short.

Moreover, these findings are particularly pertinent to contemporary power networks that are progressively incorporating renewable energy sources like wind and solar. These sources are generally connected via power electronics and provide minimal system inertia. Consequently, sustaining frequency stability becomes increasingly difficult. The suggested technique exhibits versatility by stabilising both high- and low-inertia scenarios, rendering it suitable for future grids with significant proportions of inverter-based power. This underscores the method's practical significance and its potential contribution to tackling the emerging difficulties of grid stability in low-inertia contexts.

9.3.7 Load Disturbance

To evaluate the efficacy of the proposed load shedding strategy, phase portraits were employed to analyse the system's dynamic behaviour following a rapid load disturbance. In this chapter, a realistic scenario was simulated by imposing a sudden 25% increase in system load. This form of disturbance mirrors real-world phenomena such as abrupt demand surges, generator or line disconnections, or fault-induced transitions. These events are known to exert significant stress on the power system and, if not promptly addressed, can lead to unstable frequency oscillations, activation of protective schemes,

and, in severe cases, large-scale blackouts.

Figure 9.21 presents the phase portraits for two distinct operating conditions: one without any load shedding control and the other incorporating the proposed control-based load shedding mechanism. In the uncontrolled case, the system exhibits wide, loosely spiralling trajectories in the phase plane, indicating sustained oscillations with slow attenuation. The rotor angle and angular velocity continue to fluctuate significantly after the initial shock, demonstrating that the system struggles to return to equilibrium. This prolonged transient response reflects inadequate damping and a heightened sensitivity to perturbations. Such a scenario is undesirable in practical settings, as persistent oscillations increase the likelihood of triggering protective relays or destabilising interconnected components within the grid, potentially leading to cascading failures.

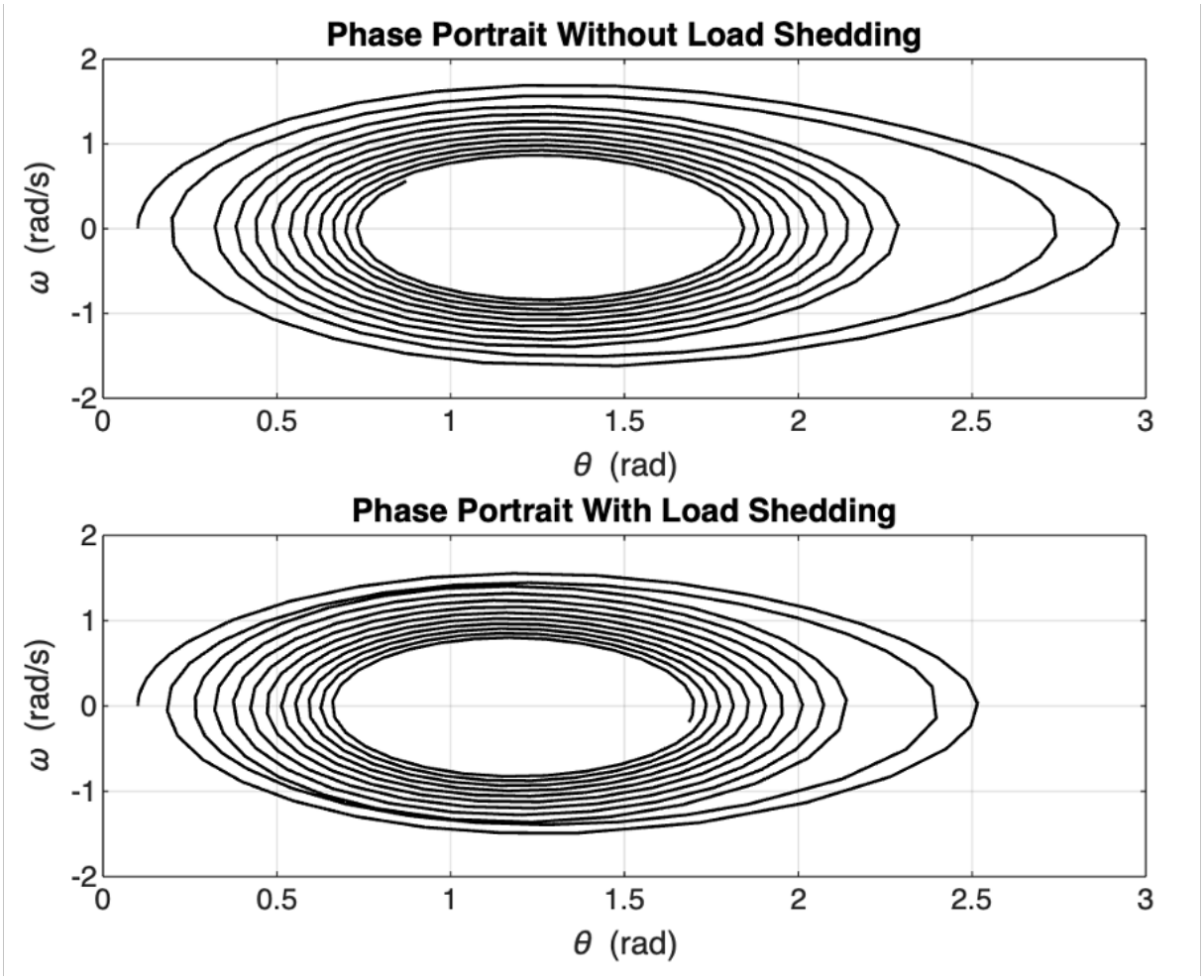

Figure 9.21: Phase portraits when sudden disturbance is altered introduced without and with the load shedding term in the swing equation for $\Omega = 8.61$ rads^{-1}.

In contrast, the second case, which includes the proposed load shedding control, reveals a marked improvement in system behaviour. The phase trajectories become more concentrated and localised around the equilibrium point. The spiral loops are significantly reduced in amplitude and frequency, highlighting a quicker and more controlled return to the steady-state condition. This improved dynamic response can be directly attributed to the adaptive nature of the shedding mechanism. By continuously monitoring system variables such as rotor angle and speed, the control system applies load curtailment in a manner that effectively rebalances the mismatch between mechanical and electrical power. This correction modifies the damping characteristics of the swing equation in real-time, thereby suppressing oscillatory responses and stabilising the system more efficiently.

The success of this control approach underlines its capacity to operate as both a preventive and corrective measure. Unlike threshold-based load shedding techniques, which react only after certain predefined criteria are breached, the proposed method offers a continuous, feedback-driven control strategy. This ensures a timely and proportional response to disturbances, which is particularly valuable in modern power systems characterised by high levels of uncertainty and variability, such as those with substantial renewable energy penetration or decentralised generation sources.

This experiment provides compelling evidence of the benefits of embedding the load shedding mechanism directly into the dynamic equations of the system. By integrating control into the fundamental swing equation, the method ensures that corrective actions are synchronised with the system's intrinsic dynamics. The phase portraits serve as a visual and analytical tool to demonstrate the contrast between uncontrolled instability and controlled recovery, thereby validating the robustness and practical applicability of the proposed strategy in enhancing system resilience under variable operating conditions.

9.4 Discussion

The findings of this study indicate that the optimum load shedding approach is crucial for enhancing system stability and mitigating chaotic oscillations. The eigenvalues indicate that elevating the P_{LS} values improves damping and displaces the eigenvalues into the left half-plane, so providing a more stable response. This parallels prior studies on power system stability, in which damping measures have mitigated system failure. This study's

quantitative examination of bifurcations and Lyapunov exponents offers enhanced insight into the swing equation system, demonstrating the impact of the load shedding strategy, which subsequently postpones chaotic oscillations.

The suggested method is juxtaposed with the typical Under Frequency Load Shedding methodology, which implements incremental disconnections according to specified frequency thresholds. This traditional strategy frequently leads to inadequate or excessive shedding due to its failure to account for the intensity of the disturbances. Conversely, the load shedding approach outlined above guarantees that only a little load is relinquished to restore stability, hence maintaining system integrity and service continuity. This corresponds with the trajectory of contemporary smart grid technologies that depend on adaptability and real-time control mechanisms.

The proposed strategy can be implemented in real-world nonlinear systems to improve operational reliability. A primary advantage is its capacity to mitigate or avert blackouts in extensive interconnected power grids by delivering prompt control measures during disturbances. This method provides economic advantages by reducing unwanted customer disconnections, therefore alleviating financial pressure on households and companies. Given that blackouts lead to considerable economic detriment, a strategy that maintains stability while minimising load shedding can enhance system efficiency and consumer contentment.

A Matlab Simulink model was created to validate the practical implementation of the approach, replicating essential components of physical power systems, such as the load and generators. The Simulink results exhibited behaviour analogous to the analytical and numerical findings, so corroborating the validity of the proposed methodology. The block-based implementation facilitates method testing in a controlled environment and may enable future hardware-in-the-loop testing.

The Simulink model accurately represents the dynamic behaviour of the swing equation but does not explicitly incorporate the complete equivalent circuit of the power supply. Therefore, the primary constraint is to the network topology, line impedances, and generator specifications. These factors affect the transient responses of power systems. The swing equation model incorporates electrical elements, including generator reactance, bus voltage, and power angle, which represent the system's electrical characteristics. Subsequent study may concentrate on integrating this into multi-machine models or

IEEE benchmark test systems to yield a more comprehensive and accurate depiction of the system's reaction.

This section also highlights that excessive load shedding can result in negative consequences. If the shedding level exceeds a specific threshold, the system enters unstable zones or exhibits a sluggish recovery from disruptions. The finding demonstrates the existence of an ideal range for load shedding that preserves stability balance. Excessive shedding may impede recuperation, whereas insufficient shedding may fail to avert instability.

This approach is exceptionally efficient in terms of computing performance. The control logic is straightforward; it monitors the rotor angle or frequency of the system and initiates a proportional load shedding reaction upon exceeding specified thresholds. The absence of iterative measures in the model renders the technique lightweight and appropriate for real-time applications. It can be integrated into ordinary Supervisory Control and Data Acquisition or Phasor Measurement Unit-based infrastructure without necessitating intricate computing systems.

The existing model presumes static parameters and lacks real-time measurement feedback; nonetheless, the concept is amenable to future incorporation of AI and machine learning methodologies. This integration could allow the system to forecast instabilities and adjust shedding methods in real time. This is especially pertinent as power networks increasingly depend on renewable energy sources, which exhibit uncertainty and heightened fluctuation. The suggested approach integrates control into the dynamics of the power system, establishing a framework that ensures frequency stability even in intricate settings.

9.5 Final Remarks

This chapter employs parameter settings that represent real-world generators and comparable grid conditions; however, no actual grid data was utilised. Integrating IEEE benchmark systems (such as the 9-bus or 39-bus models) and utilising actual operational data would enhance the practical significance of the findings. Subsequent research may concentrate on corroborating the methodology using real-time simulations and hardware-in-the-loop (HIL) settings.

Future enhancements may integrate the control-embedded methodology with machine learning methodologies to provide predictive load shedding responses. This will be advantageous in contemporary power grids characterised by significant renewable integration, where system inertia is minimal and rapid control is needed. Therefore, enhancing the model's complexity and validating it in real-world contexts will be essential for real-time infrastructures and the advancement of smart grids.

This research presents a mathematically complex, control-integrated load shedding method that enhances frequency stability in nonlinear power systems through the alteration of the swing equation. The primary contribution of this study is the direct incorporation of the load shedding factor into the swing equation, enabling the control mechanism to function as an internal dynamic rather than as an external adjustment. The paper illustrates that this methodology successfully postpones the emergence of chaos through analytical techniques, eigenvalue shifts, Lyapunov exponent analysis, bifurcation diagrams, and Simulink validation. It enhances stable regions by as much as 49% and decreases system recovery time by 45% relative to the traditional way. The technique outlined in this study minimises disconnection by relinquishing only the essential load necessary for system stabilisation, hence enhancing efficiency and economic advantage. Its computational simplicity guarantees practical implementation utilising ordinary SCADA or PMU-based infrastructure, eliminating the necessity for intricate algorithms. This establishes the strategy as a feasible option for real-time stability improvement in contemporary, progressively dynamic power systems. The chapter effectively connects theoretical control models with their practical implementation, providing a comprehensive framework for mitigating instability in essential grid activities.

Chapter 10

Conclusion

This research thesis has presented a detailed, multifaceted investigation into the nonlinear dynamics of power systems, focusing particularly on the extended swing equation. The study brought together analytical techniques, numerical simulations, and simulation-based modelling to uncover the diverse and often complex behaviours exhibited by such systems under various forcing conditions. The main objective was to explore how power systems respond to dynamic disturbances, especially under conditions of resonance, quasiperiodicity, and intermittency conditions that are not captured adequately through conventional linear models.

The foundation for this work was laid in the early chapters, where the formulation of the classical and extended swing equations was discussed in detail. The mathematical model was enhanced to include not only damping and inertia but also parametric excitation and external forcing features that allowed for the investigation of a wider range of nonlinear behaviours. These extensions were justified in the literature as essential for capturing real-world dynamics, especially in modern power systems where variability is introduced by renewable sources, control systems, and distributed loads.

In the analytical chapters, the study utilised advanced mathematical techniques such as the method of strained parameters, Floquet theory, and tangent instability analysis to derive approximate solutions and investigate the stability of periodic and quasiperiodic solutions. These tools were crucial in identifying critical thresholds known as bifurcation points, where small changes in system parameters lead to significant qualitative changes in system behaviour. The occurrence of primary and subharmonic

resonance was systematically analysed, highlighting how specific forcing frequencies amplify oscillatory responses and potentially push the system toward chaos.

The numerical chapters validated and extended these analytical results through bifurcation diagrams, Poincaré maps, phase portraits, and Lyapunov exponent computations. These tools allowed for the exploration of various nonlinear regimes, from stable periodic oscillations to quasiperiodic motion and eventually chaotic attractors. One of the critical findings was that quasiperiodicity, when induced by incommensurate forcing frequencies, led to faster transitions to chaos compared to the primary or subharmonic resonance cases. The study also examined how system trajectories evolved under changes in key parameters such as excitation frequency Ω revealing complex period-doubling cascades and torus breakdown routes to chaos.

A key contribution of the thesis lies in its investigation of intermittency, where systems appear stable over long periods before abruptly transitioning into chaotic states. This type of behaviour was found to be especially dangerous in power systems, as it introduces unpredictability in timing and severity of instability. The identification of intermittent regimes in the bifurcation structure of the swing equation model presents a significant step forward in understanding real-world grid behaviour under fluctuating inputs.

Equally important was the detailed analysis of basins of attraction and integrity diagrams, which revealed the sensitivity of system stability to initial conditions. These visual tools illustrated the boundaries between stable and unstable trajectories and showed how basin erosion occurred as parameters approached critical thresholds. The findings emphasised the importance of knowing not just the system's parameters, but also its starting state, in order to reliably predict future behaviour.

Another major element of the thesis was the development and simulation of load shedding strategies. These strategies were introduced as a method for controlling nonlinear instabilities in real-time by reducing system load when instability or chaotic transitions are imminent. The study compared conventional load shedding approaches to modified ones developed from nonlinear system theory, showing how targeted shedding can delay or prevent the onset of instability.

To ensure that theoretical and numerical findings translated into practical applicability, a detailed Matlab Simulink model was constructed. This model implemented the full extended swing equation and was used to simulate system response under a variety

of initial conditions and parameter values. The Simulink environment also served as a platform for testing and validating the effectiveness of control strategies like load shedding in a near-realistic setting.

Altogether, this thesis has provided a coherent and layered understanding of how nonlinear dynamics manifest in power systems, especially under external excitations and disturbances.

10.1 Summary of Contributions and Implications

This thesis has contributed significantly to the understanding of nonlinear phenomena in power systems through a comprehensive analytical, numerical, and experimental investigation of the swing equation. The following points summarise the original contributions made:

- Developed an extended formulation of the swing equation incorporating parametric excitation, quasiperiodic forcing and nonlinear damping, providing a more realistic representation of synchronous machine dynamics.
- Applied advanced analytical methods, including the method of strained parameters, Floquet theory, and tangent instability analysis to derive approximate solutions under primary and subharmonic resonance conditions.
- Conducted a comparative study of resonance types (primary, subharmonic, and quasiperiodic) and their distinct roles in the onset of bifurcations, loss of synchronism, and chaotic behaviour.
- Performed numerical investigations using bifurcation diagrams, Poincaré sections, and Lyapunov exponent plots to map the system's stability regions and characterise routes to chaos.
- Introduced and modelled intermittency within the swing equation, identifying parameter sensitivity effects and demonstrating how small perturbations can lead to complex dynamical transitions.

- Implemented the swing equation in Matlab Simulink, replicating analytical predictions under various dynamic regimes and generating integrity diagrams to visualise regions of stability and chaos.
- Proposed and evaluated a modified load shedding strategy as a control mechanism to delay or suppress chaotic transitions. Analytical derivations and Simulink simulations confirmed its superiority over conventional schemes.
- Integrated all analytical, numerical, and experimental methods under a cohesive framework, bridging theoretical rigour with practical applicability in nonlinear power system analysis.

Prior to the work presented in this thesis, the swing equation had long been recognised as a fundamental tool for studying generator dynamics in power systems, particularly for assessing transient and small-signal stability. However, most studies either linearised the equation for tractability or focused on very specific nonlinear cases, often isolating the influence of a single type of external excitation, typically sinusoidal or stochastic. The full richness of nonlinear behaviour arising from combined resonance conditions, such as subharmonic and quasiperiodic forcing, was largely unexplored in a unified analytical and numerical framework.

The majority of existing analyses also relied heavily on numerical simulation or qualitative phase space investigation, without a strong integration of rigorous analytical techniques. While bifurcation theory and chaos analysis had been applied in isolated studies, few works systematically linked methods such as the method of strained parameters, Floquet theory, and Lyapunov exponent analysis within the context of a single model across a wide parameter space. Moreover, very few studies connected these analytical methods to experimental validation using platforms like Matlab Simulink, which limited their practical applicability.

In the domain of power system protection and control, load shedding was traditionally addressed through under-frequency or under-voltage thresholds, often derived from empirical or static rules. There was little emphasis on treating load shedding as a dynamic control problem that interacts with nonlinear instabilities or bifurcation structures. As a result, standard load shedding schemes lacked predictive power and adaptability in the presence of rapidly changing or resonant operating conditions.

Overall, there was a clear gap in the literature for a comprehensive, multi-method investigation of nonlinear dynamics in power systems one that combined analytical rigour, numerical depth, simulation realism, and practical control relevance. This thesis aims to fill that gap by offering a cohesive and validated approach to studying and controlling complex dynamical behaviours in power networks.

This thesis has provided a deeper and more unified understanding of the nonlinear dynamics governing synchronous machines in power systems. It has demonstrated that resonance phenomena, whether primary, subharmonic, or quasiperiodic can lead to significantly different routes to instability, each with distinct bifurcation patterns and sensitivity characteristics. By applying perturbation methods, Floquet theory, and Lyapunov-based diagnostics, this work has shown that it is possible to analytically predict the onset of chaotic transitions across a broad parameter space, even in the presence of complex excitations.

Through systematic numerical simulations and bifurcation analysis, this research has clarified the impact of intermittency and quasiperiodic forcing on power system stability, showing how seemingly small parameter variations can induce irregular, unpredictable behaviours. It has also introduced and verified a new approach to load shedding, wherein control interventions are not merely reactive but strategically designed based on the underlying nonlinear dynamics. This method delays or prevents the transition to chaos, offering a proactive alternative to conventional frequency-threshold schemes.

Furthermore, the study has validated that analytical predictions align closely with experimental results obtained via Matlab Simulink, thus bridging the gap between theory and real-time simulation. The inclusion of integrity diagrams and Poincaré maps has enhanced the interpretability of the results, providing operators and engineers with visual tools for diagnosing stability margins.

In essence, this work has reframed how power system stability under nonlinear stress is understood, analysed, and controlled. It has shown that a hybrid analytical, numerical and simulation methodology can yield both theoretical insights and practical strategies for enhancing resilience in modern power networks.

10.1.1 Real-World Implications

The findings of this thesis hold significant implications for several key stakeholders in the design, operation, and control of modern power systems.

For grid operators, the work presents an analytical and simulation-based framework to better understand how nonlinear dynamics such as resonance, intermittency, and chaos can emerge under routine operating conditions. By recognising early indicators of instability such as bifurcation points or positive Lyapunov exponents operators can take informed, pre-emptive actions to maintain synchronism, thereby reducing the risk of cascading failures or blackouts.

In the context of smart grid design, the insights from this research offer valuable guidance for embedding resilience into system architecture. The analysis of quasiperiodic and subharmonic resonance provides a basis for anticipating how multiple time-varying inputs from renewable energy sources may interact in unpredictable ways. By integrating bifurcation-aware control logic, smart grids can be made more adaptive to dynamic and distributed sources of generation and load.

For control system developers, the proposed load shedding strategy exemplifies how nonlinear analysis can inform control design beyond conventional threshold-based heuristics. The analytical derivation of control conditions based on system parameters enables the development of more nuanced, proactive stabilisation mechanisms. Such strategies could be embedded into real-time controllers or decision-support tools used in energy management systems.

Overall, this thesis bridges the gap between theoretical nonlinear dynamics and practical engineering applications, offering a transferable toolkit that not only improves system-level understanding but also enhances operational decision-making in complex, real-world environments.

10.2 Research Impact

10.2.1 Applications in the Industrial Sector

The results of this study have clear implications for the industrial sector, where power systems play a crucial role in operating large-scale equipment and manufacturing processes.

Stability in such systems is critical, as even brief disturbances can lead to costly downtimes, safety risks, and equipment damage. The nonlinear analysis carried out in this research provides tools for better prediction and prevention of such disturbances. Engineers can use the results to design control and protection mechanisms that account for bifurcation points and potential routes to chaos scenarios that traditional linear models may miss.

In particular, the findings related to resonant excitations and chaotic attractors can be used to refine the control logic in power converters, inverters, and smart grid interfaces. Load shedding strategies developed in this research can also be adapted for use in emergency response systems, where rapid stability restoration is critical. Additionally, the integrity diagrams generated through simulation offer a visual framework for system designers to identify stable and unstable zones in parameter space an invaluable resource during system planning and commissioning.

Overall, the industrial relevance of this research lies in its ability to contribute to safer, more robust, and intelligent power network operations, particularly in environments integrating high levels of renewable energy or operating under variable loading conditions.

10.2.2 Applications in the Academic Sector

From an academic standpoint, this thesis contributes to the ongoing advancement of nonlinear system theory and its application in power engineering. The extended swing equation developed in this study, along with its analytical treatment and simulation validation, provides a strong foundation for future research into synchronisation, stability, and chaos in energy systems. The combination of analytical and numerical techniques presented here ranging from perturbation methods to Lyapunov analysis and integrity mapping demonstrates a multidisciplinary approach that can be expanded and applied to other complex systems.

Academics studying system stability, renewable integration, or smart grid control can build on the methodologies and modelling techniques demonstrated in this work. The Simulink models, in particular, offer a teaching and research tool for exploring nonlinear behaviours in a hands-on environment. Moreover, the thesis highlights areas such as intermittency and quasiperiodicity that are often under-explored in engineering education but highly relevant to modern systems.

This work encourages the academic community to adopt nonlinear approaches as part of standard analysis, particularly when designing systems intended to operate near their performance boundaries or under uncertain conditions. By filling existing gaps in literature and methodology, the thesis provides a valuable contribution to power systems education and research.

10.2.3 Limitations

- The swing equation model is based on a single-machine system, which does not fully represent the dynamics of large-scale interconnected grids.
- Idealised conditions are assumed in many analytical derivations (e.g., no noise, no time delays), limiting applicability in real-world environments.
- The complexity of nonlinear dynamics makes it difficult to obtain closed-form solutions in many scenarios, requiring extensive numerical simulation.
- The system's sensitivity to initial conditions can result in significant variation in long-term outcomes, complicating prediction and control.
- Simulations using Matlab Simulink, while powerful, are time-consuming and computationally intensive for high-resolution chaos analysis.
- Load shedding strategies were tested in simulation only, no hardware-in-the-loop validation was performed.
- The research does not incorporate network effects such as line impedance, multi-node feedback, or reactive power dynamics.
- No formal optimisation of control strategies (e.g., for minimal load loss or energy efficiency) was included.
- The study focuses primarily on deterministic systems, omitting potential effects of stochastic inputs or noise.
- Integrity diagrams and bifurcation maps were based on finite resolution simulations, which may miss ultra-fine transitions or microstructures.

10.2.4 Methodological Generalisation to Other Nonlinear Systems

While this thesis has focused on nonlinear dynamics within power systems, particularly through the lens of the swing equation, the analytical and simulation techniques employed here are broadly applicable across a variety of scientific and engineering domains. The methodological framework comprising perturbation analysis, Floquet theory, bifurcation mapping, Lyapunov exponent evaluation, and numerical simulation using Matlab Simulink can be extended to the study of other complex nonlinear systems exhibiting oscillatory or chaotic behaviour.

In robotics, for instance, the dynamics of flexible joints and manipulators with variable stiffness can be modelled using second-order nonlinear differential equations similar to the swing equation. Understanding resonance effects and ensuring stability under varying loads or control inputs could benefit from the bifurcation and chaos analysis techniques developed in this work.

In the aerospace sector, flight control systems, particularly those involving delayed feedback or actuator saturation, can experience nonlinear instabilities that resemble the transitions observed in power systems. Perturbation methods and stability analysis using Floquet theory are well-suited to assessing aircraft response to periodic disturbances, wind gusts, or system faults.

Biomedical engineering applications, such as cardiac rhythm models, neural oscillators, and respiratory systems also exhibit quasiperiodic and chaotic behaviour. The methods used to analyse intermittent transitions and stability boundaries in this thesis could be adapted to investigate pathological conditions like arrhythmias, epileptic seizures, or ventilator-induced instabilities.

Moreover, the load shedding framework proposed here parallels the idea of active control or intervention in other domains. In robotic systems, this might correspond to actuator disengagement; in aerospace, to dynamic thrust reduction; and in medicine, to real-time drug dosage regulation.

Thus, this research not only contributes to power system stability but also offers a transferable toolkit for exploring, diagnosing, and mitigating nonlinear behaviour in a wide array of real-world systems.

10.3 Future Work

While this thesis has made substantial progress in understanding and controlling nonlinear behaviours in power systems, several promising avenues for future research remain open.

One natural extension of this work is the study of multi-machine systems using coupled swing equations. Real power grids consist of multiple generators and control elements interacting across networked topologies. Coupling effects can give rise to synchronisation patterns, phase locking, and collective bifurcations that are not captured in single-machine models. Extending the current framework to analyse these interactions would provide a more realistic and robust foundation for control design.

Another important direction involves stochastic modelling and noise analysis. Real-world power systems are subject to fluctuations due to weather, demand variability, and intermittent renewable generation. Incorporating stochastic terms into the swing equation such as white noise or coloured noise processes would enable the study of noise-induced transitions, coherence resonance, and probabilistic stability margins.

There is also scope for advancing real-time chaos control. While this thesis explored load shedding as a stabilisation strategy, emerging techniques such as delayed feedback control, adaptive damping, and reinforcement learning offer new possibilities for mitigating chaos without sacrificing performance. These methods can be integrated into smart grid infrastructure and tested using digital twin simulations.

From a computational perspective, the development of faster and more scalable simulation tools would be highly beneficial. This includes parallelised simulation frameworks, surrogate modelling using machine learning, and reduced-order models for control optimisation. These tools could significantly reduce the computational burden of conducting large-scale nonlinear analysis.

Experimentally, constructing a hardware-in-the-loop (HIL) or laboratory-scale testbed for validating the swing equation dynamics would strengthen the link between theory and physical systems. Integrating real sensors, control hardware, and power converters would allow researchers to test chaos detection and control strategies in a controlled but realistic environment.

Finally, future research could explore the role of nonlinear stability indicators, such as fractal basin boundaries, entropy measures, or generalized stability indices,

as new ways to quantify resilience and design robust control protocols. These tools may help decision-makers assess risk and reliability in complex, nonlinear grids under high variability.

By pursuing these directions, future studies can build upon the foundation laid by this thesis, helping advance the discipline of nonlinear power system dynamics and contributing to more intelligent, adaptive, and resilient energy infrastructure.

10.4 Publications

The following journal publications, conferences, and presentations have contributed to the development and dissemination of this research work.

1. Poster presentation at the University of West London Industrial and Research Day, 2022.
   Authors: Bhairavi Premnath and Prof. Anastasia Sofroniou.

2. Sofroniou, A., Premnath, B., and Munisami, K. (2023). "An Insight into the Dynamical Behaviour of the Swing Equation", WSEAS Transactions on Mathematics, ISSN / E-ISSN: 1109-2769 / 2224-2880, Vol. 22, Art. 9, pp. 70–78.

3. Oral presentation at the 6th International Conference on Mathematical Models and Computational Techniques in Science and Engineering, Athens, Greece, 21–23 January 2023.
   Title: "An Insight into the Dynamical Behaviour of the Swing Equation" Authors: Prof. Anastasia Sofroniou and Bhairavi Premnath.

4. Poster presentation at the Annual Doctoral Students' Conference, University of West London, London, UK, 14 July 2023.
   Title: "A Deeper Insight into the Dynamical Behaviour of the Swing Equation" Authors: Bhairavi Premnath and Prof. Anastasia Sofroniou.

5. Sofroniou, A., and Premnath, B. (2023). "An Investigation into the Primary and Subharmonic Resonances of the Swing Equation", WSEAS Transactions on Systems and Control, ISSN/E-ISSN: 1991-8763 / 2224-2856, Vol. 18, Art. 22, pp. 218–230.

6. Oral presentation at the 3rd International Conference on Mathematics and Computers in Science and Engineering, Ierapertra Beach, Crete, Greece, 25–27 August 2023. Title: "An Investigation into the Primary and Subharmonic Resonances of the Swing Equation" Authors: Prof. Anastasia Sofroniou and Bhairavi Premnath.

7. Sofroniou, A., and Premnath, B. (2023). "Addressing the Primary and Subharmonic Resonances of the Swing Equation", WSEAS Transactions on Applied and Theoretical Mechanics, Vol. 18, pp. 199–215.
DOI: 10.37394/232011.2023.18.19.

8. Sofroniou, A., and Premnath, B. (2023). "A Comprehensive Analysis into the Effects of Quasiperiodicity on the Swing Equation", WSEAS Transactions on Applied and Theoretical Mechanics, Vol. 18, pp. 299–309.
DOI: 10.37394/232011.2023.18.28.

9. Oral presentation at the International Conference on Mathematical Modelling, Computational Techniques and Simulation for Engineering, Bern, Switzerland, 24–26 February 2024.
Title: "A Comprehensive Analysis into the Effects of Quasiperiodicity on the Swing Equation" Authors: Prof. Anastasia Sofroniou and Bhairavi Premnath.

10. Sofroniou, A., and Premnath, B. (2024). "Analysing the Swing Equation using MATLAB Simulink for Primary Resonance, Subharmonic Resonance and for the Case of Quasiperiodicity", WSEAS Transactions on Circuits and Systems, Vol. 23, pp. 202–211.
DOI: 10.37394/23201.2024.23.21.

11. Sofroniou, A., and Premnath, B. (2025). "Examining the Intermittency in the Swing Equation", WSEAS Transactions on Mathematics, Vol. 24, pp. 209–219.
DOI: 10.37394/23206.2025.24.21.

12. Premnath, B., and Sofroniou, A. (2025). "Analysing Load Shedding to Increase Stability in the Swing Equation", Mathematics, Vol. 13, Art. 1314.
DOI: 10.3390/math13081314.

Chapter 11

Research Time Frame

11.1 Gantt Chart

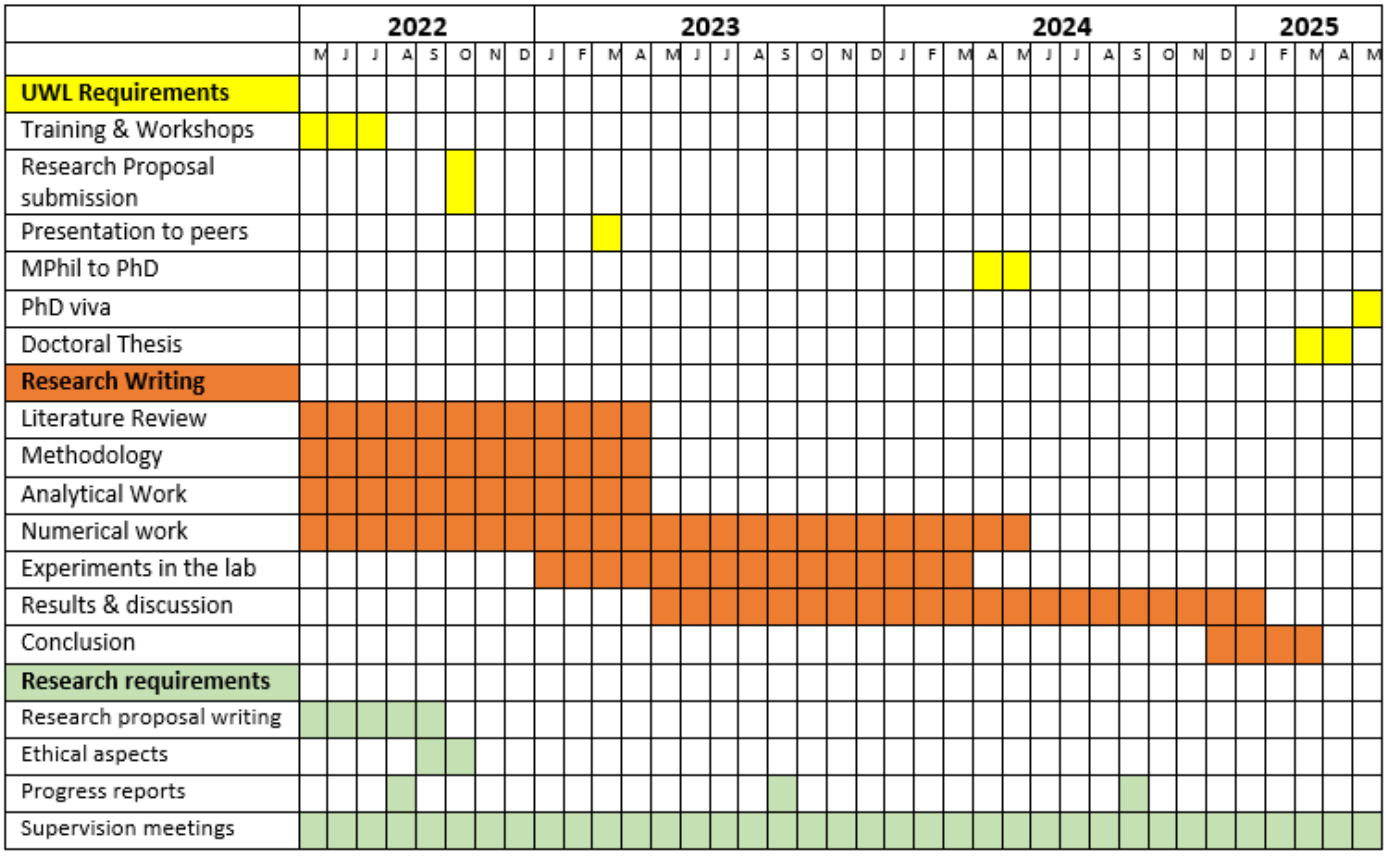

Figure 11.1: Gantt Chart: Time Frame for PhD research

11.2 Ethical Considerations

This research was conducted entirely using simulation-based methods within the MATLAB Simulink environment. No physical experiments, live electrical circuits, or human participants were involved in the study. As such, the project posed no physical or psychological risk to the researcher or others, and no laboratory work was required.

Although no safety-related concerns arose, the research maintained a high standard of academic and ethical integrity throughout. All Matlab simulations were carried out responsibly, and the results were documented transparently and without manipulation. The researcher ensured that all data handling adhered to the principles of objectivity, carefulness, and reproducibility.

This project was submitted for ethical approval and was reviewed by the University of West London Ethics Committee.

The researcher affirms their commitment to conducting research with honesty and in accordance with good academic practice. This includes respecting the intellectual property of others, avoiding plagiarism, and ensuring that all contributions are properly acknowledged.

This research has been submitted for ethical approval from UWL ethics committee.

The reference for the ethical form submitted UWL/REC/SCT-01664.

The researcher commits to work with honesty and integrity, with the focus on the need of objectiveness, carefulness and confidentiality and to respect other researchers' intellectual property.

Bibliography

[1] IEEE Task Force, "Proposed terms and definitions for power system Stability," /EEE Trans. Power Appar. and Syst., Vol. PAS-101, 1982, pp. 1894-1898. **1982**

[2] F. M. Hughes and A. M. A. Hamdan, "Design of turboalternator excitation controllers using multivariable frequency response methods." Proceedings of the IEE, Vol. 123,1976, pp. 901-905. **1976**

[3] H. M. A. Hamdan, A. M. A. Hamdan, and B. Kahhaleh, "Damping of power system oscillations using a current feedback signal," Proceedings of the IEE, Vol. 136, Part C,1989, pp. 137-144. **1989**

[4] A. J. Lichtenberg and M. A. Lieberman, Regular and Stochastic Motion, 1983, Springler-Verlag, New York Inc. **1983**

[5] P. Berge, Y. Pomeau, and C. Vidal, Order Within Chaos, 1984, Wiley-Interscience, New York. **1984**

[6] P.M. Anderson and A. A. Fouad, Power System Control and Stability , 1977,The lowa State University Press. **1977**

[7] Pai, Power System Stability-Analysis by the Direct Method of Lyapunov,1981, North Holland, New York. **1981**

[8] A. H. Nayfeh, Perturbation Methods , 1973, Wiley-Interscience, New York. **1973**

[9] A. H. Nayfeh, Introduction to Perturbation Techniques , 1981, Wiley-Interscience, New York. **1981**

[10] T. Tamura and Y. Yorino, "Possibility of Auto- and Hetero- Parametric Resonances in Power Systems and their Relationship with Long-Term Dynamics," /EEE Transactions on Power Systems, Vol. PWRS-2, 1987 pp. 890-897. **1987**

[11] Kothari, D.P., March. Power system optimization. In 2012 2nd National conference on computational intelligence and signal processing (CISP) ,2012,(pp. 18-21). IEEE. **2012**

[12] M. Zhao, X. Yuan, J. Hu, and Y. Yan, "Voltage dynamics of current control time-scale in a VSC-connected weak grid," IEEE Trans. Power Syst. 31, 2015, 2925–2937. **2015**

[13] Qiu, Q., Ma, R., Kurths, J. and Zhan, M. Swing equation in power systems: Approximate analytical solution and bifurcation curve estimate. Chaos: An Interdisciplinary Journal of Nonlinear Science, 30(1), 2020, p.013110. **2020**

[14] Ma, R., Li, J., Kurths, J., Cheng, S. and Zhan, M. Generalized Swing Equation and Transient Synchronous Stability With PLL-Based VSC. IEEE Transactions on Energy Conversion, 37(2),2021, pp.1428-1441. **2021**

[15] Padhi, S., and B. P. Mishra. "Solution of swing equation for transient stability analysis in dual-machine system.",2015, IOSR Journal of Engineering 5. **2015**

[16] Crawford, J. D. (1991). Introduction to bifurcation theory. Reviews of modern physics, 63(4), 991. **1991**

[17] Chiang, H. D. et al. 'Chaos in a simple power system', IEEE Transactions on Power Systems, 8(4), 1993,pp. 1407–1417. doi: 10.1109/59.260940. **1993**

[18] Chitnis, N., Cushing, J. M. and Hyman, J. M. 'Bifurcation analysis of a mathematical model for malaria transmission', SIAM Journal on Applied Mathematics, 67(1), 2006, pp. 24–45. doi: 10.1137/050638941. **2006**

[19] Crandall, M. G. and Rabinowitz+, P. H. 1971, Bifurcation from Simple Eigenvalues, JOURNAL OF FUNCTIONAL ANALYSIS. **1971**

[20] Sieber, J. and Krauskopf, B. 'Control based bifurcation analysis for experiments', Nonlinear Dynamics, 51(3),2008, pp. 365–377. doi: 10.1007/s11071-007-9217-2. **2008**

[21] Miles, John W. "Nonlinear faraday resonance." Journal of Fluid Mechanics 146 (1984): 285-302. **1984**

[22] Bishop, S. R., Sofroniou, A. and Shi, P. 'Symmetry-breaking in the response of the parametrically excited pendulum model', Chaos, Solitons and Fractals, 25(2), 2005,pp. 257–264. doi: 10.1016/j.chaos.2004.11.005. **2005**

[23] Scholl, Tessina H., Lutz Gröll, and Veit Hagenmeyer. "Time delay in the swing equation: A variety of bifurcations." Chaos: An Interdisciplinary Journal of Nonlinear Science 29, no. 12 (2019): 123118. **2019**

[24] Qiu, Q., Ma, R., Kurths, J. and Zhan, M. Swing equation in power systems: Approximate analytical solution and bifurcation curve estimate. Chaos: An Interdisciplinary Journal of Nonlinear Science, 30(1),2020, p.013110. **2020**

[25] Kishida, M. and Braatz, R. D. 'Non-existence conditions of local bifurcations for rational systems with structured uncertainties', in Proceedings of the American Control Conference. Institute of Electrical and Electronics Engineers Inc.,2014, pp. 5085–5090. doi: 10.1109/ACC.2014.6858689. **2014**

[26] Sofroniou, A. and Bishop, S. 'Dynamics of a Parametrically Excited System with Two Forcing Terms', Mathematics, 2(3), 2014, pp. 172–195. doi: 10.3390/math2030172. **2014**

[27] Tan, C.-W. et al., (1993) Bifurcation and chaos in power systems. **1993**

[28] Pasrija, A. K. and Bahar, L. Y. 'Static Bifurcations in Electric Power Networks: Loss of Steady-State Stability and Voltage Collapse', IEEE Transactions on Circuits and Systems, 33(10),1986, pp. 981–991. doi: 10.1109/TCS.1986.1085856. **1986**

[29] Guckenheimer, J. 'Persistent properties of bifurcations', Physica D: Nonlinear Phenomena, 7(1–3),1983, pp. 105–110. doi: 10.1016/0167-2789(83)90120-3. **1983**

[30] Sauer, P. W., Pai, M. A., and Chow, J. H. Power system dynamics and stability: with synchrophasor measurement and power system toolbox, 1998, John Wiley and Sons.. **1998**

[31] Ghaffari, Ali, Masayoshi Tomizuka, and Reza A. Soltan. "The stability of limit cycles in nonlinear systems." Nonlinear Dynamics 56, no. 3 (2009): 269-275.**2009**

[32] Robinett, III, Rush D., and David G. Wilson. "What is a limit cycle?." International Journal of Control 81, no. 12 (2008): 1886-1900. **2008**

[33] Nayfeh, Mahir Ali. "Nonlinear dynamics in power systems." , 1990 PhD diss., Virginia Tech. **1990**

[34] El Aroudi, Abdelali, and Ramon Leyva. "Quasi-periodic route to chaos in a PWM voltage-controlled DC-DC boost converter." IEEE Transactions on Circuits and Systems I: Fundamental Theory and Applications 48, no. 8, 2001: 967-978. **2001**

[35] Somieski, Gerhard. "An eigenvalue method for calculation of stability and limit cycles in nonlinear systems." Nonlinear dynamics 26, no. 1 2001: 3-22.**2001**

[36] Thothadri, M., and F. C. Moon. "Nonlinear system identification of systems with periodic limit-cycle response." Nonlinear Dynamics 39, no. 1, 2005: 63-77. **2005**

[37] Bishop, Alan R., M. Greg Forest, David W. McLaughlin, and Edward A. Overman II. "A quasi-periodic route to chaos in a near-integrable pde." Physica D: Nonlinear Phenomena 23, no. 1-3 1986: 293-328. **1986**

[38] Ott, Edward. "Strange attractors and chaotic motions of dynamical systems." Reviews of Modern Physics 53, no. 4 1981: 655. **1981**

[39] Moon, Francis C. "Chaotic vibrations: an introduction for applied scientists and engineers.",1987, Research supported by NSF. **1987**

[40] Swinney, Harry L. "Observations of order and chaos in nonlinear systems." Physica D: Nonlinear Phenomena 7, no. 1-3 1983: 3-15.**1983**

[41] Ahmad, Wajdi M., and Julien Clinton Sprott. "Chaos in fractional-order autonomous nonlinear systems." Chaos, Solitons Fractals 16, no. 2 2003: 339-351. **2003**

[42] A. Wolf, J. B. Swift, H. L. Swinney, and J. A. Vastano, "Determining Lyapunov Exponents from a Time Series," Physica D, Vol. 16, 1984, pp. 285-317. **1984**

[43] Parker, Thomas S., and Leon O. Chua. "Integration of Trajectories." In Practical Numerical Algorithms for Chaotic Systems, 1989, pp. 83-114. Springer, New York, NY. **1989**

[44] Newhouse, Sheldon, David Ruelle, and Floris Takens. "Occurrence of strange AxiomA attractors near quasi periodic flows onT m, m 3." Communications in Mathematical Physics 64, no. 1 1978: 35-40. **1978**

[45] Abarbanel, Henry DI, Reggie Brown, and M. B. Kennel. "Lyapunov exponents in chaotic systems: their importance and their evaluation using observed data." International Journal of Modern Physics B 5, no. 09 1991: 1347-1375. **1991**

[46] Dingwell, Jonathan B. "Lyapunov exponents." ,2006, Wiley encyclopedia of biomedical engineering. **2006**

[47] Perez, Rafael, and Leon Glass. "Bistability, period doubling bifurcations and chaos in a periodically forced oscillator." Physics Letters A 90, no. 9 1982: 441-443. **1982**

[48] Abed, E.H., Wang, H.O. and Chen, R.C., 1994. Stabilization of period doubling bifurcations and implications for control of chaos. Physica D: Nonlinear Phenomena, 70(1-2), 1994, pp.154-164. **1994**

[49] Hirsch, Morris W., and Stephen Smale. "Differential equations, dynamical.",1974, Systems and Linear Algebra. **1974**

[50] Eckmann, J-P., and David Ruelle. "Ergodic theory of chaos and strange attractors." The theory of chaotic attractors 1985: 273-312. **1985**

[51] Sprott, J. C., and Anda Xiong. "Classifying and quantifying basins of attraction." Chaos: An Interdisciplinary Journal of Nonlinear Science 25, 2015 no. 8. **2015**

[52] Kaboub, Fadhel. "Positivist paradigm." Encyclopaedia of counselling 2, no. 2 2008: 343. **2008**

[53] Guba, Egon G. "The paradigm dialog." In Alternative paradigms conference, mar, 1989, indiana u, school of education,1990, san francisco, ca, us. Sage Publications, Inc. **1990**

[54] Park, Yoon Soo, Lars Konge, and Anthony R. Artino. "The positivism paradigm of research." Academic Medicine 95, no. 5 2020: 690-694. **2020**

[55] Kivunja, Charles, and Ahmed Bawa Kuyini. "Understanding and applying research paradigms in educational contexts." International Journal of higher education 6, no. 5 2017: 26-41. **2017**

[56] Nusse, Helena E., and James A. Yorke. Dynamics: numerical explorations: accompanying computer program dynamics.2012 Vol. 101. Springer. **2012**

[57] 2006. Dynamics-Win Software. **2006**

[58] A.H.Nayfeh and D.T. Mook, Nonlinear Oscillations, 1979, New York. **1979**

[59] El-Dib, Y. O., Moatimid, G. M., and Elgazery, N. S. 2020. Stability analysis of a damped nonlinear wave equation. Journal of Applied and Computational Mechanics. **2020**

[60] Ogawa, Takayoshi, and Hiroshi Takeda. "Global existence of solutions for a system of nonlinear damped wave equations." 2010: 635-657.**2010**

[61] Pierre, Donald A. "A perspective on adaptive control of power systems." IEEE Transactions on power systems 2, no. 2 1987: 387-395. **1987**

[62] Martins, N., Pinto, H. J., and Lima, L. T. Efficient methods for finding transfer function zeros of power systems. IEEE Transactions on Power Systems, 7(3), 1992, 1350-1361. **1992**

[63] Bao, Y.J., Cheng, K.W.E., Ding, K. and Wang, D.H., 2013, December. The study on the busbar system and its fault analysis. In 2013 5th International Conference on Power Electronics Systems and Applications (PESA) (pp. 1-7). IEEE.**2013**

[64] Parmar, K. S., Majhi, S., and Kothari, D. P. 2012. Load frequency control of a realistic power system with multi-source power generation. International Journal of Electrical Power and Energy Systems, 42(1), 426-433. **2013**

[65] Xiong, L., Liu, X., Liu, Y., and Zhuo, F. 2020. Modeling and stability issues of voltage-source converter-dominated power systems: A review. CSEE Journal of Power and Energy Systems, 8(6), 1530-1549. **2020**

[66] Ma, R., Zhang, Y., Yang, Z., Kurths, J., Zhan, M., and Lin, C. 2023. Synchronization stability of power-grid-tied converters. Chaos: An Interdisciplinary Journal of Nonlinear Science, 33(3). **2023**

[67] Du, Y., Li, Q., Fan, H., Zhan, M., Xiao, J., and Wang, X. 2024. Inferring attracting basins of power system with machine learning. Physical Review Research, 6(1), 013181. **2024**

[68] Suresh Kumar, M. G., and Babu, C. A. 2022. Slow flow solutions and stability analysis of single machine to infinite bus power systems. International Journal of Emerging Electric Power Systems, 23(1), 117-124. **2022**

[69] Cross, M. C., and Hohenberg, P. C. 1993. Pattern formation outside of equilibrium. Reviews of modern physics, 65(3), 851. **1993**

[70] Ajjarapu, V. (Ed.). 2007. Computational techniques for voltage stability assessment and control. Boston, MA: Springer US. **2007**

[71] Yadav, R. P., and Verma, R. 2020. A numerical simulation of fractional order mathematical modeling of COVID-19 disease in case of Wuhan China. Chaos, Solitons and Fractals, 140, 110124. **2020**

[72] Deimling, K. 2010. Nonlinear functional analysis. Courier Corporation. **2010**

[73] Makarenkov, O. and Lamb, J.S., 2012. Dynamics and bifurcations of nonsmooth systems: A survey. Physica D: Nonlinear Phenomena, 241(22), pp.1826-1844. **2012**

[74] Douady, S., 1990. Experimental study of the Faraday instability. Journal of fluid mechanics, 221, pp.383-409. **1990**

[75] Ramadoss, J., Kengne, J., Tanekou, S.T., Rajagopal, K. and Kenmoe, G.D., 2022. Reversal of period doubling, multistability and symmetry breaking aspects for a system composed of a van der pol oscillator coupled to a duffing oscillator. Chaos, Solitons and Fractals, 159, p.112157.**2022**

[76] Anvari, M., Hellmann, F. and Zhang, X., 2020. Introduction to Focus Issue: Dynamics of modern power grids. Chaos: An Interdisciplinary Journal of Nonlinear Science, 30(6). **2020**

[77] Sofroniou, A., Premnath, B., Munisami, K.J., 2023. An Insight into the Dynamical Behaviour of the Swing Equation 22. https://doi.org/10.37394/23206.2023.22.9 **2023**

[78] Ji, J. C., and N. Zhang. 2010, "Suppression of the primary resonance vibrations of a forced nonlinear system using a dynamic vibration absorber." Journal of Sound and Vibration 329, no. 11: 2044-2056. **2010**

[79] Niu, Jiangchuan, Lin Wang, Yongjun Shen, and Wanjie Zhang.2022 "Vibration control of primary and subharmonic simultaneous resonance of nonlinear system with fractional-order Bingham model." International Journal of Non-Linear Mechanics 141: 103947.**2022**

[80] Wang, Xiaodong, Yushu Chen, Gang Han, and Caiqin Song. 2015, "Nonlinear dynamic analysis of a single-machine infinite-bus power system." Applied Mathematical Modelling 39, no. 10-11: 2951-2961. **2015**

[81] El-Abiad, Ahmed H., and K. Nagappan. 1996, "Transient stability regions of multimachine power systems." IEEE Transactions on Power Apparatus and Systems 2: 169-179.**1996**

[82] Sauer, P. W., and M. A. Pai. 1990, "Power system steady-state stability and the load-flow Jacobian." IEEE Transactions on power systems 5, no. 4: 1374-1383. **1990**

[83] Emam, Samir A., and Ali H. Nayfeh. 2004, "On the nonlinear dynamics of a buckled beam subjected to a primary-resonance excitation." Nonlinear Dynamics 35: 1-17. **2004**

[84] Arafat, H. N., and A. H. Nayfeh. 2003."Non-linear responses of suspended cables to primary resonance excitations." Journal of Sound and Vibration 266, no. 2: 325-354. **2003**

[85] Zhao, Chongwen, Zhibo Wang, Jin Du, Jiande Wu, Sheng Zong, and Xiangning He. 2014. "Active resonance wireless power transfer system using phase shift control strategy." In 2014 IEEE Applied Power Electronics Conference and Exposition-APEC, pp. 1336-1341. IEEE. **2014**

[86] Kavasseri, Rajesh G.2006, "Analysis of subharmonic oscillations in a ferroresonant circuit." International Journal of Electrical Power and Energy Systems 28, no. 3: 207-214. **2006**

[87] KISHIMA, Akira. 1968 "Sub-harmonic Oscillations in Three-phase Circuit." Memoirs of the Faculty of Engineering, Kyoto University 30, no. 1: 26-44. **1968**

[88] Deane, Jonathan HB, and David C. Hamill. "Instability, subharmonics and chaos in power electronic systems." In 20th Annual IEEE Power Electronics Specialists Conference, pp. 34-42. IEEE. **1989**

[89] Nayfeh, M. A., A. M. A. Hamdan, and A. H. Nayfeh. 1990, "Chaos and instability in a power system—Primary resonant case." Nonlinear Dynamics 1: 313-339. **1990**

[90] Wang, Dong, Junbo Zhang, Wei Cao, Jian Li, and Yu Zheng. 2018, "When will you arrive? estimating travel time based on deep neural networks." In Proceedings of the AAAI Conference on Artificial Intelligence, vol. 32, no. 1. **2018**

[91] Zhang, Wei, Fengxia Wang, and Minghui Yao. 2005 "Global bifurcations and chaotic dynamics in nonlinear nonplanar oscillations of a parametrically excited cantilever beam." Nonlinear Dynamics 40: 251-279. **2005**

[92] Zulli, D. and Luongo, A., 2016. Control of primary and subharmonic resonances of a Duffing oscillator via non-linear energy sink. International Journal of Non-Linear Mechanics, 80, pp.170-182. **2016**

[93] Permoon, M.R., Haddadpour, H. and Javadi, M., 2018. Nonlinear vibration of fractional viscoelastic plate: primary, subharmonic, and superharmonic response. International Journal of Non-Linear Mechanics, 99, pp.154-164. **2018**

[94] Kuznetsov, Y.A., Kuznetsov, I.A. and Kuznetsov, Y., 1998. Elements of applied bifurcation theory (Vol. 112, pp. xx+-591). New York: Springer. **1998**

[95] Alsaleem, F.M., Younis, M.I. and Ouakad, H.M., 2009. On the nonlinear resonances and dynamic pull-in of electrostatically actuated resonators. Journal of Micromechanics and Microengineering, 19(4), p.045013. **2009**

[96] Haberman, R. and Ho, E.K., 1995. Boundary of the basin of attraction for weakly damped primary resonance. **1995**

[97] Van Cutsem, T. and Vournas, C.D., 2007, June. Emergency voltage stability controls: An overview. In 2007 IEEE Power Engineering Society General Meeting (pp. 1-10). IEEE. **2007**

[98] Yılmaz, Serpil, and Ferit Acar Savacı. 2017, "Basin stability of single machine infinite bus power systems with Levy type load fluctuations." In 2017 10th International Conference on Electrical and Electronics Engineering (ELECO), pp. 125-129. IEEE.**2017**

[99] Parashar, Manu, James S. Thorp, and Charles E. Seyler. 2004, "Continuum modeling of electromechanical dynamics in large-scale power systems." IEEE Transactions on Circuits and Systems I: Regular Papers 51, no. 9: 1848-1858.**2004**

[100] Soliman, M.S., 1995. Fractal erosion of basins of attraction in coupled non-linear systems. Journal of sound and vibration, 182(5), pp.729-740. **1995**

[101] Nayfeh, M.A., Hamdan, A.M.A. and Nayfeh, A.H., 1991. Chaos and instability in a power system: subharmonic-resonant case. Nonlinear Dynamics, 2, pp.53-72. **1991**

[102] Pecora, Louis M., Thomas L. Carroll, Gregg A. Johnson, Douglas J. Mar, and James F. Heagy. 1997, "Fundamentals of synchronization in chaotic systems,

concepts, and applications." Chaos: An Interdisciplinary Journal of Nonlinear Science 7, no. 4: 520-543. **1997**

[103] Dixit, Shiva, and Manish Dev Shrimali. 2020, "Static and dynamic attractive–repulsive interactions in two coupled nonlinear oscillators." Chaos: An Interdisciplinary Journal of Nonlinear Science 30, no. 3. **2020**

[104] Al-Qaisia, A. A., and M. N. Hamdan. 2007, "Subharmonic resonance and transition to chaos of nonlinear oscillators with a combined softening and hardening nonlinearities." Journal of sound and vibration 305, no. 4-5: 772-782. **2007**

[105] Butikov, Eugene I. "Subharmonic resonances of the parametrically driven pendulum." Journal of Physics A: Mathematical and General 35, no. 30: 6209. **2002**

[106] Xize, N. and Jiajun, Q., 2002. Investigation of torsional instability, bifurcation, and chaos of a generator set. IEEE Transactions on Energy Conversion, 17(2), pp.164-168. **2002**

[107] Sourani, P., Hashemian, M., Pirmoradian, M. and Toghraie, D., 2020. A comparison of the Bolotin and incremental harmonic balance methods in the dynamic stability analysis of an Euler–Bernoulli nanobeam based on the nonlocal strain gradient theory and surface effects. Mechanics of Materials, 145, p.103403. **2020**

[108] Liu, C.W. and Thorp, J.S., 1997. A novel method to compute the closest unstable equilibrium point for transient stability region estimate in power systems. IEEE Transactions on Circuits and Systems I: Fundamental Theory and Applications, 44(7), pp.630-635. **1997**

[109] Glazier, James A., and Albert Libchaber. 1988, "Quasi-periodicity and dynamical systems: An experimentalist's view." IEEE Transactions on circuits and systems 35, no. 7: 790-809 **1988**

[110] G. Gentile, 2005, "Quasi-periodic motions in dynamical systems. Review of a renormalisation group approach", Reviews in Mathematical Physics, Vol. 17, No. 02, pp. 157-216.**2005**

[111] A. Katok and B. Hasselblatt, 1995,Introduction to the Modern Theory of Dynamical Systems, Cambridge University Press. **1995**

[112] Pogalin, Erik, Arnold WM Smeulders, and Andrew HC Thean.2008, "Visual quasi-periodicity." In 2008 IEEE Conference on Computer Vision and Pattern Recognition, pp. 1-8. IEEE. **2008**

[113] Broer, Hendrik W., George B. Huitema, and Mikhail B. Sevryuk. 1996, Quasi-periodic motions in families of dynamical systems: order amidst chaos. Vol. 1645. Springer Science and Business Media. **1996**

[114] Wyld, H.W. and Powell, G., 2020. Mathematical methods for physics. CRC Press. **2020**

[115] Sofroniou A., Premnath B., 2023, "An Investigation into the Primary and Subharmonic Resonances of the Swing Equation," WSEAS Transactions on Systems and Control, vol. 18, pp. 218-230, DOI:10.37394/23203.2023.18.22 **2023**

[116] Hitzl, D. L. 1975, "The swinging spring-invariant curves formed by quasi-periodic solutions. III." Astronomy and Astrophysics, vol. 41, no. 2, June 1975, p. 187-198. 41: 187-198. **1975**

[117] Chen, X., and Xu, X. 2017. Quasi-periodic solutions of discrete dynamical systems with mixed-type functional equations. Nonlinear Analysis: Theory, Methods and Applications, 163, 322-343. **2017**

[118] Han, Y., and Zhang, Y. 2019. Quasi-periodic solutions of a fractional differential equation. Journal of Differential Equations, 267(1), 366-395. **2019**

[119] Kuwamura, N., Shimomura, K., and Ueda, T. 2012. Quasi-periodic motion with two incommensurate frequencies in a non-autonomous differential equation. Nonlinear Dynamics, 67(1), 807-822. **2012**

[120] Li, Y., and Zhang, Y. 2018. Quasi-periodic solutions for a non-autonomous fractional differential equation with a nonlinear term. Chaos, Solitons and Fractals, 108, 229-243. **2018**

[121] Liu, Z., and Zhang, T. 2016. Quasi-periodic solutions of a class of non-autonomous differential equations with impulsive effects. Journal of Mathematical Analysis and Applications, 435(2), 696-716. **2016**

[122] Nayfeh, A. H. 1972. Quasi-periodic motions in a forced pendulum. International Journal of Non-Linear Mechanics, 7(3), 495-509 **1972**

[123] Nayfeh, A. H. 1977. The effect of damping on quasi-periodic motions in a forced pendulum. International Journal of Non-Linear Mechanics, 12(1), 44-54. **1977**

[124] Yue, Yuan, Pengcheng Miao, Jianhua Xie, and Grebogi Celso. 2016, "Symmetry restoring bifurcations and quasiperiodic chaos induced by a new intermittency in a vibro-impact system." Chaos: An Interdisciplinary Journal of Nonlinear Science 26, no. 11. **2016**

[125] Zambrano, Samuel, Inés P. Mariño, Francesco Salvadori, Riccardo Meucci, Miguel AF Sanjuán, and F. T. Arecchi. 2006, "Phase control of intermittency in dynamical systems." Physical Review E 74, no. 1: 016202. **2006**

[126] Mishra, Arindam, S. Leo Kingston, Chittaranjan Hens, Tomasz Kapitaniak, Ulrike Feudel, and Syamal K. Dana. 2020, "Routes to extreme events in dynamical systems: Dynamical and statistical characteristics." Chaos: An Interdisciplinary Journal of Nonlinear Science 30, no. 6. **2020**

[127] Pomeau, Yves, and Paul Manneville. 1980, "Intermittent transition to turbulence in dissipative dynamical systems." Communications in Mathematical Physics 74: 189-197. **1980**

[128] Keller, Gerhard, and Christoph Richard. 2018, "Dynamics on the graph of the torus parametrization." Ergodic Theory and Dynamical Systems 38, no. 3: 1048-1085. **2018**

[129] Skorokhod, Anatoli V., Frank C. Hoppensteadt, Habib Salehi, Anatoli V. Skorokhod, Frank C. Hoppensteadt, and Habib Salehi. 2002, "Dynamical Systems on a Torus." Random Perturbation Methods with Applications in Science and Engineering: 303-342. **2002**

[130] Baldovin, Marco, Angelo Vulpiani, and Giacomo Gradenigo. 2021, "Statistical mechanics of an integrable system." Journal of Statistical Physics 183, no. 3: 41. **2021**

[131] Chang, Shun-Chang. 2020, "Stability, chaos detection, and quenching chaos in the swing equation system." Mathematical Problems in Engineering 2020: 1-12. **2020**

[132] Kopell, Nancy, and R. Washburn. "Chaotic motions in the two-degree-of-freedom swing equations." IEEE Transactions on Circuits and Systems 29, no. 11: 738-746. **1982**

[133] Vittal, Vijay, James D. McCalley, Paul M. Anderson, and A. A. Fouad. Power system control and stability. John Wiley and Sons. **2019**

[134] Sofroniou A., Premnath B., 2023, "Addressing the Primary and Subharmonic Resonances of the Swing Equation," WSEAS Transactions on Applied and Theoretical Mechanics, vol. 18, pp. 199-215, DOI:10.37394/232011.2023.18.19 **2023**

[135] Rahgozar, Peyman 2020. "Free vibration of tall buildings using energy method and Hamilton's principle." Civil Engineering Journal 6, no. 5: 945-953. **2020**

[136] Náprstek, J., and C. Fischer. 2013, "Types and stability of quasi-periodic response of a spherical pendulum." Computers and Structures 124: 74-87. **2013**

[137] Kalpakides, Vassilios K., and Antonios Charalambopoulos.2021, "On hamilton's principle for discrete and continuous systems: A convolved action principle." Reports on Mathematical Physics 87, no. 2 : 225-248. **2021**

[138] Duan, Yupeng, Jinglai Wu, and Yunqing Zhang. 2024, "Quasi-Lagrangian equations and its energy-conservative numerical integration for nonlinear dynamic systems." Acta Mechanica Sinica 40, no. 1: 1-16. **2024**

[139] Daza, Alvar, Alexandre Wagemakers, and Miguel AF Sanjuán. 2022, "Classifying basins of attraction using the basin entropy." Chaos, Solitons and Fractals 159 : 112112. **2022**

[140] Zhao, Jinquan, Yaoliang Zhu, and Jianjun Tang. 2020, "Transient voltage and transient frequency stability emergency coordinated control strategy for the multi-infeed HVDC power grid." In 2020 IEEE Power and Energy Society General Meeting (PESGM), pp. 1-5. IEEE. **2020**

[141] Najar, F., Nayfeh, A.H., Abdel-Rahman, E.M., Choura, S. and El-Borgi, S., 2010. Dynamics and global stability of beam-based electrostatic microactuators. Journal of Vibration and Control, 16(5), pp.721-748. **2010**

[142] BASAK, Rasim. 2022, "Golden ratio and Fibonacci sequence: universal footprints of the golden flow." Turkish Online Journal of Design Art and Communication 12, no. 4: 1092-1107. **2022**

[143] Balcerzak, Marek, Artur Dabrowski, Barbara Blazejczyk–Okolewska, and Andrzej Stefanski. 2020, "Determining Lyapunov exponents of non-smooth systems: Perturbation vectors approach." Mechanical Systems and Signal Processing 141: 106734. **2020**

[144] Tsoutsanis, Elias, Nader Meskin, Mohieddine Benammar, and Khashayar Khorasani. 2013, "Dynamic performance simulation of an aeroderivative gas turbine using the matlab simulink environment." In ASME International Mechanical Engineering Congress and Exposition, vol. 56246, p. V04AT04A050. American Society of Mechanical Engineers. **2013**

[145] Sybille, G., and Le-Huy, H. (2000, January). Digital simulation of power systems and power electronics using the MATLAB/Simulink Power System Blockset. In 2000 IEEE Power Engineering Society Winter Meeting. Conference Proceedings (Cat. No. 00CH37077) (Vol. 4, pp. 2973-2981). IEEE. **2000**

[146] Lin, S., Yao, W., Xiong, Y., Zhao, Y., Shi, Z., Ai, X., and Wen, J. (2023). MatPSST: A Matlab/Simulink-based power system simulation toolbox for research and education. IET Generation, Transmission and Distribution, 17(10), 2272-2288. **2023**

[147] Bozin, A. S. (1998). Electrical power systems modeling and simulation using SIMULINK. **1998**

[148] Tessarolo, Alberto.2011, Modeling and simulation of multiphase machines in the Matlab/Simulink environment. IntechOpen. **2011**

[149] Airoboman, A. E., Okakwu, I. K., Alayande, A. S., and Seun, O. E. (2015). On the assessment of power system stability using Matlab/Simulink model. International Journal of Energy and Power Engineering, 4(2), 51-64. **2015**

[150] Gharaibeh, Khaled M. 2011, Nonlinear distortion in wireless systems: Modeling and simulation with MATLAB. John Wiley and Sons.

[151] Prabhakar, G., P. Nedumal Pugazhenthi, and S. Selvaperumal. 2014, "Implementation analysis of state space modelling and control of nonlinear process using PID algorithm in MATLAB and PROTEUS environment." Applied Mechanics and Materials 573: 297-303. **2014**

[152] Schwartz, Carla, and Richard Gran. 2001, "Describing function analysis using MATLAB and Simulink." IEEE Control Systems Magazine 21, no. 4: 19-26. **2001**

[153] Ondera, Martin, and Mikuláš Huba. 2009, "Simulation of nonlinear control systems represented as generalized transfer functions." In 2009 European Control Conference (ECC), pp. 1444-1449. IEEE. **2009**

[154] Raj, M. (2014) "Modelling and Simulation Lab", BHARTIYA INSTITUTE OF ENGINEERING and TECHNOLOGY, SIKAR, Lab File. (Available online: https://www.bietsikar.ac.in/documents/2923432409MODELLING%20AND%20SIMULATION%20LAB.pdf) **2014**

[155] Monshizadeh P, De Persis C, Monshizadeh N, van der Schaft AJ 2016. Nonlinear analysis of an improved swing equation. In IEEE 55th Conference on Decision and Control (CDC) (pp. 4116-4121) 2016 Dec 12. IEEE. **2016**

[156] Zhou J, Ohsawa Y. 2008 Improved swing equation and its properties in synchronous generators. IEEE Transactions on Circuits and Systems I: Regular Papers. 2008 May 7;56(1):200-9. **2008**

[157] Toirov O, Bekishev , Urakov S, Mirkhonov U. 2020 Development of differential equations and their solution using the simulink matlab program, which calculate the self-swinging of synchronous machines with traditional and longitudinal-transverse excitation. In E3S Web of Conferences(Vol. 216, p. 01116). EDP Sciences. **2020**

[158] Pirmatov N, Bekishev A, Egamov A, 2023, Shernazarov S, Isakov F, Zubaydullayev M. Mathematical modeling of the self-swinging process of synchronous generators. In AIP Conference Proceedings 15 (Vol. 2612, No. 1) March. AIP Publishing. **2023**

[159] Anastasia Sofroniou, Bhairavi Premnath, 2023, "A Comprehensive Analysis into the Effects of Quasiperiodicity on the Swing Equation," WSEAS Transactions on Applied and Theoretical Mechanics, vol. 18, pp. 299-309, DOI:10.37394/232011.2023.18.28

[160] SIMULINK toolbox, 2023. doi: 10.1016/b978-0-32-399548-1.00023-0 **2023**

[161] Poznyak EV, Radin VP, Novikova OV, Chirkov VP, Babin OA, Kuznetsov SF., 2022, Dynamic Analysis of Systems with a Nonlinear Elastomeric Isolator in Simulink. In 2022 VI International Conference on Information Technologies in Engineering Education (Inforino) Apr 12 (pp. 1-5). IEEE. **2022**

[162] Grigoriev DA, Antipov VA., 2023, Features of mathematical models of deformation of multifunctional vibration isolators with elastic-hysteresis elements made of fiber wire material. In AIP Conference Proceedings Dec 26 (Vol. 2624, No. 1). AIP Publishing. **2023**

[163] Huang Y, Yang W, Zhao Z, Yang J, Li Y, Ma W, Yang J., 2021, Nonlinear simulation of speed variation of variable-speed unit under large disturbance by Simulink. In IOP Conference Series: Earth and Environmental Science, June (Vol. 774, No. 1, p. 012140). IOP Publishing. **2021**

[164] Long-Xiang F, Shao-Bo H, Hui-Hai W, Ke-Hui S., 2022, Simulink modeling and dynamic characteristics of discrete memristor chaotic system. Acta Physica Sinica. Feb 5;71(3). **2022**

[165] Villarreal ML, Minchala LI. Approximate modeling of dynamical systems applying HAVOK: A systematic review. In 2023 IEEE Colombian Caribbean Conference (C3) November (pp. 1-6). IEEE. **2023**

[166] Domínguez E, Ardila F, Bustamante S, 2010, System Solver: an open source tool for mathematically modelling dynamical systems. Ingeniería e Investigación. Dec;30(3):157-64. **2010**

[167] Tank K, Garg MM, Narasimharaju BL., 2022, MATLAB-based Simplified Mathematical Modelling of Non-ideal Differential Mode Inverters. In2022 IEEE 19th India Council International Conference (INDICON), November (pp. 1-6). IEEE. **2022**

[168] Iyer NP., 2006, Matlab/Simulink modules for modeling and simulation of power electronic converters and electric drives (Doctoral dissertation). **2006**

[169] Bao H, Gu Y, Xu Q, Zhang X, Bao B., 2022 Parallel bi-memristor hyperchaotic map with extreme multistability. Chaos, Solitons and Fractals. Jul ;160:112273. **2022**

[170] He S, Zhan D, Wang H, Sun K, Peng Y., 2022, Discrete memristor and discrete memristive systems. Entropy. June ;24(6):786. **2022**

[171] Phan TT., 2019 MODELLING AND SIMULATION OF THE AUTOMOBILE DYNAMICS MOVEMENT USING MATLAB SIMULINK SOFTWARE. Scientific Journal of Tra Vinh University. June ;1(1):94-103. **2019**

[172] Haar S, Paulevé L, Schwoon S., 2020 Drawing the line: basin boundaries in safe Petri nets. In Computational Methods in Systems Biology: 18th International Conference, CMSB, Konstanz, Germany, September 23–25, Proceedings 18 2020 (pp. 321-336). Springer International Publishing. **2020**

[173] Karmi G, Kravetc P, Gendelman O. Analytic exploration of safe basins in a benchmark problem of forced escape. Nonlinear Dynamics. November;106:1573-89. **2021**

[174] Genda A, Fidlin A, Gendelman O., 2023 The level-crossing problem of a weakly damped particle in quadratic potential well under harmonic excitation. Nonlinear Dynamics. November;111(22):20563-78. **2023**

[175] Kravetc P, Gendelman O, Fidlin A., 2023 Resonant escape induced by a finite time harmonic excitation. Chaos: An Interdisciplinary Journal of Nonlinear Science. June ;33(6). **2023**

[176] Genda A, Fidlin A, Gendelman O., 2023 Dynamics of forced escape from asymmetric truncated parabolic well. ZAMM-Journal of Applied Mathematics and Mechanics/Zeitschrift für Angewandte Mathematik und Mechanik. September;103(9):e202200567. **2023**

[177] Engel A, Gendelman OV, Fidlin A., 2024 Escape of a particle from two-dimensional potential well. Nonlinear Dynamics. February;112(3):1601-18 **2024**

[178] Ren Z, Yang J, Xie J, Chen P, Liu X., 2023, Bifurcation and stability analysis of fractional quintic oscillator system with power damping term. International Journal of Non-Linear Mechanics. January ;148:104260. **2023**

[179] Xu H, Ren C, He D, Zhou B, Wang Q, Gao H, Wang T., 2024, Coupling vibration characteristics and vibration suppression of rolling mill rolls with dynamic vibration absorber. Journal of Manufacturing Processes. June ;120:1157-79. **2024**

[180] Shen Y, Li H, Yang S, Peng M, Han Y., 2020, Primary and subharmonic simultaneous resonance of fractional-order Duffing oscillator. Nonlinear Dynamics. November ;102:1485-97. **2020**

[181] Niu J, Zhang W, Wen S, Zhang J., 2022, Subharmonic resonance of Duffing oscillator with dry friction under foundation excitation. Journal of Computational and Nonlinear Dynamics. October;17(10):101006. **2022**

[182] Zhornyak, L., Hsieh, M.A. and Forgoston, E., 2024. Inferring bifurcation diagrams with transformers. Chaos: An Interdisciplinary Journal of Nonlinear Science, 34(5). **2024**

[183] Ryabov, P.E., 2018. Bifurcation diagram of one perturbed vortex dynamics problem. arXiv preprint arXiv:1811.10512. **2018**

[184] Karimov, T.I., Druzhina, O.S., Andreev, V.S., Tutueva, A.V. and Kopets, E.E., 2021, January. Bifurcation spectral diagrams: a tool for nonlinear dynamics investigation. In 2021 IEEE Conference of Russian Young Researchers in Electrical and Electronic Engineering (ElConRus) (pp. 119-123). IEEE. **2021**

[185] Fedoseev, D.A., 2015. Bifurcation diagrams of natural Hamiltonian systems on Bertrand manifolds. Moscow University Mathematics Bulletin, 70(1), pp.44-47. **2015**

[186] Piccirillo, V., do Prado, T.G., Marcelo Tusset, A. and Manoel Balthazar, J., 2020. Dynamic integrity analysis on a non-ideal oscillator. Mathematics in Engineering, Science and Aerospace (MESA), 11(3). **2020**

[187] Thompson, J.M.T., 2019. Dynamical integrity: three decades of progress from macro to nanomechanics. Global nonlinear dynamics for engineering design and system safety, pp.1-26. **2019**

[188] Rega, G., Lenci, S. and Ruzziconi, L., 2019. Dynamical integrity: A novel paradigm for evaluating load carrying capacity. Global nonlinear dynamics for engineering design and system safety, pp.27-112. **2019**

[189] Hedrih, K.S., 2005. The integrity of dynamical systems. Nonlinear Analysis: Theory, Methods and Applications, 63(5-7), pp.854-871. **2005**

[190] Jinli, C., Yali, X. and Xingang, L., 2014. Nonlinear Robust Control Approach Based on Integrity. TELKOMNIKA Indonesian Journal of Electrical Engineering, 12(5), pp.3366-3380.**2014**

[191] Joan Jani, 2023, "Simulation of Chaotic Operation f A Damped Driven Pendulum Using Python," WSEAS Transactions on Advances in Engineering Education, vol. 20, pp. 1-6, DOI:10.37394/232010.2023.20.1 **2023**

[192] Kartik Chandra Patra, Asutosh Patnaik, 2023, "Possibility of Quenching of Limit Cycles in Multi Variable Nonlinear Systems with Special Attention to 3X3

Systems," WSEAS Transactions on Systems and Control, vol. 18, pp. 677-695, DOI:10.37394/23203.2023.18.69. **2023**

[193] Xianwei, Chen., Xiangling, Fu., Jintao, Tan., 2020. Chaos Suppression in a Pendulum Equation through Parametric Excitation with Phase Shift for Ultra-Subharmonic Resonance. Current Journal of Applied Science and Technology, doi: 10.9734/CJAST/2020/V39I3531048 **2020**

[194] Frisch, Uriel, and Rudolf Morf, 1981 Intermittency in nonlinear dynamics and singularities at complex times. Physical review A 23, no. 5, 2673. **1981**

[195] Nguyen, Emma, Pierre Olivier, Marie-Cécile Pera, Elodie Pahon, and Robin Roche, 2024, Impacts of intermittency on low-temperature electrolysis technologies: A comprehensive review. International Journal of Hydrogen Energy 70, 474-492. **2024**

[196] Guan, Yu, Vikrant Gupta, and Larry KB Li, 2020, Intermittency route to self-excited chaotic thermoacoustic oscillations. Journal of Fluid Mechanics 894, R3. **2020**

[197] Del Rio, Ezequiel, and Sergio Elaskar, 2021, Type III intermittency without characteristic relation. Chaos: An Interdisciplinary Journal of Nonlinear Science 31, no. 4. **2021**

[198] Lozano-Durán, Adrián, and Gonzalo Arranz, 2022, Information-theoretic formulation of dynamical systems: causality, modeling, and control. Physical Review Research 4, no. 2, 023195. **2022**

[199] Ma, Zhuang, Gaofeng Wang, Tao Cui, and Yao Zheng, 2022, Interpretation of intermittent combustion oscillations by a new linearization procedure. Journal of Propulsion and Power 38, no. 2, 190-199. **2022**

[200] Huang, Hao, and Fangxing Li, 2012, Sensitivity analysis of load-damping characteristic in power system frequency regulation. IEEE transactions on power systems 28, no. 2, 1324-1335. **2012**

[201] Di Bernardo, Mario, Chris J. Budd, Alan R. Champneys, Piotr Kowalczyk, Arne B. Nordmark, Gerard Olivar Tost, and Petri T. Piiroinen. 2008, Bifurcations in nonsmooth dynamical systems. SIAM review 50, no. 4, 629-701. **2008**

[202] Liang, Xinyu, Hua Chai, and Jayashri Ravishankar, 2022, Analytical methods of voltage stability in renewable dominated power systems: a review. Electricity 3, no. 1, 75-107. **2022**

[203] Cheng, Yi, Rasoul Azizipanah-Abarghooee, Sadegh Azizi, Lei Ding, and Vladimir Terzija, 2020, Smart frequency control in low inertia energy systems based on frequency response techniques: A review.Applied Energy 279, 115798. **2020**

[204] Hartmann, Bálint, István Vokony, and István Táczi, 2019, Effects of decreasing synchronous inertia on power system dynamics—Overview of recent experiences and marketisation of services. International Transactions on Electrical Energy Systems 29, no. 12, e12128. **2019**

[205] Sofroniou, Anastasia, and Bhairavi Premnath, 2024, Analysing the Swing Equation using MATLAB Simulink for Primary Resonance, Subharmonic Resonance and for the case of Quasiperiodicity. WSEAS Transactions on Circuits and Systems 23, 202-211. **2024**

[206] Ma, Rui, Jinxin Li, Jürgen Kurths, Shijie Cheng, and Meng Zhan, 2021, Generalized swing equation and transient synchronous stability with PLL-based VSC. IEEE Transactions on Energy Conversion 37, no. 2, 1428-1441.**2021**

[207] Wolf, Alan, Jack B. Swift, Harry L. Swinney, and John A. Vastano, 1985, Determining Lyapunov exponents from a time series. Physica D: nonlinear phenomena 16, no. 3, 285-317. **1985**

[208] Laugesen, Jakob L., and Erik Mosekilde., 2011, Emergence of oscillatory dynamics. In Biosimulation in Biomedical Research, Health Care and Drug Development, pp. 69-95. Vienna: Springer Vienna. **2011**

[209] Zhusubaliyev, Zhanybai T., and Erik Mosekilde, 2003 Bifurcations and chaos in piecewise-smooth dynamical systems: applications to power converters, relay and

pulse-width modulated control systems, and human decision-making behavior. Vol. 44. World Scientific. **2003**

[210] Suresha, Suhas, R. I. Sujith, Benjamin Emerson, and Tim Lieuwen, 2016, Nonlinear dynamics and intermittency in a turbulent reacting wake with density ratio as bifurcation parameter. Physical Review E 94, no. 4, 042206. **2016**

[211] Chinni, Karthik, Pablo M. Poggi, and Ivan H. Deutsch, 2021, Effect of chaos on the simulation of quantum critical phenomena in analog quantum simulators. Physical Review Research 3, no. 3, 033145.**2021**

[212] Liu, Zeyi, Jianshe Gao, Xiaobo Rao, Shunliang Ding, and Deping Liu, 2024, Complex dynamics of the passive biped robot with flat feet: Gait bifurcation, intermittency and crisis. Mechanism and Machine Theory 191, 105500. **2024**

[213] Kundur, P., 2007. Power system stability. Power system stability and control, 10(1), pp.7-1. **2007**

[214] Oh, H., 2023. Analytic solution to swing equations in power grids with ZIP load models. Plos one, 18(6), p.e0286600. **2023**

[215] Laghari, J.A., Mokhlis, H., Bakar, A.H.A. and Mohamad, H., 2013. Application of computational intelligence techniques for load shedding in power systems: A review. Energy conversion and management, 75, pp.130-140. **2013**

[216] Rudez, U. and Mihalic, R., 2015. WAMS-based underfrequency load shedding with short-term frequency prediction. IEEE Transactions on Power Delivery, 31(4), pp.1912-1920. **2015**

[217] Ketabi, A. and Fini, M.H., 2014. An underfrequency load shedding scheme for hybrid and multiarea power systems. IEEE Transactions on Smart Grid, 6(1), pp.82-91. **2014**

[218] Tofis, Y., Timotheou, S. and Kyriakides, E., 2016. Minimal load shedding using the swing equation. IEEE Transactions on Power Systems, 32(3), pp.2466-2467. **2016**

[219] Mortaji, H., Ow, S.H., Moghavvemi, M. and Almurib, H.A.F., 2017. Load shedding and smart-direct load control using internet of things in smart grid demand response management. IEEE Transactions on Industry Applications, 53(6), pp.5155-5163. **2017**

[220] Mammoli, A., Robinson, M., Ayon, V., Martínez-Ramón, M., Chen, C.F. and Abreu, J.M., 2019. A behavior-centered framework for real-time control and load-shedding using aggregated residential energy resources in distribution microgrids. Energy and Buildings, 198, pp.275-290. **2019**

[221] Talwariya, A., Singh, P. and Kolhe, M.L., 2021. Stackelberg game theory based energy management systems in the presence of renewable energy sources. IETE Journal of Research, 67(5), pp.611-619. **2021**

[222] Dedović, M.M., Avdaković, S., Musić, M. and Kuzle, I., 2024. Enhancing power system stability with adaptive under frequency load shedding using synchrophasor measurements and empirical mode decomposition. International journal of electrical power energy systems, 160, p.110133. **2024**

[223] Paganini, F. and Mallada, E., 2019. Global analysis of synchronization performance for power systems: Bridging the theory-practice gap. IEEE Transactions on Automatic Control, 65(7), pp.3007-3022. **2019**

[224] Shariati, O., Zin, A.M., Khairuddin, A., Pesaran, M.H.A. and Aghamohammadi, M.R., 2012, March. An integrated method for under frequency load shedding based on hybrid intelligent system-part II: UFLS design. In 2012 Asia-Pacific Power and Energy Engineering Conference (pp. 1-9). IEEE. **2012**

[225] Jereminov, M., Pandey, A., Song, H.A., Hooi, B., Faloutsos, C. and Pileggi, L., 2017, September. Linear load model for robust power system analysis. In 2017 IEEE PES Innovative Smart Grid Technologies Conference Europe (ISGT-Europe) (pp. 1-6). IEEE. **2017**

[226] Lu, M., ZainalAbidin, W.A.W., Masri, T., Lee, D.H.A. and Chen, S., 2016. Under-frequency load shedding (UFLS) schemes–A survey. International Journal of Applied Engineering Research, 11(1), pp.456-472. **2016**

[227] Larik, R.M., Mustafa, M.W. and Aman, M.N., 2019. A critical review of the state-of-art schemes for under voltage load shedding. International Transactions on Electrical Energy Systems, 29(5), p.e2828. **2019**

[228] Sofroniou A., Premnath B., 2025. Examining the Intermittency in the Swing Equation. WSEAS Transactions on Mathematics. 2025;24:209-219. 10.37394/23206.2025.24.21 **2025**

[229] Premnath, Bhairavi, and Anastasia Sofroniou. 2025. "Analysing Load Shedding to Increase Stability in the Swing Equation" Mathematics 13, no. 8: 1314. https://doi.org/10.3390/math13081314 **2025**

Appendix A

A.1 Parameters of Machine Used in Chapter 3

The parameters of the machine taken are similar to that from Table D3 of Appendix D of the textbook by Anderson and Fouad (1977). They are as follows:

- Rated MVA: 160
- Rated power factor: 0.805
- Rated voltage: 15.2 kV
- Frequency: 60 Hz
- Transient reactance, X': 0.244 per unit
- Inertia constant, H: 2.36 s

The remaining parameters of the SMQIBS (Single Machine Quasi-Infinite Bus System) are:

- Line reactance, X_{line}: 0.4 per unit
- Bus voltage modulation amplitude, V_{B1}: 0.1 per unit
- Bus angle modulation amplitude, θ_{B1}: 0.1 rad
- Bus voltage magnitude, V_{B0}: 1 per unit
- Bus angle, θ_{B0}: 0.1 rad
- Total reactance, $X_G = X_{\text{line}} + X'$: 0.645 per unit
- Damping coefficient, D: varied between 0.002 and 0.016

A.2 Parameters of Machine Used in Chapter 4

The parameters of the machine taken are similar to that from Table D3 of Appendix D of the textbook by Anderson and Fouad (1977). They are as follows:

- Rated MVA: 160
- Rated power factor: 0.805
- Rated voltage: 15.2 kV
- Frequency: 60 Hz
- Transient reactance, X': 0.244 per unit
- Inertia constant, H: 2.36 s

The remaining parameters of the SMQIBS (Single Machine Quasi-Infinite Bus System) are:

- Line reactance, X_{line}: 0.4 per unit
- Bus voltage modulation amplitude, V_{B1}: 0.2 per unit
- Bus angle modulation amplitude, θ_{B1}: 0.2 rad
- Bus voltage magnitude, V_{B0}: 1 per unit
- Bus angle, θ_{B0}: 0.2 rad
- Total reactance, $X_G = X_{\text{line}} + X'$: 0.645 per unit
- Damping coefficient, D: 0.004

A.3 Codes

Code for Phase portraits, frequency-domain plots and Poincaré maps

```
clc;
clear all;
```

```
N=1000;
T=linspace(0,30,N);
H=T(2)-T(1);
F=@(X2)X2;
G=@(X1,X2,T)-0.05*X1 +0.9 - 2.1*(1 + 0.1*cos(8.27*T)*sin(X1 - (1+0.1*cos(8.27*T))));
X1=zeros(1,N);
X2=zeros(1,N);
X1(1)=0;
X2(1)=1;
for i=1:N-1
K1=F(X2(i));
L1=G(X1(i),X2(i),T(i));
K2=F(X2(i)+((H/2)*L1));
L2=G(X1(i)+((H/2)*K1),X2(i)+((H/2)*L1),T(i));
K3=F(X2(i)+((H/2)*L2));
L3=G(X1(i)+((H/2)*K2),X2(i)+((H/2)*L2),T(i));
K4=F(X2(i)+((H)*L3));
L4=G(X1(i)+((H)*K3),X2(i)+((H)*L3),T(i));
X1(i+1)=X1(i)+(H/6)*(K1+2*K2+2*K3+K4);
X2(i+1)=X2(i)+(H/6)*(L1+2*L2+2*L3+L4);
end
figure(1)
plot(T,X1)
hold on
plot(T,X2,'r');
legend('x_1(t)',' x_2(t)');
xlabel('Normalized Time');
ylabel('States of the system')
figure(2)
plot(X1,X2,'k')
xlabel('x_1'); ylabel('x_2')
[T,X] = ode45(G,T,X0');
```

n = length(T); RES =5; p = 0.035;

poincare$_x = X((n * p) : RES : n, 1)$;

poincare$_z = X((n * p) : RES : n, 1); figure(5)$;

plot(poincare$_x, poincare_z, ' r*')$;

xlabel('$\theta(t)$');

ylabel('$\dot{\theta(t)}$','interpreter','latex');

axis([1.346 1.35 1.346 1.35]);

title('Poincare map'); grid on

Npre = 200; Nplot = 100;

N=10;

Codes for Bifrucation diagrams and Lyapunov Exponents

x = zeros(Nplot,1);

for T = 0:0.01:1

x(1) = 0.5;

for n = 1:Npre

x(1) = (- 0.05*x(1) + 0.9 - 2.44*sin(x(1) - (1+0.1*cos(8.27*T))));

end

for n = 1:Nplot-1

x(n+1) = x(n)*(- 0.05*x(n) + 0.9 - 2.44*sin(x(n) - (1+0.1*cos(8.27*T))));

end

plot(T*ones(Nplot,1), x, '.', 'markersize', 2);

hold on;

end

title('Bifurcation diagram');

xlabel('r'); ylabel('x$'_n$);

set(gca, 'xlim', [2.5 4.0]);

hold off;

function LE = LEofLogisticMap(rStart, rEnd, rStep) rValues = rStart:rStep:rEnd;

nPoints = length(rValues);

nIterations = 1000;

LE = zeros(1, nPoints);

x = zeros(1, nIterations + 1);

x(1) = 0;
for k = 1:nPoints
sum = 0;
for i = 1:nIterations
x(i + 1) = - 0.03*x(i) + 0.805 - rValues*sin(x(i) - (1+0.1*cos(8.27*7)));
sum = sum + log(abs(rValues(k) - 0.5*rValues(k)*x(i)));
end
LE(k) = sum / nIterations;
end
rStart = 0.2;
rEnd = 2.8;
rStep = 0.005;
LE = LEofLogisticMap(rStart, rEnd, rStep);
figure; plot(rStart:rStep:rEnd, LE, 'k.-'); axis tight;
xlabel('r');
ylabel('Values of estimated Lyapunov exponent');
hold on;
plot(yline(0));
G = @(X1, X2, T) -0.05*X1 + 0.9 - 2.1*(1 + 0.1*cos(8.27*T)*sin(X1 - (1 + 0.1*cos(8.27*T))));
omega = 8.27;
T = 2*pi/omega;
$X1_0 = linspace(-2 * pi, 2 * pi, 1000); X2_0 = zeros(size(X1_0));$
epsilon = 0.01;
$bifurcation_points_Floquet = [];$
$bifurcation_points_tangent = [];$
$bifurcation_points_trained = [];$
for i = 1:length($X1_0$)
$X1_init = X1_0(i);$
$X2_init = X2_0(i);$
[T, X] = ode45(@(t, y) [y(2); G(y(1), y(2), t)], [0 T], $[X1_init; X2_init]$);

[, floquet$_i ndices$] = $max(abs(eig(jacobian(@(t, y)[y(2); G(y(1), y(2), t)], 0, X(end, :$
$)))));$

bifurcation$_p oints_F loquet$ = $[bifurcation_p oints_F loquet; X(end, 1) floquet_i ndices]$;

[T, X] = ode45(@(t, y) [y(2); G(y(1), y(2), t) + epsilon*y(1)], [0 T], [X1$_i nit; X2_i nit$]);

[, tangent$_i ndices$] = $max(abs(eig(jacobian(@(t, y)[y(2); G(y(1), y(2), t) + epsilon *$
$y(1)], 0, X(end, :)))));$

bifurcation$_p oints_t angent$ = $[bifurcation_p oints_t angent; X(end, 1) tangent_i ndices]$;

[T, X] = ode45(@(t, y) [y(2); G(y(1), y(2), t) + epsilon*y(1) + epsilon^2*$y(1)^2$], $[0T], [X1_i nit; X2_i nit]$);

[, strained$_i ndices$] = $max(abs(eig(jacobian(@(t, y)[y(2); G(y(1), y(2), t) + epsilon *$
$y(1) + epsilon^2 * y(1)^2], 0, X(end, :)))));$

bifurcation$_p oints_s trained$ = $[bifurcation_p oints_s trained; X(end, 1) strained_i ndices]; end$

figure;

plot(bifurcation$_p oints_F loquet(:, 1), bifurcation_p oints_F loquet(:, 2), '.', 'DisplayName', 'FloquetMethod$

hold on;

plot(bifurcation$_p oints_t angent(:, 1)$,

bifurcation$_p oints_t angent(:, 2), '.', 'DisplayName', 'TangentInstabilities')$;

plot(bifurcation$_p oints_s trained(:, 1)$,

bifurcation$_p oints_s trained(:, 2), '.', 'DisplayName', 'MethodsofStrainedParameters')$;

xlabel('X1');

ylabel('Bifurcation Indices');

legend;

title('Bifurcation Diagram');

Codes for Basins of Attractions

x$_m in$ = -15;

x$_m ax$ = 10;

num$_p oints$ = 200;

x = linspace(x$_m in, x_m ax, num_p oints)$;

y = linspace(x$_m in, x_m ax, num_p oints)$;

[X, Y] = meshgrid(x, y);

basins = zeros(num$_p oints$);

t$_s pan$ = [010];

for i = 1:num$_p oints$

for j = 1:num$_p oints$
IC = [X(i,j), Y(i,j)];
[t, x] = ode45(@myODE, t$_s pan, IC$);
final$_p oint = x(end, :)$;
data$_p oints(i, j, :) = final_p oint$;
end
end
data$_p oints = reshape(data_p oints, [], 2)$;
num$_c lusters = 5$;
[idx,] = kmeans(data$_p oints, num_c lusters$);
basins = reshape(idx, num$_p oints, num_p oints$);
figure;
pcolor(X, Y, basins);
colormap('jet');
shading interp;
colorbar;
xlabel('Real part of initial condition');
ylabel('Imaginary part of initial condition');
title('Basins of Attraction');
ylim([-15,10])
xlim([-15,10])
function attractor = determine$_a ttractor(final_p oint)$
attractor = abs(final$_p oint(1)) < 1e-3 abs(final_p oint(2)) < 1e-3$;
end

Basins of attractions for load shedding clc; clear; close all;
x$_m in = -15$;
x$_m ax = 10$;
num$_p oints = 200$;
x = linspace(x$_m in, x_m ax, num_p oints$);
y = linspace(x$_m in, x_m ax, num_p oints$);
[X, Y] = meshgrid(x, y);

$\mathrm{P}_L S_v als = [0, 0.05, 0.1, 5];$
titles = 'No Load Shedding', '$\mathrm{P}_{LS} = 0.05'$,' $P_{LS} = 0.1'$,' $P_{LS} = 1.2'$;
figure; for p = 1:length($\mathrm{P}_L S_v als$)
$\mathrm{P}_L S = P_L S_v als(p); basins = zeros(num_p oints);$
$\mathrm{t}_s pan = [010];$
for i = 1:$\mathrm{num}_p oints$
for j = 1:$\mathrm{num}_p oints$
IC = [X(i,j), Y(i,j)];
[t, x] = ode45(@(t, x) myODE(t, x, $\mathrm{P}_L S$), $t_s pan, IC$);
$\mathrm{final}_p oint = x(end, :);$
$\mathrm{data}_p oints(i, j, :) = final_p oint;$
end end
$\mathrm{data}_p oints_r eshaped = reshape(data_p oints, [], 2);$
$\mathrm{num}_c lusters = 5; [idx, \ ] = kmeans(data_p oints_r eshaped, num_c lusters);$
basins = reshape(idx, $\mathrm{num}_p oints, num_p oints$);
subplot(2,2,p);
pcolor(X, Y, basins);
colormap('jet');
shading interp;
colorbar;
xlabel('Real part of initial condition');
ylabel('Imaginary part of initial condition');
title(titlesp);
ylim([-15,10]);
xlim([-15,10]); end
function dxdt = myODE(t, x, $\mathrm{P}_L S$)$r = 2.5; dxdt = zeros(2, 1);$
dxdt(1) = x(2);
dxdt(2) = -0.03*x(2) + 0.805 - r*sin(x(1) - (1 + 0.1*cos(19*4))) - $\mathrm{P}_L S$;
end

Lyapunov Exponents for laod shedding

clc; clear; close all;

Npre = 200;

Ncalc = 1000; delta0 = 1e-8;

$r_values = 0 : 0.005 : 4;$

$P_LS_values = [0, 0.235, 0.25, 9.8]; titles = 'NoLoadShedding',' P_{LS} = 0.05',' P_{LS} = 0.1',' P_{LS} = 1.2';$

figure;

for k = 1:length(P_LS_values)

$P_LS = P_LS_values(k);$

LyapunovExp = zeros(length(r_values), 1);

for idx = 1:length(r_values)

$r = r_values(idx);$

x = 0.05;

$x_perturbed = x + delta0; delta = delta0;$

for n = 1:Npre

x = -0.03*x + 0.805 - r*sin(x - (1 + 0.1*cos(8.27*7))) - P_LS;

$x_perturbed = -0.03 * x_perturbed + 0.805 - r * sin(x_perturbed - (1 + 0.1 * cos(8.2 * 7))) - P_LS;$

end

$sum_log_delta = 0;$

for n = 1:Ncalc

x = -0.03*x + 0.805 - r*sin(x - (1 + 0.1*cos(8.27*7))) - P_LS;

$x_perturbed = -0.03 * x_perturbed + 0.805 - r * sin(x_perturbed - (1 + 0.1 * cos(8.27 * 7))) - P_LS;$

delta = abs($x_perturbed - x$);

if delta ¡ 1e-10

delta = delta0;

end $sum_log_delta = sum_log_delta + log(delta/delta0);$

$x_perturbed = x + delta0 * sign(x_perturbed - x); end$

LyapunovExp(idx) = $sum_log_delta/Ncalc; end$

subplot(2, 2, k);

plot($r_values, LyapunovExp,' b–',' LineWidth', 1.2$);

hold on; yline(0, 'r–', 'LineWidth', 1);

title(titlesk);

xlabel('r');

ylabel('Lyapunov Exponent');

grid on;

legend('Lyapunov Exponent', 'Zero Line', 'Location', 'Best'); end

Phase portrait for load shedding clc; clear; close all;

H = 6.5; D = 0.8; Pm = 1.5; VG = 1.2; XB = 0.5;

VB0 = 1.0; VB1 = 0.15; thetaB0 = 1.0; thetaB1 = 0.08;

Omega = 2.25; phi$_v = 0; phi_0 = 0; omega_R = 2.0$;

g = @(theta, dtheta, t) 1.2 * sin(theta) .* exp(-0.5 * t) + 0.3 * dtheta .* (1 - exp(-0.5*t));

tspan = [0 300];

theta0 = [0.9; 0];

swingEq1 = @(t, y) [y(2);

(omega$_R/(2 * H)) * (Pm - (VG * (VB0 + VB1 * cos(Omega * t + phi_v))/XB) *$ ...$sin(y(1) - (thetaB0 + thetaB1 * cos(Omega * t + phi_0))) - D * y(2))]$;

swingEq2 = @(t, y) [y(2);

(omega$_R/(2*H))*(Pm-(VG*(VB0+VB1*cos(Omega*t+phi_v))/XB)*...sin(y(1)-(thetaB0 + thetaB1 * cos(Omega * t + phi_0))) - (3.4 * D + 0.5) * y(2) - g(y(1), y(2), t))]$;

[t1, y1] = ode45(swingEq1, tspan, theta0);

[t2, y2] = ode45(swingEq2, tspan, theta0);

figure;

subplot(3,1,1);

plot(t1, y1(:,2), 'r', 'LineWidth', 1.2); hold on;

plot(t2, y2(:,2), 'b', 'LineWidth', 1.2);

xlabel('Time (s)');

ylabel('d$\theta/dt(rad/s)'$);

title('Rotor Speed Time Series');

legend('Without Load Shedding', 'With Load Shedding');

grid on;

subplot(3,1,2);

plot(y1(:,1), y1(:,2), 'r', 'LineWidth', 1.2);

xlabel('$\theta(rad)$');
ylabel('d$\theta/dt(rad/s)$');
title('Phase Portrait Without Load Shedding');
grid on;
xlim([0.8, 2.4]);
ylim([-0.3, 0.5]);
subplot(3,1,3);
plot(y2(:,1), y2(:,2), 'b', 'LineWidth', 1.2);
xlabel('$\theta(rad)$');
ylabel('d$\theta/dt(rad/s)$');
title('Phase Portrait With Load Shedding');
grid on;
xlim([0.8, 2.4]);
ylim([-0.3, 0.5]);

Poincare map for load shedding clear; clc;
r = 2.0;
D = 0.03;
Omega = 7.5;
tspan = [0 300];
x0 = [0.1; 0];
$P_L S_v alues = [0, 1.2]$;
labels = 'Without Load Shedding', 'With Load Shedding';
T = 2*pi / Omega;
$\text{sampling}_p oints = T * (1 : 150)$;
figure;
for i = 1:2
$P_L S = P_L S_v alues(i)$;
[t, x] = ode45(@(t, x) $\text{swing}_e q(t, x, D, r, P_L S, Omega), tspan, x0)$;
$\text{theta}_p = interp1(t, x(:, 1), sampling_p oints)$;
$\text{omega}_p = interp1(t, x(:, 2), sampling_p oints)$;
subplot(1,2,i);

plot(theta$_p, omega_p,' k.',' MarkerSize', 4)$;

title(['Poincaré Map - ' labelsi]);

xlabel('$\theta(rad)$');

ylabel('$\omega(rad/s)$');

axis tight; grid on; end

function dxdt = swing$_e q(t, x, D, r, P_L S, Omega) dxdt = zeros(2, 1)$;

dxdt(1) = x(2);

VB = 1 + 0.1*cos(Omega * t);

dxdt(2) = -D*x(2) + 0.805 - r*sin(x(1) - VB) - P$_L S; end$

Phase portraits clc; clear; close all;

H = 2.36;

D = 0.8;

Pm = 1.5;

VG = 1.2;

XB = 0.5;

VB0 = 1.0;

VB1 = 0.15;

thetaB0 = 1.0;

thetaB1 = 0.08;

Omega = 1.2;

phi$_v$ = 0;

phi$_0$ = 0;

omega$_R$ = 2.0;

g = @(theta, dtheta, t) 1.2 * sin(theta) .* exp(-0.5 * t) + 0.3 * dtheta .* (1 - exp(-0.5*t));

tspan = [0 300];

theta0 = [0.9; 0];

swingEq1 = @(t, y) [y(2);

(omega$_R/(2 * H)) * (Pm - (VG * (VB0 + VB1 * cos(Omega * t + phi_v))/XB) * sin(y(1) - (thetaB0 + thetaB1 * cos(Omega * t + phi_0))) - D * y(2))$];

swingEq2 = @(t, y) [y(2);

(omega$_R$/(2∗H))∗(Pm−(VG∗($VB0$+$VB1$∗cos($Omega$∗t+phi_v))/XB)∗sin($y(1)$−($thetaB0 + thetaB1 * cos(Omega * t + phi_0)$))) − $(3.4 * D + 0.5) * y(2) - g(y(1), y(2), t)$)];

[t1, y1] = ode45(swingEq1, tspan, theta0); [t2, y2] = ode45(swingEq2, tspan, theta0);

figure;

subplot(2,1,1);

plot(t1, y1(:,1), 'r', 'LineWidth', 1.2); hold on;

plot(t2, y2(:,1), 'b', 'LineWidth', 1.2);

xlabel('Time (s)'); ylabel('$\theta(rad)$');

title('Rotor Angle Time Series');

legend('Without Load Shedding', 'With Load Shedding');

grid on;

subplot(2,1,2);

plot(t1, y1(:,2), 'r', 'LineWidth', 1.2); hold on;

plot(t2, y2(:,2), 'b', 'LineWidth', 1.2);

xlabel('Time (s)'); ylabel('d$\theta/dt(rad/s)$');

title('Rotor Speed Time Series');

legend('Without Load Shedding', 'With Load Shedding');

grid on;

sgtitle('Time Series of Rotor Angle and Speed');

figure;

subplot(2,1,1);

plot(y1(:,1), y1(:,2), 'r', 'LineWidth', 1.2);

xlabel('$\theta(rad)$'); $ylabel('d\theta/dt(rad/s)')$;

title('Phase Portrait Without Load Shedding');

grid on;

grid on;

xlim([0.8, 2.4]);

ylim([-0.3, 0.5]);

subplot(2,1,2);

plot(y2(:,1), y2(:,2), 'b', 'LineWidth', 1.2);

xlabel('$\theta(rad)$'); $ylabel('d\theta/dt(rad/s)')$;

title('Phase Portrait With Load Shedding');

grid on;
xlim([0.8, 2.4]);
ylim([-0.3, 0.5]);

Stability increase clc; clear; close all;
$\mathrm{P}_L S_v als = linspace(0, 1.2, 30)$;
$\mathrm{stability}_i ncrease_o riginal = [0, 10.5, 21.6, 29.5, 35.2, 40.8, 44.1, 46.8, 48.5, 49.21]$;
$\mathrm{P}_L S_o riginal = [0, 0.02, 0.05, 0.1, 0.2, 0.4, 0.6, 0.8, 1.0, 1.2]$;
$\mathrm{stability}_i ncrease = interp1(P_L S_o riginal, stability_i ncrease_o riginal, P_L S_v als, ' pchip')$;
figure;
$\mathrm{plot}(\mathrm{P}_L S_v als, stability_i ncrease, ' bo-', ' LineWidth', 1.5, ' MarkerSize', 6, ' MarkerFaceColor', ' b')$;
grid on;
xlabel('Load Shedding (P_{LS})');
ylabel('Stability Region Increase (
xlim([0 $\max(\mathrm{P}_L S_v als)$]);
ylim([0 $\max(\mathrm{stability}_i ncrease) + 5$]);
set(gca, 'FontSize', 12);
legend('Stability Increase', 'Location', 'Best');

Time series for control clc; clear; close all;
H = 6.5;
D = 0.8;
Pm = 1.5;
VG = 1.2;
XB = 0.5;
VB0 = 1.0;
VB1 = 0.15;
thetaB0 = 1.0;
thetaB1 = 0.08;
Omega = 1.2;
$\mathrm{phi}_v = 0$;
$\mathrm{phi}_0 = 0$;
$\mathrm{omega}_R = 2.0$;

g = @(theta, dtheta, t) 1.2 * sin(theta) .* exp(-0.5 * t) + 0.3 * dtheta .* (1 - exp(-0.5*t));

tspan = [0 300];

theta0 = [0.9; 0];

swingEq1 = @(t, y) [y(2);

(omega$_R$/(2 * H)) * (Pm − (VG * ($VB0$ + $VB1$ * $cos(Omega * t + phi_v)$)/XB) * $sin(y(1) - (thetaB0 + thetaB1 * cos(Omega * t + phi_0)))$ − $D * y(2)$)];

swingEq2 = @(t, y) [y(2);

(omega$_R$/(2∗H))∗(Pm−(VG∗($VB0$+$VB1$∗$cos(Omega$∗t+phi_v$))/$XB$)∗$sin(y(1)$− $(thetaB0 + thetaB1 * cos(Omega * t + phi_0)))$ − $(3.4 * D + 0.5) * y(2) - g(y(1), y(2), t))$];

[t1, y1] = ode45(swingEq1, tspan, theta0); [t2, y2] = ode45(swingEq2, tspan, theta0);

plot(t1, y1(:,2), 'r', 'LineWidth', 1.2); hold on;

plot(t2, y2(:,2), 'b', 'LineWidth', 1.2);

xlabel('Time (s)'); ylabel('d$\theta/dt(rad/s)'$); $legend('WithoutLoadShedding','WithLoadShedding'); grid$

Heat map

Npre = 200;

Nplot = 200;

r$_v alues$ = 0 : 0.005 : 4;

n$_v alues$ = 1 : $Nplot$;

x = zeros(length(r$_v alues$), $Nplot$); $foridx = 1 : length(r_v alues)$

r = r$_v alues(idx); x_c urrent = 0$;

for n = 1:Npre

x$_c urrent = -0.03 * x_c urrent + 0.805 - r * sin(x_c urrent - (1 + 0.1 * cos(18.5 * 7)))$;

end for n = 1:Nplot

x$_c urrent = -0.03 * x_c urrent + 0.805 - r * sin(x_c urrent - (1 + 0.1 * cos(18.5 * 7)))$;

x(idx, n) = x$_c urrent$;

end end figure;

imagesc(n$_v alues, r_v alues, mod(x, 2 * pi)); colormap('hot'); colorbar$;

xlabel('n (iterations)');

ylabel('r'); hold on; plot([0, Nplot], [2.68, 2.68], 'b–', 'LineWidth', 1.5);

legend('Intermittency Region');

Quasiperiodicity Bifurcation

function bifurcation$_d iagram_q uasi_p eriodic2$

Npre = 200;

Nplot = 100;

x = zeros(Nplot, 1);

omega$_p rimary_r esonance = pi/2.5$;

for r = 0:0.005:4 x(1) = 0;

for n = 1:Npre

x(1) = -0.01 * x(1) + 0.8 - r * sin(x(1) - (1.7 + 0.15 * cos(omega$_p rimary_r esonance *$ 7)));

end

for n = 1:Nplot-1

x(n+1) = -0.01 * x(n) + 0.8 - r * sin(x(n) - (1.7 + 0.15 * cos(omega$_p rimary_r esonance *$ 7)));

end

plot(r * ones(Nplot, 1), x, '.', 'markersize', 4);

hold on;

end

xlabel('r');

ylabel('$\theta(t)$');

set(gca, 'xlim', [0 4], 'ylim', [-5 5]);

end

Quasiperiodicity Analysis

function quasi$_p eriodic_a nalysis$

f = 0.1;

omega$_p rimary_r esonance = pi/2.5$;

r$_r ange = 0 : 0.005 : 4$;

Npre = 200;

Nplot = 100;

Ncalc = 500;

delta0 = 1e-8;

x = zeros(Nplot, length(r_range));

LyapunovExp = zeros(length(r_range), 1);

$heatmap_data = zeros(length(r_range), Nplot)$;

for j = 1:length(r_range)

$r = r_range(j)$;

$x_current = 0$;

$x_perturbed = x_current + delta0$;

for n = 1:Npre

$x_current = -0.01*x_current+0.8-r*sin(x_current-(1.7+0.15*cos(omega_primary_resonance*7)))$;

$x_perturbed = -0.01*x_perturbed+0.8-r*sin(x_perturbed-(1.7+0.15*cos(omega_primary_resonance*7)))$;

end

for n = 1:Nplot

x(n, j) = -0.01 * $x_current+0.8-r*sin(x_current-(1.7+0.15*cos(omega_primary_resonance*7)))$;

$x_current = x(n, j)$;

$heatmap_data(j, n) = mod(x_current, 2 * pi)$;

end

$sum_log_delta = 0$;

$x_current = 0$;

$x_perturbed = x_current + delta0; delta = delta0$;

for n = 1:Ncalc $x_current = -0.01 * x_current + 0.8 - r * sin(x_current - (1.7 + 0.15 * cos(omega_primary_resonance * 7)))$;

$x_perturbed = -0.01*x_perturbed+0.8-r*sin(x_perturbed-(1.7+0.15*cos(omega_primary_resonance*7)))$;

delta = abs($x_perturbed - x_current$);

if delta ¡ 1e-10 delta = delta0;

end

$sum_log_delta = sum_log_delta + log(delta/delta0)$;

$x_perturbed = x_current + delta0 * sign(x_perturbed - x_current)$;

end LyapunovExp(j) = $sum_log_delta/Ncalc$;

```
end
figure;
plot(r_range, x,'.','markersize', 2);
xlabel('r');
ylabel('x_n');
title('Quasi-Periodic Bifurcation Diagram');
ylim([-5 5]);
xlim([0 4]);
grid on;
figure;
imagesc(1:Nplot, r_range, heatmap_data);
colormap('hot');
colorbar;
xlabel('n (iterations)');
ylabel('r');
title('Heatmap of Quasi-Periodic System Dynamics');
figure;
plot(r_range, LyapunovExp,'b-','LineWidth', 1);
xlabel('r');
ylabel('Lyapunov Exponent'); grid on;
hold on;
yline(0, 'r–', 'LineWidth', 1);
legend('Lyapunov Exponent', 'Zero Line');
end
```